

INTERNATIONAL HARMONIZED RESEARCH ACTIVITIES (IHRA) STATUS REPORT OF THE BIOMECHANICS WORKING GROUP

Rolf H. Eppinger

National Highway Traffic Safety Administration
United States
Paper Number 05-0459

ABSTRACT

A summary of the continued efforts of the Biomechanics Working Group to complete its original task given to it by the International Harmonized Research Activities Steering Committee, determining specifications for a Universal Side Impact Anthropomorphic Test Devices is presented.

INTRODUCTION

This report summarizes the continued activities of the International Harmonized Research Activities (IHRA) Working Group on Biomechanics Research (BWG) for the period from its last report, given at the May 2003 in Nagoya, Japan on the occasion of the 18th International Technical Conference on the Enhanced Safety of Vehicles, to the present. The Biomechanics Working Group continues to concentrate its efforts to develop a rationale for and specifications of a universal side impact Anthropomorphic Test Device (ATD). This task remains the primary focus of the Biomechanics however; discussions of possible new initiatives have also taken place.

DISCUSSION

Emphasis of the BWG's Current Efforts:

The BWG continues to concentrate the majority of its efforts on the completion of its Side Impact Report. These efforts encompass four major topics:

- Characterization of the Global Side Impact Problem (which seeks to identify the commonalities and differences of the side impact problem throughout the world),
- Anthropometric Characterization of Crash Victims (which investigates the size and mass attributes of the world's side impact population at risk and seeks to determine the necessary and sufficient type and number of test dummies necessary to effect broad safety benefits),

- Biofidelic Impact Response Specifications (which seeks to characterize and generalize human impact responses into dummy design requirements and provide a quantitative evaluation methodology for assessing the ability of various dummy designs to meet them), and
- Injury Criteria and Associated Performance Limits (which seeks, through thorough review and analysis, appropriate injury criteria for the various body areas at risk that can link features of an occupant's impact response with estimations of the extent and severity of expected injuries. Performance limit recommendations that would provide sufficient reduction of the current side impact injury situation will also be proposed).

Steady progress has been achieved in each of the four major research areas with updated versions of the final report having been redrafted. However, developing and reaching consensus in the area of Biofidelic Impact Response Specifications area remains the most difficult technical challenge to the BWG. The difficulties stem from deciding what is the set of *necessary* response requirements and when do they become the set of *sufficient* response requirements. This is further complicated because some response requirements determine how a dummy should interact with its impact environment while others deal with those requirements necessary for good injury prediction. Various, recent technical publications in this area have tried to address this issue and the BWG feels that with these new concepts, it can find a reasonable consensus of opinion to resolve this issue and allow finalizing the needed response requirements.

Efforts to develop Biofidelic Impact Response Specifications for a family of frontal test dummies have also been informally initiated. The BWG has decided to use, as an initial bases, the response specifications derived and used for the design and development of NHTSA's advanced frontal test dummies, the 50th percentile male and the 5th percentile female THOR dummies. Evaluation of the

appropriateness, adequateness, and sufficiency of these and other existing requirements will most certainly become major discussion topics for upcoming meetings of the BWG group.

SUMMARY

To accomplish its task of developing and providing necessary and sufficient specifications to develop a universal side impact anthropomorphic test device(s) with associated injury criteria and performance limits, the BWG continues to review crash data, anthropometrical data, biomechanical response and

injury data. As it stands today, the current consensus among the BWG's participants is that the world side impact problem possesses sufficient significant similarities to allow a definition of a single family of dummy test devices to be made. This single family should be able to appropriately represent the diversity of the world's nationalities as well as be able to monitor and/or control all significant injury and crash modes they experience. The BWG also believes that sufficient information exists to define the dummy's impact response characteristics to assure that it adequately response like a human and those responses can be interrogated to make accurate estimations of injury. The BWG hopes to complete this undertaking in the near future and provide the Steering Committee a draft of the Side Impact report as it has requested.

KINEMATICALLY BASED WHIPLASH INJURY CRITERION

Shashi Kuppa, James Saunders, Jason Stammen

National Highway Traffic Safety Administration

Ann Mallory

Transportation Research Center Inc.

U.S.A

05-0211

ABSTRACT

NHTSA recently published the final rule that upgrades the FMVSS No. 202 head restraint standard (69 FR 74848). The rule provides requirements that would make head restraints higher and closer to the head so as to engage the head early in the event of a rear impact. The rule also has provisions for a rear impact sled test option with a Hybrid III dummy that is intended in particular for active head restraints that do not meet the head restraint position requirements.

This paper presents a whiplash injury criterion for use with the Hybrid III dummy in rear impacts and its application in rear impact tests. The injury risk curve, based on the head-to-torso rotation of the Hybrid III dummy, was developed using insurance claims data, and rear impact sled tests with the Hybrid III dummy. The feasibility of the application of this injury criterion in rear impact vehicle crash tests and sled tests has also been presented. The sled test data indicates that the developed whiplash injury criterion correctly predicts improved performance of head restraint and seat systems in the field.

INTRODUCTION

NHTSA estimates that between 1988 and 1996, there were annually, 805,851 occupants in outboard seating positions of passenger cars, light trucks and vans who sustained whiplash injuries. The annual cost of these whiplash injuries was approximately \$8.0 billion (Final Regulatory Impact Analysis for FMVSS No. 202 Head Restraints, NHTSA-2004 19807, No. 1 at <http://dms.dot.gov>). When insurance claims are considered, whiplash injuries account for 70 percent of all bodily injury claims, 43 percent of medical costs, and overall cost approaching 9 billion dollars (Viano, 2003).

NHTSA recently published the final rule that upgrades the FMVSS No. 202 head restraint standard (69 FR 74848). The rule provides requirements that would make head restraints higher and closer to the head so as to engage the head early in the event of a rear impact. The rule also has provisions for a rear impact sled test option with a Hybrid III dummy that is intended in particular for active head restraints that do not meet the static head restraint position

requirements such as head restraint height and backset.

Though some studies suggest that the BioRID II and RID 2 are more biofidelic than the Hybrid III dummy in low speed rear crashes, they are still undergoing change and have not attained universal acceptance in the biomechanical community (Prasad, et al., 1997, Kim, et al., 2001, 2003). The Hybrid III dummy was found to successfully rank OEM seats according to their associated frequency of whiplash injury claims (Heitplatz et al., 2003). It was also found to be a good tool for the design of effective head restraints (Viano, 2001, 2003). Therefore, NHTSA decided on the use of the Hybrid III dummy for whiplash injury assessment in the optional dynamic sled test of the FMVSS No. 202 upgrade.

INJURY CRITERION TO ASSESS WHIPLASH INJURY IN FMVSS NO. 202 DYNAMIC TEST OPTION

The symptoms associated with whiplash injury include pain in the neck, shoulders, or upper back, vision disorder, dizziness, headaches, unconsciousness, and neurological symptoms in the upper extremities. These symptoms may be short term or long term. The term “whiplash” to describe these injuries is derived from the neck kinematics during a rear impact. Initially, the unsupported head lags behind the torso due to inertia (retraction) and then rotates backward, forcing the neck into extension.

Yang et al. (1996) hypothesized that the relative motion of the head with respect to the torso results in shearing action causing relative motion between adjacent vertebrae that may be pronounced in the lower cervical vertebrae where the facet angle is less steep. This may cause stretching of lower cervical vertebrae facet capsules beyond the normal physiological range, resulting in injury and pain. Lee et al. (2004) demonstrated a relationship between facet joint distraction and capsular ligament strain resulting from whiplash kinematics, and pain using an in vivo animal model.

The various symptoms resulting from whiplash injury lead to various hypotheses of the mechanisms of injury and as a consequence different injury criteria. A description of the various proposed

whiplash injury mechanisms and criteria has been presented in a technical report (Kuppa, 2004) in support of the FMVSS No. 202 Final Rule.

Some studies have demonstrated that the neck forces and moments along with head and T1 accelerations of the Hybrid III dummy in low speed rear impacts may not exhibit very good biofidelity. Therefore, whiplash injury assessment using NIC (Bostrom et al., 1996, Svensson et al., 2000), Nij (FMVSS No. 208, 2000), or Nkm (Muser et al., 2000, Schmitt et al., 2001) with the Hybrid III dummy responses may not be adequate.

While there remains a lack of consensus on the underlying whiplash injury mechanism, many agree that limiting the relative head-to-torso motion may reduce the incidence of whiplash injuries (Viano, 2002, Yoganandan, 2000, Langweider, 2000). Sunderarajan et al. (2004) examined the effect of the head restraint position with respect to the head/neck on cervical facet stretch during low speed rear impacts with human post-mortem subjects. The study demonstrated that the maximum facet stretch was greater when the head-to-head restraint distance increased, suggesting an increase in whiplash injury potential.

Viano (2003a), using the Hybrid III dummy in rear impact sled tests, demonstrated that an increase in head-to-head restraint distance results in an increase in head-to-torso rotations of the Hybrid III dummy in rear impact sled tests. Therefore, head-to-torso rotation measurements on the Hybrid III dummy may be able to distinguish poor head restraint designs from the good designs. Tencer et al. (2003) found that a displacement based injury criterion was best suited to predict intervertebral displacements associated with whiplash injury. This further suggests that injury criteria based on relative head-to-torso motion of the Hybrid III dummy may be adequate in assessing whiplash injury risk.

Viano, et al. (2002) proposed the Neck Displacement Criteria (NDC) that rates seat and head restraint systems on the basis of the relative motion of the Hybrid III head with respect to its torso in rear impact tests. However, he did not associate the relative head motion with the risk of whiplash injury. One method of estimating whiplash injury risk as a function of Hybrid III dummy head/neck kinematics, is to relate whiplash injury risk for specific OEM seat systems in rear impact crashes in the field to Hybrid III neck kinematics in rear impact sled tests at different speeds with the same OEM seats.

Kuppa (2004) used whiplash injury claims data of the Saab 900 and Saab 9-3 along with corresponding rear impact sled tests with the Hybrid III dummy to develop a whiplash injury risk curve based on head-to-torso rotation of the Hybrid III dummy (Figure 1

and Equation 1). Though NDC developed by Viano (2002a) considers the head-to-torso rotation as well as the head-to-torso translation, Kuppa found the head-to-torso translation was highly correlated to the head-to-torso rotation ($R^2=0.98$) and so did not add any new information for evaluating whiplash potential of seat systems.

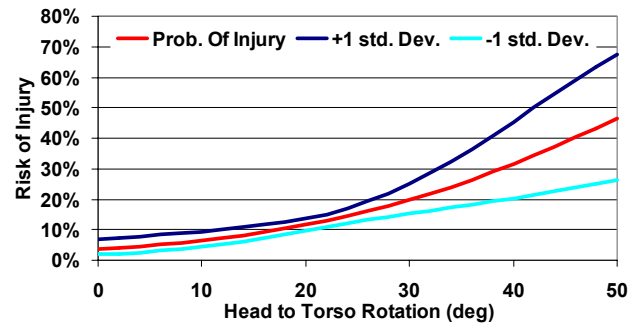


Figure 1. Risk of whiplash injury as a function of head-to-torso rotation of the 50th percentile adult male Hybrid III dummy in 16 km/h rear impact sled tests.

$$\text{prob. of whiplash injury} = \frac{1}{1 + e^{3.295 - 0.063 \text{ H/T rotation (deg)}}} \quad (1)$$

INSTRUMENTATION FOR MEASUREMENT OF HEAD-TO-TORSO ROTATION

The instrumentation used in rear impact tests to obtain head-to-torso rotation needs to be durable, allow unrestricted motion of the head and torso, and be lightweight and small so as not to change the dummy mass and inertial properties. NHTSA examined different instrumentation (accelerometers, electrogoniometers, gyro and magneto-hydrodynamic angular rate sensors) for obtaining head-to-torso rotations. In various research programs sponsored by NHTSA, magnetohydrodynamic (MHD) angular rate sensors (ARS) were successfully employed for determining joint rotations. The MHD ARS are based on the principle that relative motion between a magnetic field and a conductive fluid produces an electropotential that is measured by the sensor (Laughlin, 1992).

MHD ARS were previously used to determine human foot position relative to the tibia during a plantar foot impact, position of the forearm relative to the upper arm during side air bag loading, and to determine neck extension angle during out-of-position airbag loading (Hall et al. 1997). The three dimensional position of a body segment with respect to another was determined by transforming the three-dimensional angular rates and linear accelerations

into Eulerian space. The accuracy of the computed position and relative rotation was verified by demonstrating that the ARS results agreed to within 2 percent of ankle potentiometer data from an anthropomorphic crash test dummy (Hall et al., 1996). Tests on the spine and neck demonstrated that ARS was more accurate than photographic methods. Based on this prior experience for measuring joint motion, the dummy's head and torso was instrumented with Applied Technology Associates (ATA) magnetohydrodynamic (MHD) angular rate sensors (ARS).

Typical ATA ARS have low cross axis and linear acceleration sensitivity and have a bandwidth in the range of 1 Hz to 1000 Hz. The extremely broad frequency bandwidth capability enables the MHD rate sensors to measure high frequency and transient angular motions reasonably well.

The low frequency of the MHD angular rate sensors can be extended well below 0.1 Hz by use of digital filtering of the post processing of the measurement data. The compensation filter (Laughlin, 1998) is supplied by ATA (ATA- Sensors) and is specific to the MHD ARS used. Voo et al. (2003) employed ATA MHD ARS in rear impact sled tests and demonstrated that the head rotation obtained from the uncompensated angular rate signal underestimated the extension neck rotation and overestimated the flexion rotation in rear impact tests while the compensated signal matched that from video analysis reasonably well.

Voo et al. (2003) evaluated three different measurement methods for angular rotation of a dummy head and torso in a rear impact crash environment and found the compensated signals from the ATA MHD angular rate sensors yielded rotation data closely matching the results from high-speed video images to within 3 degrees with a total displacement range up to 110 degrees. Linear acceleration data generally yielded less accurate angular displacement results.

APPLICATION OF ANGULAR RATE SENSORS IN REAR IMPACT TESTS

Voo et al. (2003, 2004) and Kleinberger et al. (2003) conducted rear impact sled tests with the 50th percentile Hybrid III dummy in seats with different head restraint heights and seatback strength. The dummy, positioned in a seat in accordance to FMVSS No. 202, was restrained with the available

lap/shoulder belts. The seatback was inclined to 25° from the vertical and the dummy was positioned so that its H-point was aligned with the H-point of the seat (Figure 2).

The dummy was instrumented with tri-axial angular rate sensors at the center of gravity (CG) of the head and the dummy thorax. The ARS mounting cube could accommodate the linear accelerometers at the CG and was about the same mass as the existing accelerometer cube in the Hybrid III head. There was negligible change of the head mass and the head moment of inertia by replacing the existing mounting cube with the ARS cube at the CG of the head. Another ARS cube was attached to the spine box such that it had no effect on the dummy interaction with the seat back.

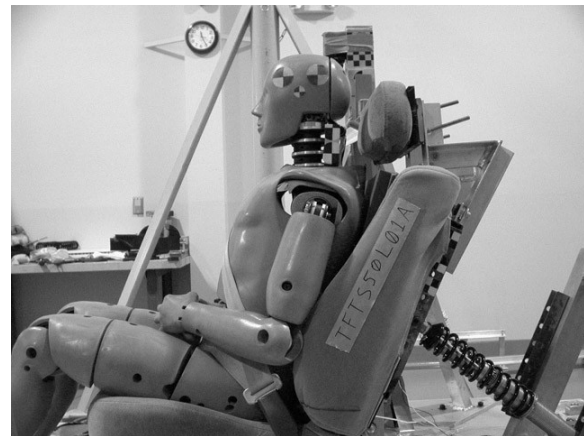


Figure 2. Instrumented Hybrid III dummy seated in a modified production seat.

Due to the symmetry of the dummy and the test condition, the head and torso rotated mainly in the sagittal plane. Therefore, rotational velocity data about the y-axis of the dummy provided reasonably good estimates of the rotation of the head and torso. The compensated angular rate signals along the y-axis at the head CG and the spine box were integrated (trapezoid integration) to obtain angular displacement of the head and the torso in degrees. The angular torso displacement was then subtracted from that of the head to obtain relative angular displacement (degrees) of the head with respect to the torso.

Sled tests were conducted using a sinusoidal sled pulse that fit within the FMVSS No. 202 dynamic test corridor with a nominal peak of 9 gs and duration of 90 milliseconds (Figure 3).

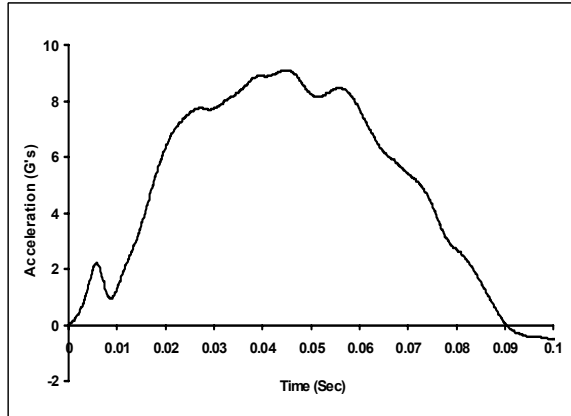


Figure 3. Sled pulse for rear impact tests complying with the FMVSS No. 202 specified sled pulse corridor.

Voo et al. (2003, 2004) and Kleinberger et al. (2003) found that the peak head-to-torso rotation of the dummy not only depended on the head restraint position (height and backset) but also on the rigidity of the head restraint, recliner stiffness and seat cushion stiffness. Seats with low recliner stiffness resulted in greater seat back rotation, later contact time of the head with the head restraint, and greater head and torso rotation. Sled tests with different types of head restraints suggested that a more rigid head restraint might have a protective advantage over a more flexible one in rear impacts. Kleinberger et al. (2003) also reported repeatable head and torso rotation values obtained from the ATA MHD angular rate signals.

NHTSA conducted 3 repeat FMVSS No. 301 type rear impact crash tests of a 2004 Jeep Liberty. The crash involved a flat barrier impacting a stationary vehicle in the rear at 30 mph. The average change in velocity of the Jeep Liberty was 26.4 km/h. The head restraint height from the H-point along the torso line was 836 mm and the backset was 85 mm (according to the measurement procedure in FMVSS No. 202 upgrade). While the head restraint height met the head restraint height requirement specified, it did not meet the backset requirement of 55 mm as per FMVSS No. 202 final rule.

The seat back was inclined to 25 degrees from vertical and along with the standard instrumentation on the Hybrid III 50th percentile male dummy, it was also instrumented with ATA MHD ARS-06 angular rate sensors at the CG of the dummy head and at the spine to obtain head-to-torso rotation.

The HIC15 values of the driver and passenger in the three tests were less than 100 and the coefficient of variance was 1.3 percent (Figure 4). The mean head-to-torso rotation in the three tests for the driver was 45 degrees while that for the rear passenger was

30 degrees. The coefficient of variation of head-to-torso rotation for the driver and rear passenger was less than 10 percent (Figure 4).

The sled test data from Kleinberger et al. (2003) and the vehicle crash tests suggest that the head-to-torso rotation obtained from MHD ARS are repeatable in sled and vehicle crash test environment.

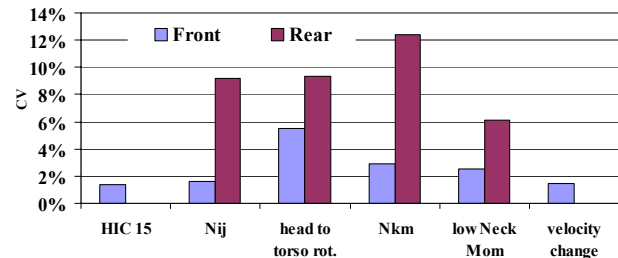


Figure 4. Coefficient of variation of injury measures from three repeat FMVSS 301 type rear impact tests with the Jeep Liberty.

VALIDATION OF HEAD-TO-TORSO ROTATION MEASUREMENT FOR WHIPLASH INJURY ASSESSMENT

Farmer et al. (2002) examined the effects of head restraint and seat redesign on neck injury risk in rear end crashes by examining automobile insurance claims. The results indicated that the improved geometric fit of head restraints observed in many newer vehicle models reduced the risk of whiplash injury. In particular, Farmer examined the improved geometry of the 2000-2001 Ford Taurus head restraints over that of the 1999 Ford Taurus. The 1999 Ford Taurus head restraint received a “poor” rating based on the IIHS evaluation procedure (IIHS, 2004) while the 2001 Ford Taurus received an “acceptable” rating. After controlling for the effect of crash severity, Farmer estimated an 18 percent effectiveness of the 2000-2001 Ford Taurus over that of the 1999 Ford Taurus in mitigating whiplash injuries.

Mallory and Stammen (2005) conducted low speed rear impact tests with the 50th percentile male Hybrid III dummy in 1999 and 2001 Ford Taurus seats. The objective of these tests was to investigate the ability of head-to-torso rotation and other whiplash injury criteria to distinguish the performance of the 1999 and 2001 Model year Ford Taurus in rear impacts in comparison to the relative effectiveness reported by Farmer et al. (2002).

Rear impact sled tests using sled pulses that were within the FMVSS 202 specified corridor were conducted with 1999 and 2001 Ford Taurus seats. The Hybrid III dummy was instrumented to measure head and T1 accelerations, as well as upper and lower neck loads. In addition, ATA MHD ARS-06 angular

rate sensors were attached at the head CG and the dummy spine to measure head and torso angular rates. Head-to-head restraint contact time was determined using a contact switch on the head restraint and confirmed using high-speed video.

The neck injury measures Nij, Nkm, and NIC were computed as reported by Kleinberger et al. (2003). Nij, head-to-torso rotation, and corrected lower neck moments (moment at the base of the neck as per Prasad (1997)) were lower in the 2001 Taurus than the 1999 Taurus suggesting that all three injury measures correctly predict the improved effectiveness of the 2001 Taurus head restraint over that of the 1999 Taurus (Table 1). However, NIC and Nkm were higher for the 2001 Taurus than the 1999 Taurus suggesting a reverse trend from field observations.

Since the head-to-torso rotation injury measure has an associated whiplash injury risk curve, the relative effectiveness of the 2001 Taurus over the 1999 Taurus model can be developed using head-to-torso rotations obtained in tests with these two seats.

Table 1. Injury measures of the Hybrid III dummy in 1999 and 2001 Ford Taurus in FMVSS No. 202 type rear impact sled tests.

Injury Measure	1999 Taurus	2001 Taurus
HIC15	30.7	28.5
NIC (m^2/s^2)	19.5	23.9
Nij	0.21	0.08
Nkm	0.35	0.36
Head-to-torso rotation (deg)	38.1	29.5
Corr. Lower neck moment (Nm)	69.3	54.6
Tl accel. (gs)	10.8	12.1
Head to head rest. contact time (ms)	120.5	111.7
Upper neck shear force Fx (N)	302.2	264.7
Upper neck tension force Fz (N)	1038	489

The risk of whiplash injury estimated by head-to-torso rotation for the 1999 Taurus is 29 percent while that for the 2001 Taurus is 19.5 percent (obtained using Equation 1). The whiplash injury risk is 9.5 percent lower in the 2001 Taurus resulting in 33 percent improved effectiveness over the 1999 Taurus. The improved effectiveness of the 2001 Taurus seat over that of the 1999 Taurus seat estimated from the sled test data (Table 1) is higher than the 18 percent reported by Farmer (2004). This higher effectiveness in the sled tests may be related to the fact that the sled tests were conducted with the head restraints in

the highest position while in the real world, adjustable head restraints are not always optimally positioned and many times left unadjusted in their lowest position (Lubin and Sehmer (1993)).

Figures 5 and 6 present the timing of the peaks of various measures along the head-to-torso rotation time-history. Peak chest acceleration and NIC occur early in the impact event, about the time of head-to-head restraint contact, while the peaks of Nij, upper and lower neck extension moment, Nkm occur closer to the time of peak head-to-torso rotation. Kuppaa (2004) found that peak corrected lower neck extension moment of the Hybrid III dummy was correlated ($R^2=0.96$) to its head-to-torso rotation in rear impact sled tests. Figures 5 and 6 indicate that lower neck moment peaks a little earlier than peak head-to-torso rotation.

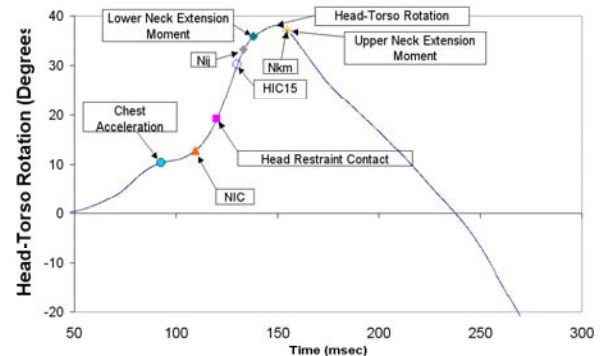


Figure 5. Relative timing of injury measures overlaid on the head-to-torso rotation time history curve in the rear impact test with the 1999 Ford Taurus

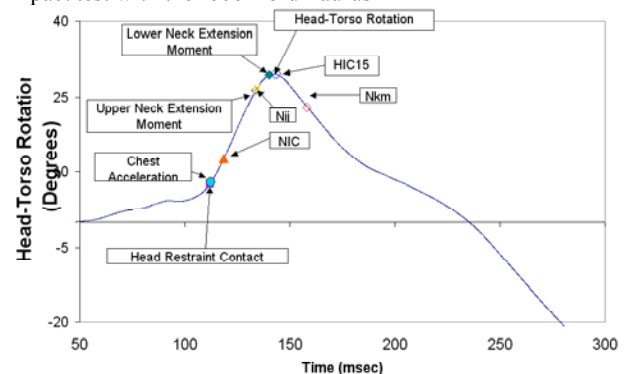


Figure 6. Relative timing of injury measures overlaid on the head-to-torso rotation time history curve in the rear impact test with the 2001 Ford Taurus

DISCUSSION

The head-to-torso rotation of the Hybrid III dummy, obtained from ATA MHD angular rate sensors, in rear impact sled tests and vehicle crash tests was found to be reasonably accurate and repeatable. This demonstrates the feasibility of head-

to-torso rotation as a whiplash injury measure to evaluate head restraint/seat systems in the FMVSS No. 202 optional dynamic test.

Linder et al. (2004) conducted sled test reconstructions of real world rear impacts and correlated whiplash injury risk observed in the field to dummy measurements and various injury criteria. From the test data of 25 real world reconstructions using the BioRID II dummy, the researchers found NIC, Nkm, T1 acceleration, upper neck shear force (Fx) and axial force (Fz), and head-to-head restraint contact time to correlate well with whiplash injury risk. Linder proposed injury threshold levels for NIC of 16.7, Nkm of 0.37, T1 acceleration of 9.6 gs upper neck shear force (Fx) of 178 N and upper neck axial force (Fz) of 659 N that correspond to less than 10 percent of whiplash injury persisting for more than one month.

The Insurance Institute for Highway Safety (IIHS, 2004) recently released the International Insurance Whiplash Prevention Group (IIWPG) procedure for rating of seats and head restraints for neck injury prevention that is somewhat based on the Linder (2004) study. Seat systems that obtain a “good” or “acceptable” rating according to the IIHS geometric evaluation of their head restraints, are put through a dynamic rear impact sled test with the BioRID II dummy simulating a rear crash with a velocity change of 16 km/h. The evaluation is based on seat design parameters and test dummy response parameters. The seat design parameters are time to head restraint contact and maximum forward T1 acceleration that are classified into “pass” and “fail” categories. The test dummy response parameter is based on a vector sum of maximum upper neck tension and upper neck rearward shear force and is classified into “low”, “moderate”, and “high” neck force categories. The vector sum of neck tension and shear has no biomechanical interpretation but is merely a statistical interpretation of data obtained from dynamic sled tests of 102 seats with good static geometric ratings. The seat design and neck force classifications are combined, resulting in a dynamic rating of the seat ranging from “good” to “poor”.

The sled pulse corridor specified in FMVSS No. 202 is similar to the IIWPG 16 km/h sled pulse. While FMVSS No. 202 employs head-to-torso rotation of the Hybrid III dummy to assess whiplash injury potential, the IIWPG uses head-to-head restraint contact time, maximum T1 acceleration, and a vector sum of upper neck tension and shear forces of the BioRID II to evaluate head restraint/seat systems.

The 2001 and the 1999 Taurus seats used in the Mallory et al. study (2005) did not meet the head restraint position requirements (at least 800 mm head

restraint height along torso line above H-point and a backset no greater than 55 mm) of the FMVSS No. 202 Final Rule in 69 FR 74848 (Table 2). IIHS geometric head restraint rating for the 1999 and 2001 Taurus models was “poor” and “acceptable”, respectively.

Table 2. Head restraint geometric position measurement according to that specified in FMVSS No. 202.

Vehicle	Horizontal (mm)		Vertical (mm)	
	Down	Up	Down	Up
1999 Taurus	125	85	695	714
2001 Taurus	65	70	747	794

In the tests with the 1999 and 2001 model Ford Taurus, the head-to-torso rotations of 38.1 and 29.5 degrees (Table 1), respectively, were higher than the 12 degree limit specified in FMVSS No. 202.

The head-to-head restraint contact time of the 1999 and 2001 Taurus were greater than 70 msec and the peak T1 accelerations exceeded 9.5 gs (Table 1) resulting in the two Taurus models receiving a “fail” rating of the seat design criteria proposed by IIWPG. The maximum upper neck tensile force of 1038N and 489 N and the upper neck shear of 302 N and 265 N for the 1999 Taurus and the 2001 Taurus, respectively, give the two Taurus models a IIWPG neck force classification of “high”. Though the IIWPG ratings are based on the BioRID II dummy measurements, the Hybrid III measurements applied to the IIWPG rating would give the 1999 and 2001 Ford Taurus an overall “poor” rating.

Mallory and Stammen (2005) also conducted low speed rear impact sled tests using the BioRID II dummy in 1999 and 2001 model year Ford Taurus seats. The sled pulses were identical to those used in the tests with the Hybrid III dummy in the Ford Taurus seats presented earlier in this paper. The injury measures in the tests with the BioRID II are presented in Table 3. In both the tests with the Ford Taurus seats, the T1 accelerations of the BioRID II exceeded 9.5 gs and the time to head restraint contact exceeded 70 ms. The measured upper neck shear and tensile force of the BioRID II are in the high force range of the IIWPG neck force classification. This results in an IIWPG rating of the 1999 and 2001 Ford Taurus of “poor”.

The IIWPG procedure for rating seats and head restraints rated the 1999 and the 2001 Ford Taurus seats as “poor” when applied to the rear impact sled test data with the BioRID II as well as with the Hybrid III dummy.

Table 3. Injury measures of the BioRID II dummy in 1999 and 2001 Ford Taurus in FMVSS No. 202 type rear impact sled tests.

Injury Measure	1999 Taurus	2001 Taurus
HIC15	35.1	47.9
NIC (m^2/s^2)	36.9	40.1
Nij	0.39	0.13
Nkm	0.93	0.72
Head-to-torso rotation (deg)	18.4	2.6
Lower neck moment (Nm)	17.1	41.5
T1 accel. (gs)	12.3	14.4
Head to head rest. contact time (ms)	155.2	104
Upper neck shear force Fx (N)	609.8	364.8
Upper neck tension (N)	1090	716.7

This poor rating, along with the failure of both Taurus seats to meet the updated FMVSS No. 202 requirements suggest that though the 2001 Taurus demonstrated improved performance over the 1999 Taurus in mitigating whiplash injury, substantial improvements are still needed. IIHS also suggested the need for further improvement by giving the 2004-05 Ford Taurus head restraint and seat a “marginal” rating according to the IIWPG evaluation procedure.

CONCLUSIONS

This paper presents a kinematically based injury measure (head-to-torso rotation) to evaluate whiplash injury potential in rear impact tests using the Hybrid III 50th percentile male dummy. Head-to-torso rotation obtained from magnetohydrodynamic angular rate sensors in rear impact tests were found to be reasonably accurate and repeatable. Peak head-to-torso rotation of the HIII dummy in FMVSS No. 202 dynamic sled tests was able to correctly rank the effectiveness of head restraint/seat systems according to their observed field effectiveness.

REFERENCES

ATA Sensors, “Extending the Frequency Response of the MHD Angular Rate Sensors,” Application Note AN-01 Rev A, http://www.atasensors.com/Sensors2/application_note_an01_rev_a.htm.

Bostrom, O., et al., “A New Neck Injury Criterion Candidate Based on Injury Findings in the Cervical

Spinal Ganglia After Experimental Neck Extension Trauma,” Proceedings of the IRCOBI Conference, 1996.

Farmer, C., Wells, J., Lund, A., “Effects of Head Restraint and Seat Redesign on Neck Injury Risk in Rear-End Crashes,” Report of Insurance Institute for Highway Safety, October, 2002.

Hall, G., Crandall, J., Klopp, G., Pilkey, W., “Angular Rate Sensor Joint Kinematics,” Shock and Vibration, Vol. 4, pp. 223-229, 1997.

Hall, G., Crandall, J., Klisch, S., Klopp, G., Pilkey, W., “Measurement of Joint Motion Using Magnetohydrodynamic Angular Rate Sensors,” Technical Note, Shock and Vibration Digest, 28(5), 1996.

Heitplatz, F., Sferco, R., Fay, P., Reim, J., Kim, A., Prasad, P., “An evaluation of Existing and Proposed Injury Criteria with Various Dummies to Determine their Ability to Predict the Levels of Soft Tissue Neck Injury Seen in Real World Accidents,” 18th International Technical Conference on the Enhanced Safety of Vehicles, 2003.

Insurance Institute for Highway Safety (IIHS), “Procedure for Rating Seats/Head Restraints,” <http://www.hwysafety.org/vehicle%5Fratings/head%5Frestraints/head.htm>, 2004.

Insurance Institute for Highway Safety (IIHS), “Rationale for IIWPG Ratings of Seats and Head Restraints for Neck Injury Prevention – International Insurance Whiplash Prevention Group,” http://www.iihs.org/vehicle_ratings/iwpg_rationale.pdf, December, 2004.

Kim, A., et al., “A Comparison of the Hybrid III and BioRID II Dummies in Low Severity, Rear Impact Sled Tests,” Proceedings of the Forty-Fifth Stapp Car Crash Conference, Paper No. 01S-22, 2001.

Kim, A., Anderson, K., Berliner, J., Hassan, J., Jensen, J., Mertz, H., Pietsch, H., Rao, A., Scherer, R., Sutterfield, A. “Comparison Tests of BioRID II and RID 2 with Regard to Repeatability, Reproducibility and Sensitivity for Assessment of Car Seat Protection Potential in Rear-End Impacts, Stapp Car Crash Journal, Vol. 47, October, 2003.

Kleinberger, M., et al., “Development of Improved Injury Criteria for the Assessment of Advanced Automotive Restraint Systems, NHTSA Docket 98-4405-9, U.S. DOT, Washington, D.C.

Kleinberger, M., Voo, L., Merkle, A., Bevan, M., Chang, S., “The Role of Seatback and head Restraint Design Parameters on Rear Impact Occupant Dynamics,” 18th International Technical Conference on the Enhanced Safety of Vehicles, Nagoya, Japan, 2003.

Kuppa, S., “Injury Criteria and Anthropomorphic Test Devices for Whiplash Injury Assessment,”

- NHTSA Docket No. 19807,
<http://dmses.dot.gov/docimages/p80/313219.pdf>.
- Langweider, K., Hell, W., Schick, S., "Evolution of a Dynamic Seat Test Standard Proposal for a Better Protection After Rear End Impact," Proceedings of the International Conference on the Biomechanics of Impact, 2000.
- Laughlin D., "A magnetohydrodynamic angular motion sensor for anthropomorphic test device instrumentation," Proceedings of the 33rd Stapp Car Crash Conference, Society of Automotive Engineers, Inc., Warrendale, PA, 1989.
- Laughlin DA, "Digital Filtering for Improved Automotive Vehicle and Crash Testing with MHD Angular Sensors," Applied Technology Associates, 1998.
- Lee, K., Davis, M., Mejilla, R., Winkelstein, B., "In Vivo Cervical Facet Capsule Distraction: Mechanical Implications for Whiplash and Neck Pain," Stapp Car Crash Journal, Vol. 48, pp. 373-396, November, 2004.
- Linder, A., Avery, M., Kullgren, A., Krafft, M., "Real-World Rear Impacts Reconstructed in Sled Tests," Proceedings of the International Conference on the Biomechanics of Impact (IRCOBI), Graz, Austria, September 2004.
- Lubin, S., and Sehmer, J., "Are Automobile Head Restraints Used Effectively?" Canadian Family Physician 39:1584-1588, 1993.
- Mallory, A., Stammen, J., "Comparative Evaluation of Rear Impact Dummies – Static Seat Interaction and Dynamic Testing," NHTSA Docket No. 19807, 2005
- Muser, M., Walz, F., Zellmer, H., "Biomechanical Significance of the Rebound Phase in Low Speed Rear End Impacts," Proceedings of IRCOBI Conference, 2000.
- Prasad, P., Kim, A., Weerappuli, D., "Biofidelity of Anthropomorphic Test Devices for Rear Impact," Proceedings of the Forty-First Stapp Car Crash Conference, pp. 387-415, SAE Paper No. 973342, 1997.
- Schmitt, K., Muser, M., Niederer, P., "A New Neck Injury Criterion Candidate for Rear-End Collisions Taking into Account Shear Forces and Bending Moments," 17th ESV Conference, Paper No. 124, 2001.
- Sundararajan, S., Prasad, P., Demetropoulos, C., Tashman, S., Begeman, P., Yang, K., King, A., "Effect of Head-Neck Position on Cervical Facet Stretch of Post Mortem Human Subjects During Low Speed Rear-End Impacts," Stapp Car Crash Journal, Vol. 48, pp. 331-372, November, 2004.
- Svensson, M., Bostrom, O., Davidsson, J., Hansson, H., et al., "Neck Injuries in Car Collisions – A Review Covering a Possible Injury Mechanism and the Development of a New Rear Impact Dummy," Accident Analysis and Prevention, 32: 167-175, 2000.
- Tencer, A., Mirza, S., Huber, P., "A Comparison of Injury Criteria used in Evaluating Seats for Whiplash Protection," Traffic Injury Prevention, 5:56-66, 2004.
- Viano, D., Olsen, S., "The Effectiveness of Active Head Restraint in Preventing Whiplash," Journal of Trauma, 51: 959-969, 2001.
- Viano, D., Davidsson, J., "Neck Displacements of Volunteers, BioRID P3 and Hybrid III in Rear Impacts: Implications to Whiplash Assessment by a Neck Displacement Criterion (NDC)," Traffic Injury Prevention, 3: 105-116, 2002.
- Viano, D. C., "Role of the Seat in Rear Crash Safety," Society of Automotive Engineers, Inc., Warrendale, PA, 2003.
- Voo, L., Merkle, A., Shin Sung, C., Kleinberger, M., "Comparison of Three Rotation Measurement Techniques in Rear Impact Application," Society of Automotive Engineer, Inc., Warrendale, PA, 2003.
- Voo, L., Merkle, A., Wright, J., Kleinberger, M., "Effect of Head Restraint Rigidity on Whiplash Injury Risk," Society of Automotive Engineers Congress, 2004.
- Yang, K. H., Begeman, P., Muser, M., Niederer, P., Walz, F., "On the Role of Cervical Facet Joints in Rear End Impact Neck Injury Mechanisms," SAE 970497, in Motor Vehicle Safety Design Innovations, 1997.
- Yoganandan, N., Pintar, F., "Mechanics of Head Ache and Neck Pain in Whiplash, In: Eds. Yoganandan, N; Pintar, F.,: Frontiers in Whiplash Trauma, IOS Press, The Netherlands, ISBN 1 58603 012 4, pp. 173-185.

ON THE DEVELOPMENT OF A THEORETICALLY BASED, STATISTICALLY JUSTIFIED, THORACIC INJURY CRITERION

J. Quinn Campbell

Rabih E. Tannous

AASA, Inc.

Erik G. Takhounts

Peter Martin

Rolf Eppinger

National Highway Traffic Safety Administration

Thuvan Nguyen

CSMI Inc.

ABSTRACT

Advanced crash test dummies are being designed with multiple deflection measuring capabilities in the thorax to allow better characterization of the chest's local response to impact and thus, better optimization of performance from systems such as belt/bag combinations or four-point restraints. Historically, the injury criteria used to interpret thoracic impact responses were derived empirically from simple parameters, such as peak acceleration and deflection, that were extracted from available experimental data. This study takes a different approach. It combines the vast knowledge of structural responses and interactions embodied in our finite element modeling technologies in a model of the thorax, validates the model's impact response capability by mimicking the experiments by Kroell et al. (1972) and demonstrates that applying the measured x-y deformation-time histories of two points on the anterior chest wall of a dummy to the model, is sufficient for the model to accurately reproduce the complete two-dimensional deformation shape of the entire thoracic slice. This then allows the potential for the prediction of injury to be made on the basis of local stresses and strains occurring throughout the entire slice over time. Discussion of the development and validation of the slice model concept of post processing of dynamic dummy response output using FE models, verification of minimum necessary dummy inputs, and validation of predictive capabilities are all presented.

INTRODUCTION

Thoracic injuries are ranked second only to head injuries for automobile collisions in three categories: area most often injured (Ruan et al., 2003), overall number of fatalities and serious injuries (Cavanaugh, 1993), and overall societal harm

(Malliaris, 1985). Injuries to the thorax were found to account for approximately 13% of all AIS 1-2 injuries and 29% of all AIS 3-6 injuries (Ruan et al., 2003). A better understanding of the mechanisms involved in these thoracic injuries will lead to improved restraint systems that have the ability to reduce injuries and save lives.

Thoracic injuries occur in the presence of numerous contributing factors, such as crash speed and intrusion, as well as the presence of restraint systems, including airbags, seatbelts, load limiters, and seatbelt pretensioners. While experimental research using cadavers and crash test dummies is an important step to understanding thoracic injury mechanisms, computer models offer increased flexibility at a lower cost. Computer models also offer more detailed observations of stress and strain than are possible with cadavers and test dummies. The information from chest deflection and spine acceleration can be used to calculate many thoracic injury criteria, but they do not provide much guidance in how to improve a design. The flexibility and increased measurement possibilities allow researchers to pinpoint what dummies need to measure, which will improve the ability to regulate more effectively.

In order to design more effective restraint systems and improve regulations, researchers must be able to investigate "what if" scenarios, not just focus on passing a specific metric. In fact, focusing on a single metric could lead someone in the wrong direction. Instead of a specific metric, computer models provide a variety of outcome measures which are all related to injury risk. This paper presents a 2-D finite element model of the human thorax designed to study injury mechanisms and restraint conditions in an automotive crash environment.

METHODS

The purpose of this study was to create a finite element model of the human thorax with which to study injury mechanisms under different restraint conditions, and use the model in conjunction with multiply measured thoracic deflection time-histories obtained on THOR, the advanced frontal impact dummy developed by the NHTSA, to predict injury. The complexity of the model was determined by balancing computational issues, such as including enough complexity to accurately represent the response of the thorax while still maintaining a relatively fast run time on a PC. For this purpose, a 2D model was selected over a 3D model. After creating the mesh for the 2D thorax, the model's response was validated against thoracic impact experiments. Once the model was validated,

simulations were run to test the response of the model under various restraint conditions. Specifically, the model was tested to determine if it can differentiate between the concentrated loading condition of a torso belt from the distributed loading condition of an airbag. Next, applied displacements were used to replicate the restraint loading and determine if points corresponding to the THOR crux points, i.e., those sights on the anterior chest wall where deflection sensing instrumentation is attached, were sufficient to replicate the simulations. Finally, simulations were conducted to correlate stresses and strains in the model to injury. A large set of cadaveric impact tests were used to derive and apply displacements to the model corresponding to THOR crux points. A variety of model outputs were analyzed and a criterion was developed to predict injury.

Model Description

The finite element model of the thorax was modeled using the LS-Dyna software package. The model represents a 50th percentile male thorax. As previously stated, it was created in two dimensions to allow simulation of the overall thorax response while dramatically reducing the solution time. The thorax model (Figure 1) contains six parts: rib, sternum, viscera, elastic spine, rigid spine, and spine/rib joint.

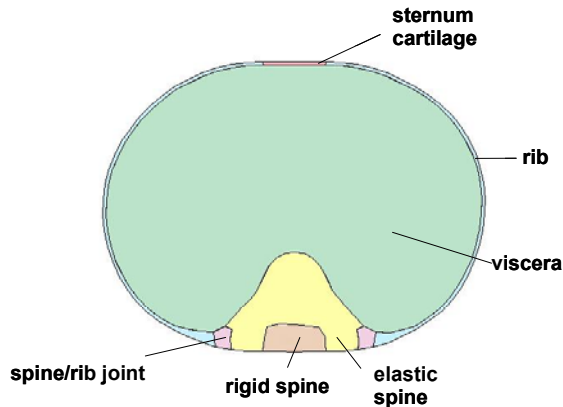


Figure 1. 2-D Thorax Finite Element Model.

The material properties for the model are shown in Table 1 and were determined through a review of the literature. A variety of material models were considered and tested for the deformable parts in the model, including elastic, viscoelastic, and piecewise linear plasticity models. The piecewise linear plasticity material was used because it provided the most biofidelic behavior when tested. This material scales the yield stress based on the strain rate as shown in equation 1:

$$\sigma_y(\varepsilon_{eff}^p, \dot{\varepsilon}_{eff}^p) = \sigma_y^s(\varepsilon_{eff}^p) + SIGY * (\dot{\varepsilon}_{eff}^p / C)^{1/p} \quad (1)$$

where $\sigma_y(\varepsilon_{eff}^p, \dot{\varepsilon}_{eff}^p)$ = effective stress, $\sigma_y^s(\varepsilon_{eff}^p)$ = static stress, SIGY = yield stress, $\dot{\varepsilon}_{eff}^p$ = strain rate, and C and p are user defined coefficients (LS-Dyna User's Manual, 2003).

Table 1.
Material Properties of the thorax finite element model, (Granik and Stein, 1972, Deng, 2000).

Part Name	Density (kg/m ³)	Stiffness (kPa)	Yield Stress (kPa)
Sternum	2.5e-6	1200000	3445
Rib	1.1e-6	10335000	85284
Viscera	2.9e-6	207	0.69
Spine/Rib Joint	1.1e-6	1200000	3445
Elastic Spine	1.1e-6	25982190	N/A
Spine (rigid)	1.1e-6	rigid	N/A

The rib properties required some modification because the model is two-dimensional. Specifically, the space between the ribs in the full thorax cannot be directly modeled in two dimensions. The stiffness of the thorax is dependent on the total cross-sectional area of ribs in the thorax. An extruded 2-D thorax model would have one solid rib without any space between ribs, making the model too stiff. Therefore, to ensure the proper response of the model, the cross sectional area of the rib in the model was reduced to account for the space between the ribs, while the rib modulus was kept constant. First, an average rib cross sectional area was determined to be 0.73 cm² (Pintar & Yoganandan, 1998). A rectangular cross section was assumed with a height of 1.27 cm and a thickness of 0.58 cm. Next, the average sternum length, from rib 1 to rib 10, of a 50th percentile male was found to be 29 cm (Robbins, 1983). Based on the average cross section the ribs should take up 7.3 cm² leaving 9.52 cm² space between the ribs. Therefore, the ribs take up 44% of the area. To account for the space between the ribs, the cross sectional area of the rib in the 2-D model should be 44% of the average rib. The thickness of the rib in the 2-D model was reduced to a thickness of 0.25 cm; with a height of 1.27 cm the rib has a cross sectional area of 0.32 cm².

The mass of the model was determined by comparing the mass and area of the full thorax to the mass and area of the 2-D thorax model. The mass of a 50th percentile male is 76.3 kg, with a thorax mass

of 23.6 kg (Robbins, 1983). The contact area on the 3-D thorax is 161 cm² (Kroell, 1974) and the contact area of the 2-D thorax is 18 cm². Therefore, the mass of the 2-D thorax was determined by multiplying the full thorax mass by the ratio of the thorax areas as shown in equation 2, resulting in a 2-D mass of 2.7 kg.

$$2\text{-D Mass} = 3\text{-D Mass} * (2\text{-D Area} / 3\text{-D Area}) \quad (2)$$

Model Validation

Fourteen experimental tests from Kroell et al., 1971 and 1974 (shown in Table 2) were simulated to validate the response of the thorax model under impact. These included ten free back tests and four fixed back tests. For the simulation of the fixed back tests, the rigid spine was restrained in all directions. Four of the free back tests had the skin on the thorax removed. For each simulation, the model was scaled based on the size and mass of the cadaver for that test. Each test was simulated using a representation of a 15.2 cm diameter impactor with the same initial velocity as in the experiments. The impactor was modeled as two-dimensional and its mass was scaled in the same manner as the mass of the model, based on the ratio of the 3-D and 2-D surface areas (Equation 2). Only initial conditions were provided, and each simulation then proceeded forward in time according to the laws of mechanics.

The results of each simulation were evaluated using force displacement curves, force time histories, and displacement time histories. Because the simulations used a 2-D model with scaled down masses, the forces in the simulation had to be scaled back up before they were compared to the experimental data. It should also be noted that a different scale factor was used for the tests that had the skin on the thorax removed than for the tests that did not. An assumption was made that the tests in which the skin on the thorax was intact would have a contact area that included the entire surface of the impactor (161 cm²), due to the skin's distribution of the load to the underlying structures. In contrast, the tests with the skin removed will have a lower contact area (105 cm²) because the impactor force will only be distributed over the ribs and sternum, and not the interstices. The force scale factors were calculated using the ratio of the 3-D contact area to the 2-D contact area (18 cm² in both cases). Therefore, the scale factor for the tests with the skin intact was 8.8 and the scale factor for the tests with skin removed was 5.8.

Table 2.
List of Tests Simulated for Validation * = Fixed Back Test, ** = Skin Removed.

Test No	Initial Velocity (kph)	Impactor Mass (kg)	Chest Depth (cm)	Cadaver Mass (kg)
92	48	1.6	18	41
96	30	19	24	59
99	26	19	23	75
104	35	23	25	74
171	18	23	22	55
177	18	23	25	64
182*	25	10	23	65
186*	26	10	23	60
187*	24	10	25	82
188*	26	10	22	52
7**	14	19	20	38
10**	18	19	19	43
6**	19	19	25	77
5**	19	19	26	86

Restraint Combination Simulations

Thirty simulations were run to test the 2-D thorax model's performance under different loading combinations of hypothetical restraint systems. Loads were applied to the model to simulate either pure airbag loading, seatbelt loading, or a combination of the two. Airbag loading was distributed evenly over the chest anterior surface as shown in Figure 2, while concentrated seatbelt loading was at an angle of 25 degrees and distributed across three adjacent nodes with 44% of the load applied on the center node and 28% on each side. Two seatbelt positions were simulated (Figures 3 and 4): a center position to simulate where the seatbelt crosses at the upper thorax (near rib 4) and a lateral position to simulate where the belt crosses the lower thorax (near rib 8). In all of the simulations the rigid spine was allowed to translate in the x and y directions but no rotation was allowed.

Loading was applied as a triangle pulse starting at 0, reaching 100% of the applied load at 100 ms, and returning to 0 again at 125 ms. A base loading level was assumed at a force level that resulted in a reasonable chest deflection and 50 m/s² spine acceleration. Three different total loading levels were simulated by applying the force across three adjacent nodes: 125%, 100% and 75% of the base loading level. The sum of the airbag and seatbelt loads resulted in the total load specified for

that simulation. The list of the various simulation loading combinations is provided in Table 3.

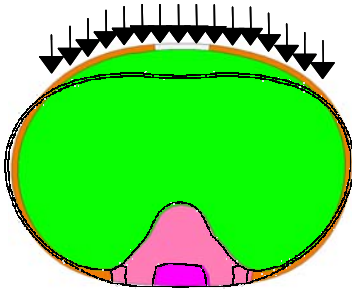


Figure 2. Distribution of Airbag Only Loading.

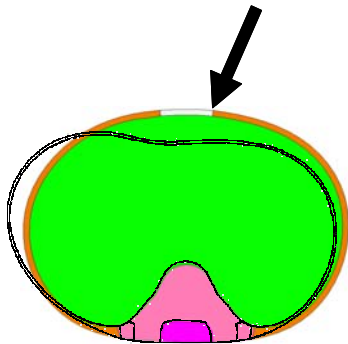


Figure 3. Location of Center Position Seatbelt Loading.

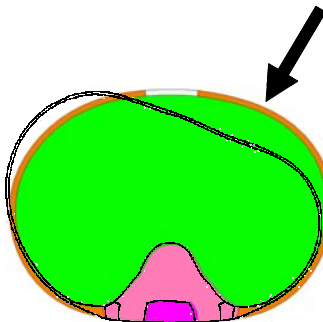


Figure 4. Location of Lateral Position Seatbelt Loading .

Table 3.
List of Tests in Restraint Combination Simulations.

Test No	Total Load	Belt Position	% Belt Loading	% Airbag Loading
1	100%	Center	100%	0%
2	100%	Center	75%	25%
3	100%	Center	50%	50%
4	100%	Center	25%	75%
5	100%	Center	0%	100%
6	125%	Center	100%	0%

7	125%	Center	75%	25%
8	125%	Center	50%	50%
9	125%	Center	25%	75%
10	125%	Center	0%	100%
11	75%	Center	100%	0%
12	75%	Center	75%	25%
13	75%	Center	50%	50%
14	75%	Center	25%	75%
15	75%	Center	0%	100%
16	100%	Lateral	100%	0%
17	100%	Lateral	75%	25%
18	100%	Lateral	50%	50%
19	100%	Lateral	25%	75%
20	100%	Lateral	0%	100%
21	125%	Lateral	100%	0%
22	125%	Lateral	75%	25%
23	125%	Lateral	50%	50%
24	125%	Lateral	25%	75%
25	125%	Lateral	0%	100%
26	75%	Lateral	100%	0%
27	75%	Lateral	75%	25%
28	75%	Lateral	50%	50%
29	75%	Lateral	25%	75%
30	75%	Lateral	0%	100%

Applied Crux Simulations

To determine how well the deformation of the slice model induced by the variety of force/area/time profiles discussed above can be duplicated by having only knowledge of the THOR's two x-and-y CRUX displacement time histories as the model's stimulus, the previous simulations were rerun by applying only the calculated CRUX displacements obtained from the previous calculations force stimulated simulations. Sixty additional simulations were conducted; two tests were run for each of the tests in Table 3, one with applied upper crux displacements, one with applied lower crux displacements. In each test the spine was fixed in all directions. The simulations with applied displacements were then compared to the original simulations using applied forces and the respective deformations, stresses, and strains compared.

Injury Correlation

To answer the question “How similar would the deformation of the thorax cross section be if, rather than loading the thoracic slice model with a particular force, area, time history, one only used the two dimensional (x,y) displacements of the anterior CRUX measurement points that the force-area-time loading produced,” 54 frontal impact cadaver sled tests were selected from the NHTSA database. The upper chestband data was processed for each test by a program written to derive the x and y displacements of points corresponding to the THOR crux points relative to the spine. The initial points were chosen based on which points were closest to the THOR crux points based on the x distance from the sternum. Once the initial points were selected, the x and y displacement time histories for each point were used as load curves for the thorax model. A simulation was run for each test based on the upper crux displacements. Each simulation was analyzed and processed to output peak stresses and strains during the simulation. Next, logistic regression was performed to correlate the injuries found in the sled tests to the outputs of the model. Injury in the sled tests was determined by the number of rib fractures found. Regressions were performed with injury thresholds at 2-6 rib fractures to determine the best cutoff point for injury. Regressions were also performed by correlating either only upper thoracic fractures (ribs 1-5) or fractures for the full thorax. While 54 tests were initially chosen, the number of tests for each regression varied depending on the quality control of chestband data and if the tests had full reports to determine upper from lower rib fractures.

RESULTS

Model Validation

Each test in Table 2 was simulated using the slice model and the experimentally observed peak displacements and forces were compared with those predicted by the model. Figures 5 and 6 illustrate results for peak displacement and force respectively. Figures 7 through 13 illustrate comparisons of individual simulated and experimentally observed force-time, displacement-time, or force-displacement/displacements from representative tests. Examples are given for each type of test: free back with skin, free back without skin, and fixed back. Time histories for the tests without skin are not shown because the experimental data was not available.

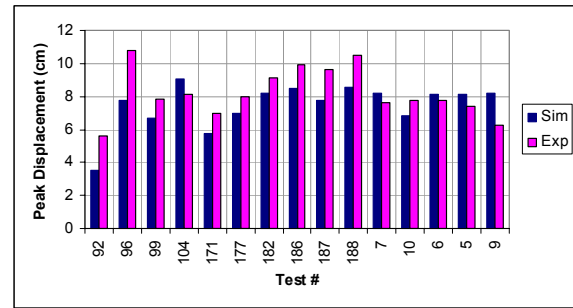


Figure 5. Comparison of Peak Displacements.

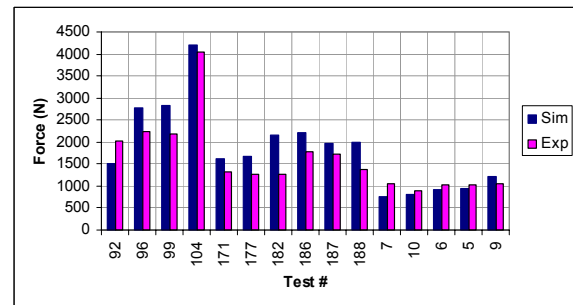


Figure 6. Comparison of Peak Forces.

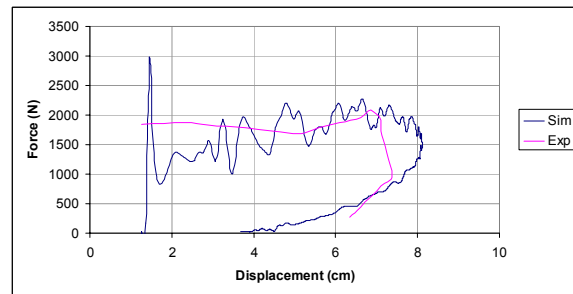


Figure 7. Force Displacement Curve, Test 7, Free Back Without Skin.

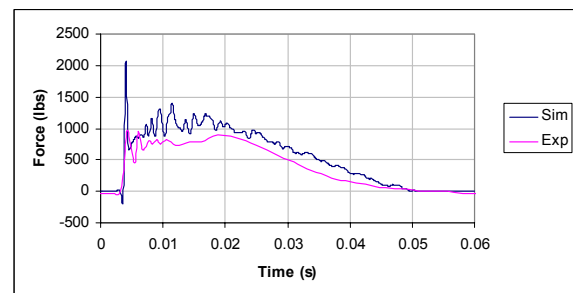


Figure 8. Force Time History, Test 99, Free Back With Skin.

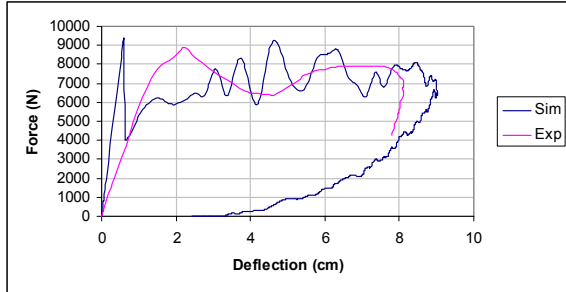


Figure 9. Force Displacement Curve, Test 104, Free Back With Skin.

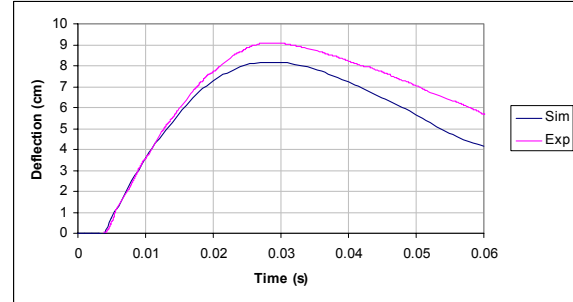


Figure 13. Displacement Time History, Test 182, Fixed Back With Skin.

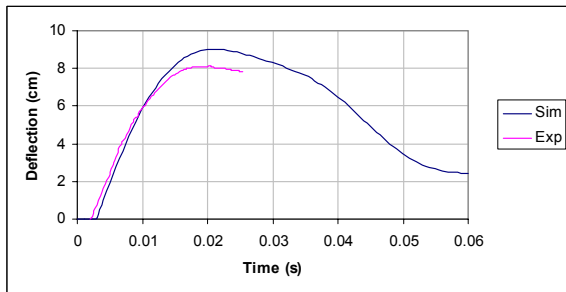


Figure 10. Displacement Time History, Test 104, Free Back With Skin.

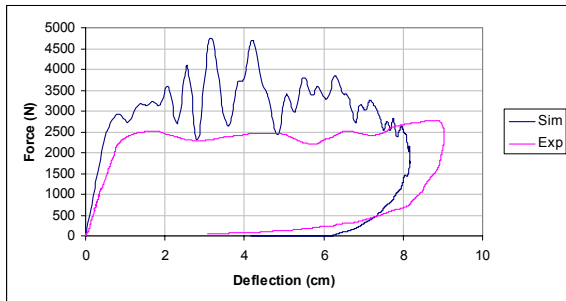


Figure 11. Force Displacement Curve, Test 182, Fixed Back With Skin.

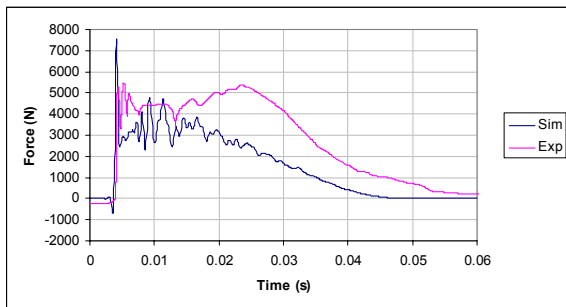


Figure 12. Force Time History, Test 182, Fixed Back With Skin.

Restraint Combination Simulations

Each loading condition described in Table 3 was simulated using the slice model and the x and y displacements of the two upper and two lower anterior THOR crux points to determine a maximum stress and strain in the rib. Examples are shown comparing the different test conditions: restraint combinations, belt positions, and loading levels (Figures 14-19). Figures 14, 16, and 18 present the initial position and maximum displacement of the anterior crux points with respect to the spine under the various force loading conditions.

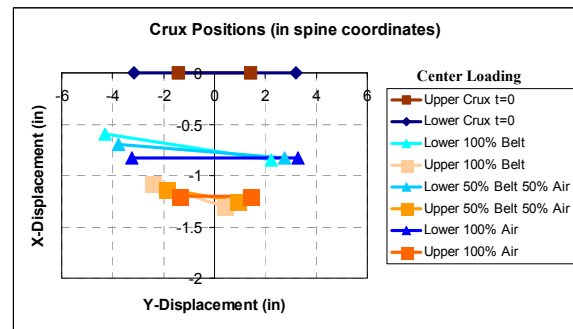


Figure 14. Comparison of Crux Displacements for Different Restraint Combinations.

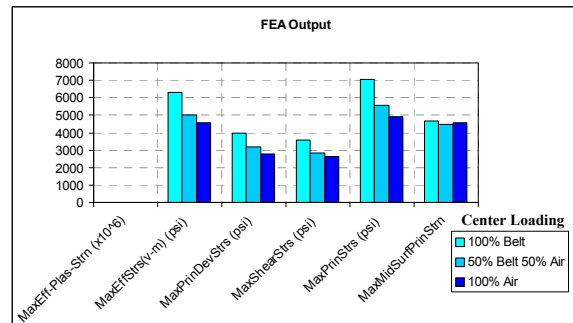


Figure 15. Comparison of Rib Stress and Strain for Different Restraint Combinations.

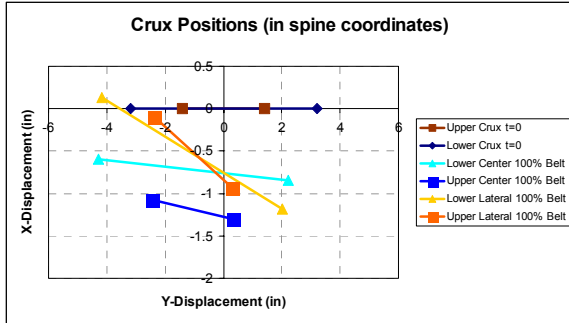


Figure 16. Comparison of Crux Displacements for Different Belt Positions.

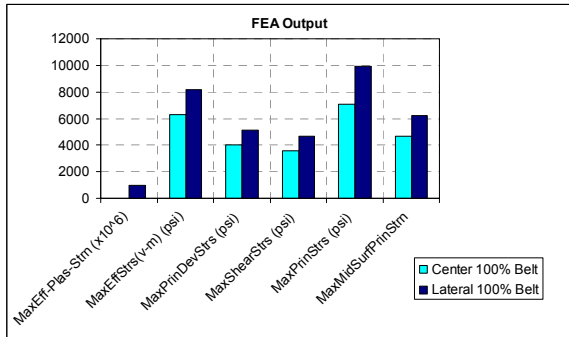


Figure 17. Comparison of Rib Stress and Strain for Different Belt Positions.

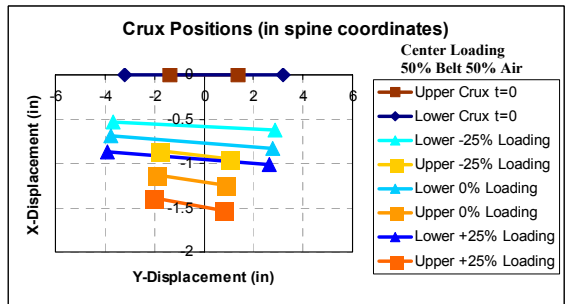


Figure 18. Comparison of Crux Displacements at Different Loading Levels.

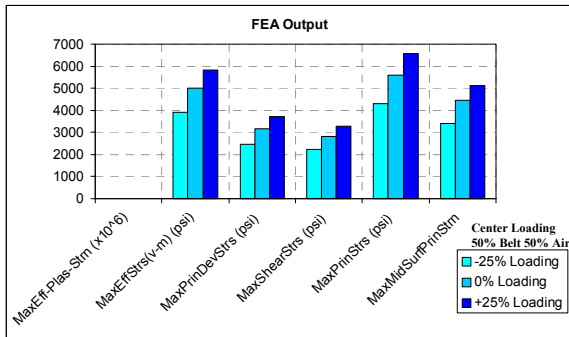


Figure 19. Comparison of Rib Stress and Strain at Different Loading Levels.

Applied Crux Simulations

Each test in Table 3 was also simulated using only applied upper or lower crux displacements obtained from the previous 30 tests just discussed. All tests were processed to compare the overall deformation of the displacement-stimulated model with the deformation of the force stimulated model. Good replication of deformation shape was noted. The following charts provide a comparison between the original loading simulations, applied upper crux simulations, or applied lower crux simulations (Figures 20-23). Due to limited space, examples are shown only for select restraint combinations.

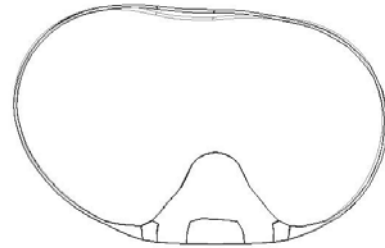


Figure 20. Overlay showing both the original loading (grey) and applied lower crux (black) rib contours for the 100% center belt loading condition.

These results strongly suggest that post processing THOR generated upper and lower chest deflections using the slice model can provide a reasonable estimate of the stress/strain distributions found in a force deformed thorax and the potential for damage/injury throughout the entire event. To investigate this further, the slice model was displaced by applying the two crux displacement time histories obtained when conducting the kinetic force applications previously discussed and the error between the two stresses compared.

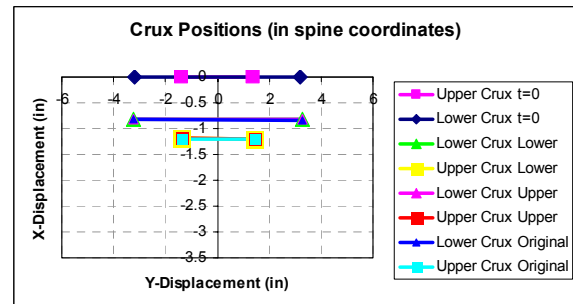


Figure 21. Comparison of Crux Positions for 100% Airbag Loading.

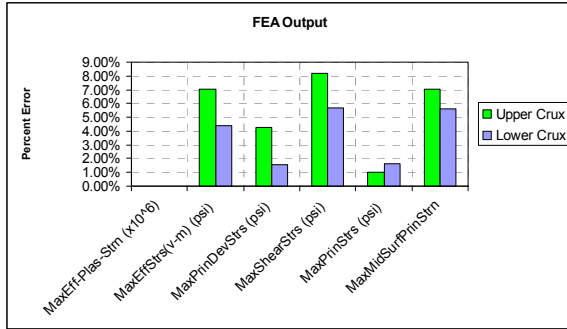


Figure 22. Comparison of Error in Rib Stress and Strain for 100% Airbag Loading.

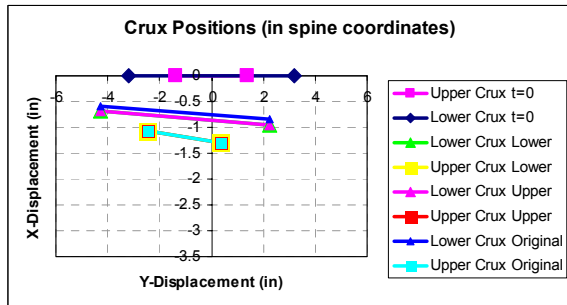


Figure 23. Comparison of Crux Displacements for 100% Center Belt Loading.

Injury Correlation

The 54 frontal impact cadaver sled tests were simulated using the slice model and chestband data from each experimental test. Each simulation was analyzed and processed to output peak stresses and strains seen in the slice model during the simulation. Logistic regressions were performed to correlate the injuries found in the sled tests to the outputs of the model. An example of the rib contours at peak deflection from the chestband alone and upper crux simulation using only crux displacements for test 2910 is shown in figure 24.

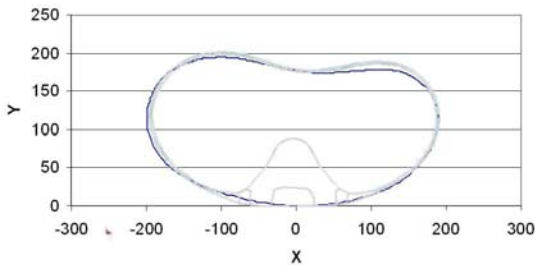


Figure 24. Rib contours at peak deflection from test 2910, upper crux simulation (grey), cadaver chestband (black).

Numerous logistic regressions were performed on the data from the chestband

simulations: using different outputs from the simulations, injury thresholds from 2-6 rib fractures, and separate correlations for upper rib fractures versus all rib fractures. Various confounding variables were tested in the regressions as well, including cadaver age, weight, and sex. The regression with the most significance (p-value 0.0001) and highest Chi2 (18.0) used maximum principal strain from the upper crux simulation with cadaver age to predict injury defined as greater than 2 rib fractures in the entire thorax. 84% of the tests used in the regression had correct prediction of injury using the model (ROC=0.84). Figure 25 shows the probability of injury for this model at different ages.

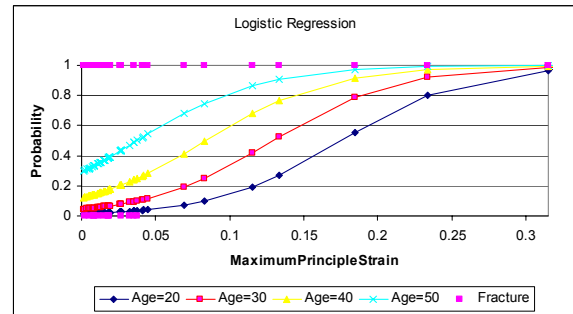


Figure 25. Logistic Regression with injury defined as greater than 2 rib fractures.

DISCUSSION

Model Validation

The 2-D finite element model of the thorax shows reasonable correlation with the impact experiments of Kroell et al. The force displacement curves and time histories show that the model has a biofidelic response through the entire event, including at the peaks. The force scaling methods seem to allow accurate comparison of 3-D and 2-D force measurements. This is demonstrated in the accurate simulation of cases with and without skin. However, overall the results suggest that the model may be too stiff based on slightly higher forces and lower displacements seen throughout the simulations. It is possible that these results could be improved by altering the average rib cross section that was used, since the cross section of ribs varies greatly both along their length and at different levels within the thorax. Overall, the model performs relatively well in both fixed and free back conditions and the model can be used to evaluate restraint conditions with seatbelts and/or airbags.

Restraint Combination Simulations

The thirty simulations using various combinations of airbag and seatbelt loading, various seatbelt positions, and three loading levels, showed that the 2-D thorax model can appropriately differentiate between different restraint systems. A comparison of the belt positions in Figure 17 shows that lateral belt loading is more severe than center belt loading, 100% lateral belt loading being the most severe condition tested. Figure 19 shows that increasing the overall load results in higher stresses and strains, as expected. Figure 15 shows that the 100% belt loading condition results in higher stresses and strains than either combined loading or airbag loading. 100% airbag loading had the lowest stress and strain levels of any restraint combination. Logistic regression showed that all of the stress components examined had the ability to differentiate the 100% seatbelt condition from the others ($p=0.003-0.002$), while the maximum effective plastic strain and the maximum principal strain had less ability to differentiate the restraint conditions, $p=0.024$ and $p=0.154$ respectively. The ability for the 2-D thorax model to differentiate seatbelt loading from other types of restraint conditions is an important ability because field research has shown seatbelt only restraints to be more likely to produce injuries (Trosseille et al., 2001).

Applied Crux Simulations

The results from the applied crux simulations show that in general the model has the ability to replicate the contours, stresses, and strains in a variety of loading conditions using only the planar (x,y) displacements of two crux points. However, the simulations show that with increased loading levels and/or increased belt loading the error increases between the applied crux simulations and the original simulations. Also, the results show that the belt position affects the ability for the applied crux simulations to replicate the loading. When upper crux displacements are applied there is more error in the lateral belt loading position, while when the lower crux displacements are applied there is more error in the center belt loading position. This is a result of the upper crux points being close to the center of the chest while the lower crux points are spread out more laterally. Figure 26 shows the error in maximum principal Von Mises stress for each

simulation. While there is some error when simulating thoracic loading with applied crux displacements, the contours and stresses are close enough to provide useful information that isn't available from the crux displacements alone. Therefore, using the 2-D thorax model in conjunction with THOR makes it a useful research tool to differentiate differences in restraint performance.

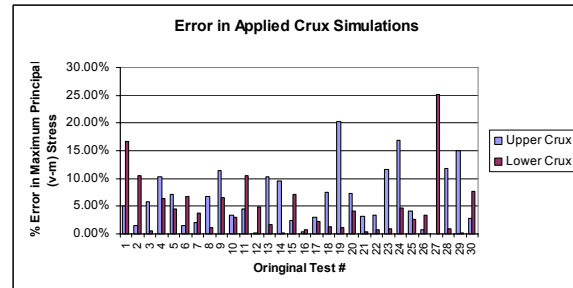


Figure 26. Error in Von Mises Stress for Applied Crux Simulations.

Injury Correlation

The results from the simulations of the cadaver tests showed that the best model for predicting injury used maximum principal strain from the simulations with cadaver age as a confounder. This model is promising because maximum principal strain is physically linked to fracture. The ability for the model to predict injury accurately in 84% of the tests shows the models ability to differentiate injury from non-injury. One potential problem with the model is that at high ages it is very unlikely to predict non-injury, even at low strains. This may be due to limits of the analysis techniques used or the nature of the test data available and may be remedied using the full range of available tests.

CONCLUSIONS

- The 2-D finite element model of the thorax correlates well to the impact experiments of Kroell et al.
- The force scaling methods seem to allow accurate comparison of 3-D and 2-D force measurements.
- The model has a biofidelic response through the entire impact event, including at the peaks.
- The model performs relatively well in both fixed and free back conditions.
- The model can be used to evaluate restraint conditions with seatbelts and/or airbags.
- The model has the ability to differentiate belt loading from other restraint conditions based on higher stresses and strains.

- Upper or lower THOR crux displacements can be applied to the 2-D thorax model to replicate loading simulations.
- A logistic regression model using maximum principal strain and age has a high probability of predicting thoracic injury.

REFERENCES

[1] CAVANAUGH, J. (1993) The biomechanics of thoracic trauma. In *Accidental Injury Biomechanics and Prevention*, ed. A. Nahum and J. Melvin, pp. 362-390. Springer-Verlag, New York.

[2] DENG, Y.C. and CHANG, F. (2000) F8B: Development of A Finite Element Human Thorax Model, Final Report. GM North America Car Group.

[3] GRANIK, G and STEIN, I. (1973) Human ribs: static testing as a promising medical application. *J Biomech.* May;6(3):237-40.

[4] KROELL, C.K., SCHNEIDER, D.C., NAHUM, A.M. (1971) Impact Tolerance and Response of the Human Thorax. Proc. 15th Stapp Car Crash Conference, pp 84-134. Society of Automotive Engineers, Warrendale, PA.

[5] KROELL, C.K., SCHNEIDER, D.C., NAHUM, A.M. (1974) Impact Tolerance and Response of the Human Thorax II. Proc 18th Stapp Car Crash Conference, pp 383-412. Society of Automotive Engineers, Warrendale, PA.

[6] LS-DYNA Keyword User's Manual (2003) Vol I and II, Version 960, Livermore Software Technology Corporation, Livermore, CA.

[7] MALLIARIS, A. C., et al. (1985) Harm causation and ranking in car crashes. Paper 8500090, Society of Automotive Engineers, Warrendale, PA.

[8] YOGANANDAN, N. and PINTAR F.A. (1998) Biomechanics Of Human Thoracic Ribs. *J Biomech Eng.* Feb;120(1):100-4.

[9] ROBBINS, D.H. (1983) Anthropometric Specifications for Mid-Sized Male Dummy. UMTRI Report Number 83-53-2, Anthropometry of Motor Vehicle Occupants. Volume 2 - Mid-Sized Male. U.S. Department of Transportation. National Highway Transportation Safety Administration.

[10] RUAN, J., EL-JAWAHRI, R., CHAI, L., BARBAT, S., PRASAD, P. (2003) Prediction and Analysis of Human Thoracic Impact Responses and Injuries in Cadaver Impacts Using a Full Human Body Finite Element Model. Proc. 47th Stapp Car Crash Conference, pp. 299-321. Society of Automotive Engineers, Warrendale, PA.

[11] TROSSEILLE, X., FORET-BRUNO, J-Y., PAGE, Y., HUERE, J-F., LE COZ, J-Y., BENDJELLAL, F., DIBOINE, A., PHALEMPIN, T., VILLEFORCEIX, D., BAUDRIT, P., GUILLEMOT, H., and COLTAT, J-C. (2001) Comparison of Thoracic Injury Risk in Frontal Car Crashes for Occupant Restrained Without Belt Load Limiters and Those Restrained With 6kN and 4kN Belt Load Limiters. Proc. 45th Stapp Car Crash Conference, pp. 205-224. Society of Automotive Engineers, Warrendale, PA.

A STUDY OF CURRENT NECK INJURY CRITERIA USED FOR WHIPLASH ANALYSIS. PROPOSAL OF A NEW CRITERION INVOLVING UPPER AND LOWER NECK LOAD CELLS.

D. Muñoz¹, A. Mansilla^{1,2}, F. López-Valdés^{1,2}, R. Martín¹

¹ Fundación CIDAUT

² Department of Mechanical Engineering and Engineering of Materials. University of Valladolid
Spain

Paper Number 05-0313

ABSTRACT

Nowadays several injury criteria are being used in the analysis and evaluation of whiplash risk in automotive rear impacts (NIC, Nkm, LNL, etc.). This study presents a review of the most accepted injury mechanisms and evaluates the advantages and inconveniences of the commonest criteria at present. Taking into account the conclusions arrived at during this comparison, a new criterion is proposed using the signals registered in the upper and lower neck load cells of a crash test dummy, trying to minimize the disadvantages previously found in the other criteria. In order to validate this study a series of sled tests with a BioRID-II dummy have been performed and its results analyzed, confirming the assumptions made during the review of the present criteria and showing a very promising response to the new one. In conclusion, the use of injury criteria involving the load cells situated in both ends of the neck at the same time is recommended as the best way to deal with the dynamics produced during the whiplash movement in a rear impact.

INTRODUCTION

In a rear-end car crash, even at low speed, the head of the occupants of the struck vehicle normally suffers a motion related to the torso that produces sudden distortions of the neck. Although in the most severe cases this movement can produce the fracture of cervical vertebrae, the commonest related lesions are only classified as minor injuries (AIS 1) [1]. Nevertheless, these lesions, known as whiplash-associated disorders (WAD) or simply whiplash, produce painful and often long-term or even chronic symptoms, causing huge economic costs to the society at the same time.

During the last few years a certain number of experimental procedures have appeared trying to evaluate the capacity of the automotive seats to protect the occupants in a rear-end crash. Currently the most accepted of these procedures (IIWPG [2][3], Folksam [4], ADAC, etc.) are using dynamic sled tests and the crash test dummy BioRID-II [5][6][7]. One of the main problems in the development of this kind of procedures has been related to the lack of a full understanding of

whiplash injury mechanisms, even though several theories have been proposed trying to give an explanation to the observed symptoms. At the same time, a certain number of injury criteria have been developed looking for a correlation with the different proposed mechanisms. At present there is still a debate about which of these criteria should be taken into account to describe the ability of a seat to protect the neck of the occupants in a rear-end impact properly. In this situation, the groups that are developing new test procedures are adopting either several criteria simultaneously ([4]) or none of them, basing their assessment on the direct comparison of loads and accelerations ([3]). At this point, the lack of a criterion unifying the different injury mechanisms that can be used easily on a test protocol is clear.

The main objective of the presented work was to make a critical review of the commonest injury criteria used at present, trying to analyze the advantages and disadvantages of each one of them. The results would provide a better understanding about the different criteria themselves and, if possible, give guidelines for the definition of a new criterion solving the possible problems found.

METHODS

Keeping this objective in mind, the first question is: how do we evaluate a whiplash injury criterion? or even better, what do we expect from it?. The points found by the authors to answer this question are the following:

1. The criterion must be representative of one or more injury mechanisms, indicating and quantifying the probability of injury. It must be sensitive to the factors related to these injuries and able to give an assessment about different impact conditions. It must be able, for instance, to determine which seat is safer for an occupant with regard to the considered mechanisms when using a particular acceleration pulse.
2. At the same time it should be repeatable and stable. Values measured in similar situations should not be too different.
3. It should not be sensitive to other processes

different to the mechanism analyzed. Variables not related with the injury mechanism should not have a great influence on its value.

4. When possible, for practical reasons, the criterion should be easily and quickly calculated. It should use values directly measured during the test and avoid non automatic operations.

These points evidence that in order to proceed to the evaluation of the different criteria it is convenient to get the best possible understanding about what happens where and when in a typical rear-end impact. The dynamics of the neck and head have been studied both in the literature and with results of tests using the BioRID-II dummy. In addition, a review of the most accepted injury mechanisms has been done.

After these reviews, the most common injury criteria have been analyzed trying to understand their weak and strong points. A series of four sled tests with seat, dummy and seat belt have been done in order to validate the obtained conclusions. All the tests have been carried out at CIDAUT, using a MTS inverse catapult and a BioRID-II Rev.f fully instrumented dummy. The forces at the seat belt were measured using a Messring belt load cell, in order to get extra information about the rebound phase. The seating procedure was based on [2]. The position of several characteristic points of the dummy was registered with a FaroArm portable 3D measurement system, in order to guarantee its reproduction when using similar seats. The sled was accelerated using the IIWPG 16 Km/h pulse [2] (Figure 1 shows the acceleration measured in the different tests). Four Redlake high-speed digital cameras were used during the tests in both on-board and off-board positions, taking images at 1000 fps. When necessary, image analysis was done using the software Falcon eXtra. All the signs and axis mentioned on the present paper are according SAE J1733 standard ([8]).

Two models of seats have been chosen for the tests. As none of them has been specifically designed to prevent whiplash, we will refer to them as Seat “A” and Seat “B”. Seat “A” is a common car driver seat, while Seat “B” is a minibus rear seat with an integrated 3-point seat belt. This forces its structure to be very rigid and, therefore, is expected to give worst results with regard to whiplash protection. Three tests were done with “A” type new seats (numbers 001, 002 and 003), and a fourth one was done with a seat “B”, also new (number 004). In this way we could analyze the repeatability and sensitivity of the different criteria. Figure 2 shows the rotation of the backrest in the tests, measured from the high speed images. The difference of stiffness between both models of

seats appears clearly here (the rotation on the fourth test has been quite lower than on the other ones). The variability of the behaviour of the “A” seats can also be observed, even when using similar acceleration pulses. This can be used as a reference when studying the repeatability of the criteria.

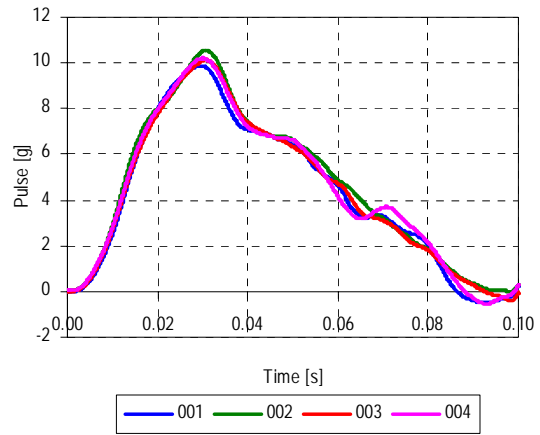


Figure 1. Acceleration pulses of the tests.

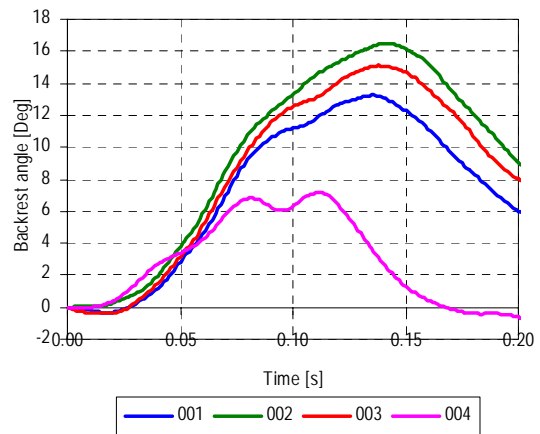


Figure 2. Rotation of the backrest during the tests.

In order to have numeric values to compare the sensitivity and the repeatability of the different criteria, a method has been defined using the Russell criterion for comparison of curves [9]. This criterion is normally used to compare two different series of data $f_1(i)$ and $f_2(i)$ defined by N points each, giving a numeric value ε_c closer to 0 when the curves are similar and greater when the curves are different. The expressions used are the following:

$$\begin{aligned}
 A &= \sum_{i=1}^N f_1(i)^2 \\
 B &= \sum_{i=1}^N f_2(i)^2
 \end{aligned}
 \tag{1}$$

$$C = \sum_{i=1}^N f_1(i) f_2(i)$$

$$m = \frac{A - B}{\sqrt{AB}}$$

$$p = \frac{C}{\sqrt{AB}}$$

$$\varepsilon_p = \frac{\cos^{-1}(p)}{\pi}$$

$$\varepsilon_m = \text{sign}(m) \cdot \log^{10}(1 + |m|)$$

$$\varepsilon_c = \sqrt{x(\varepsilon_m^2 + \varepsilon_p^2)}$$

The values ε_m and ε_p represent respectively the errors associated to differences in magnitude and phase, and x is a reference constant that, in this case, has been defined as $\pi/4$.

To get an indicator of the repeatability of the injury criteria the first three tests have been compared to each other (001 to 002, 001 to 003 and 002 to 003), obtaining three ε_c values as results. The average of these values has been considered to be representative of the repeatability. The indicator for sensitivity has been calculated in a similar way, comparing the three first tests with the fourth one and calculating the average of the three obtained ε_c . As defined, the repeatability is assumed to be better when its indicator is closer to zero, and the sensitivity is better when its indicator is higher. To be used as a reference, the indicators of repeatability of the acceleration pulses (high repeatability and low sensitivity) and the rotations of the backrest (relative low repeatability and high sensitivity) were 0.028 and 0.108 respectively, while its sensitivities were 0.022 and 0.482.

HEAD-NECK MOVEMENTS DURING A REAR-END IMPACT

In order to be able to analyze the results of the tests and to try to identify the time when the possible injury mechanisms happen, it is indispensable to understand the kinematics of the neck and the head during a typical low speed rear-end impact. This movement is well documented and has been described by several authors using different techniques ([5], [10], [11], [12] and [13] among others). The main phases of the motion are shown in Figure 3.

In the initial state the subject is seated on the seat in normal position. When the vehicle is struck, the acceleration of the structure is transmitted to the seat through its anchorages, producing a movement forward with regard to the occupant. The first zone of the subject in receiving the pressure of the seat is normally the pelvis and the lumbar zone, followed

by the thorax. When the spine, originally curved according to its physiological shape, is pushed forward, it tends to straighten, moving the base of the neck (vertebra T1) upwards and producing some compression on it. This phenomenon can be amplified by the movement upwards of the whole thorax due to the angle of the seat and the acceleration of the base. This is commonly called “ramping up”. Although the thorax begins to move, the head at this point remains in its original position. The T1 vertebra, which was originally situated behind the centre of gravity of the head, passes to be in front of it, and the previous compression of the neck becomes traction, with the thorax pulling on the head. The movement of T1 makes the cervical vertebrae work as a chain, transmitting the motion from the lower end upwards, while at the upper end the inertia of the head produces resistance to the movement. The combination of these effects produces a transitory biphasic state known as “s-shape” in which the lower part of the neck (vertebrae C5-C7) presents a very pronounced extension, while the upper part is in flexion. The rearwards movement of the head referred to T1 is called retraction

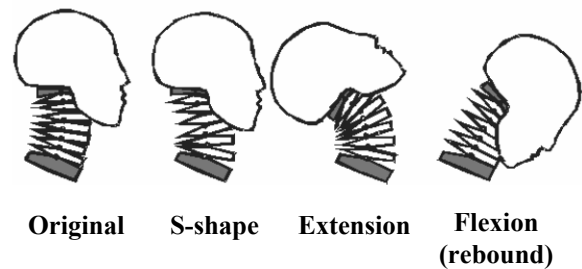


Figure 3. Different phases of the motion of the head in a typical rear-end impact.

When finally the head begins to rotate, the whole neck arrives in a state of extension with the head being pulled on by the thorax. When the acceleration of the base drops, the elastic energy stored on the seat and the occupant begins to be released, producing a rebound movement with a rotation forward of all the torso of the subject around the pelvis. The seat belt begins to tense over the pelvis and the thorax approximately when the body returns to its original position, producing a violent flexion of the neck. Finally, due to the tension of the belt, the body is stopped, and returns to the backrest.

THEORIES ABOUT WHIPLASH INJURY MECHANISMS

Up to the present a wide number of research works have been done trying to identify the origin of the symptoms related to whiplash associated disorders. As a result of these studies several injury

mechanisms have been proposed, the coexistence of some of them being the most accepted hypothesis. If we want to analyze the different injury criteria it is necessary to understand the origin of the lesions as well as possible, in order to be able of relate them with the magnitudes measured in the lab. A review of the most accepted mechanism has been done keeping this idea in mind. Some of the main ones appear below:

Hyperextension

The hyperextension of the neck was the first hypothesis trying to explain the whiplash phenomenon. It was proposed in the sixties by Macnab [14], and suggested the movement of extension of the neck to be the cause of the whiplash injuries, producing lesions on the lower cervical spine. In 1969 the incorporation of head restrains in the new cars sold in USA was made compulsory, trying to limit this movement. However, this fact did not reduce the number of reported whiplash cases in the expected proportion, making evident the necessity for further research. Although hyperextension is still a possible cause of injuries, today the extended use of head restraints has limited it to particular cases, such as misuse or failure of the headrest.

Cervical flexion during the rebound phase

Opposite to the previous mechanism, Macnab also proposed the flexion of the neck due to the movement produced by the head when the seat belt acts on the rebound phase as a probable origin of injuries [15]. This was suggested after the observation of a higher frequency of cervical injuries on people using seat belt, and later confirmed by other authors ([16], [17] and [18] among others).

Pressure gradients on the spinal canal

In 1986 Aldman [19] predicted that volume changes produced inside the spinal canal during sudden movements of the cervical spine on the sagittal plane could be the origin of injuries in the intervertebral tissues. In 1993, Svensson et al. [20] confirmed this hypothesis, measuring the pressure changes on the spinal canal of anesthetized pigs and reporting damage to the spinal ganglia that could explain many of the typical symptoms of whiplash. In these experiments the highest pressure oscillations were related to the phase shift from the s-shape to the extension, and the highest pressures were registered at the level of the C4 vertebra during the s-shape.

Localized cervical compression and tension during the s-shape

Nowadays the most accepted cause of whiplash injuries is probably the one related to the hyperextension observed in the lower part of the neck during the formation of the s-shape (vertebrae C5, C6 and C7). In 1998 Panjabi et al. [21] reported that the intervertebral movements observed at these levels during in vitro tests exceeded their physiological limits, being the cause of lesions in the capsular ligaments and facet joints at the C5-C6 level. Similar findings have been done later by other authors ([22], [23] and [24] among others).

COMPARISON OF THE MOST USED CRITERIA

Figure 4 shows the sensors that at present are being included in a BioRID-II dummy as normal instrumentation. The signals of these sensors and the measurements done by image analysis on the sequences registered with high speed cameras are the current available tools to quantify the ability of a seat to protect the neck of an occupant during a low speed rear impact. Several criteria have been developed in order to quantify the risk of having whiplash related disorders, based either on accelerations, displacements or loads. The most accepted among these criteria have been evaluated critically by the authors trying to understand their virtues and defects. Below the results of the evaluation and its application to the tests are presented:

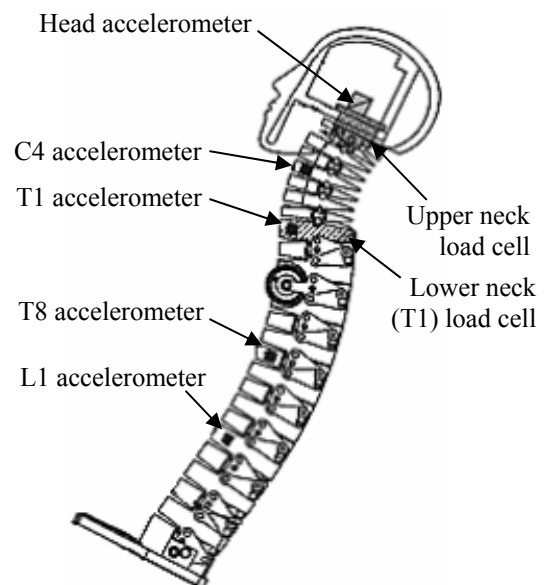


Figure 4. Standard instrumentation in spine and head of BioRID-II (Adapted from R. A. Denton drawing 5834 www.dentonatd.com).

NIC

NIC (Neck Injury Criterion) was proposed by Boström et al. in 1996 [25], as a value to correlate the movement of the head related to the base of the neck (T1 vertebra) with the damage found in the cervical spinal ganglia produced by transient pressure changes in the spinal canal. It uses the difference of accelerations in the longitudinal direction (x axis) between the centre of gravity of the head and the T1 vertebra, being therefore representative of the movement of the neck during the retraction phase. NIC is calculated as follows:

$$\begin{aligned} NIC &= a_{rel} \cdot 0.2 + v_{rel}^2 \\ a_{rel} &= a_x^{T1} - a_x^{Head} \\ v_{rel} &= \int a_{rel} dt \end{aligned} \quad (2).$$

The maximum reached by this expression during the first 150 milliseconds of the test is called NIC_{max} , and for years has been considered as one of the main indicators of whiplash.

Figure 5 and Table 1 show the NIC values achieved during the tests. The repeatability of the results of the first three tests is very good (with an indicator of 0.084), and even impressive looking at the maximum values. It is necessary to mention here that such a high repeatability of the maximum values is not that common in practice. On the other hand, the different behavior of the seats A and B has been well characterized, having a value of 0.407 on the sensitivity indicator.

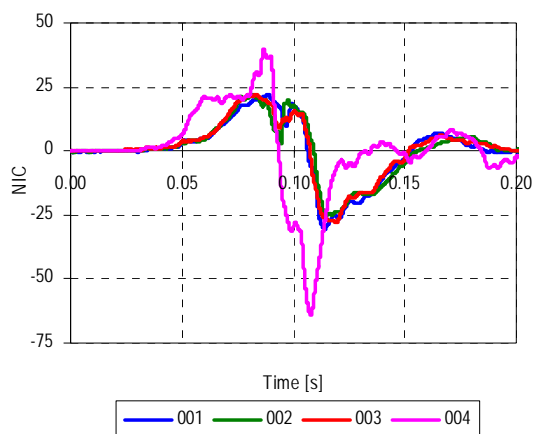


Figure 5. NIC.

Table 1. Maximum NIC values.

Test	001	002	003	004
NIC_{max}	21.94	21.94	21.93	40.08
Time (ms)	88.6	79.9	81.8	86.7

When analyzing the causes that can produce different accelerations in the longitudinal axis between the head and the T1 vertebra and, therefore, cause a modification on the value of the NIC, we observe that this difference can not only be produced by distortions in the neck, but also by any rotation of the head and T1 around the transversal axis (Y) as a rigid body. This movement does not cause any deformation in the neck, and, apart from extreme cases, should not be a direct cause of injury. We can see a scheme of this in Figure 6.

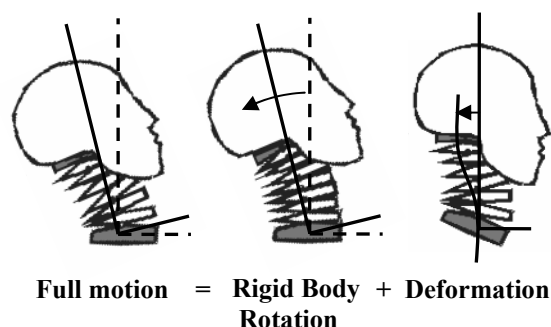


Figure 6. Decomposition of movements producing NIC values.

The influence of this effect can be estimated dividing the relative acceleration used in the NIC definition in two terms:

$$a_{rel} = a_{rotation} + a_{deformation} \quad (3).$$

If we refer to the angular acceleration of T1 as α and the distance between the centre of gravity of the head and the accelerometer at T1 as d , we can then calculate the acceleration term corresponding to the deformation:

$$a_{deformation} = a_{rel} - \alpha \cdot d \quad (4).$$

Although d is not fixed for all the configurations of the neck (it is deformable) we can consider 0.2 metres as an average, and we can estimate α from the double derivation of the angle of the T1 vertebra measured on the images (Figure 7).

If we use $a_{deformation}$ instead a_{rel} in expression (2) we get the curves shown in Figure 8. We will refer to these values as NIC^* , calculated only with the term related to deformation. Table 2 shows that the maximum values obtained in this way can differ up to 30% from the original NIC values. This variation is produced by factors not directly related to the distortion of the neck.

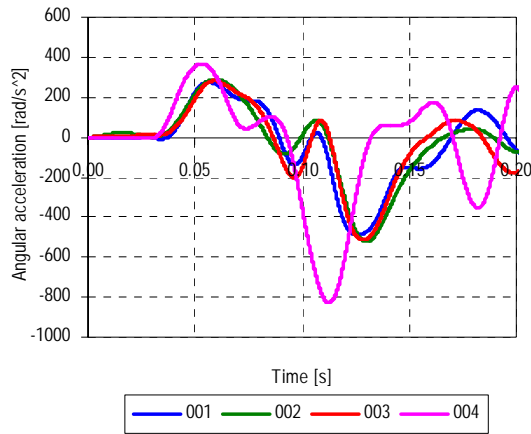


Figure 7. T1 angular acceleration.

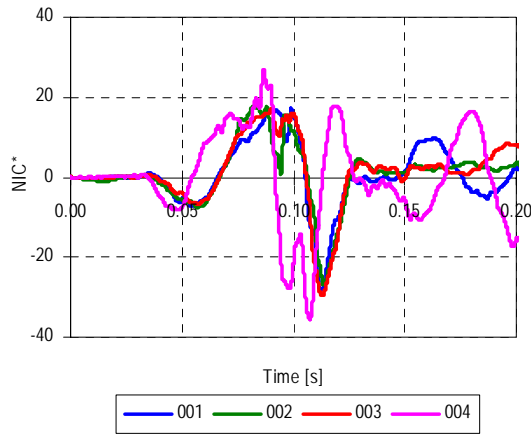


Figure 8. NIC* (without effect of T1 rotation).

Table 2. Maximum NIC* values and deviation with regard to the original NIC.

Test	001	002	003	004
NIC* _{max}	17.30	17.72	17.20	26.95
Deviation	21.2%	19.2%	21.6%	32.8%

This fact supports the observations made by Suffel during the fourth BioRID User Meeting [26], who reported the carrying out of some tests blocking the movement of the neck relative to the T1 vertebra, but obtaining NIC values around $8 \text{ m}^2/\text{s}^2$.

In short, NIC has shown to have a good repeatability and distinguishes well between the two different seats. It also takes into account the kinematics of the head with regard to the thorax trying to describe the retraction movement, but on the other hand, it is sensitive to effects not related

to the distortion of the neck, due to the use of accelerations for its calculation (for instance, the rotation of the seatback produces the effect previously described).

N_{km}

In 2001 Schmitt et al. [27] proposed the N_{km} criterion, based on the linear combination of shear forces (F_x) and sagittal bending moments corrected to the occipital condyle ($M_{y,OC}$), measured with the upper neck load cell. This criterion distinguishes among four possible situations depending on the sign of M_y and F_x (see Table 3)

Table 3. Cases of N_{km} .

Case	M_y	F_x
N_{fa} (Flexion Anterior)	> 0	> 0
N_{fp} (Flexion Posterior)	> 0	< 0
N_{ea} (Extension Anterior)	< 0	> 0
N_{ep} (Extension Posterior)	< 0	< 0

The criterion is calculated as follows:

$$N_{km} = \frac{|F_x|}{F_{int}} + \frac{|M_{y,OC}|}{M_{int}} \quad (5)$$

$$F_{int} = 845N$$

$$M_{y,OC} > 0 \Rightarrow M_{int} = 88.1N \cdot m$$

$$M_{y,OC} < 0 \Rightarrow M_{int} = 47.5N \cdot m$$

Figure 9 shows two possible representations of the results of N_{km} applied to the tests, and Table 4 the maximum values achieved. After these results we can see that the criterion distinguishes both models of seats very well. With regard to the repeatability, it seems to be lower than that observed on the NIC. The maximum on the test 002 is reached during the phase of extension anterior (N_{ea}), instead of during the phase of flexion anterior (N_{fa}), as happens in the tests 001 and 003. This makes the time of the maximum differ between them. The indicators of repeatability and sensitivity have worse values than the ones obtained for the NIC, being 0.137 and 0.307 respectively.

Table 4. Maximum N_{km} .

Test	001	002	003	004
N_{km} max.	0.33	0.20	0.27	0.62
Time (ms)	128.6	112.6	128.1	108.7
Case	FA	EA	FA	FA

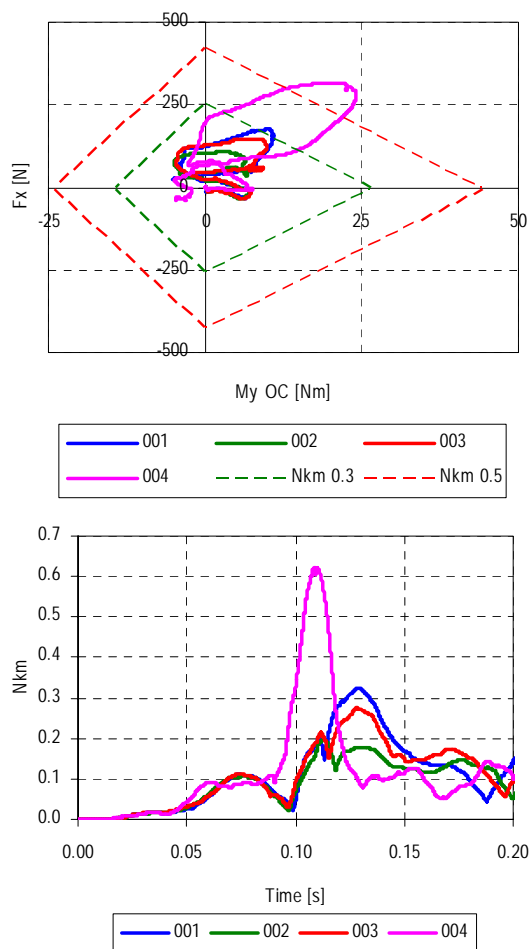


Figure 9. Two representations of N_{km} criterion.

The main advantage found for this criterion is the use of forces and moments, directly related to the loads of the neck, not being affected by other effects such as rotations. Another positive point is its definition in cases, depending on the sign of F_x and $M_{y\ OC}$. This allows the criterion to consider different values and limits depending on the load case. On the other hand, a possible disadvantage is related to the use of the signals measured only on the upper neck load cell, located at the occipital condyle, while the most common injuries have been described between the vertebrae C5 and C7, nearer to the base of the neck. Despite this, the combination of F_x and $M_{y\ OC}$ seems to correlate well with the time in which the s-shape is produced, at least in the studied cases.

Additionally, although the observed influence is not high, it was noticed that the mathematical definition of the criterion as a lineal combination depending on the load case can produce local minimums, oscillations or variations on the tendencies (discontinuities on the derivatives of the curves) at the points of change of case. This can be

understood more easily by looking at the first representation of the criterion in Figure 9. The rhomboidal lines represent the points with 0.3 and 0.5 constant values of N_{km} . If we intended to have a continuous value of the criteria on the zones of the corners (change of case) we should follow a line with this shape, producing a change in the tendencies of some of the magnitudes (force or moment, depending on the corner) when changing the case, and therefore a discontinuity on its derivative. In practise, the change of the definition of the N_{km} results in discontinuities on its derivative and possible local minimums related only to its mathematical formulation, although, as mentioned above, the influence of this effect has not been decisive in any of the studied cases.

LNL

In 2002 (one year after the proposal of the N_{km} criterion) the prototype of a new load cell placed on the T1 vertebra of the BioRID-II dummy was presented, designed to give information about the loads on the lower end of the neck, next to the vertebrae that had been more often related to injury mechanisms (C5-C7). In March 2003 the version “P” of the dummy was released, already equipped with this load cell. Taking advantage of this new instrument the LNL criterion (Lower Neck Load) was proposed, defined as follows:

$$LNL = \frac{|M_{y\ lw}|}{C_{moment}} + \frac{|F_{x\ lw}|}{C_{shear}} + \frac{|F_{z\ lw}|}{C_{tension}} \quad (6).$$

In this expression $M_{y\ lw}$, $F_{x\ lw}$ and $F_{z\ lw}$ are the moment and forces measured with the T1 load cell, and C_{moment} , C_{shear} and $C_{tension}$ reference values (15 N·m, 250 N and 900 N respectively). The value to be used for the evaluation of the seats is the maximum of this curve.

The curves obtained when applying this expression to the data of the tests are shown in Figure 10, and the maximums in Table 5. Looking at these results, we can see that the repeatability for the first three tests is excellent throughout the curves (with an indicator value of 0.044), including the maximums, but the criterion has not been able to differentiate well between seats A and B, at least in the maximum values. The indicator for sensitivity has a value of 0.250.

Table 5. Maximum LNL.

Test	001	002	003	004
LNL max.	3.98	4.09	4.01	3.88
Time (ms)	119.3	123.3	120.7	107.3

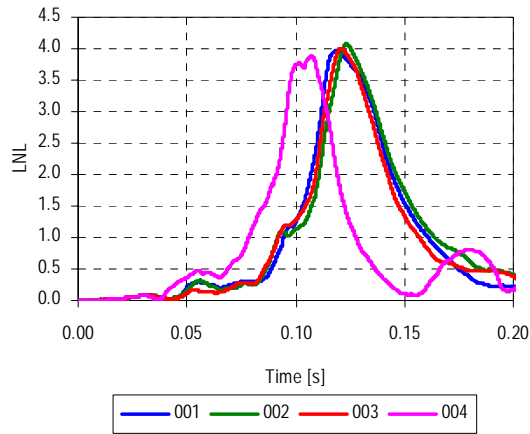


Figure 10. LNL.

The advantages found for this criterion are very similar to the ones found for the N_{km} . It is a criterion based directly on loads, and therefore easy to implement, and does not have the influence of other effects. It is also defined by segments (because of the modulus in the mathematical expression), although it only changes the sign of the reference values for positive and negative data. Besides, the load cell used is the nearest one to the vertebrae where the incidence of injuries is supposed to be higher, and the repeatability shown is very good. On the other hand, the definition by segments presents the same problem already mentioned for the N_{km} , and it has not been able to differentiate between two seats supposed to be very different in terms of whiplash protection.

Neck displacement based criteria (ND)

Viano and Davidsson have proposed a criterion based on the displacements and rotations of the occipital condyle with regard to the T1 vertebra [13]. This criterion, called Neck Displacement Criterion (NDC), was developed from the analysis of the kinematics of volunteers, and is based on two graphs, with the vertical displacement and rotation of the occipital condyle in abscissa and the rearwards horizontal movement of the occipital condyle in ordinate, all of them referred to the T1 vertebra (Z_{OC-T1} , θ_{OC-T1} and X_{OC-T1} respectively). According to the zones occupied by the curves the behaviour is classified as excellent, good, acceptable or poor. This classification was done considering the natural range of motion of both dummies and volunteers.

In order to get numeric values to compare with other criteria, Tencer, Mirza and Huber [28] have defined $Nd_{distraction}$, $Nd_{extension}$ and Nd_{shear} as the quotient between the data used by the NDC criterion and reference values, as described in (8):

$$\begin{aligned} Nd_{distraction} &= \frac{Z_{OC-T1}}{-15mm} \\ Nd_{extension} &= \frac{\theta_{OC-T1}}{25^\circ} \\ Nd_{shear} &= \frac{X_{OC-T1}}{35mm} \end{aligned} \quad (7).$$

Using experimental results with volunteers and in vitro tests, and comparing several criteria, they arrived at the conclusion that the best predictors of injury are Nd_{shear} , $Nd_{extension}$ and $Nd_{distraction}$, following this order, instead of other criteria such as N_{km} or NIC, and therefore they recommended the use of criteria based on displacements.

Figure 11 shows the Nd_{shear} calculated for the tests. We can see that the curves of the tests 001, 002 and 003 have a repeatability worse than the previous criteria (0.163), and seat B has been well differentiated (sensitivity of 0.343). Table 6 shows the relative maximums achieved during the formation of the s-shape (100-150 ms).

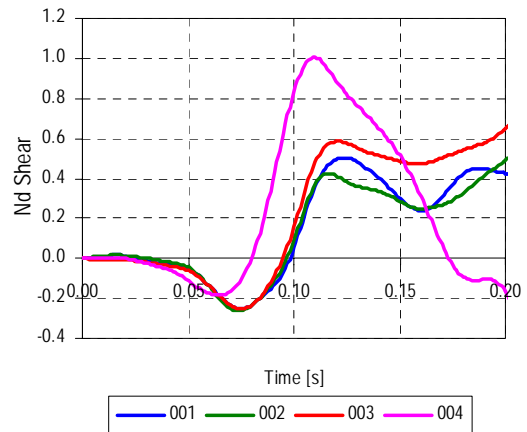


Figure 11. Nd_{shear} .

Table 6. Maximum Nd_{shear} .

Test	001	002	003	004
Nd_{shear} max.	0.50	0.42	0.59	1.00
Time (ms)	124	116	121	109

The main advantage of these criteria is that they represent the real kinematics of the neck, taking into account the whole movement of the head with regard to T1. On the other hand, the main disadvantage seems to be the necessity of displacements measurement using motion analysis software, which, although available, represents additional operations, time of analysis and cost in practise.

Rebound

Several authors ([15], [16], [17] and [18] among others) have reported the risk of injury during the rebound phase when the seat is not able to absorb energy during the impact. This phase can be divided into two different stages. In the first one the dummy receives the released elastic energy from the seat, moving forward freely. The second phase starts when the seat belt begins to act on the dummy, stopping the pelvis and the thorax, and producing a sudden flexion of the neck. Figure 12 shows the data measured with the seat belt load cell during the tests and the rotation of the occipital condyle referred to the T1 vertebra measured by image analysis. We can observe how a violent flexion of the neck is produced when the forces in the seat belt grow. This is reflected also in the loads of the neck, as can be seen in the N_{km} values on this phase (Figure 13). It can be observed also that the maximum values in some of the cases (tests 001, 002 and 003) are considerably higher than the ones registered when observing only the first stages of the movement.

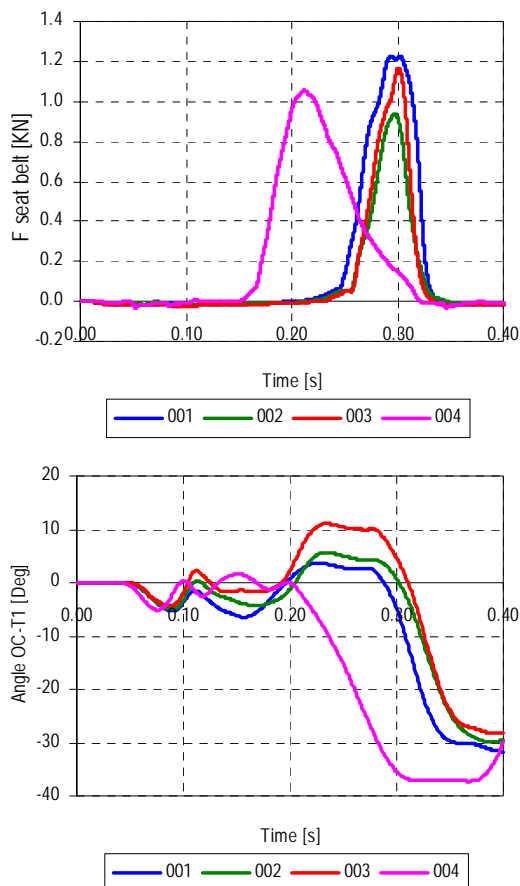


Figure 12. Forces measured at the seat belt and angle of the occipital condyle referred to T1.

At present the capacity of the seats to prevent injuries during the rebound phase is evaluated mainly by measuring the speed of the centre of

gravity of the head when it comes back to the position that it occupied at the beginning of the movement (the results of this operation for the fulfilled tests are shown in Table 7). This is supposed to happen just before the seat belt begins to work, so the behaviour of the seat belt is not taken into account. Normally this approximation should be enough, when using seat belts with similar mechanical characteristics on the strap and spool out (the loads are too low so as to be affected by load limiters working at common levels), but this can change in special cases, such as when using pretensioner systems or, as in the case of the seat “B” (test 004), when the points of fixation of the seat belt are fixed to parts of the seat that displace during the impact. Having a look at Table 7 and Figure 13 we can see that, while the rebound speeds are similar for all the tests, the loads on the neck at the rebound are somewhat higher on the fourth test. This fact points to the convenience of reproducing the seat belt configuration in the injury assessment in this phase, at least in the mentioned particular cases.

Table 7. Rebound velocity and time of measure.

Test	001	002	003	004
Rebound velocity (m/s)	3.98	3.96	3.75	4.04
Time (ms)	242	260	259	184

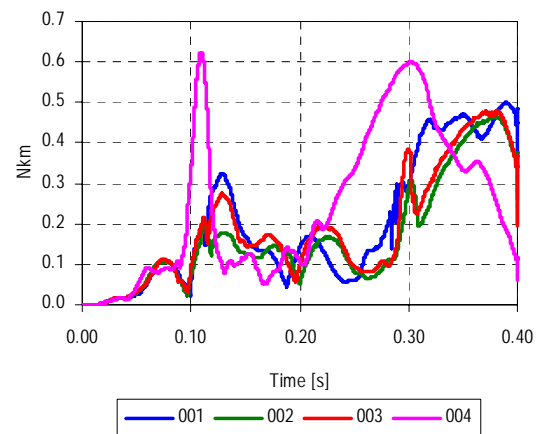


Figure 13. N_{km} extended to the rebound phase.

In conclusion for the rebound phase, a criterion based on loads seems to give more information for injury assessment than the calculation of the speed at a particular point. Considering that the possible injuries of the neck in this phase are better understood (the movements are similar to the ones produced in frontal crashes), a general criterion could be used, such as maximum loads at occipital condyle or N_{km} . Besides, the current method to calculate the rebound velocity supposes normally

the use of image analysis, with the practical disadvantages already commented on in the case of displacement based criteria.

RESULTS

The study of these criteria has evidenced weak and strong points in all the cases. The advantages more esteemed by the authors on the underlying concepts of the different criteria have been the following:

1. Capacity to describe the dynamics of the whole neck, taking into account the upper and the lower parts (NIC and ND). Conceptually this should provide a better description of multiphasic states of the neck, particularly the s-shape.
2. Avoidance of distortions due to facts not directly related to the studied injury mechanism (NDC and Rebound speed), such as the angular accelerations found in the NIC (produced by the use of accelerometers at different points) or the mathematical definition in the change of case for the N_{km} and LNL.
3. Facility of calculation (NIC, LNL and N_{km}), avoiding the use of image analysis or complicated algorithms. For practical reasons, the results of the criteria should be available to be analyzed immediately after the test without extra operations.

Other considerations, such as the repeatability or the capability to distinguish different seats are not chosen in the design of the criterion, but are a consequence of the selection of the magnitudes or expressions used in the calculation.

Considering all this, we can draw some guidelines to be applied in the definition of a whiplash injury criterion, focusing on the advantages and avoiding the disadvantages of the studied ones:

1. It should be representative of the dynamics of the whole neck. Taking into account the importance given to the s-shape by the currently accepted injury mechanisms, it should work with values at both ends of the neck in order to be able to detect and quantify this biphasic state.
2. It should avoid the use of accelerations in more than one point, in order to eliminate the sensitivity to the rotations of the seatback.
3. For practical reasons, it should also avoid the use of displacements or velocities measured by

image analysis.

4. It would be desirable that its mathematical expression was simple, avoiding the definition in segments.

Taking into account these guidelines and the current instrumentation of the BioRID-II dummy, the simplest solution seems to be the use of the two load cells that the dummy has in the upper and lower ends of neck within only one simple mathematical expression.

PROPOSAL OF A NEW WHIPLASH INJURY CRITERION (WIC)

Having described the previous guidelines, the next step was to determine whether the complex movement of the neck during a rear-end impact could be described by only one mathematical expression using just load magnitudes. As most authors coincide in pointing to the s-shape of the neck as the most probable cause of whiplash injuries, it was decided to look for a function that had a maximum when it happened. As we have seen, the s-shape is a biphasic stage in which the upper end of the neck suffers a flexion at the same time as a hyperextension occurs at the lower end. When using the sign convention stated by the SAE J1733 recommended practice [8], the extension movement is characterized by positive moments in the sagittal axis (Y) of both neck load cells, while the flexion moment is defined by negative moments. Therefore, during the s-shape of the neck, there must be a positive Y moment on the upper end of the neck and a negative Y moment on the lower end (see Figure 14). Taking this into account, the function WIC (Whiplash Injury Criterion) was defined as the most evident solution to the problem:

$$WIC = M_{y_{OC}} - M_{y_{lw}} \quad (8).$$

In this expression $M_{y_{OC}}$ represents the Y moment around the Occipital Condyle (at the upper end of the neck), and $M_{y_{lw}}$ represents the Y moment measured at the T1 load cell.

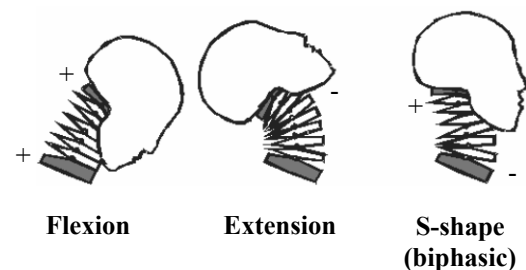


Figure 14. SAE J1733 sign convention for neck moments in "Y" axis.

Figure 15 shows the result of the application of this function to the data obtained in the tests. The maximum values registered were 25.10 Nm, 19.34 Nm and 22.32 Nm respectively for the three first tests (seat “A”) and 38.67 Nm for the fourth test (seat “B”).

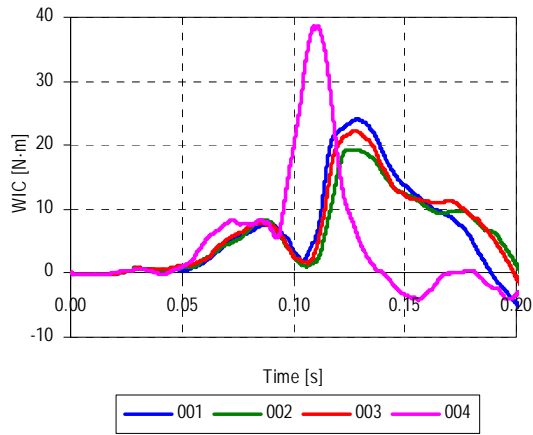


Figure 15. WIC.

After the evaluation of the results we can make the following observations:

1. The curves are very clear and easy to understand. There is a first peak corresponding to the time of the ramping up and spine straightening effects (50-100 milliseconds), coincident with the compression force measured on the lower neck load cell, and a second one, much more marked, during the time when the s-shape is more accentuated (100 to 150 milliseconds).
2. The repeatability in the curves for similar seats (tests 1, 2 and 3) is quite good, having an indicator value of 0.097 (Table 8 shows a comparison of the different values achieved by the indicators of repeatability and sensitivity by the different criteria). We can see also in Table 9 that maximum values for these first three tests happen at very similar times, within a range smaller than that observed by any other criterion.
3. There is a clear differentiation between the curves of the two different seats (sensitivity value of 0.359). The criterion has proved to be sensitive to the seat used and has indicated correctly the inferior seat with regard to neck protection.
4. Looking at the biomechanical aspects, the criterion was designed seeking a function to describe the s-shape, based on the studies that pointed to it as the origin of the more common

whiplash injuries. Figure 16 shows a detail of the neck and head of the dummy at the times when the s-shape seemed to be more pronounced visually. We can appreciate that, as expected, the s-shape was significantly more accentuated in the fourth test (the seat was much more rigid than in the other tests, so the thorax accelerated before and the retraction movement happened more violently).

5. Table 9 presents the times in which the different criteria had a maximum, compared to the times when the most accentuated s-shape in the videos were observed (Figure 16). We can see how the proposed criterion was in general, next to N_{km} , the nearest one to the observed times. Besides, it quantified the magnitude of the loads, indicating clearly which seat produced a more pronounced s-shape.
6. Finally, it is easily implemented, neither image analysis being necessary, nor additional instrumentation or complicated algorithms. It can also be easily applied to previously done tests using the version “f” of the dummy (the first one implementing the lower neck load cell) or later.

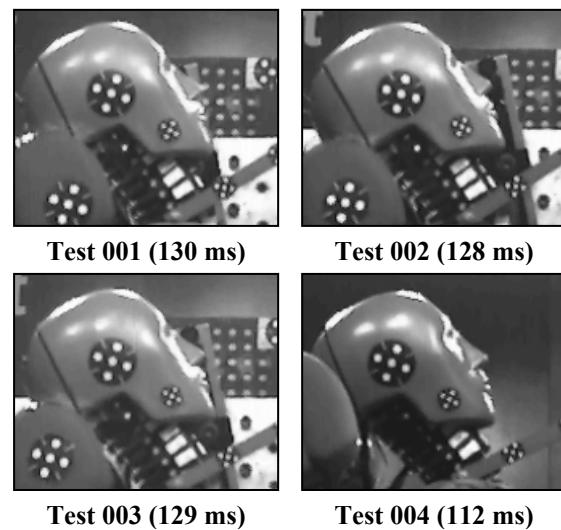


Figure 16. Detail of the head and neck at the time of the most accentuated observed s-shape during the tests.

Table 8. Indicators for repeatability and sensitivity.

	Repeatability (lower better)	Sensitivity (higher better)
WIC	0.097	0.359
NIC	0.084	0.407
N_{km}	0.137	0.307
LNL	0.044	0.250
Nd_{shear}	0.163	0.343

Table 9. Times of maximum values (ms).

Test	001	002	003	004
Observed S-shape	130	128	129	112
WIC	<u>128.6</u>	<u>126.3</u>	127.7	<u>110.2</u>
NIC	88.6	79.9	81.8	86.7
N_{km}	<u>128.6</u>	112.6	<u>128.1</u>	108.7
F_x (upper)	128.4	121.2	121.2	108.1
F_z (upper)	115.3	123.1	119.9	98.9
LNL	119.3	123.3	120.7	107.3
Nd_{Shear}	124	116	121	109

This study could not have been finished without a critical review of the new criterion. The observed points were the following:

1. This criterion only takes into account the injury mechanisms associated with the formation of the s-shape in the neck. It does not reveal other possible mechanisms such as, for instance, damages produced during the rebound phase or simple hyperextension. To consider them it should be complemented with another criterion for general use (for instance, maximum loads on the occipital condyle or N_{km})
2. The dynamics of the whole neck has only been represented by the two sagittal moments. Of course, this is a simplification, and a more complex criterion could be defined using additional parameters, such as forces, one acceleration or derivative terms. On the other hand, the criterion has shown to be able to detect and quantify the formation of the s-shape, which was its main objective. This could be enough to evaluate the protection for the most accepted whiplash injury mechanisms. Further studies are suggested in order to analyze this point and the convenience of developing a more complete criterion using this one as a base.

CONCLUSIONS

The original aim of this study was the critical review of the commonest injury criteria used to evaluate whiplash protection, analyzing the advantages and disadvantages of each one of them in order to get a more thorough knowledge of their use. A review of the current theories about the motion of the head and the injury mechanisms was done in order to provide a better understanding of the whiplash phenomenon. Four tests with a BioRID-II dummy were fulfilled to provide data to be used in the comparison of the criteria. As a result, some guidelines to define a new criterion were drawn up focusing on the advantages and

avoiding the disadvantages of those previously studied. To resume, it should be based on measurements done at both ends of the neck, in order to be able to describe accurately the biphasic state of the s-shape, and, at the same time, it should avoid the use of several accelerometers or image analysis. Therefore, the clearest solution was to use the upper and lower neck load cells at the same time.

Following these directives a new criterion called “WIC” (Whiplash Injury Criterion) was proposed and evaluated under the same conditions that had been used for the study of the other criteria. The results have been very promising, having shown a good repeatability, sensitivity to the seat and capacity to predict and quantify the s-shape of the neck.

In conclusion, some ideas are suggested for future studies:

1. Further evaluation of the new criterion with previously done tests, in order to confirm the first results.
2. Definition of limit values for evaluation of seats, based either on biomechanical studies, on statistical results (taking into account the values given by different types of seats, as done by IIWPG to define their current limits [3]), or using either tests or simulations of real-world accidents with known injury outcomes and recorded crash pulses, as done by Eriksson and Kullgren [29] or Linder et al. [30].
3. More in depth biomechanical analysis, researching into the convenience or not of defining a more complex criterion based on the same guidelines.

REFERENCES

- [1] (1998) “The Abbreviated Injury Scale (AIS) 1990 - Update 98”. Association for the Advancement of Automotive Medicine (AAAM). Des Plaines, USA.
- [2] (2004) “IIWPG Protocol for the dynamic testing of motor vehicle seats for neck injury prevention DRAFT V 1.4”. International Insurance Whiplash Prevention Group (IIWPG). iiwpg.iihs.org.
- [3] (2004) “Rationale for IIWPG ratings of seats and head restraints for neck injury prevention”. International Insurance Whiplash Prevention Group (IIWPG). iiwpg.iihs.org.
- [4] (2004) “Standard test method for rear end

impact crash tests". Folksam, Swedish national road administration. Sweden. www.vv.se.

[5] Davidsson J. (2000) "Development of a mechanical model for rear impacts: Evaluation of volunteer response and validation of the model", Chalmers University of Technology, Goteborg, Sweden.

[6] (2002) "BioRID II User's guide". Denton ATD, Inc. USA.

[7] Svensson M. Y., Boström O., Davidsson J., Hansson H.A., Håland Y., Lövsund P., Suneson A. and Säljö A. (1999) "Neck injuries in car collisions – A review covering a possible injury mechanism and the development of a new rear-impact dummy". Whiplash Associated Disorders World Congress, Vancouver, Australia.

[8] (1994) "SAE J1733. Sign Convention for vehicle crash testing. Issued DEC94". Society of Automotive Engineers (SAE) USA.

[9] Russell D. M. (1997) "Error measures for comparing transient data – Part I: Development of a comprehensive error measure". 68th Shock and Vibration Symposium. Hunt valley, Maryland. USA.

[10] McConnell W. E., Howard R. P., Poppel J. V., Krause R., Guzman H. M., Bomar J. B., Raddin J. H., Benedict J. V. and Hatsell C. P. (1995) "Human head and neck kinematics after low velocity rear-end impacts – Understanding whiplash". Society of Automotive Engineers (SAE) Paper Number 982724. USA.

[11] Grauer J. N., Panjabi M. M., Cholewicki J., Nibu K., Dvorak J. (1997) "Whiplash produces an S-Shaped curvature of the neck with hyperextension at lower levels". Spine 22:2489-2494.

[12] Ono K., Kaneoka K., Wittek Q., Kajzer J. "Cervical injury mechanism based on the analysis of human cervical vertebrae motion and head-neck-torso kinematics during low speed rear impacts" 41st STAPP Car Crash Conference. Society of Automotive Engineers (SAE) Paper Number 933340. USA.

[13] Viano D. C., Davidsson J. (2002). "Neck displacements of volunteers, BioRID P3, and Hybrid III in rear impacts: Implications to whiplash assessment by a neck displacement criterion (NDC)". Traffic Injury Prevention Vol. 3, Number 2, 105-116.

[14] Macnab I. (1966). "Whiplash injuries of the

neck". Manitoba Med. Rev. 46. 172-174.

[15] Macnab I. (1971) "The whiplash syndrome". Orthop. Clin. North. Am. 2: 389.

[16] Von Koch M., Nygren Å. and Tingvall C. (1994) "Impairment pattern in passenger car crashes, a follow-up of injuries resulting in long term consequences". 14th ESV conference. Munich. Germany.

[17] Muser M. H., Walz F. H. And Zellmer H. (2000) "Biomechanical significance of the rebound phase in low speed rear end impacts". International IRCOBI conference on the Biomechanics of Impacts, Montpellier, France.

[18] Hell W., Langwieder K., Walz F., Muser M. Kramer M. and Hartwig E. (1999) "Consequences for seat design due to rear end accident analysis, sled tests and possible test criteria for reducing cervical spine injuries after rear-end collision" International IRCOBI conference on the Biomechanics of Impacts, Sitges, Spain.

[19] Aldman B. (1986). "An analytical approach to the impact biomechanics of head and neck". Proceedings of the 30th Annual AAAM Conferences.

[20] Svensson M. Y., Aldman B., Lövsund P., Hansson H. A., Seeman T., Suneson A. and Örtengren T. (1993). "Pressure effects in the spinal canal during whiplash extension motion – a possible cause of injury to the cervical spinal ganglia". International IRCOBI conference on the Biomechanics of Impacts, Eindhoven, The Netherlands.

[21] Panjabi M. M., Cholewicki J., Nibu K., Grauer J. N., Babat L. and Dvorak J. (1998). "Mechanism of whiplash injury". Clinical Biomechanics 13 239-249.

[22] Kaneoka K., Ono K., Inami S., Ochiai N. and Hayashi K. (2002) "The human cervical spine motion during rear-impact collisions: A proposed cervical facet injury mechanism during whiplash trauma". Journal of Whiplash & Related Disorders, Vol 1(1), 85-97.

[23] Cusick J., Pintar F. A., and Yoganandan N. (2001) "Whiplash syndrome, Kinematic factors influencing pain patterns". Spine 26, 1252-1258.

[24] Siegmund G. P., Myers B. S., Davis M. B., Bohnet H. F., Winkelstein B. A. (2000). "Human cervical motion segment flexibility and facet capsular ligament strain under combined posterior shear, extension and axial compression". STAPP

[25] Boström O., Svensson M. Y., Aldman B., Hansson H., Håland Y., Lövsund P., Seeman T., Suneson A., Säljö A. and Örtengren T, (1996) “A new neck injury criterion candidate based on injury findings in the cervical spine ganglia after experimental neck extension trauma”. International IRCOBI conference on the Biomechanics of Impacts, Dublin, Ireland.

[26] (2003) “Minutes of 4th European BioRID user meeting (BUM)”. BioRID Users Meeting, Stadthagen, Germany. www.rcar.org.

[27] Schmitt K. U., Muser M. H. and Niederer P. (2001) “A new injury criterion candidate for rear-end collisions taking into account shear forces and bending moments”. 17th ESV Conference. Amsterdam, Netherlands.

[28] Tencer A. F., Mirza S. and Huber P. (2003) “A comparison of injury criteria used in evaluating seats for whiplash protection”. 18th ESV Conference. Tokyo. Japan.

[29] Eriksson L., Kullgren A. (2003) “Influence of seat geometry and seating position on NIC_{MAX} and N_{km} AISI neck injury predictability”. International IRCOBI conference on the Biomechanics of Impacts, Lisbon, Portugal.

[30] Linder A., Avery M., Kullgren A., Krafft M. (2004) “Rear-world rear impacts reconstructed in sled tests”. International IRCOBI conference on the Biomechanics of Impacts, Graz, Austria.

NON-CENSORED RIB FRACTURE DATA FROM DYNAMIC BELT LOADING TESTS ON THE HUMAN CADAVER THORAX

Stefan Duma

Joel Stitzel

Andrew Kemper

Craig McNally

Eric Kennedy

Virginia Tech – Wake Forest, Center for Injury Biomechanics
United States

Fumio Matsuoka

Toyota Motor Corporation

Paper Number 05-03603

ABSTRACT

The purpose of this paper is to present data from dynamic belt loading tests on the thorax of human cadavers where the exact timing of all rib fractures is known. In order to generate non-censored rib fracture data, a total of 47 strain gages were placed throughout the thorax of two human cadavers (1 male, 1 female). In order to simulate thoracic loading from a severe car crash, a table-top belt loading device was developed that utilizes a servo-hydraulic test machine to apply a dynamic input. The belt load pulse was configured to result in 40% chest compression through a 150 ms load and unload cycle. Potentiometers and accelerometers measured the chest compression and acceleration at three locations, load cells in line with the belt provided belt loads, and load cells on the posterior side of the thorax measured the reaction loads. The time histories of each strain gage were analyzed to determine the time of fracture which could then be compared directly to the reaction loads and chest displacements at that exact time, thereby creating a non-censored data set. In both cadavers, all fractures (20 for female and 12 for male) occurred within the first 35% compression of the thorax. As a general trend, the first series of fractures were on the left side of the thorax where the belt passed over the abdomen. The peak strain at failure ranged from 1.1 % to 2.5 %. By utilizing this technique, the exact timing of an injury level can be characterized relative to the mechanical parameters. For example, using rib fractures as the parameter for AIS scores in the female test, it is shown that AIS 1 injury occurs at a chest compression of 21%, AIS 2 at 22%, AIS 3 at 24 %, and AIS 4 at 34%.

INTRODUCTION

The vast majority of thoracic impact research has focused on developing global criteria for predicting injury. These include force, acceleration, and

displacement based criteria, as well as combinations of the above [5, 13, & 15]. Recent work has focused on the prediction of injury due to different restraint systems. For example, the increase in thoracic injury severity with increased age for a given occupant size, restraint type, and crash type is well documented [1, 5, 6, 7, 16 & 20]. The most common injury that occurs during sled tests with belted cadavers is rib fracture [4, 8 & 20]. Also, it is known that rib fracture patterns vary by restraint type [8]. Kent *et al.* [10] evaluated the injury predictive value of hard tissue criteria by varying restraint condition and found compression is the best indicator of fracture risk. Moreover, the noted that there is a significant effect on the fracture patterns due to belt only, airbag only, and combined belt and airbag loading.

Kent [9] also notes one of the problems with global methods used to develop thoracic injury criteria is that the criteria correlate with injury without necessarily being functionally related to injury, in contrast to stress and strain. This is the critical limitation of previous studies designed to develop global thoracic injury criteria. In summary, all previous studies aimed at determining thoracic injury criteria generally rely on the same set of cadaver impact tests, which all provide censored injury data. In other words, it is not possible to determine the exact loads, accelerations, or displacements at the time of fracture. Rather, one only knows that an injury occurred as some point during the impact test. In order to reduce this limitation, this study presents a method to generate non-censored rib fracture data. Although previous studies have shown the ability to detect selected rib fractures, no method has been successful at mapping the exact fracture timing of the entire thorax during dynamic belt loading. Therefore, the purpose of this study is to develop a method for determining non-censored rib fracture data and to present results from

dynamic belt loading tests on the human cadaver thorax using this method.

METHODS

Dynamic belt tests were performed on two cadavers (one male, one female) instrumented with 47 single axis and rosette strain gages on the ribs, sternum, and clavicle. The primary components of the belt loading system were a tensile testing machine (MTS 810, 22 kN, Eden Prairie, MN) and rigid loading table (Figure 1). The thorax of each cadaver was placed over a rigid plate that distributed the applied load over four load cells to measure the reaction loads of the thorax which were used to compensate for inertial effects. The 5 cm wide nylon

loading belt was situated 40° from the sagittal plane of the body. The orientation of the belt simulated a passenger side seat belt, going over the right clavicle and left side of the abdomen. A series of wire cables and pulleys connected the hydraulic piston to a Material Testing System (MTS 810, 22 kN, Eden Prairie, MN) used to load the cable/belt system at the desired rate. The locations of the pulleys were adjustable to accommodate cadavers of various sizes as well as to alter the angle of the belt relative to the table top. A slack reducer, connecting the primary wire rope to two secondary wire ropes, served to displace the ends of the loading belt equally, as well as remove slack from the system.

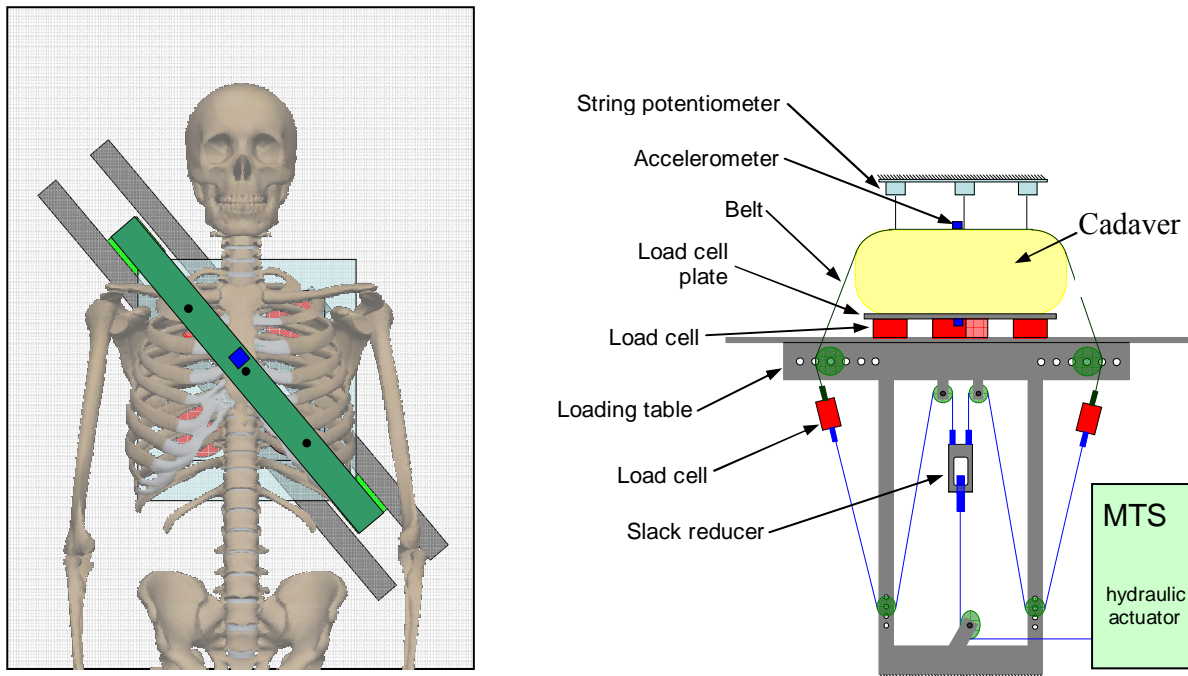


Figure 1. Top and Oblique View of Belt Loading System.

Once all the cables and instrumentation were connected, each cadaver was preconditioned prior to each test. This was done by placing a large flat 9.07 kg mass on the thorax five times for 10 seconds at one minute intervals. Before each test the MTS was used to pretension slightly the belt (75-80 N for the male, 58-75 N from the female). In order to model *in vivo* conditions, the test subjects' pulmonary systems were inflated to 14 kPa immediately prior to each test, which corresponded to the mean inspiration pressure, with a tracheostomy connected to pressure regulator. The depth of the inflated chest was then measured and recorded. Finally, the MTS machine

loaded the cable system at a rate of 1.5 m/s in order to simulate a severe car crash.

Instrumentation

Each cadaver was instrumented with a total of 47 strain gages; 26 single axial strain gages (Vishay Measurements Group, CEA-06-062UW-350, Malvern, PA) and 7 rectangular rosette strain gages (Vishay Measurements Group, CEA-06-062UR-350, Malvern, PA). The deflection of the thorax was measured using three string potentiometers (Space Age Control, 160, Palmdale, CA) that were attached

to the belt at the sternum and situated approximately 90 mm apart along the length of the belt (Figure 1). Additionally, an accelerometer (Endevco, 7264B, 2000 g, San Juan Capistrano, CA) was mounted on the belt at the sternum and load cell plate to acquire chest acceleration and table vibration. Belt tension was measured with two load cells (Interface, SSM-AJ, 13kN, Scottsdale, AZ). Four additional load cells (Denton, 5768, 11 kN, Rochester Hills, MI), (Denton, 1968, 22 kN, Rochester Hills, MI), (Denton, 1716A, 13 kN, Rochester Hills, MI) located between the cadaver and loading table, measured the force response of the body.

Test Subject Information

Two fresh frozen human cadavers were used in these tests (Table 1). It should be noted that chest depth measurements were taken from the middle of the sternum to the back of the thorax. Also, the percent compression was defined as the ratio of chest depth during the test to the chest depth measured prior to the test. For comparison with the standard population, Osteograms® were performed. The left hand of each cadaver was x-rayed and scanned by Compumed Incorporated (Los Angeles, CA). The BMD results are reported with respect to the normal population (Table 2). The t-score is used to compare the cadaver’s bone mineral density with that of the general population. The z-score is used to compare the bone mineral density of the female subjects with the average for their age. The t-score is expected to be low for these elderly cadavers with respect to the general population. A t-score of -1 corresponds to one standard deviation below the mean for the general population (30 year olds), meaning the individual is at or above the -63rd percentile for bone mineral density, or close to normal. T-scores of 2 and 3 correspond to 97th and 99th percentiles, respectively.

Table 2.
Subject Osteogram Results.

Cadaver Number	SM35	SF33
BMD Index	75.7	73.7
T-Score	-3.2	-3.4
Z-score	-1.4	-0.7

Table 1.
Subject Anthropometric Data.

Cadaver Number	SM35	SF33
Sex	Male	Female
Age	73	73
Weight	84.36 kg	45.35 kg
Height	154 cm	154 cm
Height (head to heal)	1730 mm	1540 mm
Sternum Length	210 mm	150 mm
Chest Circumference (Largest part)	1140 mm	700 mm
Chest Circumference (Center of Sternum)	1070 mm	740 mm
Linear Breadth (Center of Sternum)	370 mm	280 mm
Chest Depth (Center of Sternum)	230 mm	165 mm
Chest Circumference (Center of Thorax no Superficial Tissue)	840 mm	610 mm

Stain Gage Locations

The strain gages were located on the lateral sides of ribs 2-10 as well as the anterior side of ribs 3, 4, and 5 (Figures 2). The only difference between the two is the orientation of the rosettes on the left 7th and 9th ribs. The first “R” in the rib strain gage labels stands for “Rib”. Similarly, the first letters on the clavicle and sternum strain gage labels “CR”, “SU”, and “SL” stand for clavicle, upper sternum, and lower sternum respectively. The first number represents the number of the rib. The second letter “R” or “L” stands for the right side or left side of the thorax, respectively. The first letter after the dash, “S” or “R”, stands for single axis or rosette strain gage. The gages were numbered one to three bilaterally for ribs containing multiple gages. The number “1” gage corresponded to the gage closest to the sternum on each side, and the number “3” gage was the most distal gage from the sternum. The last letter “A”, “B”, or “C” only concerned the rosette strain gages and identifies the gage position within the rosette. For example, the strain gage label R3R-R3A stands for gage A of a rosette on the lateral right side of rib 3.

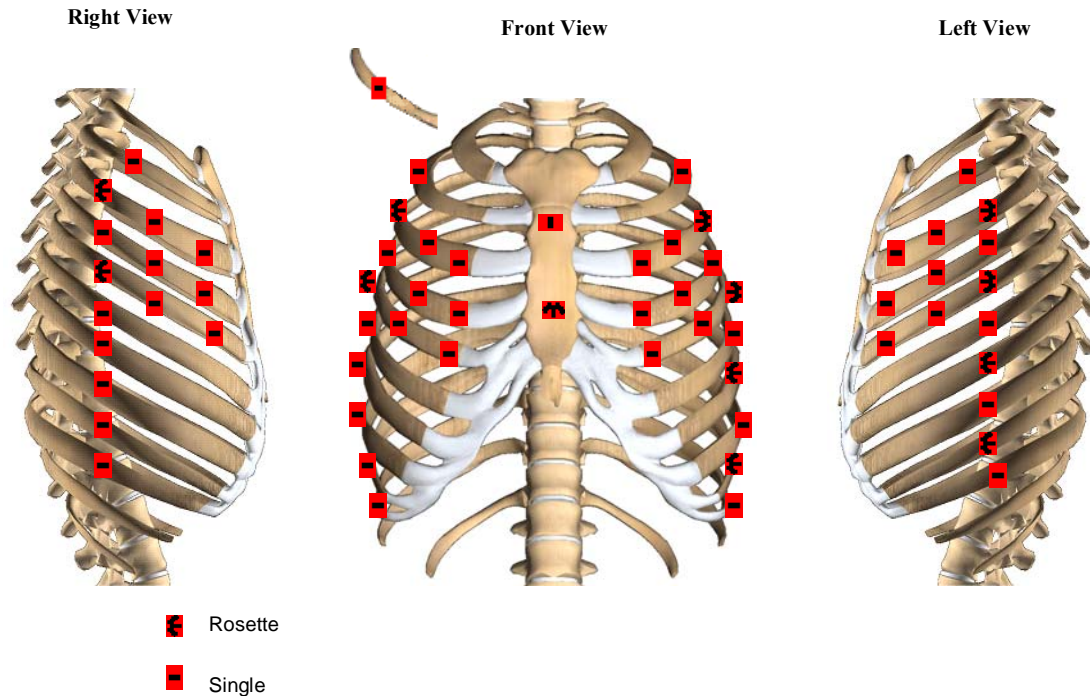


Figure 2. Strain Gage Positioning on the Thorax.

Strain Gage Attachment

Once the location of each strain gage was determined the surface of the bone was then swabbed with either and allowed to dry. Upon drying, Conditioner A an acidic solution, was applied to the surface with a clean piece of gauze in order to etch the surface of the bone. Then Neutralizer 5A a basic solution, was applied to the surface in order to neutralize the acidic solution. The gage was removed from its case and prepared by applying M-Bond Catalyst to the underside of the gage. Next, M-Bond 200 Adhesive was applied to the bone and the gage was quickly pushed over the adhesive in a rolling manner. The strain gage covered with a small piece of latex was held with firm pressure for 3 minutes (Figure 2.-7). Special care was taken to align each gage so that it was in line with the axis of the rib. The strain output from the three gages that composed each rosette was used to calculate the first and second principle strains and the angle Phi (Φ). Phi was defined as the angle from the gage reference axis (labeled X-Y) to the first principal axis.

RESULTS

In order to validate that these tests were representative of an actual sever crash, the data was

compared to data obtained from an actual sled test preformed (Figure 3). It can be seen that the compression rates produced from these tests closely match those seen in an actual sled test. The full travel of the MTS (15 cm) was used to fully compress the chest, causing 55% compression of the female thorax and 37% of the male thorax. This corresponded to 91.39 mm for the female and 100.36 mm for the male. The MTS was actuated at 150 cm/s, which compressed the thorax of the female at a rate of 94 cm/s and the male at 97 cm/s. The difference in the rate of the MTS and the rates seen by the cadavers was due to inertial effects and friction in the cable system.

The peak strains and strain rates vary from gage to gage for both the male and female cadavers (Table 3, Table 4). The highest absolute value for each gage was reported as the peak strain. The majority of the gages reported tensile loading. The strain rate was determined from the most linear portion of the initial strain loading. The majority of the gages reported tensile loading. The male cadaver had peak strain ranging from 1,533 to 39,812 (μ strain) in tension and from 1612 to 15,332 (μ strain) in compression. The female cadaver had peak strain ranging from 1,716 to 33,614 (μ strain) in tension and from 1,223 to 17,193 μ strain in compression. The rib strain rates seen by

the male cadaver ranged from -0.376 to 0.880 (strain/s), while strain rates seen by the female cadaver ranged from -0.468 to 0.547 (strain/s). The plots of strain vs. time for all the strain gages on both

the male and female are located in Appendixes A and B, respectively.

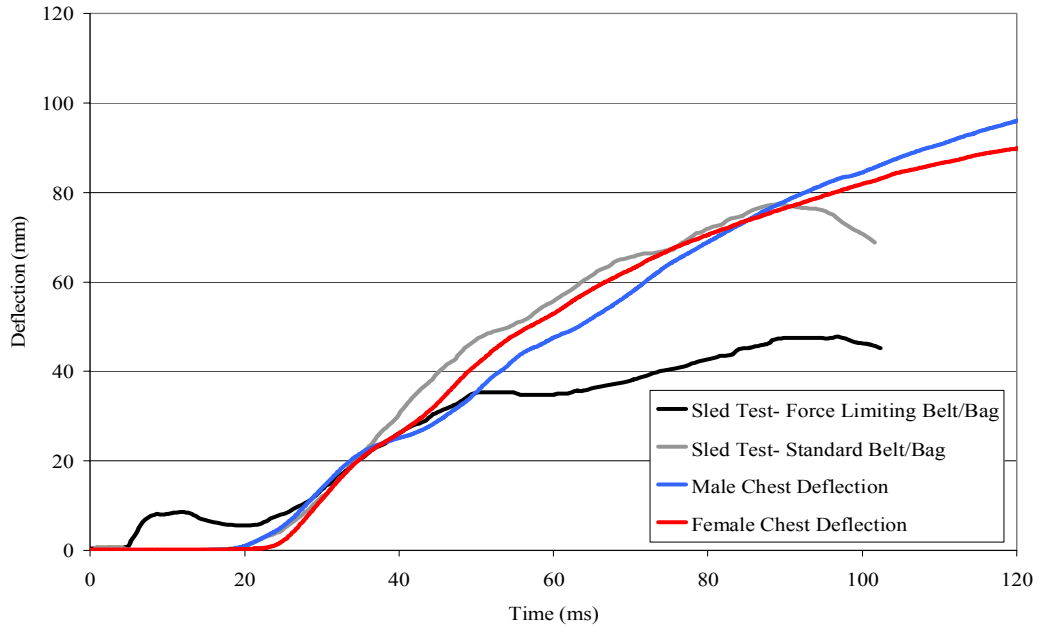


Figure 3. Chest Compression Rate of Cadavers in a 48 km/hr Sled Test (Kent, 2001) versus Presented Belt Loading Data.

Table 3.
Peak Strains and Strain Rates for all Strain Gages on Male Cadaver.

Strain Gage Number	Thorax Location	Rib Number	Gage Type	Rib Location	Peak Strain (μ strain)	Time (ms)	Strain Rate (strain/s)
R2R-S3	Right Side	2	Single	3	13680	79.3	0.243
R3R-S1	Right Side	3	Single	1	11353	89.5	0.134
R3R-S2	Right Side	3	Single	2	11595	89.2	0.209
R3R-R3A	Right Side	3	Rosette	3	1941	89.3	0.071
R3R-R3B	Right Side	3	Rosette	3	22111	88.9	0.459
R3R-R3C	Right Side	3	Rosette	3	12574	88.9	0.225
R4R-S1	Right Side	4	Single	1	5083	95.6	0.143
R4R-S2	Right Side	4	Single	2	13758	95.2	0.268
R4R-S3	Right Side	4	Single	3	12561	95.3	0.179
R5R-S1	Right Side	5	Single	1	4848	82.6	0.243
R5R-S2	Right Side	5	Single	2	7252	82.6	0.267
R5R-R3A	Right Side	5	Rosette	3	3335	82.9	0.054
R5R-R3B	Right Side	5	Rosette	3	8165	82.6	0.145
R5R-R3C	Right Side	5	Rosette	3	3577	82.6	0.055
R6R-S3	Right Side	6	Single	3	10480	136.2	0.095
R7R-S3	Right Side	7	Single	3	7014	132.3	0.080
R8R-S3	Right Side	8	Single	3	4557	132.7	0.062
R9R-S3	Right Side	9	Single	3	1286	118.2	0.015
R10R-S3	Right Side	10	Single	3	2810	121.5	0.079
CR-S3	Right Clavicle	N/A	Single	N/A	-6577	95.5	-0.122
SU-S	Upper Sternum	N/A	Single	N/A	-7711	69.1	-0.376
SL-RA	Lower Sternum	N/A	Rosette	N/A	13331	69.4	4.098
SL-RB	Lower Sternum	N/A	Rosette	N/A	39812	77.2	3.256
SL-RC	Lower Sternum	N/A	Rosette	N/A	7960	76.7	0.581
R2L-S3	Left Side	2	Single	3	11589	53.9	0.535
R3L-S1	Left Side	3	Single	2	10478	56.1	0.413
R3L-S2	Left Side	3	Single	3	13328	55.9	0.577
R3L-R3A	Left Side	3	Rosette	3	4624	55.9	0.172
R3L-R3B	Left Side	3	Rosette	3	5936	55.8	0.267
R3L-R3C	Left Side	3	Rosette	3	1839	56.1	0.144
R4L-S1	Left Side	4	Single	1	9290	51.4	0.449
R4L-S2	Left Side	4	Single	2	15576	51.4	0.880
R4L-S3	Left Side	4	Single	3	7948	51.5	0.410
R5L-S1	Left Side	5	Single	1	11741	47.3	0.603
R5L-S2	Left Side	5	Single	2	14128	47.3	0.706
R5L-R3A	Left Side	5	Rosette	3	3674	47.6	0.204
R5L-R3B	Left Side	5	Rosette	3	6499	47.6	0.342
R5L-R3C	Left Side	5	Rosette	3	1533	47.7	0.059
R6L-S3	Left Side	6	Single	3	6961	44.7	0.385
R7L-R3A	Left Side	7	Rosette	3	3772	42.6	0.215
R7L-R3B	Left Side	7	Rosette	3	6618	42.7	0.451
R7L-R3C	Left Side	7	Rosette	3	1822	117.1	0.117
R8L-S3	Left Side	8	Single	3	5080	136.0	0.318
R9L-R3A	Left Side	9	Rosette	3	2310	35.9	0.183
R9L-R3B	Left Side	9	Rosette	3	3026	35.8	0.251
R9L-R3C	Left Side	9	Rosette	3	-1673	52.7	-0.086
R10L-S3	Left Side	10	Single	3	-15332	126.1	-0.287

Table 4.
Peak Strains and Strain Rates for all Strain Gages on Female Cadaver.

Strain Gage Number	Thorax Location	Rib Number	Gage Type	Rib Location	Peak Strain (μ strain)	Time (ms)	Strain Rate (strain/s)
R2R-S3	Right Side	2	Single	3	-5504	111.2	0.138
R3R-S1	Right Side	3	Single	1	5508	85.8	0.300
R3R-S2	Right Side	3	Single	2	8000	111.1	0.191
R3R-R3A	Right Side	3	Rosette	3	2410	78.3	0.104
R3R-R3B	Right Side	3	Rosette	3	5246	57.2	0.225
R3R-R3C	Right Side	3	Rosette	3	4755	57.2	0.179
R4R-S1	Right Side	4	Single	1	3338	62.7	0.345
R4R-S2	Right Side	4	Single	2	7076	62.5	0.202
R4R-S3	Right Side	4	Single	3	5490	95.1	0.175
R5R-S1	Right Side	5	Single	1	2709	52.5	0.111
R5R-S2	Right Side	5	Single	2	4846	58.6	0.137
R5R-R3A	Right Side	5	Rosette	3	-1223	56.8	-0.044
R5R-R3B	Right Side	5	Rosette	3	7391	108.0	0.146
R5R-R3C	Right Side	5	Rosette	3	n/a	n/a	n/a
R6R-S3	Right Side	6	Single	3	10642	105.5	0.153
R7R-S3	Right Side	7	Single	3	7785	133.1	0.094
R8R-S3	Right Side	8	Single	3	4633	111.1	0.144
R9R-S3	Right Side	9	Single	3	2971	118.2	0.062
R10R-S3	Right Side	10	Single	3	1716	107.3	0.123
CR-S3	Right Clavicle	N/A	Single	N/A	-9020	74.4	-0.248
SU-S	Upper Sternum	N/A	Single	N/A	-2947	115.4	-0.195
SL-RA	Lower Sternum	N/A	Rosette	N/A	-2109	70.1	-0.058
SL-RB	Lower Sternum	N/A	Rosette	N/A	-7683	132.7	-0.316
SL-RC	Lower Sternum	N/A	Rosette	N/A	7729	84.2	0.300
R2L-S3	Left Side	2	Single	3	20681	72.8	0.531
R3L-S1	Left Side	3	Single	2	-8174	61.7	0.520
R3L-S2	Left Side	3	Single	3	33641	92.2	0.682
R3L-R3A	Left Side	3	Rosette	3	2593	119.7	0.034
R3L-R3B	Left Side	3	Rosette	3	3095	111.0	0.058
R3L-R3C	Left Side	3	Rosette	3	-3954	93.7	-0.069
R4L-S1	Left Side	4	Single	1	-7257	50.2	-0.301
R4L-S2	Left Side	4	Single	2	9028	49.1	0.385
R4L-S3	Left Side	4	Single	3	9139	49.2	0.350
R5L-S1	Left Side	5	Single	1	-17193	50.3	-0.468
R5L-S2	Left Side	5	Single	2	3008	45.5	0.129
R5L-R3A	Left Side	5	Rosette	3	6326	47.6	0.218
R5L-R3B	Left Side	5	Rosette	3	10109	47.5	0.460
R5L-R3C	Left Side	5	Rosette	3	7025	47.0	0.364
R6L-S3	Left Side	6	Single	3	12211	46.9	0.547
R7L-R3A	Left Side	7	Rosette	3	-3124	61.4	0.252
R7L-R3B	Left Side	7	Rosette	3	11357	46.1	0.491
R7L-R3C	Left Side	7	Rosette	3	8260	45.4	0.547
R8L-S3	Left Side	8	Single	3	-5254	51.7	0.275
R9L-R3A	Left Side	9	Rosette	3	n/a	n/a	n/a
R9L-R3B	Left Side	9	Rosette	3	-6217	621	0.320
R9L-R3C	Left Side	9	Rosette	3	3523	54.5	0.184
R10L-S3	Left Side	10	Single	3	9297	73.1	0.316

Rib Fracture Identification

The rib fractures locations were determined by performing a post-test injury analysis on each cadaver using a detailed necropsy of the thorax. The fracture locations were photographed and documented for each cadaver. The time of fracture was determined from the plots of strain gage output vs. time (Figure 4). The male cadaver sustained 12 fractures on 12 ribs [8 on the left, 4 on the right], as well as one fracture on the right clavicle (Figure 5). For the female cadaver, 20 rib fractures were detected on 12 ribs [14 on the left, 6 on the right] as well as one fracture to the sternum (Figure 6). The strain rates seen by the ribs of the male cadaver that fractured varied from 0.133 to 0.648 (strain/s), and from -0.581 to 0.559 (strain/s) for the female cadaver.

The male cadaver sustained two fractures directly under strain gages, and the female sustained 7. The fractures that occurred directly under gages are of particular interest because the peak strain at the time of fracture could be obtained from these gages.

In both cadavers, all rib fractures occurred within the first 35% compression of the thorax (Figure 7, Figure 8). As a general trend, the first series of fractures were on the left side of the thorax where the belt passed over the abdominal region. The ribs in the upper thoracic region on the right side fractured next.

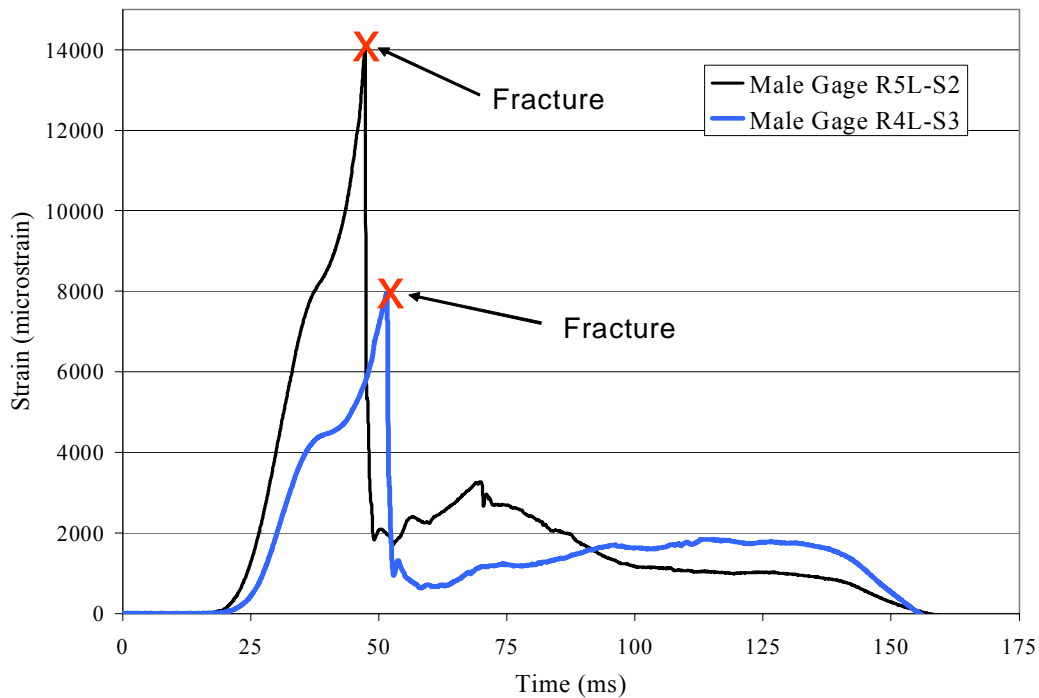


Figure 4. Determination of Rib Fracture Timing.

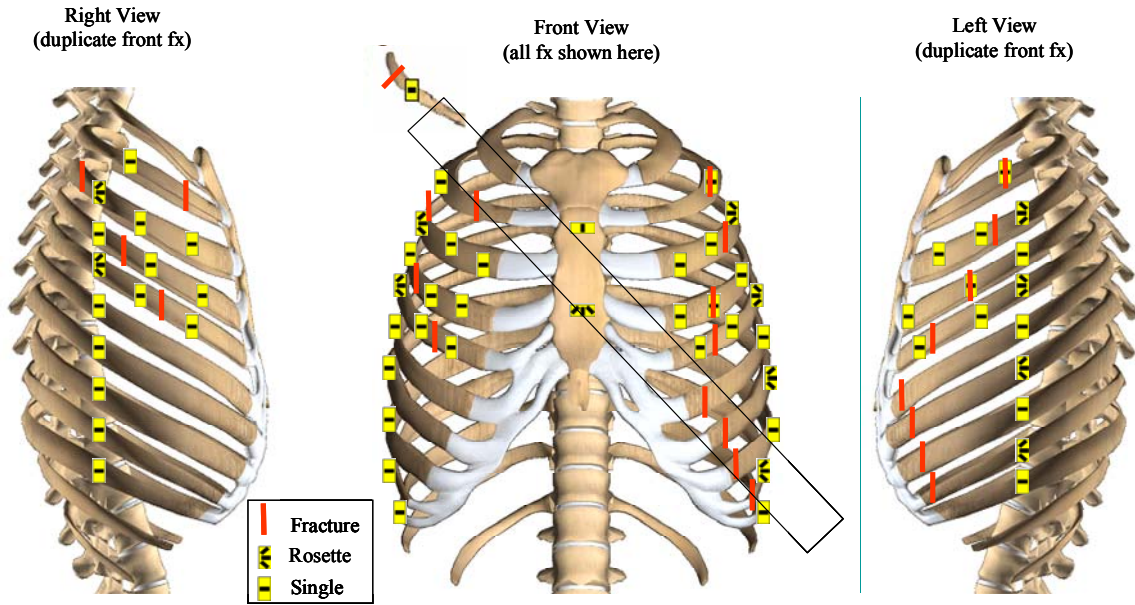


Figure 5. Location of Strain Gages and Fractures for Male Cadaver.

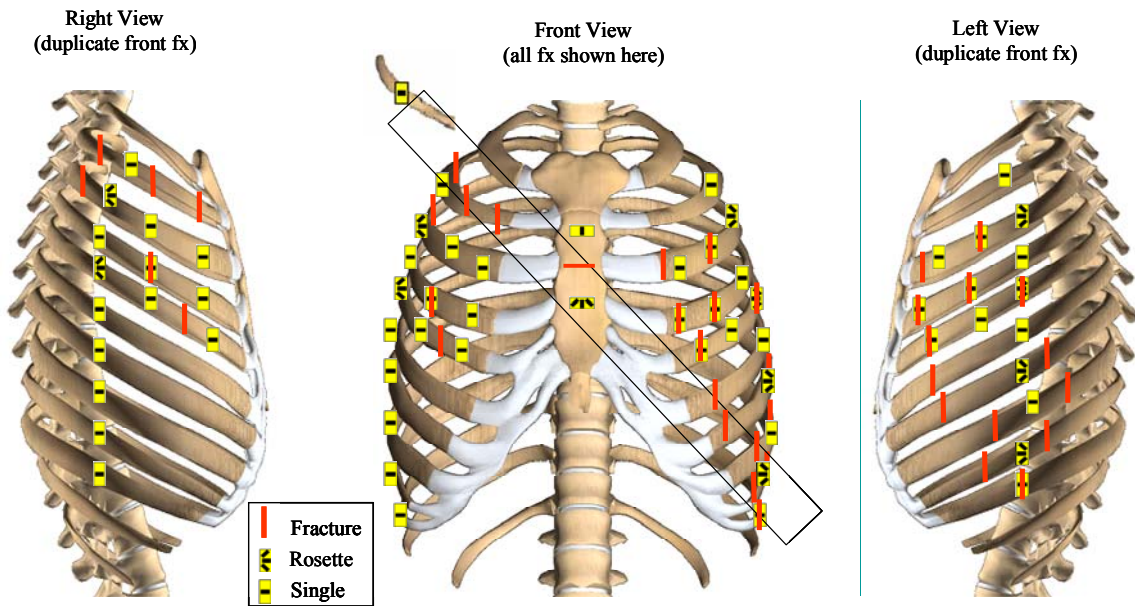


Figure 6. Location of Strain Gages and Fractures for Female Cadaver.

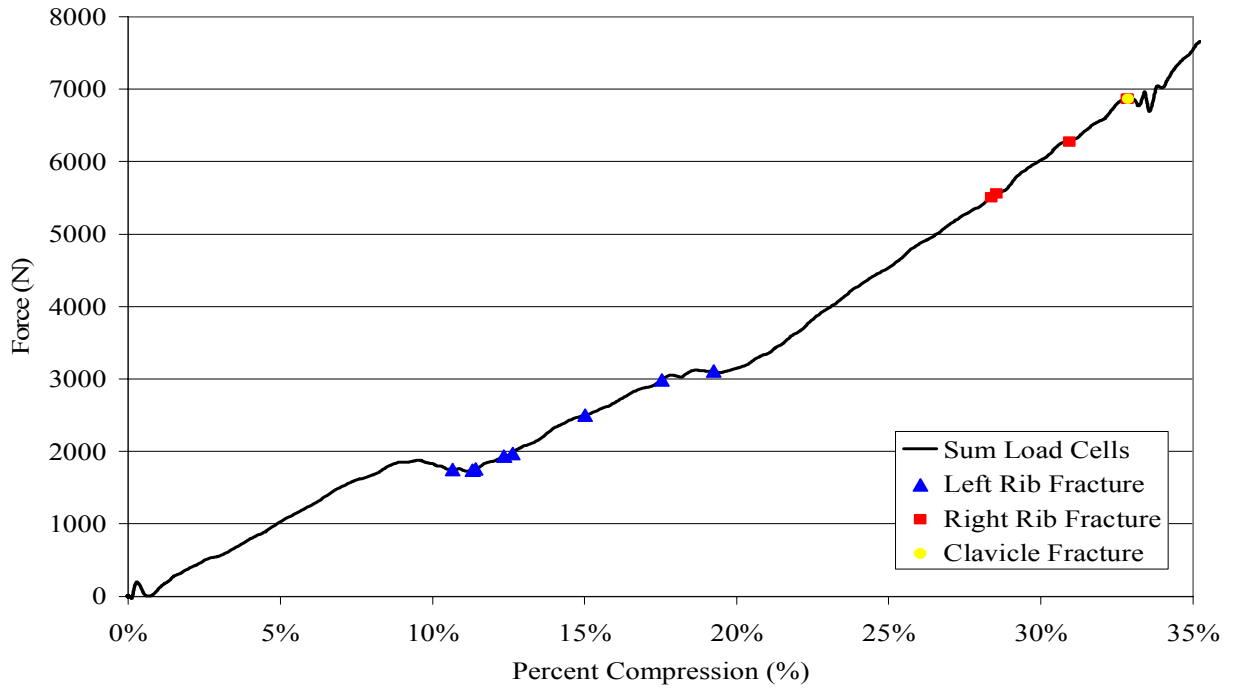


Figure 7. Rib Fracture Progression of Male Cadaver.

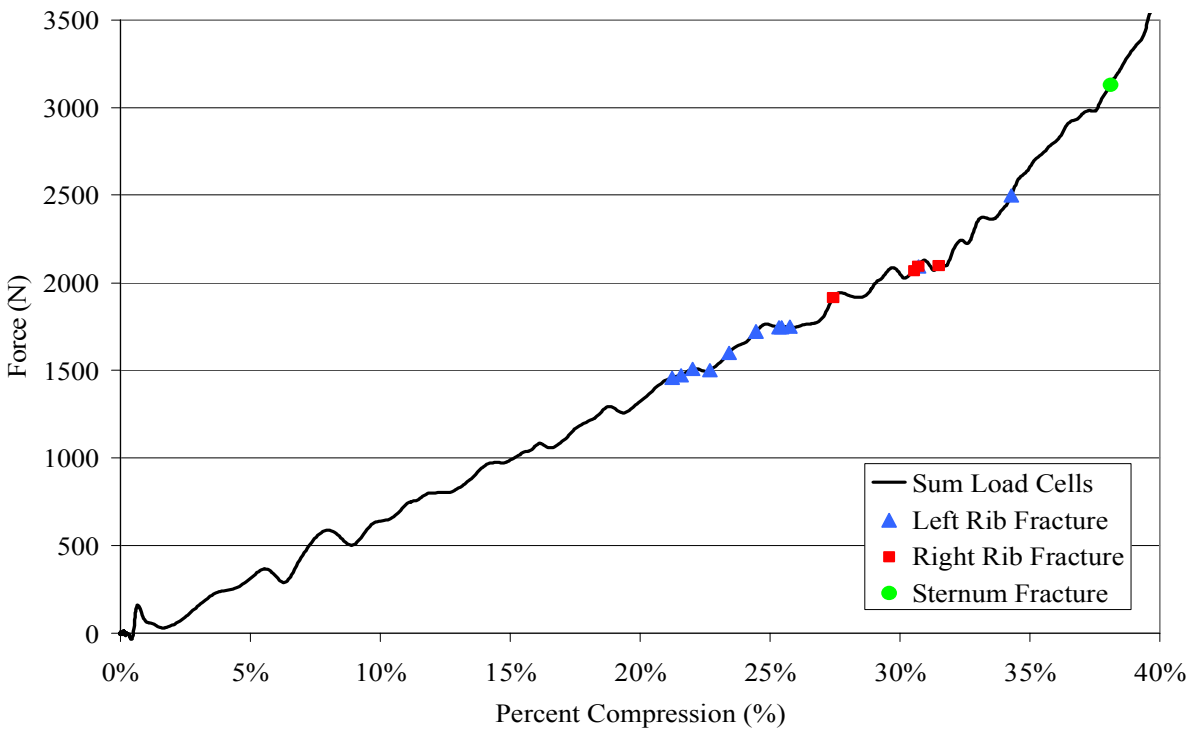


Figure 8. Rib Fracture Progression of Female Cadaver.

Principle Strain Results

The first principle strain, second principle strain, and the axial strain were plotted along with the angle from the axis of the rib to the first principal axis (Figure 9, Figure 10). In general, it was found that the first principle strain and the axial strain closely matched up to the time of the first fracture. In some cases the first principle strain and the axial strain continued to follow each other after the fracture and in other cases they did not. This could be due to either broken or damaged gages and or the complex loading seen after the fracture. The plots of first principle strain, second principle strain, axial strain, and theta for the other rosettes on the male and female cadavers are located in Appendixes A and B.

The maximum of the first and second principle strain before or at the first fracture were compared to the peak axial strain for each cadaver (Table 5, Table 6). The peak strains before or at the time of the first fracture were used because the strain could no longer be reported with confidence after the rib fractures due to the complexity of loading and possibility of damage to the gage. If no fracture occurred, then the strains reported were those that corresponded to the time at which the absolute maximum strain out of the three occurred. In some cases the rib was too small to adequately support all three gages of the rosette the data was suspect and thereby not reported in this section. Additionally, if one of more of the gages that composed each rosette broke during the test the data was omitted from this section.

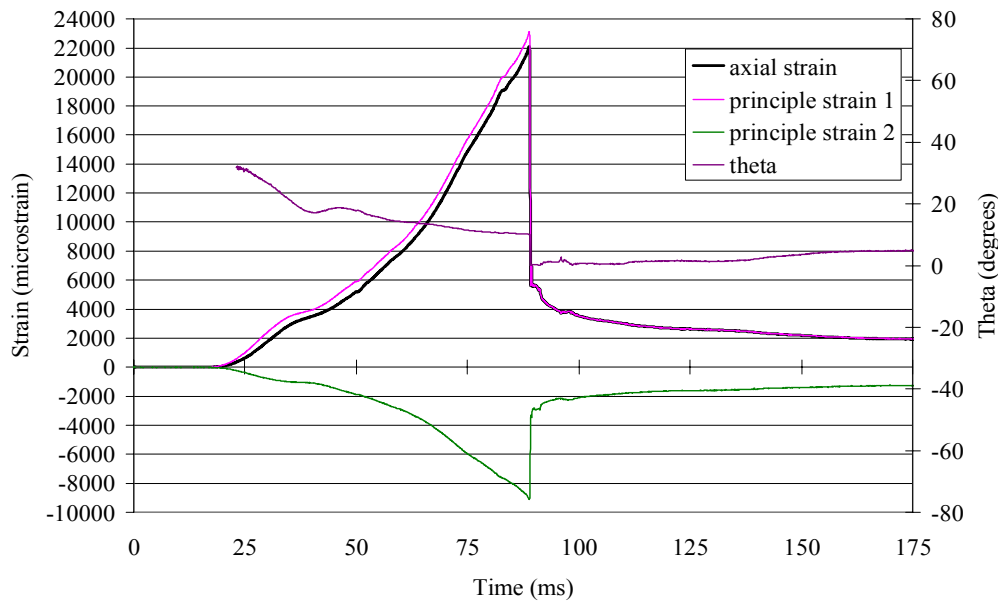


Figure 9.: Axial Strain, First and Second Principle Strain, and Theta vs. Time for Rosette R3R on the Male Cadaver.

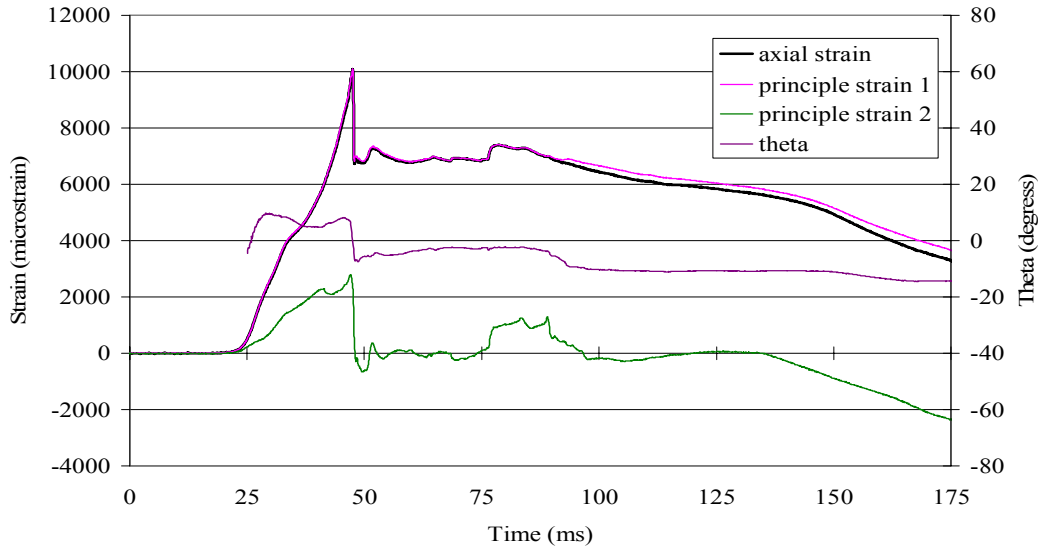


Figure 10. Axial Strain, First and Second Principle Strain, and Theta vs. Time for Rosette R5L on the Female Cadaver.

Table 5.

Comparison of Peak Axial Strain from Gage B of Rosette to Peak First Principle Strain for the Male Cadaver.

Rosette	Thorax Location		Peak Gage B Strain	Peak Principle Strain 1	Percent Difference	Peak Principle Strain 2	θ
R3R	Rib 3	Right Side	22111	23105	4.4	-8996	10.2
R5R	Rib 5	Right Side	8165	8223	0.7	-2465	3.8
R3L	Rib 3	Left Side	5890	6406	8.4	-636	-15.1
R5L	Rib 5	Left Side	6499	6661	2.5	-1605	-8.1
R7L	Rib 7	Left Side	6618	6773	2.3	-1792	-7.8
R9L	Rib 9	Left Side	3033*	3482*	13.8*	1844*	-17.0*

* = not measured at a time of fracture

Table 6.

Comparison of Peak Axial Strain from Gage B of Rosette to Peak First Principle Strain for the Female Cadaver.

Rosette	Thorax Location		Peak Gage B Strain	Peak Principle Strain 1	Percent Difference	Peak Principle Strain 2	θ
R3R	Rib 3	Right Side	5246	6142	15.7	-1581	19.9
R5R	Rib 5	Right Side	4641	4986	7.2	-3386	10.8
SL	Sternum	Lower	-4860*	12819*	444.3*	-5864*	76.6*
R3L	Rib 3	Left Side	2046	2325	12.8	-896	-18.1
R5L	Rib 5	Left Side	10109	10109	0.0	2735	0.1
R7L	Rib 7	Left Side	11357	11881	4.5	-674	12.6

* = not measured at a time of fracture

DISCUSSION

The reaction force data was plotted vs. percent chest deflection data for these tests with the fracture timing and corresponding Abbreviated Injury Scale (AIS) score (Figure 11, Figure 12). This was used to compare the definition of an AIS=3 for the human rib cage as defined by NHTSA to the injury criteria for an AIS=3 for the 50th percentile male and 5th percentile female hybrid III dummies. An AIS=3 for the rib cage was defined to be greater than 3 rib fractures on one side of the ribs and no more than 3 on the other side. NHTSA has defined the injury criteria of the 50th percentile male dummy as a chest

deflection of 63 mm, which corresponds to a 28%-30% percent chest deflection. The injury criteria for the 5th percentile female hybrid III dummy has been defined as a chest deflection of 52 mm which corresponds to a 22%-24% percent chest deflection. The range of percent chest deflections is due to the variations in dummy chest thickness as a result of tolerances set by the manufacturer, Denton ATD. As seen in Figures 4.2-1, and 4.2-2, an AIS= 3 occurred at 13% chest deflection for the male and 23% chest deflection for the female.

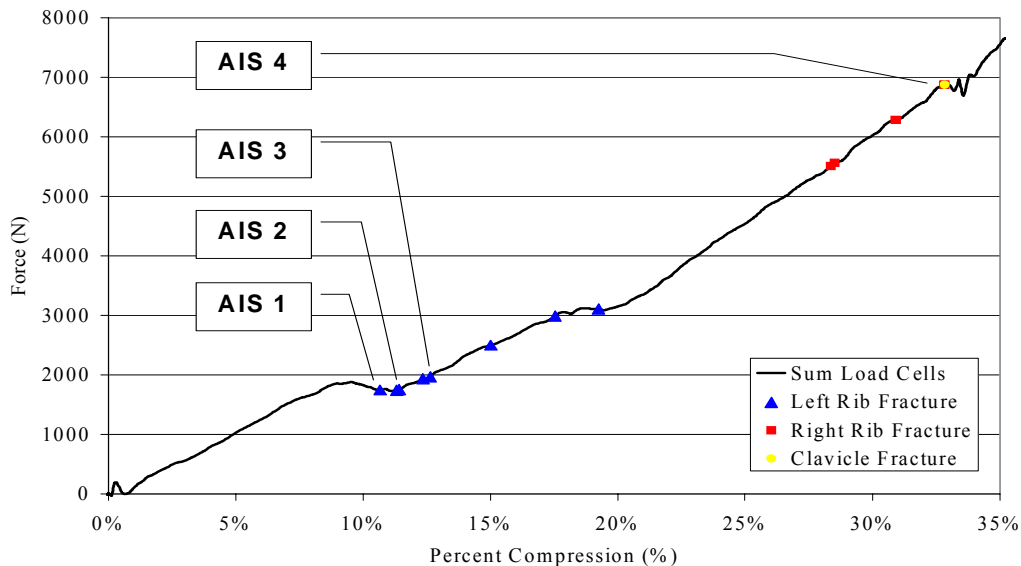


Figure 11. Rib Fracture Progression of Male Cadaver with AIS Levels.

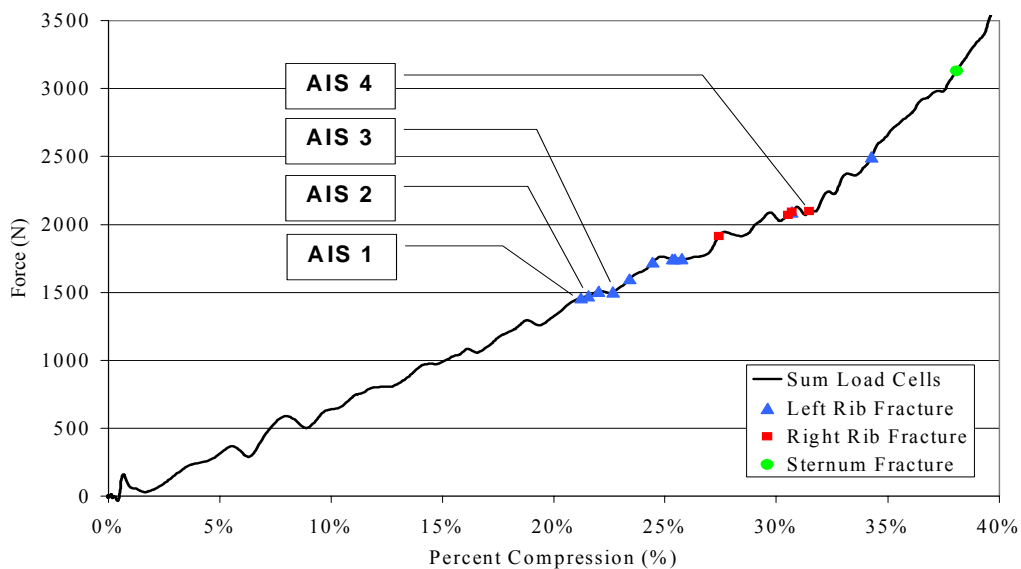


Figure 12. Rib Fracture Progression of Female Cadaver with AIS Levels.

Effective Stiffness

The thoracic testing conditions presented in this paper are similar to that presented by Kent [11] in that they present thoracic data due to diagonal belt loading at a rate that corresponds to the thoracic loading rate seen in a 48 km/h crash. Kent determined the effective stiffness of the thorax under these conditions by performing a linear regression of the force vs. percent deflection plots. These effective stiffness values for the male tests varied from 6,459-9,919 (N/ % deflection) and from 7,102-15,420 (N/ % deflection) for the female. The same method was performed on the force vs. percent compression data presented in his paper before the first fracture occurred. The effective stiffnesses for the male and female tests presented in the current study at Virginia Tech were 19,449 and 6,624 (N/ % deflection). However, there were large oscillations in the Kent data that were seen in the initial ramp up region of the force graphs such that the force fell below zero during these oscillations. This suggests a tension force while the thorax was being compressed. Therefore, the Kent data is likely lower than actual response during the initial loading phase.

CONCLUSIONS

The novel strain gaging technique presented in this report, in which the thorax was instrumented with the exception of a few gages, were usually the rosette element gages not aligned with the axis of the rib (i.e. gages A, and C), the clavicle gage, or the gages on the sternum.

The strain rates varied from gage to gage and from rib to rib for each cadaver. The strain rates sustained by the ribs ranged from -0.376 to 0.880 (strain/s) for the male cadaver and from -0.468 to 0.547 (strain/s) for the female cadaver.

The comparison of principle strain to axial strain resulted in four important findings. One, all the ribs with strain gage rosettes failed in tension. Second, the first principle strain was greater than or equal to the axis strain. However, the difference in values was small until the time of the fracture and therefore the value of theta (θ) was small. This meant that the direction of the first principle strain was not very far away from the axis of the rib. Third, the second principle strain was less than or equal to the axial strain, and in most cases was in negative (compression). Fourth, the confidence in the principle

with 47 single axis and rosette strain gages, has allowed for the precise determination of the time of fracture for each rib for the first time in the history of thoracic research. In addition, for the first time the exact point at which the different thoracic AIS scores occurred could be identified with the time of rib fracture data.

All rib fractures occurred within the first 35% compression of the thorax for both cadavers, and were side dependant for both cadavers. The first series of fractures were on the left side of the thorax where the belt passed over the abdominal region. The ribs on the upper right hand side of the thorax fractured second.

The effective thorax stiffnesses for the male and female cadavers presented in this paper were 19,449 and 6,624 (N/ % deflection) respectively, which were similar to values reported by Kent (2001). However, the data presented in this report is linear due to the robust design of the Virginia Tech belt tester, it does not have the problems of oscillations.

The strain gage data showed that majority of the ribs sustained tensile loading until the time of fracture. The male and female cadaver had peak tensile strains ranging from 1,533 to 39,812 (μ strain) and 1,716 to 33,614 (μ strain) respectively. The gages that showed predominately compressive loading, strain after fracture was low. This was due to the complex loading that occurred in the broken rib as well as the possibility of the damage that could have been sustained by the gage itself.

REFERENCES

- [1] Alem, N.M., Bowman, B.M., Melvin, J.W., and Benson, J.B. (1978) Whole-body human surrogate response to three-point harness restraint. *Stapp Car Crash Journal* 22: 361-399. SAE 780895.
- [2] Cesari, D. and Bouquet, R. (1990) Behavior of Human Surrogates under Belt Loading. *Proc. 34th Stapp Car Crash Conference*, pp. 73-82, Society of Automotive Engineers, Warrendale, PA.
- [3] Cesari, D. and Bouquet, R., (1994) Comparison of Hybrid III and Human Cadaver Thoracic Deformations." *Proceedings of the 38th Stapp Car Crash Conference*, Paper 942209, Society of Automotive Engineers, Warrendale, PA.

- [4] Crandall, J.R., Bass, C.R., Pilkey, W.D., Miller, H.J., Sikorski, J., and Wilkins, M. (1997) Thoracic response and injury with belt, driver side airbag and force limited belt restraint systems. *International Journal of Crashworthiness* 2(1): 119-132.
- [5] Eppinger, R.H. (1976) Prediction of thoracic injury using measurable experimental parameters. *Proc. 6th International Technical Conference on the Enhanced Safety of Vehicles: 770-779.*
- [6] Kallieris, D., and Mattern, R. (1979) Shoulder belt forces and thorax injuries. *Proc. 7th International Research Council on the Biomechanics of Impact: 171-183.*
- [7] . Kallieris, D., Schmidt, G., Barz, J., Mattern, R., and Schulz, F. (1974) Response and vulnerability of the human body at different impact velocities in simulated three-point belted cadaver tests. *Proc. 2nd International Research Council on the Biomechanics of Impact: 196-209*
- [8] Kallieris, D., Zerial, P.D., Rizzetti, A., and Mattern, R. (1998) Prediction of thoracic injuries in frontal collisions. *Proc. 18th International Technical Conference on the Enhanced Safety of Vehicles: 1550-1563.*
- [9] Kent, R.W. (2002) Dynamic response of the thorax: Restraint specific hard tissue injury. Ph.D. Dissertation, University of Virginia.
- [10] Kent, R.W., Crandall, J.R., Bolton, J., Prasad, P., Nusholtz, G.S., and Mertz, H.J. (2001) The influence of superficial soft tissues and restraint condition on thoracic skeletal injury prediction. *Stapp Car Crash Journal* 45: 183-204. SAE 2001-22-0008.
- [11] Kent R., Sherwood C., Lessley D., Overby B., (2003). Age-Related Changes in the Effective Stiffness of the Human Thorax Using Four Loading Conditions. *International Research Council on the Biomechanics of Impact, Lisbon Portugal.*
- [12] Kroell, C., Schneider, D., Nahum, A., (1974) Impact Tolerance and Response of the Human Thorax II. Paper number 741187, Society of Automotive Engineers, Warrendale, Pennsylvania.
- [13] Kuppa, S.M., and Eppinger, R.H. (1998) Development of an improved thoracic injury criterion. *Stapp Car Crash Journal* 42: 139-154. SAE 983153.
- [14] L'Abbe, R., Dainty, D., Newman, J., (1982) An Experimental Analysis of Thoracic Deflection Response to Belt Loading." *Proceedings of the 7th International Research Council on the Biomechanics of Impact Conference, Bron, France, pp. 184-194.*
- [15] Morgan, R.M., Eppinger, R.H., Haffner, M.P., Kallieris, D., Miltner, E., Mattern, R., Yoganandan, N., Pintar, F.A., Sances, A., Kuppa, S.M., Sharpless, C.L., Crandall, J.R., Pilkey, W.D., and Klopp, G.S. (1994) Thoracic trauma assessment formulations for restrained drivers in simulated frontal impacts. *Stapp Car Crash Journal* 38: 15-34. SAE 942206.
- [16] Patrick, L.M., Anderson, A., and Bohlin, N. (1974) Three-point harness accident and laboratory data comparison. *Stapp Car Crash Journal* 18: 201-282. SAE 741181.
- [17] Ramet, M., and Cesari, D. (1979) Behavior of restrained dummies and cadavers in frontal impacts. *Proc. 7th International Research Council on the Biomechanics of Impact: 210-219.*
- [18] Stitzel J.D., Cormier J. M., Barretta J.T., Kennedy E. A., (2003). Defining Regional Variation in the Material Properties of Human Rib Cortical Bone and its Effect on Fracture Prediction. *Stapp Car Journal, 47.*
- [19] Stitzel J.D., Cormier J. M., Barretta J.T., Kennedy E. A., (2003). Elderly Thorax Properties for Model Development. IBL Report Number 2003-020, Virginia Tech.
- [20] Viano, D.C. (1978) Thoracic injury potential. *Proc. 6th International Research Council on the Biomechanics of Impact: 142-156.*

CHALLENGES IN THE DEVELOPMENT OF A REGULATORY TEST PROCEDURE FOR NECK PROTECTION IN REAR IMPACTS: STATUS OF THE EEVC WG20 AND WG12 JOINT ACTIVITY

D Hynd

TRL Limited, UK
On behalf of EEVC WG20

M van Ratingen

TNO Science and Industry, NL
On behalf of EEVC WG12

Paper Number 05-0048

ABSTRACT

A new EEVC Working Group, WG20 (Rear Impact test procedure(s) and the mitigation of neck injury), was given the task to develop test procedures for rear end collisions, with a prime focus on neck injury reduction (whiplash). The work is carried out in collaboration with the EEVC WG12 (Advanced Anthropometry Adult Crash Dummies). WG20 is responsible for the definition of the test conditions and the overall coordination of this activity. WG12 is responsible for the selection of an appropriate crash test dummy and identification of biomechanically based injury criteria with known injury risk functions.

WG20 carried out a review of field accident data, clinical data, available sled test methods, biomechanical research on injury causation and human subject dynamic response, proposed injury criteria, available impact dummies, and instrumentation and dummy positioning methods. The findings of the WG20 review provide the basis for the future work of the group and are summarised here.

WG20 has a work programme to develop and validate a test procedure to assess the geometry of head restraints as a first stage in their approach to whiplash injury mitigation. In the longer term a sled-based dynamic assessment of injury risk or seat performance will be developed and validated.

WG12 has defined draft biofidelity requirements for rear impact crash test dummies and will evaluate the available rear impact dummies against these requirements once they are finalised. This paper summarises the chosen biofidelity requirements and the criteria by which they were selected. It also outlines the further work programme of the group to evaluate and validate biomechanically based injury criteria for rear impact crash testing.

INTRODUCTION

No regulatory test exists in Europe to assess injury risk in rear impacts, in particular low severity rear impacts. A number of accident studies and claims statistics coming from the insurance industry clearly indicate that low-speed rear impact can lead to neck injuries causing long-term disablement and discomfort. These injuries, often referred to as whiplash injuries, are usually classified as AIS 1 (Abbreviated Injury Scale).

Outside of the regulatory framework a number of organisations have been investigating WAD injury (Whiplash Associated Disorder). Two EC projects have supported some areas of this work. A rear impact, sled based test procedure, against which to assess vehicle seats has been proposed to GRSP and ISO. As of the year 2000, the EEVC had not developed a viewpoint on rear impact and WAD type injury. As a result, the EEVC Steering Committee asked EEVC WG12 to create an *ad hoc* Working Group to investigate the possibility of developing an EEVC view on rear impact and WAD injury.

The *ad hoc* Group [EEVC WG12, 2002] found that there was a significant amount of research data available and that interesting and promising research projects were ongoing. It recommended that the EEVC Steering Committee start up a new activity with the aim of developing a proposal for a new European regulatory test for whiplash injury (AIS1 neck injury) protection in rear impacts.

The EEVC Steering Committee formed a new Working Group, WG20, to develop and evaluate a test procedure, or range of test procedures, suitable for regulatory use. The test procedures should have a prime focus on neck injury reduction, but should give due regard to the potential for injuries to other body regions. The EEVC Steering Committee also gave WG12 additional terms of reference regarding the selection of an appropriate crash dummy and injury criteria for a rear impact test procedure.

This paper will summarise a state-of-the-art review of rear impact accidents and injuries undertaken by the members of EEVC WG20. This review will form the basis for the further work of the Group. The paper will also summarise the work of WG12 to develop biofidelity requirements for a rear impact dummy and to evaluate the suitability of existing dummies that have been proposed for use in rear impact test procedures.

Finally, the paper will outline the further work programmes of the two Groups.

EEVC WG20 STATE-OF-THE-ART REVIEW

As its first action, EEVC WG20 undertook a review of the current state of knowledge on rear impact accidents and injuries. This review built upon and updated the work of the WG12 rear impact *ad hoc* group [EEVC WG12, 2002]. A summary of the findings of the review is given in the sections below.

Accident Data and Insurance Statistics

From accident data and insurance statistics the impact severity in rear impacts is relatively well known, both when the occupants are uninjured and when they report whiplash injury. From crash recorder data at Folksam, obtained from a single make of car, it was found that long-term WAD symptoms are rare at mean accelerations below 3 g [Krafft *et al.*, 2001; Krafft *et al.*, 2002; Kullgren *et al.*, 2003]. The finding is also supported by several volunteer test studies [McConnell *et al.*, 1995; Ono and Kaneoka, 1997; Siegmund *et al.*, 1997]. Based on accident statistics from several countries, the majority of whiplash injuries are reported in crashes at medium impact severity, typically at a change of velocity between 10 and 15 km/h. Women have about twice the injury risk compared to men [Krafft, 1998; Hell *et al.*, 1999; Ydenius and Kullgren, 2001; Berglund, 2002]. Most of the reported injuries were short-term injuries where the occupants recovered within a couple of weeks [Spitzer *et al.*, 1995].

Furthermore, there is knowledge regarding the impact severity when occupants sustain more long-term WAD symptoms. Based on crash recorder data from real world accidents (from a single car make), the average change of velocity and the mean acceleration was quantified [Krafft *et al.*, 2001]. Those injuries leading to WAD symptoms lasting more than one month was found to occur at approximately 20 km/h and 5 g respectively, while those recovering within a month had approximately 10 km/h and 4 g respectively. The average values for occupants classified as WAD Grade 2 and 3 [Spitzer *et al.*, 1995] was approximately 16 km/h

and 5 g. Therefore a proposed test speed and acceleration will vary, depending on whether the test is focusing on all reported whiplash injuries or on the more severe ones.

At higher impact speeds there is an increased risk of uncontrolled seat back deflection or failure, with an attendant risk of serious injuries. A seat-back deflection test or a high-speed test could be added to cover this situation. To ensure that sub-optimisation is avoided, a low severity test could also be added.

Current accident data show similar trends world wide (except deviations from different social security and insurance systems in various countries).

Biomechanics

WAD injury symptoms are well documented, but the injuries causing the acute symptoms are not completely known. The relation between acute injury and chronic pain is also not fully understood. The kinematics of the head and neck during rear impact is relatively well known. Derived from the known kinematics, a number of biofidelity requirements have been formulated and were used as a basis for the development of several rear impact dummies.

Several injury criteria have been suggested. Three principal ways of verifying injury criteria were identified:

1. By identification, in the clinic, of the actual acute injury that causes chronic pain. This would probably tell us which injury mechanism is the cause and give an indication as to which injury criterion to use.
2. An alternative would be to evaluate proposed criteria against experimental data where certain injuries have been caused and where injury threshold levels can be identified (this will however leave an uncertainty about the relationship between the observed injuries and the symptoms experienced by living patients).
3. By high quality evaluation of injury criteria against field accident data. Reconstruction crash tests and computer modelling may be used in parallel.

Some currently proposed injury criteria are acceleration based, like NIC [Boström *et al.*, 2000]; velocity based (T1 rebound velocity); displacement based like, for instance, IV-NIC [Panjabi *et al.*, 1999] and NDC [Viano and Davidsson, 2001]; or load based, like N_{km} [Muser *et al.*, 2000] and LNL [Heitplatz *et al.*, 2003]. A few of these proposed injury criteria, e.g. NIC, have been used in different versions and this must be taken into account when

making comparisons. The International Insurance Whiplash Prevention Group (IIWPG) uses a combination of such measurements in a seat performance criterion. An injury criterion that correlates to injury risk is a requirement for a future test procedure. It would however be possible to identify such a criterion even if the injury and injury mechanism is not fully known. (Medical symptoms can often be treated even if the origin of the symptom is not fully understood.) The term WAD Risk Assessment Parameters (WAD-RAP) was introduced as a replacement for “injury criteria” in the present situation where the actual injury causing the WAD symptoms is unknown.

From a regulatory perspective it is essential that there is a good correlation between the WAD-RAP and risk. Any given WAD-RAP should be accompanied by a risk function. Some recent findings, verified according to method 3 above, indicate that N_{max} and N_{km} fulfil these requirements [Eriksson and Kullgren, 2003; Linder *et al.*, 2004]. These findings are based on data from a few Toyota car models. A wider data sample covering more car models as well as an evaluation of the applicability of the criteria in sled testing would be desirable.

Dummy Development

Currently, the dummies that are most likely to be useful for rear impact testing, are the BioRID II [Davidsson *et al.*, 1999] and the RID2 [Cappon *et al.*, 2001] or RID^{3D} [Cappon *et al.*, 2003]. Each of these has been based on a different set of biofidelity requirements [Philippens *et al.*, 2002]. A third alternative for rear impact is the American frontal impact dummy prototype, THOR, which has been evaluated with partly promising results. The BioRID II has the advantage of being more established and more widely used in automotive industry, while the RID is more recently released. The prototype RID^{3D} is a further development of the RID2 with improvements in the rebound phase and in ramping. One advantage of the RID2 / RID^{3D} is that it has a slightly more comprehensive instrumentation capability, with a lumbar load cell, and is intended to be able to handle oblique impacts.

All three dummies still have practical limitations, which are likely to be solved throughout the course of their use. There is an ongoing world wide evaluation of the dummies, which has led to stepwise adjustments. This process is expected to make them acceptable for use in a regulatory framework. Appropriate setting up and certification procedures are also evolving during this evaluation process. The Hybrid III, although it is being used world wide, is not considered suitable for low

severity rear impact testing due to its limited biofidelity in low-speed rear impact conditions [Philippens *et al.*, 2002].

For head restraint geometry evaluation the H-point machine was extended with a Head Restraint Measuring Device (HRMD) which is used in a rating procedure by the Research Council for Automobile Repairs (RCAR) [RCAR, 2001]. Various versions of the H-point machine exist and the difference between the versions requires investigation.

Car and Seat Design

Vehicle structures are reported to have become stiffer since the mid 1990s and this trend in increasing stiffness is continuing [Muser *et al.*, 2000; Avery and Zuby, 2001]. This may be due to enhanced crash performance driven by, among other requirements, the low speed insurance impact test and high speed frontal impact regulatory and consumer tests, and may have led to an increase in whiplash type injuries. Although some attempt could be made at the local softening of perimeter structures of the vehicle, the biggest gains in mitigating whiplash injuries are expected to come from the enhancement of seat back and head restraint performance.

Within seat design, good head restraint geometry has been shown to be important in mitigating soft tissue neck injuries [Farmer *et al.*, 1999], although occupant kinematic control and effective energy management have also been shown to be of importance. Seat back yield-strength has increased and along with other parameters is coincident with a rise in reported injuries. Current research suggests that where high seat back yield strength is used in conjunction with ‘good’ head restraint geometry a reduction in injuries is observed.

New, improved head restraint and seat systems have been shown to be effective at improving the neck injury protection in terms of a reduction in insurance claims. For such systems to be effective, energy absorbing capability could be employed to reduce occupant energy whilst controlling head and thorax motion, and good head restraint geometry could be utilised to control head kinematics early in the crash event (by gaining early contact between head and head restraint).

Any future dynamic whiplash test assessment may have to feature a range of impact velocities to prevent sub-optimisation of these systems.

Test Procedures

Several proposals for procedures for whiplash protection assessment in rear impact have been proposed or implemented in different fora (e.g. ISO, IIWPG, SRA, ADAC, EuroNCAP, NHTSA) in recent years. Static as well as dynamic test procedures have been developed. Most of the test procedures have the same origin and are gradual upgrades that have been included as new knowledge has become available.

Most of the procedures include a dynamic sled test of the seat using a modern rear impact dummy. The speed changes proposed are typically 15 to 16 km/h, and in some cases additional tests in the range 10 to 30 km/h have been proposed. The low-speed tests are intended to avoid sub-optimisation and the high-speed tests are proposed for evaluating seat integrity. Currently, a generic acceleration pulse is commonly used and several injury criteria or assessment parameters have been suggested. A static geometrical head restraint rating is currently used by RCAR [RCAR, 2001].

Ongoing and Finalised Research Programmes

A number of ongoing or finalised research initiatives, relevant for the development of a rear impact test procedure, were identified:

- EU Whiplash I (finished);
- EU Whiplash II (on going at the time of the review, now finished);
- Swedish research programs (Chalmers University, Folksam, Swedish Road Administration, Volvo Car, Saab Automobile);
- The International Insurance Whiplash Prevention Group (IIWPG). The objective of this working group is to develop dynamic test procedures to evaluate and compare seat/head restrain designs;
- ISO (on going). A test procedure was finalised during 2004, but it does not include a decision on a crash dummy nor on any injury criterion;
- OSRP/USCAR (on going). The Occupant Safety Research Partnership of the United States Council for Automotive Research has conducted a rear impact evaluation program to compare the BioRID II and Hybrid-III dummies;
- NHTSA is working on upgrades of FMVSS 202 and 203. An evaluation of the currently available dummies was carried out;
- UK spinal injury: volunteer and dummy testing plus human and dummy modelling, including the derivation of design target corridors;
- ACEA: repeatability and reproducibility of proposed rear impact whiplash protection test procedures.
- Examples of other active research laboratories:
 - TU Graz, Austria
 - Allianz ZT, Germany
 - ETH, Switzerland
 - Medical College of Wisconsin, USA: PMHS tests, thesis on facet injury mechanism
 - Wayne State University, USA: PMHS tests, thesis on facet injury mechanism
 - JARI, Japan: volunteer tests, thesis on facet injury mechanism
 - MacInnis Engineering, Canada: volunteer tests, dummy evaluation

Conclusions from the State-of-the-Art Review

- Rear impact and WAD-type (Whiplash Associated Disorder) injury is a serious problem in terms of both injury and cost to society. A lot of work has taken place in trying to quantify the problem and determine effective means of injury and cost reduction. The WAD symptoms are well documented, but the actual injury remains to be established, although several injury locations and injury mechanisms have been suggested. The dynamic motion of the human head-neck system during a low-speed rear impact is known from volunteer test data.
- To date, several special test dummies and test devices have been developed for the assessment of WAD injury and several test procedures have been developed, both static and dynamic.
- Both mean and peak acceleration appear to be important crash severity parameters together with delta-v.
- Women have about twice the injury risk compared to men.
- Energy absorbing seats, active head restraints and good head restraint geometry all seem to be beneficial, based on claims evidence.
- Multiple test severities must be considered to avoid optimisation for a single condition and to test seat integrity at higher severity.
- The proposed WAD risk assessment parameters NIC_{max} and N_{km} appear to correlate to real world risk of WAD causation and risk curves have been presented based on field accident findings from a limited number of car models from a single manufacturer. Further work is therefore needed before a WAD risk assessment parameter (LNL, N_{km} , T1-rebound velocity, NIC, NDC, IV-NIC, etc.) can be finally established. The exact injury site has still not been established and thus, no biomechanical explanation to the injury causation is available. A biomechanical evaluation of an injury criterion is not expected in the near future.

- Injuries other than neck injuries and impact types other than pure rear impacts need to be considered in the definition of the test procedure.
- The BioRID II and the RID2/RID^{3D} are the best suited dummies for rear impact whiplash prevention testing.

EEVC WG12 REAR IMPACT DUMMY BIOFIDELITY REQUIREMENTS

In order to respond to the request by the EEVC Steering Committee to select an appropriate dummy and injury criteria for the WG20 rear impact test procedure, WG12 adopted a work plan consisting of the following steps:

- Identification of the expected use of the dummy in the new test procedure, and the constraints following from this for the dummy such as anthropometry, reproducibility, durability, required adjustments, and so forth;
- Development of biofidelity impact response requirements for low severity rear impact loading of the spine (including the rebound phase), defining how the dummy should behave both in kinematic and dynamic responses in agreement with human volunteers and/or PMHS;
- Review of biomechanical evidence that may support the use of various injury criteria for neck injury assessment, including definition of measurements to be taken by the dummy;
- Review of existing dummy designs and performance with respect to the requirements developed by WG12. This will lead to a recommendation on the best dummy to use for the WG20 rear impact test procedure.

Rear Impact Dummy Biofidelity Requirements

Of these tasks, the development of biofidelity requirements for a rear impact dummy is the most advanced. The criteria for the selection of rear impact biofidelity test conditions included:

- The availability of the full data set;
- Quality of the test set-up and instrumentation;
- Reproducibility;
- Relevance of the test conditions, loading condition and velocity change;
- Distribution of subject anthropometry, gender and age;
- The number of tests and test subjects.

Nineteen sets of rear impact volunteer and PMHS data that could be used to define biofidelity requirements for a rear impact dummy have been assessed. To date, five data sets have been chosen and documented in detail. They include four volunteer and one PMHS test programme with a

variety of impact conditions. Even this small sample of biofidelity test conditions gives rise to a large number of biofidelity requirements. The draft biofidelity test conditions and requirements are summarised below.

GDV / Allianz (Whiplash II)

GDV and Allianz undertook two series of five rear impact sled tests with five volunteers, two male and three female, as part of the Whiplash 2 EC project. The mean age of the subjects was 35 years (18 to 43), their mean height was 1.67 m (1.57 to 1.78 m) and their mean mass was 74 kg (60 to 95 kg). The impacts had a delta-v of 7 and 9 km.hr⁻¹, with a peak acceleration of 35 and 40 m.s⁻¹ respectively.

A specially designed yielding seat, with a head restraint, was used (see Figure 1). Accelerometers and film markers were attached to the head and T1. Head angular accelerations were also measured.



Figure 1: The GDV / Allianz sled, volunteer and yielding seat.

Response parameters included:

- Head centre of gravity (CG) trajectory (2D)
- Head flexion angle
- T1 trajectory (2D)
- T1 flexion angle
- Head CG acceleration
- Head angular acceleration
- T1 acceleration

JARI

These volunteer tests were carried out 1997 and 1998 at the Japanese Automobile Research Institute (JARI) and are summarised in [Davidsson *et al.*, 1999]. Seven healthy male volunteers (25 ± 4 years old) of approximately 50th percentile stature were exposed to a total of 28 rear impact deceleration sled tests at delta-v's of 1.9 to 2.6 m.s⁻¹ (7.0 to 9.3 km.hr⁻¹) and mean peak decelerations of 36.2 to 39.0 m.s⁻².

Both standard car seats (13 tests) and a rigid ECE Regulation 16 bench (15 tests) were used. In 22 tests a standard driving posture was used (see Figure 2) and in six tests the subject was leaning forward 10° from the standard driving posture at the time of impact. No head restraint was used in any of the tests.

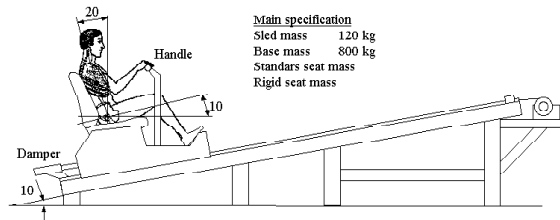


Figure 2: Schematic of the JARI sled, volunteer and Regulation 16 seat.

Film markers were mounted at the head, T1 sternum and iliac crest, and accelerometers were fitted to the head and T1. The location of the accelerometers and film targets (except the iliac crest marker) relative to the occipital condyle was determined from X-ray images of the instrumented volunteer. A Tekscan pressure sensor mat with 48 x 40 cells each 10 x 10 mm square covered the seat back surface.

Biofidelity requirements (mean \pm σ) were developed for:

- Linear and angular displacements of the head, T1, occipital condyle and iliac crest;
- Head angular acceleration and T1 and pelvis linear accelerations
- Upper neck forces and moments.

TRL

TRL performed a series of rear impact tests with ten male volunteers with a mean age 26.4 years, height of 1.79 m and weight of 77.5 kg [Roberts *et al.*, 2002; Hynd *et al.*, 2004]. A rigid seat based on the ECE Regulation 44 bench was used, with the seat back raised to support the shoulders and a head restraint added (Figure 3).

A sled-to-sled impact system was used, with a block of aluminium honeycomb used between the sleds to give the desired acceleration pulse. The delta-v was 1.9 m.s⁻¹ (7 km.hr⁻¹) and the acceleration was limited to approximately 20 m.s⁻².

Film markers and accelerometers were placed on the head and T1 and an accelerometer was placed on the sacrum. Seat back and head restraint inertia-compensated forces were measured and a Tekscan 5315 mat was used to measure seat back pressure distribution.

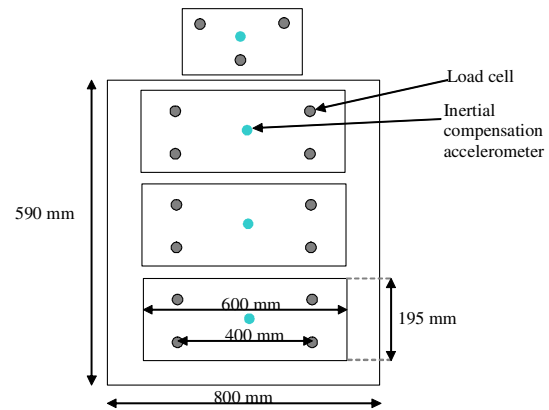


Figure 3: Schematic of the TRL seat back and head restraint, showing the force plates, load cells and inertia compensation accelerometers.

Biofidelity corridors were developed according to the method of EEVC WG9 [Roberts *et al.*, 1991]. Corridors were developed for:

- Head and T1 linear and angular displacements;
- Head, T1 and pelvis linear accelerations.

Seat back pressure distributions versus time are also available for qualitative assessment of the seat back interaction of rear impact dummies.

Allianz ZT / Chalmers

The kinematic responses of four volunteer subjects (in five tests) with anthropometry close to the 50th percentile male were extracted from a larger database with 13 subjects (subset 7V) [Davidsson *et al.*, 1998]. A custom made seat (see Figure 4) was mounted on a stationary sled which was impacted by a second sled. The delta-v was 1.9 m.s⁻¹ (7.0 km.hr⁻¹), with a peak acceleration of the target sled of about 33 m.s⁻².

The seat back consisted of four stiff panels covered by 20 mm thick soft Tempur foam and 30 mm thick medium Tempur foam and all covered with the same cloth fabric as used in a Volvo car seat. The seat back and head restraint were all mounted on springs to give the same stiffness characteristics as a Volvo 850 car seat, and the seat base was a standard cushion from a 1993 Volvo 850.

Head, T1 and iliac crest accelerations were measured and film markers were placed on the seat back frame, head, T1, shoulder, upper torso, chest, knees and H-point.

The following biofidelity response requirements were defined (mean \pm σ):

- Head x and z displacement with respect to the sled co-ordinate system;
- T1 x and z displacement with respect to the sled co-ordinate system;
- Head relative to T1 x and z displacement;

- Head angular displacement with respect to the sled co-ordinate system;
- T1 angular displacement with respect to the sled co-ordinate system;
- Head relative to T1 angular displacement;

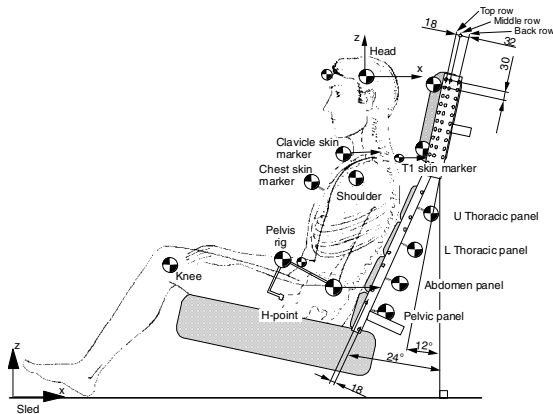


Figure 4: Schematic of the volunteer and AZT / Chalmers seat.

LAB (Whiplash I)

Six acceleration sled tests were performed with three different PMHS subjects [Bertholon *et al.*, 2000]. A rigid seat, without headrest, was subjected to a rear impact with an impact velocity of 10 km.hr⁻¹ and an acceleration of 160 m.s⁻² (Figure 5).

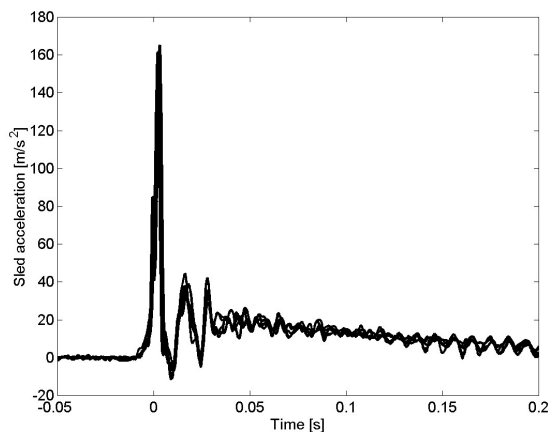


Figure 5: LAB sled acceleration pulse.

The subjects, all male, had a mean age of 80 years, height of 1.64 m and weight of 50 kg. The subject was strapped to the seat at the thigh, pelvis and thorax.

The subjects were instrumented with accelerometers on the head and film markers placed on the head, and T1. Biofidelity requirements (mean ± σ) were defined for:

- Head angle with respect to the sled co-ordinate system;
- Head angle with respect to a rotating T1 co-ordinate system;
- T1 angle with respect to the sled;
- Head CG x- and z-displacement with respect to a rotating T1 co-ordinate system;
- T1 x- and z-displacement with respect to the sled;
- Head CG x- and z-acceleration;
- Head angular acceleration.

Summary of Rear Impact Biofidelity Requirements

To date, five rear impact volunteer and PMHS test conditions have been selected by EEVC WG12 to define biofidelity requirements for rear impact dummies. The test conditions and biofidelity requirements, in the form of target corridors, are being documented in detail so that they can be reproduced with the candidate dummies for the WG20 rear impact test procedure.

FUTURE WORK

WG20

WG20 are considering the development of a geometric assessment of head restraints (which may be a static test, a dynamic test, or both) as a first stage in the mitigation of injuries in low-speed rear impacts. In the longer term, the Group will develop a sled-based test procedure for the dynamic assessment of seat performance.

Geometric Test Procedure

Several groups have raised concerns regarding the repeatability and reproducibility of the 3D-H machine and HRMD, used in some current test procedures for the static geometric assessment of head restraints. WG20 have planned a work programme to evaluate the variability in the geometric evaluation of head restraints using these tools and to isolate the sources of any variability. Potential sources of variability may be the test tools, the test procedure or variability in the seats. The programme will also assess the influence of lumbar support and seat back angle. A cost-benefit study of the implementation of a geometric requirement for head restraints in Regulation is also in progress. The EEVC Steering Committee have set a one year time frame for the development of a geometric test procedure.

Sled-based Test Procedure

The second, longer term task for WG20 is the development of a sled-based rear impact test

procedure. Issues that need to be considered in the development of such a procedure include:

- Impact pulse – vehicle specific or generic, delta-v and acceleration profile. These should be defined by knowledge of injury-causing real-world accident characteristics.
- Seat mounting and restraint systems – how the seat should be mounted to the sled (e.g., is it necessary to reproduce the vehicle floor pan accurately?), whether generic or vehicle-specific restraint systems, such as seat-belts and pre-tensioners, should be fitted and deployed.
- Cost-benefit analysis.

Recommendations on the dummy and injury criteria to be used for the test procedure will be made by EEVC WG12. A two year timescale for the development of a dynamic sled-based test procedure has been set by the EEVC Steering Committee.

WG12

Whiplash Dummy Selection

WG12 have been tasked with recommending a dummy for the WG20 rear impact test procedure. Rear impact biofidelity requirements have been drafted and the candidate rear impact dummies will be evaluated against these requirements. However, there are many requirements for a test tool other than biofidelity. The following will also be considered by WG12 (some are dependent on the parameters of the test procedure that the dummy is to be used in, so close collaboration will be maintained with WG20):

- Dummy size and gender;
- Dummy posture and seat interaction;
- The velocity and acceleration range at which the dummy will be used;
- Sensitivity, repeatability and reproducibility.

Also important in the choice of a rear impact dummy is the selection of biomechanically based injury criteria. Currently, WG12 is collating detailed information on the injury criteria that have been proposed in the literature, including determining a single definition of how each criterion is calculated as this has often changed over time. It is important to understand these changes when evaluating the biomechanical evidence presented for the criteria. This understanding will form the basis for evaluating the proposed injury criteria and for selecting and validating injury criteria to be used in the WG20 sled test procedure.

CONCLUSIONS

The EEVC Steering Committee has formed a new Working Group, WG20, with the aim of developing

a test procedure, or test procedures, to be proposed as a new European regulatory test for whiplash injury protection in rear impacts. The test procedures should have a prime focus on neck injury reduction, but should give due regard to the potential for injuries to other body regions. WG12 has been tasked with recommending a dummy and injury criteria for the WG20 test procedures.

WG20 has reviewed the background information that is available and is to develop and validate a geometric approach to head restraint assessment as the first stage of their approach to whiplash injury mitigation. In the longer term, they will develop and validate a dynamic, sled-based test procedure to stimulate further a reduction in the incidence of whiplash injuries.

WG12 has developed draft biofidelity requirements for a rear impact dummy. The available rear impact dummies will be evaluated against these requirements once they are finalised. Work has also started on the evaluation and validation of a biomechanically based injury criterion for rear impact crash testing.

ACKNOWLEDGEMENTS

The authors would like to acknowledge the financial support of the Government and industry bodies that support WG20 and WG12. They would also like to acknowledge the contributions of all of the members of EEVC WG20 and WG12.

The WG20 members are: Hans Cappon (TNO, NL); David Hynd (Chairman, TRL, UK); Anders Kullgren (Secretary, Folksam Research, SE); Massimo La Rocca (Fiat Auto, I); Bernd Lorenz (BAST, DE); Ricardo Satue (IDIADA, ES); and Jean-Pierre Verriest (INRETS, F). The WG20 technical advisors are: Matthew Avery (Thatcham, UK); Ola Boström (Autoliv, SE); François Minne (UTAC, F); and Raimondo Sferco (Ford, DE).

The WG12 members are: François Bermond (Secretary, INRETS, F); Giulio Gertosio (Fiat Auto, I); David Hynd (TRL, UK); Luis Martinez (INSIA, ES); Claus Pastor (BAST, DE); Michiel van Ratingen (Chairman, TNO, NL); and Mats Svensson (Chalmers, SE). The WG20 technical advisors are: Håkan Öhrn (Volvo, SE); Klaus Bortenschlager (Audi/PDB, DE); Sven Siems (Volkswagen, DE); and Xavier Trosseille (LAB).

Special thanks are extended to Mats Svensson for Chairing WG20 from its inception until February 2005.

REFERENCES

- Avery, M and Zubry, D (2001). *BioRID responses and the effect of crash pulse characteristics*. IIWPG/IRCOBI Symposium: Dynamic testing for whiplash injury risk, Isle of Man, UK, IIWPG and IRCOBI Secretariat.
- Berglund, A (2002). On associations between different factors and whiplash injury. Stockholm, Sweden, Karolinska Institute.
- Bertholon, N, Robin, S, Le Coz, J-Y, Potier, P, Lassau, J and Skalli, W (2000). *Human head and cervical spine behaviour during low-speed rear-end impacts: PMHS sled tests with a rigid seat*. IRCOBI Conference, Montpellier, France, IRCOBI Secretariat.
- Boström, O, Håland, Y, Lövsund, P and Svensson, M (2000). Neck Injury Criterion (NIC) and its relevance to various possible neck injury mechanisms. *Frontiers in Whiplash Trauma*. N. Yoganandan and F. Pintar, IOS Press, NL.
- Cappon, H, Philippens, M, van Ratingen, M and Wismans, J (2001). *Development and evaluation of a new rear-impact crash dummy: the RID2*. 45th Stapp Car Crash Conference.
- Cappon, H, Philippens, M, van Ratingen, M, Wismans, J, Svensson, M and Schmitt, K-U (2003). *Reduction of whiplash injury in other modes than rear-end impact*. International Whiplash Trauma Congress, Denver, CO, USA.
- Davidsson, J, Deutscher, C, Hell, W, Linder, A, Lövsund, P and Svensson, M (1998). *Human volunteer kinematics in rear-end sled collisions*. IRCOBI Conference, Goteborg, Sweden, IRCOBI Secretariat.
- Davidsson, J, Lövsund, P, Ono, K, Svensson, M and Inami, S (1999). *A comparison between volunteer, BioRID P3 and Hybrid III performance in rear impacts*. IRCOBI Conference, Sitges, Spain, IRCOBI Secretariat.
- EEVC WG12 (2002). Whiplash *ad hoc* group final report, European Enhanced Vehicle-safety Committee (www.eevc.org).
- Eriksson, L and Kullgren, A (2003). *Influence of seat geometry and seating posture on NICmax and Nkm AISI neck injury predictability*. IRCOBI Conference, Lisbon, Portugal, IRCOBI Secretariat.
- Farmer, C, Wells, J and Werner, J (1999). *Relationship of head restraint positioning to driver neck injury to rear-end crashes*. *Accident Analysis and Prevention* **31**: 719-28.
- Heitplatz, F, Sferco, R, Fay, P, Reim, J, Kim, A and Prasad, P (2003). *An evaluation of existing and proposed injury criteria with various dummies to determine their ability to predict the levels of soft tissue neck injury seen in real world accidents*. 18th International Technical Conference on the Enhanced Safety of Vehicles, Nagoya, Japan, NHTSA.
- Hell, W, Langwieder, K and Walz, F (1999). *Occurance of reported cervical spine injuries in car accidents and improved safety standards for rear-end impacts*. WAD Conference, Vancouver.
- Hynd, D, Willis, C and Roberts, A (2004). *TRL rear impact volunteer testing: methods and measurements*. APSN Biomechanics Workshop, Graz, Austria, APSN.
- Krafft, M (1998). Non-fatal injuries to car occupants. Folksam Research. Stockholm, Sweden.
- Krafft, M, Kullgren, A, Ydenius, A and Tingvall, C (2001). *Influence of crash pulse characteristics on whiplash associated disorders in rear impacts - crash recording in real-life crashes*. IIWPG/IRCOBI Symposium: Dynamic testing for whiplash injury risk, Isle of Man, UK, IIWPG and IRCOBI Secretariat.
- Krafft, M, Kullgren, A, Ydenius, A and Tingvall, C (2002). *Influence of crash pulse characteristics on whiplash associated disorders in rear impacts - crash recording in real-life crashes*. *Crash Prevention and Injury Control*.
- Kullgren, A, Eriksson, L, Boström, O and Krafft, M (2003). *Validation of neck injury criteria using reconstructed real-life rear-end crashes with recorded crash pulses*. 18th International Technical Conference on the Enhanced Safety of Vehicles, Nagoya, Japan, NHTSA.
- Linder, A, Avery, M, Kullgren, A and Krafft, M (2004). *Real world rear impacts reconstructed in sled tests*. IRCOBI Conference, Graz, Austria, IRCOBI Secretariat.
- McConnell, W, Howard, R, van Poppel, J, Krause, R, Guzman, H, Bomar, J, Raddin, J, Benedict, J and Hatsell, C (1995). *Human head and neck kinematics after low velocity rear-end impacts - understanding 'whiplash'*. 39th Stapp Car Crash Conference, Coronado, CA, USA, SAE.
- Muser, M, Walz, F and Zellmer, H (2000). *Biomechanical significance of the rebound phase in low speed rear end impacts*. IRCOBI Conference, Montpellier, France, IRCOBI Secretariat.
- Ono, K and Kaneoka, K (1997). *Motion analysis of human cervical vertebrae during low-speed rear impacts by simulated sled*. IRCOBI Conference, Hannover, Germany, IRCOBI Secretariat.
- Panjabi, M, Wang, J-L and Delson, N (1999). *Neck injury criterion based on intervertebral motions and its evaluation using an instrumented neck dummy*.

IRCOBI Conference, Sitges, Spain, IRCOBI Secretariat.

Philippens, M, Cappon, H, van Ratingen, M, Wismans, J, Svensson, M, Sirey, F, Ono, K, Nishimoto, N and Matsuoka, F (2002). *Comparison of the rear impact biofidelity of BioRID and RID2*. 46th Stapp Car Crash Conference, SAE.

RCAR (2001). A procedure for evaluating motor vehicle head restraints, Research Council for Automobile Repairs (www.rcar.org): 15.

Roberts, A, Hynd, D, Dixon, P, Murphy, O, Magnusson, M and Pope, M (2002). *Kinematics of the human spine in rear impact and the biofidelity of current dummies*. IMechE Vehicle Safety 2002, London, England, IMechE.

Roberts, A, Lowne, R, Beusenberg, M and Cesari, D (1991). *Test procedures for defining biofidelity targets for lateral impact test dummies*. 13th International Conference on Experimental Safety Vehicles, Paris, France, US Department of Transportation, National Highway Traffic Safety Administration.

Siegmund, G, King, D, Lawrence, J, Wheeler, J, Brault, J and Smith, T (1997). *Head/neck kinematic response of human subjects in low-speed rear-end collisions*. 41st Stapp Car Crash Conference, Lake Buena Vista, USA, SAE.

Spitzer, W, Skovron, M, Salmi, R, Cassidy, D, Duranceau, J, Suissa, S and Zeiss, E (1995).

Scientific monograph of the Quebec task force on whiplash associated disorders: Redefining 'whiplash' and its management. Spine **20** (8S).

UN ECE Regulation 16 Uniform provisions concerning the approval of: i) safety-belts, restraint systems, child restraint systems and ISOFix restraint systems for occupants of power-driven vehicles ii) vehicles equipped with safety-belts, restraint systems, child restraint systems and ISOFix child restraint systems. Geneva, United Nations Economic Commission for Europe.

UN ECE Regulation 44 Uniform provisions concerning the approval of restraining devices for child occupants of power driven vehicles ('child restraint system'). Geneva, United Nations Economic Commission for Europe.

Viano, D and Davidsson, J (2001). *Neck displacements of volunteers, BioRID P3 and Hybrid III in rear impacts: implications to whiplash assessment by a neck displacement criterion (NDC)*. IIWPG/IRCOBI Symposium: dynamic testing for whiplash injury risk, Isle of Man, UK, IIWPG and IRCOBI Secretariat.

Ydenius, A and Kullgren, A (2001). *Injury risk functions in frontal impacts using recorded crash pulses*. IRCOBI Conference, Isle of Man, UK, IRCOBI Secretariat.

CORRELATION OF VEHICLE AND ROADSIDE CRASH TEST INJURY CRITERIA

Douglas Gabauer
Rowan University
United States

Robert Thomson
Chalmers University
Sweden
Paper Number 05-0283

ABSTRACT

The vehicle safety and roadside safety communities utilize full-scale crash tests to assess the potential for occupant injury during collision loadings. While the vehicle community uses instrumented full-scale crash test dummies (ATDs), the roadside community relies on the flail space model and the Acceleration Severity Index (ASI) models, which are based primarily on the deceleration of the test vehicle. Unfortunately, there has been little research relating the roadside injury criteria to those used in the vehicle community. This paper investigates the correlation of these differing metrics to gain insight to potential differences in threshold occupant risk levels in the roadside and vehicle safety communities.

Full-scale vehicle crash tests are analyzed to compare the flail space model and ASI to ATD-based injury criteria for different impact configurations, including frontal and frontal offset crash tests. The Head Injury Criterion (HIC), peak chest acceleration, peak chest deflection, and maximum femur force are each compared to the ASI, and flail space parameters. With respect to the vehicle crash test injury criteria, the occupant impact velocity and ASI are found to be conservative in the frontal collision mode. The occupant ridedown acceleration appears to have the strongest correlation to HIC while the ASI appears to have the strongest correlation to peak chest acceleration.

INTRODUCTION

Full-scale crash testing is the traditional method of evaluating both vehicles and roadside safety hardware. A critical part of these evaluations is the assessment of occupant risk potential. Although the basic goal is the same, the vehicle and roadside communities approach the assessment differently. The vehicle safety community has developed impact configuration-specific crash test dummies to serve as a surrogate for the human response. Due to the propensity for oblique collisions but a lack of

mechanical test devices, the roadside safety community has developed occupant risk models, such as the flail space model and the Acceleration Severity Index (ASI), that utilize only the measured vehicle kinematics. Note that the roadside hardware occupant risk guidelines are set forth in NCHRP Report 350 [1] while the occupant risk procedures for vehicle crashworthiness are set forth in FMVSS 201 [2], FMVSS 208 [3], and FMVSS 214 [4].

Both the roadside and vehicle safety communities have attempted to link the respective criteria to the probability of actual occupant injury. Little is known, however, with respect to how these criteria relate to one other. As the update to NCHRP 350 is eminent, this issue is especially crucial to the roadside safety community.

OBJECTIVE

The purpose of this study is to compare roadside crash test injury criteria to vehicle crashworthiness test injury criteria utilizing full-scale crash test data.

BACKGROUND INFORMATION

Roadside Crash Test Injury Criteria

Flail Space Model Prior to the flail space model, a majority of the roadside occupant risk criteria were based simply on limiting the lateral and longitudinal vehicle accelerations during impact [5], [6]. In an attempt to better define the occupant risk criteria, Michie introduced the flail space concept in 1981 [7]. The model assumes that the occupant is an unrestrained point mass, which acts as a “free-missile” inside the occupant compartment. Prior to impacting the vehicle interior, the point-mass occupant is allowed to “flail” 0.6 meters in the longitudinal direction (parallel to the typical direction of vehicle travel) and 0.3 meters in the lateral direction. Measured vehicle kinematics are used to compute the difference in velocity between the occupant and occupant compartment at the instant the occupant has reached either 0.3 meter laterally or 0.6

meter longitudinally. For ease of computations, the vehicle yaw, pitch, and roll motions are ignored, all motion is assumed to be in the horizontal plane, and the lateral and longitudinal motions are assumed to be independent. At the instant of occupant impact, the largest difference in velocity (lateral and longitudinal directions are handled independently) is termed the occupant impact velocity (V_I). The occupant ridedown acceleration is the maximum 10 ms moving average of the accelerations subsequent to the occupant impact with the interior. Again, the lateral and longitudinal directions are handled separately producing two maximum occupant ridedown accelerations.

To ensure that the device does not create undo risk to the occupants of an impacting vehicle, the V_I and subsequent occupant ridedown acceleration are compared against established thresholds. Table 1 summarizes the current threshold values, as prescribed in NCHRP 350. Although values below the “preferred” are desirable, values below the “maximum” category are considered acceptable. Note that the “maximum” thresholds correspond to serious but not life-threatening occupant injury [7].

Table 1.

Current US Occupant Risk Threshold Values. [1]]

Occupant Impact Velocity Limits

Component Direction	Preferred Value	Maximum Value
Lateral and Longitudinal	9 m/s	12 m/s

Occupant Ridedown Acceleration Limits

Component Direction	Preferred Value	Maximum Value
Lateral and Longitudinal	15 g	20 g

European test procedures (CEN) utilize the flail space concept to compute the Theoretical Head Impact Velocity (THIV) and Post-Impact Head Deceleration (PHD), which are analogous to V_I and the occupant ridedown acceleration, respectively [8]. Unlike the NCHRP 350 version, the CEN version of the model utilizes the coupled equations of motion, includes vehicle yaw motion, and computes the resultant velocities and accelerations rather than resolving them into components. To ensure adequate occupant protection, the THIV and PHD are compared to established threshold values. The THIV threshold is 33 km/hr (~9 m/s), which corresponds to the

“preferred” NCHRP 350 V_I value, while the PHD threshold is 20 g, equal to the “maximum” NCHRP 350 ridedown acceleration threshold.

The Acceleration Severity Index

Using measured vehicle acceleration information, CEN test procedures [8] indicate the ASI is computed using the following relationship:

$$ASI(t) = \left[\left(\frac{\bar{a}_x}{\hat{a}_x} \right)^2 + \left(\frac{\bar{a}_y}{\hat{a}_y} \right)^2 + \left(\frac{\bar{a}_z}{\hat{a}_z} \right)^2 \right]^{\frac{1}{2}}$$

where \bar{a}_x , \bar{a}_y , and \bar{a}_z are the 50-ms average component vehicle accelerations and \hat{a}_x , \hat{a}_y , and \hat{a}_z are corresponding threshold accelerations for each component direction. The threshold accelerations are 12 g, 9 g, and 10 g for the longitudinal (x), lateral (y), and vertical (z) directions, respectively. Since it utilizes only vehicle accelerations, the ASI inherently assumes that the occupant is continuously contacting the vehicle, which typically is achieved through the use of a seat belt. The maximum ASI value over the duration of the vehicle acceleration pulse provides a single measure of collision severity that is assumed to be proportional to occupant risk. To provide an assessment of occupant risk potential, the ASI value for a given collision acceleration pulse is compared to established threshold values. Although a maximum ASI value of 1.0 is recommended, a maximum ASI value of 1.4 is acceptable [8]. Note that if two of the three vehicular accelerations components are zero, the ASI will reach the recommended threshold of unity only when the third component reaches the corresponding limit acceleration. If more than one component is non-zero, however, the unity threshold can be attained when the components are less than their corresponding limits. According to the EN-1317 [8], the ASI preferred threshold corresponds to “light injury, if any”. No corresponding injury level, however, is provided for the ASI maximum threshold.

Although the CEN procedures do not provide detail regarding the basis for ASI threshold values, the computation of the ASI is identical to the “severity index” proposed by researchers at Texas Transportation Institute investigating injury in slope-traversing events in the early 1970’s [9]. The maximum threshold values proposed in the TTI study for the longitudinal, lateral, and vertical directions are shown in Table 2, based on the level of occupant restraint. Note that the “lap belt only” limits

correspond to those utilized in the current version of the ASI. According to Chi [10], these limits are based principally on a military specification for upward ejection seats [11] and a study done by Hyde in the late 1960's [12]. Chi also notes that neither study provides any "supporting documentation or references" for the presented information.

Table 2.
Tolerable Acceleration Limits [9]

Restraint	Maximum Acceleration (G)		
	Longitudinal	Lateral	Vertical
Unrestrained	7	5	6
Lap Belt Only	12	9	10
Lap and Shoulder Belt	20	15	17

Vehicle Crashworthiness Injury Criteria

The Head Injury Criterion A refinement of the Gadd Severity Index [13], the Head Injury Criterion (HIC) was first defined in 1971 by Versace [14] as follows:

$$HIC = \max \left[\left[\frac{\int_{t_1}^{t_2} a(t) dt}{t_2 - t_1} \right]^{2.5} (t_2 - t_1) \right]$$

Where $a(t)$ is the resultant linear acceleration time history (G's) of the center of gravity of the head, and t_1 and t_2 are two particular time values that maximize the above expression. Traditionally, the National Highway Traffic Safety Administration (NHTSA) has limited the separation between t_1 and t_2 to no more than 36 milliseconds. Based on this separation, the maximum value for the HIC for an adult mid-size male anthropomorphic test dummy is 1000 [3]. Recent research completed by NHTSA in 2000, however, has led to the addition of a 15 millisecond HIC with a corresponding limit of 700 [15].

Chest Injury Criterion Several injury criteria have been developed to predict chest injuries in humans. Most notable perhaps is the viscous criterion developed by Viano and Lau [16] which is based on the assumption that a certain level of injury will occur if the product of the compression and rate of compression of the chest exceeds a particular limiting value. Currently, NHTSA mandates a variation of this idea that accounts for the chest compression as

well as chest acceleration independently. For chest acceleration, NHTSA prescribes a maximum of 60 G's, except in cases where the duration of the peak is less than 3 ms (often referred to as simply the "3 ms Clip"). For chest deflection, a maximum value of 76 mm (3 inches) was previously prescribed. This criterion is based on a study by Neathery [17] that analyzed previous cadaver data to estimate that a 33% chest compression (or 76 mm in a 50th percentile male) would result in severe but not life threatening injury (AIS value of 3). In conjunction with the update to the HIC requirements, NHTSA reduced the maximum chest compression value to 63 mm (2.5 inches) [15].

Lower Extremity Injury Traditionally, lower extremity injury has focused on limiting the axial force in the femur. NHTSA requires that the peak force in each femur should not exceed 10 kN and 6.8 kN for the 50th percentile male and 5th percentile female crash test dummies, respectively [4]. A comprehensive study of femur impact test data, done by Morgan et al [18] found that the femur force is a good predictor of knee and upper leg injury and that the 10 kN threshold value corresponds to a 35 percent probability of fracture.

CORRELATION BETWEEN INJURY CRITERION

Despite a long history of injury criteria usage in both the roadside safety and vehicle safety communities, there has been only a relatively small amount of research aimed at establishing a correlation between the criteria. As a critical goal for both groups is to provide enhanced protection for the vehicle occupant, regardless of the collision type, an understanding of this link is advantageous to both parties.

As part of the development of the current roadside safety crash testing guidelines, Ray et al. [19],[20] investigated the correlation of the flail space model to the HIC. A total of 7 sled tests were performed using a 1979 Honda Civic body buck: 3 frontal impacts (25, 35, and 45 fps) using a 5th percentile female dummy and 4 side impacts (20, 30, 35, and 45 fps) using a 50th percentile side impact dummy (SID). Note that in both test types, the surrogate occupant was not restrained. For each sled test, the crash dummy response was compared to the respective flail space occupant risk value. A 40 fps (12 m/s) occupant impact velocity was estimated to coincide with HIC₃₆ value of 1000 while an occupant impact velocity of 35 fps (10 m/s) appeared to coincide with a peak chest acceleration of 60 G's. With respect to

the lateral flail space limits, the sled tests indicated that the roadside criteria may be overly conservative as a 25 fps (8 m/s) occupant impact velocity corresponded to a mild 316 HIC and a relatively low Thoracic Trauma Index (TTI) of 113 (16% probability of AIS 3 injury or greater). Note that the results from this study led to the subsequent increase in the lateral occupant impact velocity from 30 fps (9 m/s) to 40 m/s (12 m/s) in NCHRP Report 350.

More recently, Shojaati [21] correlated the ASI to risk of occupant injury via HIC. For nine lateral sled tests, the HIC determined from a Hybrid III dummy was plotted against the ASI as determined from the measured vehicle acceleration. The available data suggested an exponential relation between HIC and the ASI. Up to an ASI value of 1.0, Shojaati approximates that the value of the HIC is below 100. Likewise, ASI values of 1.5 to 2.0 are estimated to correlate to HIC values ranging between 350 and 1000.

APPROACH

The general approach of this portion of the analysis is to use full-scale vehicle crash tests, with reported vehicle injury criteria, and compute the roadside injury criteria based on the available vehicle kinematics information. For each selected full-scale crash test, the occupant impact velocity, occupant ridedown acceleration, and ASI values are computed for comparison purposes.

Case Selection Using the crash tests available from NHTSA, an attempt was made to select tests with varying impact speeds. A particular emphasis was placed on the frontal and frontal offset configurations due to the availability of these test types. Table 3 summarizes the data selected for analysis.

A total of 24 crash tests are evaluated which results in a total of 44 occupant responses (a number of tests have crash test dummies in the right and left front seats). Approximately fifty percent of the vehicles chosen are passenger cars while the remaining fifty percent are LTV type vehicles including pickup trucks, sport utility vehicles as well as full size vans and minivans. Although vehicle type would not be expected to have a large impact on any correlation between the criteria, an effort was made to choose tests with varied vehicle types. Also note that all tests utilized the Hybrid III 50th percentile male crash test dummy.

Table 3.

Summary of Selected NHTSA Crash Test Data

Test Speed/Type	Number of Tests	Occupant Responses	Restraint Status
25 MPH/ Frontal	4	8	Airbag Only
30 MPH/Frontal	4	8	Airbag Only
35 MPH/Frontal	12	24	Airbag and Belt
40 MPH/Frontal Offset (40%)	3	3	Airbag and Belt
40 MPH/Frontal	1	1	Airbag and Belt
Totals	24	44	

Flail Space Computations As the NHTSA full-scale crash tests provide measured vehicle kinematics analogous to those recorded in a roadside hardware crash test, the computation of the occupant impact velocity and occupant ridedown acceleration is identical to the procedures outlined in NCHRP Report 350 [1]. Accelerometer data was chosen as close to the vehicle center of gravity as possible to best describe the movement of the occupant compartment. Typically, utilized sensors included those attached to the vehicle rear floor pan, rear sill, or rear seat. The raw acceleration data from the selected channel is filtered using CFC 180 filter prior to integrating for velocity of position. Note that for the frontal offset tests that both the lateral and longitudinal vehicle accelerations are considered whereas the purely frontal collisions only consider longitudinal information.

ASI Computations For the frontal offset tests, the procedure for the ASI computations is identical to that outlined in both NCHRP Report 350 and the EN-1317 [8]. The same accelerometer channel used for the flail space computations is also used for the ASI computations. A slightly modified procedure is adopted for the computation of the ASI in the purely frontal tests since only information in the longitudinal direction is provided. For these cases, it is assumed that the lateral and vertical motions of the vehicle are negligible. The ASI relation then simplifies to the maximum 50 ms average acceleration over the duration of the pulse divided by the respective acceleration limit in the longitudinal direction (12 G).

RESULTS

Correlation of Roadside Criteria to HIC

Based on the analysis of the full-scale vehicle crash tests, the roadside criteria are plotted as a function of HIC. Figure 1, Figure 2 and Figure 3 show the occupant impact velocity, ASI, and occupant ridedown acceleration as a function of HIC, respectively. Each figure is divided by crash type: the “open” points represent full frontal collisions while the “closed” points represent the frontal offset crashes. Note that differing impact speeds for the full frontal collisions are signified through the use of differently shaped data points. For instance, the square points correspond to the 25 mph tests in the data set while the diamond-shaped points indicate the 30 mph tests.

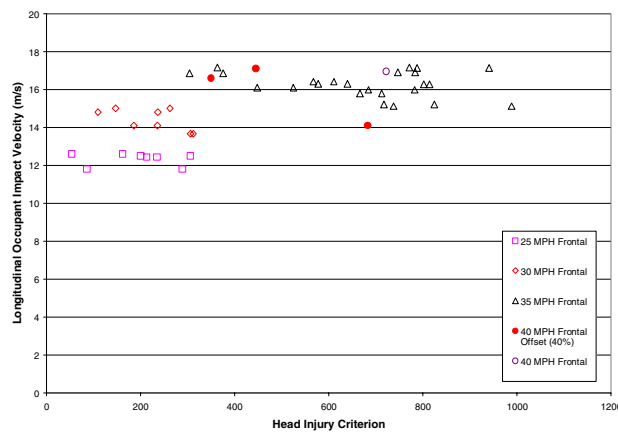


Figure 1. Occupant Impact Velocity and HIC

Especially evident in Figure 1 and Figure 2 is the relatively small variation in the roadside criteria (occupant impact velocity and ASI) while there is a large variation of HIC. The range of occupant impact velocity is approximately 12 m/s to 17 m/s while the range of ASI values is approximately 1.4 to 2.35. Unlike the variation observed in these roadside criteria, the HIC ranges from 50 to approximately 1000; essentially a zero value to the current maximum threshold specified by NHTSA for a 36 millisecond time separation. As expected, this reinforces that the vehicle occupant risk criteria is much more dependent on the occupant restraints than the roadside criteria. It is also noteworthy to view these plots with respect to the threshold values. Essentially, all of the ASI values in Figure 2 are greater than the current prescribed maximum limit of 1.4. A similar observation can be gleaned from Figure 1 as all but 2 of the data points are in excess of the occupant impact velocity maximum threshold of 12 m/s. Although both of the roadside criteria

indicate unacceptable levels of occupant risk, all HIC values in the plot fall below the maximum limit of 1000 suggesting that the ASI and occupant impact velocity may be conservative in comparison to HIC in the frontal collision mode.

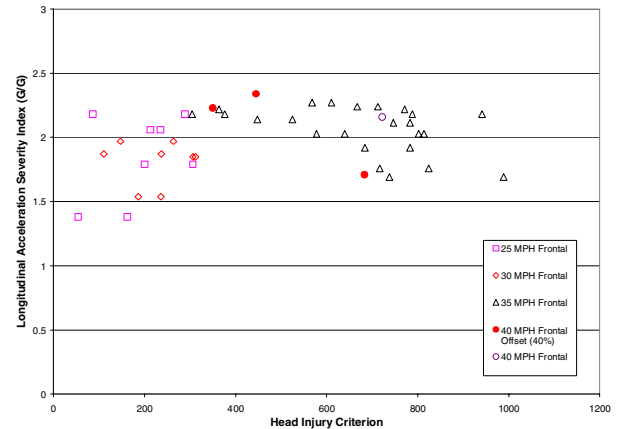


Figure 2. ASI and HIC

Unlike the occupant impact velocity and the ASI, however, the occupant ridedown acceleration appears to show evidence of a correlation to HIC. Although there is evidence of scatter in Figure 3, a trend of increasing occupant ridedown acceleration values is apparent as the value of HIC increases. More data points and statistical analysis would be necessary to quantify the level of correlation. Another interesting difference is the distribution of the points with respect to the corresponding threshold limits. Unlike the occupant impact velocity and ASI, all but one case is at or below the maximum occupant ridedown acceleration of 20 G.

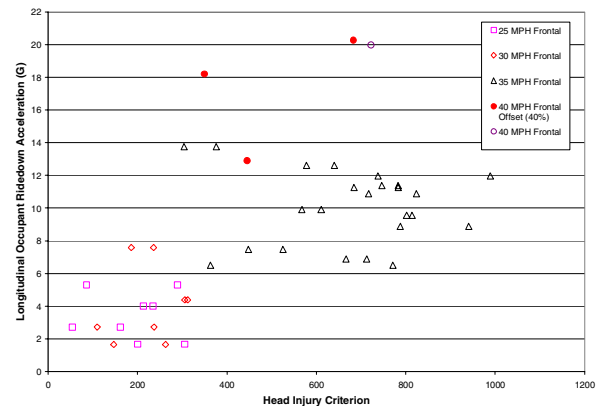


Figure 3. Occupant Ridedown Acceleration and HIC

Correlation of Roadside Criteria to Chest 3-ms Clip

Based on the analysis of the full-scale vehicle crash tests, the roadside criteria are plotted as a function of chest 3 millisecond clip. Figure 4, Figure 5, and Figure 6 show the occupant impact velocity, ASI and occupant ridedown acceleration as a function of chest 3 millisecond clip, respectively. Each figure is divided by crash type: the “open” points represent full frontal collisions while the “closed” points represent the frontal offset crashes. Again, note that the full frontal collisions use differing shapes to differentiate between the vehicle impact speeds.

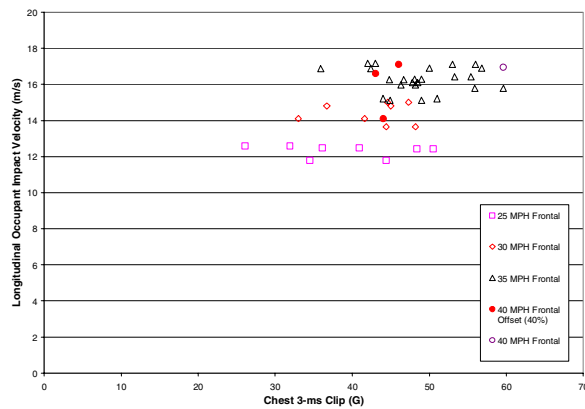


Figure 4. Occupant Impact Velocity and 3 ms Chest Clip

The obvious observation from this series of plots is the much smaller range of chest 3 ms clip values, especially in comparison to the analysis involving HIC. In Figure 4, the range of the occupant impact velocity remains between 12 and 18 m/s while the corresponding range for 3 ms clip is between 26 and 60. Although still a large range, in terms of percentage of the limiting value, it is about half of that observed in the HIC analysis. The same holds for Figure 5 involving the ASI. There does, however, appear a stronger relation between the ASI and chest 3 ms clip than evident in the occupant impact velocity data. Perhaps the ASI is more indicative of an occupant subjected to the damped accelerations of the vehicle caused by the interaction with the seat belt. With respect to the differences in occupant restraint systems, the smaller range of 3 ms clip values may suggest that this vehicle injury criterion is less sensitive to changes in the restraints. Again, however, it is interesting to note that both the occupant impact velocity and ASI are in excess of the current recommended maximum limits while all 3 ms clip values are below the recommended limit of 60 G.

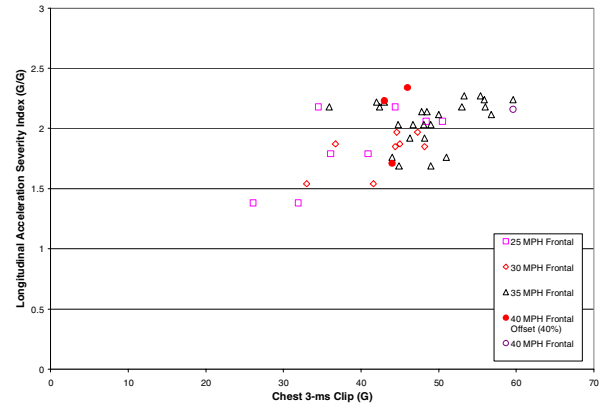


Figure 5. ASI and 3 ms Chest Clip

Although evidence of a correlation between the HIC and occupant ridedown acceleration is evident, Figure 6 appears to imply a weaker correlation to chest 3 ms clip. This may be a result of the timing of the ridedown acceleration. If the peak acceleration value occurs later in the collision when the dummy is interacting with the belt and bag system, vehicle accelerations will be transferred mechanically to the occupant. However, if the peak accelerations occur earlier in the collision before the occupant has taken up all the seatbelt slack, then the chest acceleration will not be directly influenced by the accelerations. The latter situation is more dependent on the relative speed of the occupant and vehicle when the occupant begins to load the restraint system. Based on the available data, the occupant ridedown acceleration appears to increase at a faster rate than the peak chest acceleration when the impact speed is increased. As with the HIC investigation, more data coupled with a statistical analysis would be necessary to determine the level of correlation.

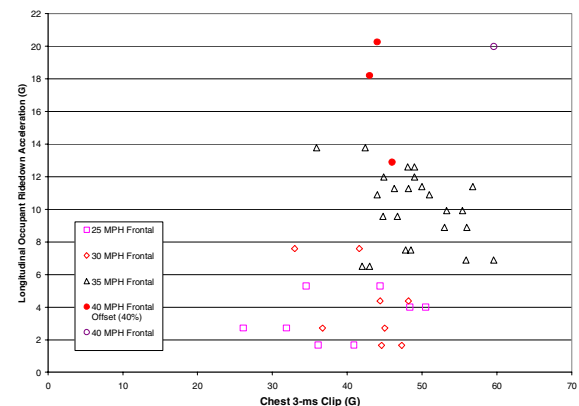


Figure 6. Occupant Ridedown Acceleration and 3 ms Chest Clip

Correlation of Roadside Criteria to Chest Deflection

Based on the analysis of the full-scale vehicle crash tests, the roadside criteria are plotted as a function of chest deflection. Figure 7, Figure 8, and Figure 9 show the occupant impact velocity, ASI, and occupant ridedown acceleration plotted as a function of chest deflection, respectively. Each figure is divided by crash type: the “open” points represent full frontal collisions while the “closed” points represent the frontal offset crashes. Again, note that the full frontal collisions use differing shapes to differentiate between the vehicle impact speeds.

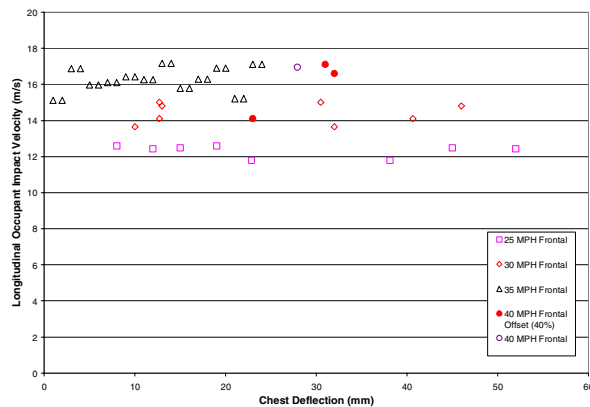


Figure 7. Occupant Impact Velocity and Chest Deflection

For the occupant impact velocity and ASI, the plots as a function of chest deflection exhibit the characteristics observed in the HIC plots. Both Figure 7 and Figure 8 indicate a large amount of variation in the chest deflection compared to a relatively small change occupant impact velocity and ASI, respectively. Likewise, all the chest deflection values are within acceptable FMVSS limits while a majority of the ASI and occupant impact velocity values exceed the currently prescribed thresholds.

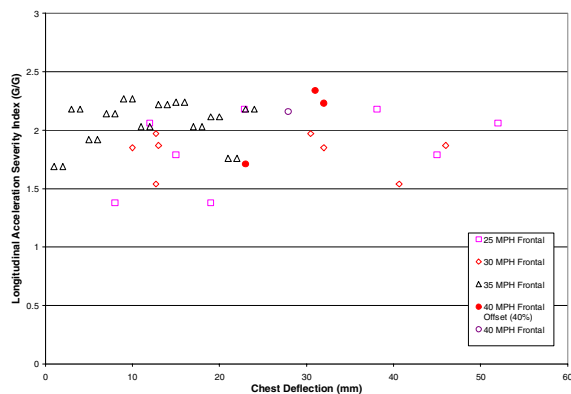


Figure 8. ASI and Chest Deflection

Based on Figure 9, there is no evidence of a strong correlation between the occupant ridedown acceleration and chest deflection. Again, the distribution of both criteria is analogous: approximately all the data points fall at or below the current threshold limits. The available data does appear to suggest a weak inverse relation between the ridedown acceleration and chest deflection. As expected, this suggests that the chest deflection criterion is a more crucial injury mechanism in lower speed collisions. Conversely, the weakly positive relation evident in Figure 6 suggests that the peak chest acceleration is the more significant criteria in higher speed collisions.

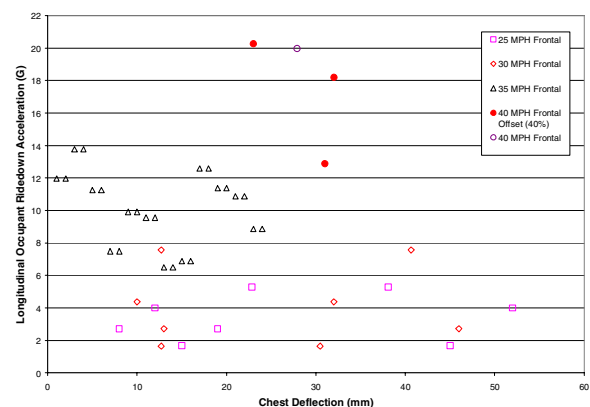


Figure 9. Occupant Ridedown Acceleration and Chest Deflection

Correlation of Roadside Criteria to Maximum Femur Force

Based on the analysis of the full-scale vehicle crash tests, the roadside criteria are plotted as a function of maximum femur force. Figure 10, Figure 11, and Figure 12 show the occupant impact velocity, ASI and occupant ridedown acceleration as a function of maximum femur force, respectively. Each figure is divided by crash type with the “open” points representing full frontal collisions and the “closed” points representing the frontal offset crashes. Again, the various data point shapes distinguish the differing impact speeds of the analyzed full frontal crash tests.

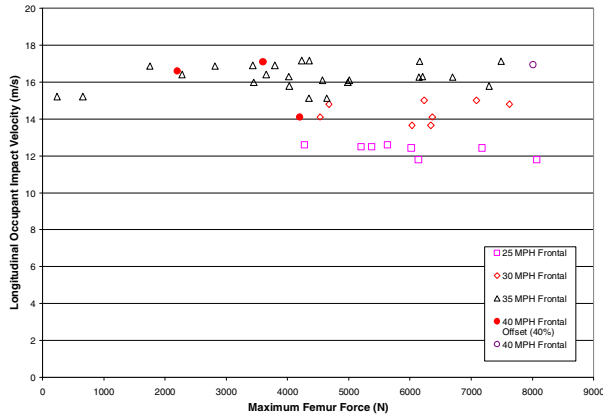


Figure 10. Occupant Impact Velocity and Maximum Femur Force

Figure 10 and Figure 11 demonstrate a scatter of the maximum femur force analogous to that observed in the HIC analysis. This variation may be due to the differences in vehicle structures (especially with respect to the toe pan area) for the chosen crash tests. Note the higher levels of femur force in the 25 and 30 mph crashes which is due to the unbelted crash test dummy. Again, the levels of the occupant impact velocity and ASI are in excess of the prescribed maximum values while the femur loads are within current NHTSA limits. The lack of correlation in Figure 11 is surprising due to the findings of Morgan et al [18] indicating a strong correlation of femur force to injury as well as the findings of Gabauer and Gabler [22] indicating a statistically significant correlation between ASI and low severity injury to the lower extremities.

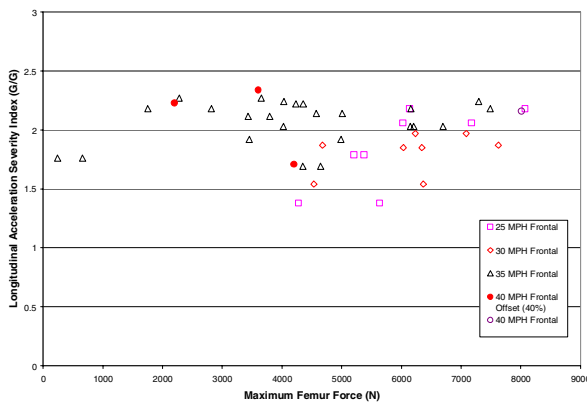


Figure 11. ASI and Maximum Femur Force

Consistent with the chest deflection plots, the occupant ridedown acceleration appears to have a negative correlation to the maximum femur force. This is more evident in Figure 12 than in Figure 9. Additional data coupled with a statistical analysis,

however, would be needed to confirm this correlation. As with the chest deflection, note the higher femur forces in the lower speed frontal impact tests, presumably due to the unrestrained surrogate occupant.

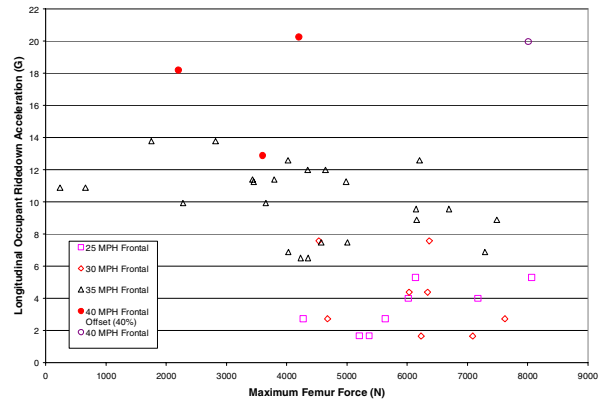


Figure 12. Occupant Ridedown Acceleration and Maximum Femur Force

CONCLUSIONS

The following conclusions can be drawn from the available data:

1. HIC and chest deflection appear severely dependent on the vehicle's restraint system. This is especially evident when comparing these criteria to the occupant impact velocity and the ASI.
2. The occupant ridedown acceleration appears to have the strongest correlation to HIC of the three examined roadside injury criteria.
3. The ASI appears to have the strongest correlation to the maximum chest acceleration of the three examined roadside injury criteria.
4. With respect to vehicle crash test injury criteria, the occupant impact velocity and ASI appear conservative in the frontal collision mode.

ACKNOWLEDGEMENTS

The authors wish to acknowledge the efforts of Lyn Hampton and Jennifer Lake, student research assistants at Rowan University.

REFERENCES

- [1] Ross, Hayes E., Sicking, D.L., Zimmer, R.A., and J.D. Michie. *Recommended Procedures for the Safety Performance Evaluation of Highway Features*. NCHRP

- Report 350, TRB, National Research Council, Washington, D.C., 1993.
- [2] NHTSA. Federal Motor Vehicle Safety Standards: Occupant Protection in Interior Impact. 49 C.F.R., Part 571.201.
- [3] NHTSA. Federal Motor Vehicle Safety Standards: Occupant Crash Protection. 49 C.F.R., Part 571.208.
- [4] NHTSA. Federal Motor Vehicle Safety Standards: Side Impact Protection. 49 C.F.R., Part 571.214.
- [5] Bronstad, M.E. and J. D. Michie. *Recommended Procedures for Vehicle Crash Testing of Highway Appurtenances*, NCHRP Report No. 153, Washington, DC, 1974
- [6] Transportation Research Circular Number 191. *Recommended Procedures for Vehicle Crash Testing of Highway Appurtenances*. Transportation Research Board, Washington, DC, February, 1978.
- [7] Michie, J. D. Collision Risk Assessment Based on Occupant Flail-Space Model. In *Transportation Research Record 796*, TRB, National Research Council, Washington, D.C., 1981, pp 1-9.
- [8] European Committee for Standardization (CEN). *Road Restraint Systems – Part 2: Performance Classes, Impact Test Acceptance Criteria and Test Methods for Safety Barriers*. European Standard EN 1317-2. 1998.
- [9] Weaver, G.D. and H.L. Marquis. *The Safety Aspects of Roadside Slope Combinations*. Conference Proceedings of the 53rd Annual Meeting of the Highway Research Board, January 1974.
- [10] Chi, M. *Assessment of Injury Criteria in Roadside Barrier Tests*. Report FHWA-RD-75-74. FHWA, U.S. Department of Transportation, Washington, D.C., 1976.
- [11] US Military Specification. General Specification for Seat System: Upward Ejection, Aircraft. MIL-S-9479A, United States Air Force, June 16, 1967.
- [12] Hyde, A.S. *Biodynamics and Crashworthiness of Vehicle Structures*. Wyle Laboratories Report WR68-3, Volume III, March 1968.
- [13] Gadd, Charles. Use of a Weighted-Impulse Criterion for Estimating Injury Hazard. Proceedings of the 10th Stapp Car Crash Conference, Paper 660793, November 8-9, 1966.
- [14] Versace, J. Review of the Severity Index, SAE 710881, *Proceedings of the 15th Stapp Car Crash Conference*, pp 771-796, 1971.
- [15] Eppinger, et. al. Supplement: Development of Improved Injury Criteria for the Assessment of Advanced Automotive Restraint Systems – II. National Highway Traffic Safety Administration, March 2000.
- [16] Viano, D.C., Lau, I.V. A Viscous Criterion for Soft Tissue Injury Assessment. *Journal of Biomechanics*, Volume 21, Number 5, pp 387-99, 1988.
- [17] Neathery, R.F. Prediction of Thoracic Injury from Dummy Responses. SAE 741187. *Proceedings of the 19th Stapp Car Crash Conference*, San Diego, pp 295-316, 1975.
- [18] Morgan, R., Eppinger, R. H., Marcus, J. Human Cadaver Patella-Femur-Pelvis Injury Due to Dynamic Frontal Impact to the Patella. *The Twelfth International Conference on Experimental Safety Vehicles*. 1989.
- [19] Ray, M.H., Michie, Jarvis D., Hunter, W.W., and J. Stutts. *Evaluation of Design Analysis Procedures and Acceptance Criteria for Roadside Hardware, Volume IV: The Importance of the Occupant Risk Criteria*. FHWA RD-87/099, US Department of Transportation, Washington, DC, 1987.
- [20] Ray, Malcolm H., Michie, Jarvis D., and Martin Hargrave. Events That Produce Occupant Injury in Longitudinal Barrier Accidents. In *Transportation Research Record 1065*, TRB, National Research Council, Washington, D.C., 1986, pp. 19-30.
- [21] Shojaati, M. Correlation Between Injury Risk and Impact Severity Index ASI. *Proceedings of the 3rd Swiss Transport Research Conference*, Monte Verita/Ascona, March 19-21, 2003.
- [22] Gabauer, D. and Hampton C. Gabler. Evaluation of the Acceleration Severity Index Threshold Values Utilizing Event Data Recorder Technology. Proceedings of the 84th Annual Meeting of the Transportation Research Board, Washington, D.C., January 9-13, 2005.

A DETAILED ANALYSIS OF THE CHARACTERISTICS OF EUROPEAN REAR IMPACTS

Volker Eis
Raimondo Sferco
Paul Fay

Ford Motor Company, Germany and UK
Paper Number 05-0385

ABSTRACT

A detailed analysis of rear impacts was carried out using data from the German In-Depth Accident Study ("GIDAS") including accidents from 1996 to 2004. The frequency of rear impacts compared to other modes was investigated, followed by an in-depth review of single rear impacts and rear impacts in multiple impact crash sequences. Crash characteristics such as the distributions of crash severity, overlap and masses of striking and struck cars were examined. The effect of crash severity on injury severity was investigated for cases including soft tissue neck injuries and / or other injuries. The types of injuries sustained and the effects of occupant gender, age and height, seating position and restraint use were analysed.

This analysis has provided a valuable summary of the characteristics of rear impacts in Europe. In general, it was found that rear impacts did not result in high levels of severe (AIS3+) injuries but many occupants were reported as suffering AIS1 level soft tissue neck injuries, often in the absence of other injuries. Many of these injuries occurred at low crash severities and with high levels of overlap. Where they did occur, most of the more severe (AIS3+) injuries were to the head and thorax and included concussion and rib cage fractures. Moderately severe injuries to the upper and lower extremities also occurred, albeit with low frequency. This analysis has provided a useful new perspective on rear impacts and a better understanding of their characteristics.

BACKGROUND

In recent years, much attention has been given to the protection of car occupants in front, side and rollover crashes. Rear impact is regarded by many people as the next area for attention. However, apart from the large amount of analysis (e.g. [1][2][3][4]) carried out on soft tissue neck injuries ("whiplash"), very little published analysis of characteristics of rear impact has been published. This may be due to the overall low accident severity of rear impact accidents.

This paper presents a detailed analysis of rear impacts carried out using data from the German In-Depth Accident Study ("GIDAS") including accidents from 1996 to 2004.

FREQUENCY OF REAR IMPACTS IN EUROPEAN TRAFFIC ACCIDENTS

To identify the characteristics of rear impacts in real world accidents, the impact configuration of each individual passenger car involved in a traffic accident is important. Three quarters of all passenger cars involved in accidents have only one impact, one quarter of the passenger cars have two or more impacts so called multiple impacts. The most frequently occurring impact type is the single frontal impact with 44 %. Single side impacts have a share of 20 % and only 10 % of the cars have a single rear impact. Multiple impacts can be further divided into multiple impacts without rear impact and multiple impacts with at least one rear impact. The latter have a share of 9 %, 16 % of the cars have multiple impacts but no rear impact (Figure 1). Finally 19 % of all passenger cars involved in an accident have at least one rear impact, regardless if single or multiple.

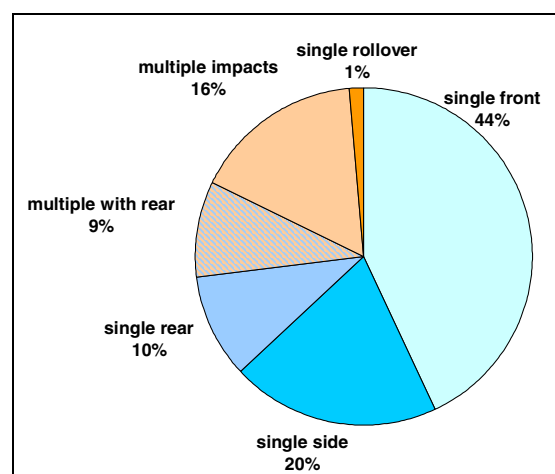


Figure 1. Distribution of impact types in passenger car accidents (n=12,968).

The overall injury level of rear impacts (as characterised by MAIS) is compared with other

impact modes in Figure 2. This analysis only covers occupants with MAIS2 to MAIS6 injuries.

Single rear impacts have the lowest proportion of MAIS3+ injuries. Only 11 % of the occupants with MAIS2+ injuries received MAIS3+ injuries compared with 32 % in single frontal impacts and 40 % in single side impacts. In multiple impacts the presence of the rear impact has no significant influence on injury severity. The share of occupants with MAIS3+ injuries (34 %) is as high as for occupants in cars involved in multiple impacts with no rear impact.

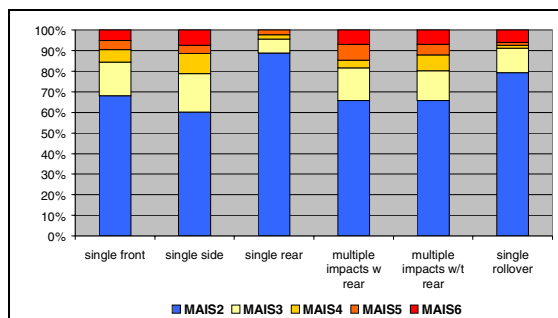


Figure 2. Injury severity (occupants with MAIS2+) of different accident types (n=1,917).

IN-DEPTH ANALYSIS OF SINGLE REAR IMPACTS

Impact configuration and impact severity

A deeper look into the individual data shows that more than 70 % of the passenger cars involved in a single rear impact have an impact to another passenger car (Figure 3). For 11.5 % of the passenger cars the collision partner is a commercial vehicle and 18.4 % collided with 2 wheelers, pedestrians or objects on or near the street.

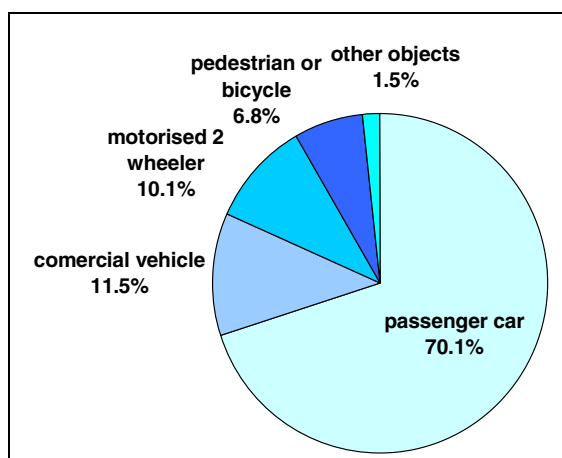


Figure 3. Collision partners of passenger cars in single rear impacts (n=1274).

In general, the impact severity in single rear impacts is relatively low. One indicator of the impact severity is velocity change (delta v). In single rear impacts 90 % of the cars received a delta v lower than 22 km/h, 50 % received a delta v lower than 10 km/h (Figure 4). In car-to-car collisions the share of delta v between 0 and 10 km/h is slightly lower.

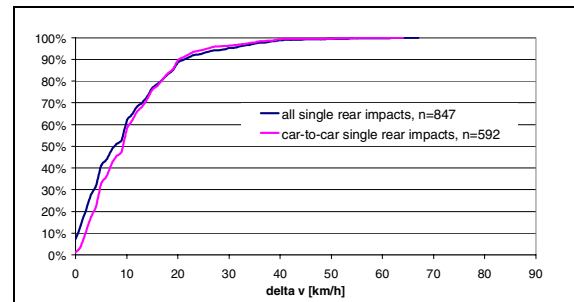


Figure 4. Delta v of the struck cars in single rear impacts.

70 % of the car-to-car single rear impacts occur in urban areas so that 90 % of the striking cars in single rear impacts have an impact speed lower than 55 km/h (Figure 5).

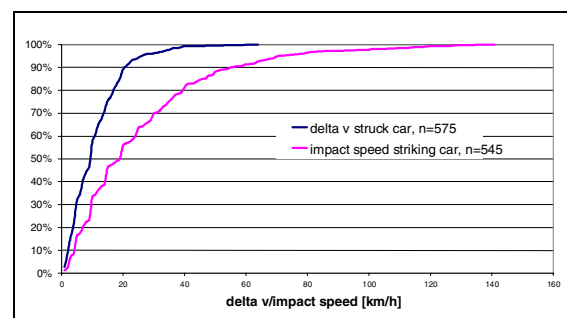


Figure 5. Delta v of the struck car and impact speed of the striking car in single rear, car-to-car impacts.

90 % of the cars have a kerb weight of 1500 kg or less (Figure 6). The average kerb weight for the struck cars (with rear impact) is 1143 kg, the striking cars are slightly lighter than the struck cars with 1096 kg on an average.

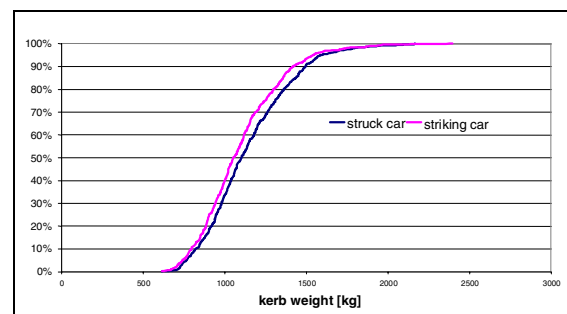


Figure 6. Kerb weight of the struck and the striking car in single rear, car-to-car impacts.

Typically most of the car-to-car impacts in single rear impacts occur between cars in the same lane. Well over half of the cars had an overlap >80 %, irrespective of whether they were the struck or striking car (Figure 7).

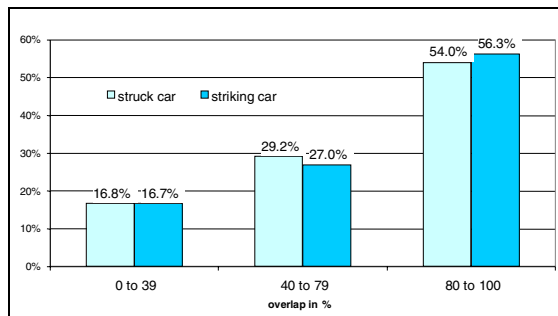


Figure 7. Overlap of the struck car and of the striking car in single rear, car-to-car impacts.

Injury severity of the front seat occupants in single rear impacts

To have an adequate number of occupants with comparable seat environment, the analysis of injury severity and description focuses on the front seat occupants. Due to the fact that the impact severity in single rear impacts is relatively low compared to the other impacts, almost 59 % of the front seat occupants in cars involved in a single rear impact were uninjured. 39.3 % of the front seat occupants had MAIS1 injuries and only 1,6 %/ 0,2 % of the front seat occupants received MAIS2/MAIS3+ injuries (Figure 8).

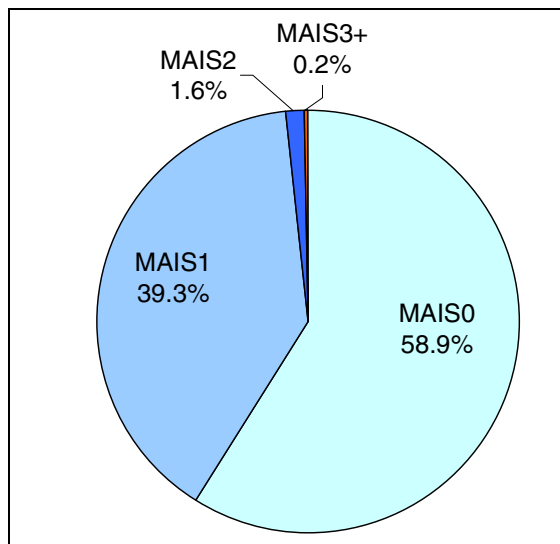


Figure 8. MAIS distribution of front seat occupants in single rear impacts (n=1724).

Because soft tissue neck injury plays an important role in rear impacts, the injured front seat occupants have been differentiated into 3 groups (Figure 9): occupants with soft tissue neck injury as their unique injury (only STNI); occupants with

soft tissue neck injury and other injuries (STNI+), and occupants with no soft tissue neck injury but with other injuries (no STNI). Seventy-eight percent of the injured front seat occupants received a soft tissue neck injury, (65 % as unique injury), 13 % received a STNI and additional other injuries (STNI+), and only 22 % received no STNI but other injuries.

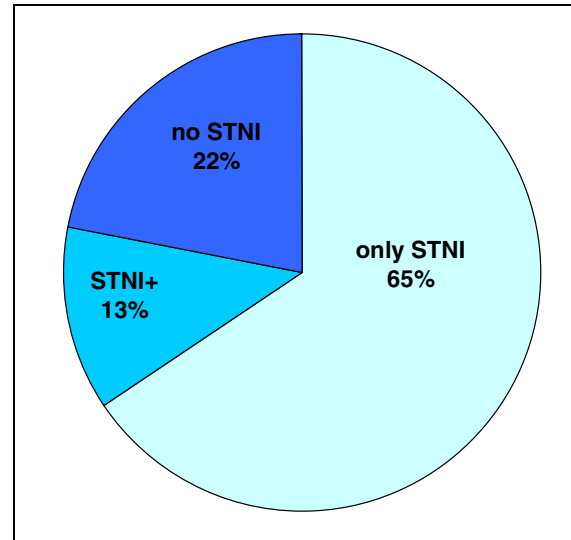


Figure 9. STNI distribution of injured front seat occupants in single rear, car-to-car impacts (n=718).

These three groups also differ regarding the impact severity of the rear impact. The group of front seat occupants who only received an STNI as a unique injury is the group with the lowest delta v level (Figure 10). For the group of occupants with no STNI but with other injuries, it can be stated that these occupants experienced the highest delta v level in this comparison.

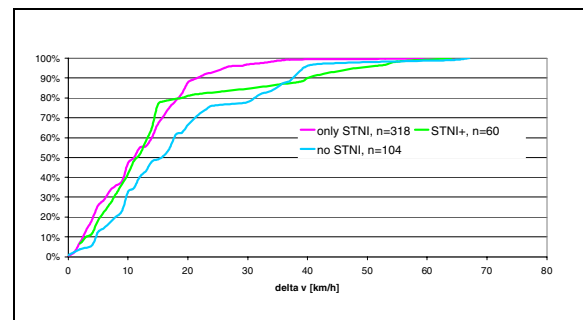


Figure 10. Delta v in single rear impacts and STNI specification of the front seat occupants.

Effects of occupant parameters on STNI

Seat belt use

The overall belt-wearing rate for front seat occupants in Germany has maintained a steady high level (between 90 % and 96 %) for many

years [5]. This explains the very low share of unbelted front seat occupants (1.3 % of the sample). However, for unbelted front seat occupants the risk of receiving a soft tissue neck injury is lower than for belted front seat occupants (Figure 11).

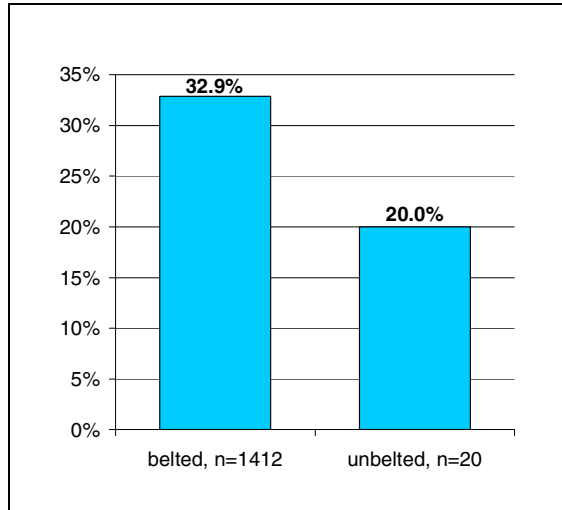


Figure 11. STNI risk of front seat occupants in single rear impacts by belt use.

Age

In the most frequent age groups between 18 and 45 years (66 % of the sample) the risk of receiving a soft tissue neck injury is at its highest level, between 35 % and 37 %, with no significant change with increasing age. For occupants older than 45 years the risk of receiving a soft tissue neck injury decreases with increasing age. This is particularly noticeable for occupants older than 65 years, who have a STNI risk of 16 % well below the average of 34 % (Figure 12).

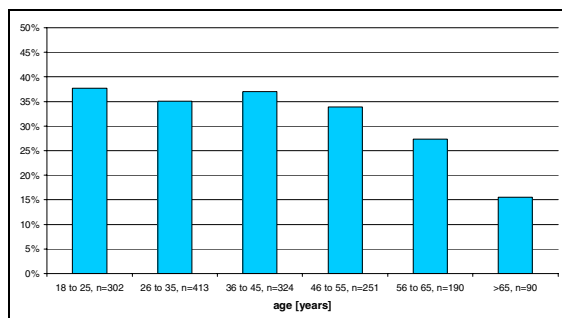


Figure 12. STNI risk of front seat occupants in single rear impacts by age.

Gender and seating position

Overall, female front seat occupants are at higher risk of receiving an STNI. It seems that the STNI risk for front seat passengers tends to be slightly

higher than for the driver (Figure 13), regardless of the gender.

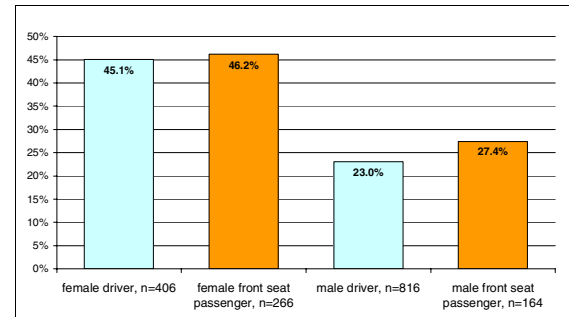


Figure 13. STNI risk of front seat occupants in single rear impacts by gender and seating position.

Body height

Regarding body height, no significant influence for male front seat occupants is detectable but for female front seat occupants the STNI risk seems to increase with body height (Figure 14). The taller the women are, the higher is their risk of receiving a soft tissue neck injury.

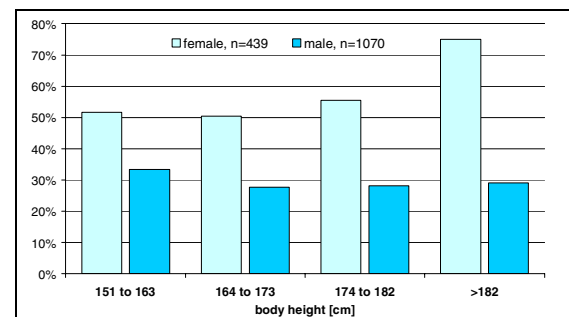


Figure 14. STNI risk of front seat occupants in single rear impacts by gender and body height.

Other injuries than STNI, severity and description

Soft tissue neck injuries are the most frequent injury type in single rear impacts. Other injuries especially those with higher severity (MAIS3+) occur rarely. The group of occupants with STNI and other injuries (STNI+) generally only have injuries of minor or moderate severity (AIS1 or AIS2). Head, thorax and upper and lower extremities are the most frequently affected body regions (Figure 14).

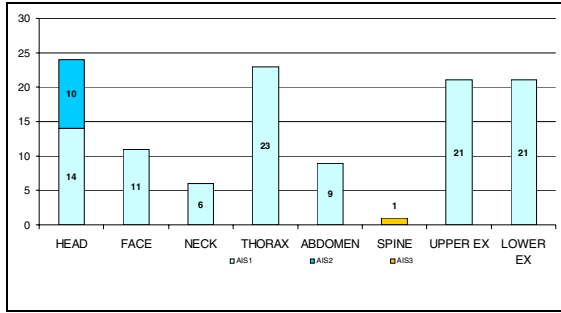


Figure 14. Injured body regions in single rear impacts, belted and unbelted occupants with STNI and other injuries (n=91 occupants).

The majority of the AIS1 injuries are skin contusions and abrasions (105 individual injuries). Concussions are the most frequent AIS2 injuries, other injuries are listed in table 1.

	AIS2/3	AIS1 (without skin contusions and abrasions)
Head/Neck/Face	<ul style="list-style-type: none"> 10 concussions (AIS2) 1 major laceration 	<ul style="list-style-type: none"> 2 minor lacerations 1 broken tooth 1 vagus nerve injury 1 nasal bone fracture 1 laceration of the ear
Thorax	-	<ul style="list-style-type: none"> 1 rib contusion 2 sternum contusions 1 single rib fracture
Spine	<ul style="list-style-type: none"> 1 spinal cord contusion (AIS3) 	-
Upper Extremities	-	<ul style="list-style-type: none"> 1 acromioclavicular joint contusion 1 shoulder contusion

Table 1. Description of the injuries for belted and unbelted front seat occupants with STNI and other injuries (n=91).

Occupants with no STNI more frequently receive MAIS3+ injuries, possibly due to the fact that this group of occupants receive relatively higher velocity changes. The most frequently affected body parts are again head and thorax but, in addition, spine injuries have a higher frequency (Figure 15)

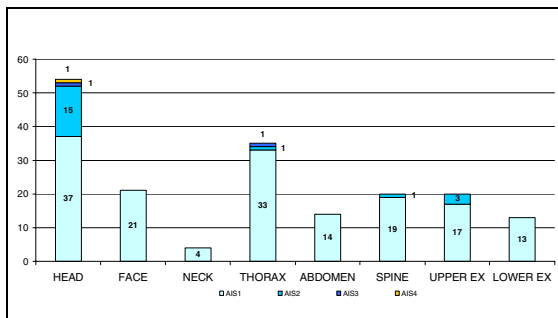


Figure 15. Injured body regions in single rear impacts, belted and unbelted front seat occupants with no STNI but with other injuries (n=157).

Apart from skin contusions and abrasions, minor lacerations and skeletal contusions are the most frequent type of injury. The main type of AIS2 injury is again concussion, but fractures of the

upper extremities and spine also occur (Table 2). The three AIS3+ injuries are a contusion of the small cerebrum, a subarachnoid bleeding and a multiple rib fracture.

	AIS3+	AIS2	AIS1 (without skin contusions and abrasions)
Head/Neck/Face	<ul style="list-style-type: none"> 1 subarachnoid bleeding (AIS4) 1 small cerebrum contusion (AIS3) 	<ul style="list-style-type: none"> 14 concussions 1 major scalp laceration 	<ul style="list-style-type: none"> 15 minor lacerations 1 vagus nerve injury 1 nasal bone fracture 1 mandible joint injury NFS
Thorax	<ul style="list-style-type: none"> 1 multiple fracture 4th to 8th rib (AIS3) 	<ul style="list-style-type: none"> 1 sternum fracture 	<ul style="list-style-type: none"> 7 rib contusions 1 single rib fracture
Abdomen	-	-	<ul style="list-style-type: none"> 2 uterus injuries NFS
Spine	-	<ul style="list-style-type: none"> 1 minor compression fracture at thoracic vertebra 	<ul style="list-style-type: none"> 9 contusions 3 strain injuries
Upper Extremities	-	<ul style="list-style-type: none"> 2 clavicular fractures 1 dislocation of acromioclavicular joint 	<ul style="list-style-type: none"> 1 tendon laceration
Lower Extremities	-	-	<ul style="list-style-type: none"> 1 laceration 1 knee contusion

Table 2. Description of the injuries for belted and unbelted occupants without STNI but with other injuries (n=157).

IN-DEPTH ANALYSIS OF REAR IMPACTS IN MULTIPLE IMPACTS

Impact configuration

In the total accident population, multiple impacts play an important role [6]. In the database used, we have similar numbers of passenger cars with single rear impacts (n=1274) and passenger cars with multiple impacts with at least one rear impact (n=1119). To consider the nature of the multiple impacts, the number of impacts in total is relevant. Approximately three quarters of the passenger cars with multiple impacts had only 2 impacts, 18 % had 3 impacts and only 10 % had more than 3 impacts (Figure 16).

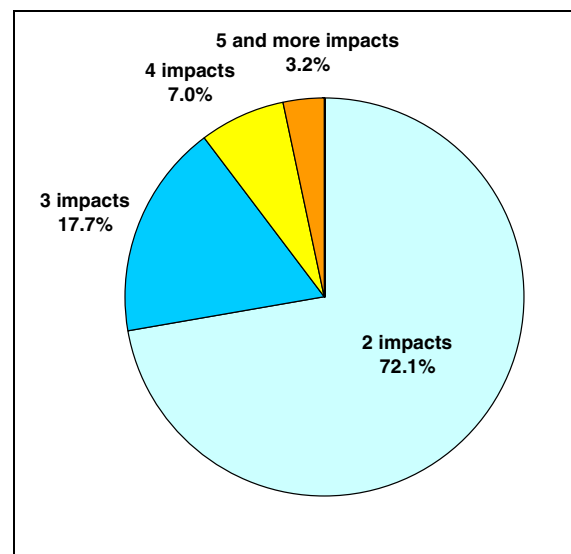


Figure 16. Number of impacts for cars with multiple impacts with at least one rear impact (n=1119).

The position of the rear impact in the multiple impact sequence is another important factor in characterising the impact situation. For more than half of the cars, the rear impact is the first impact. In 30 % of the cases the rear impact is the second impact and in 16 % the rear impacts follows two or more other impacts (Figure 17).

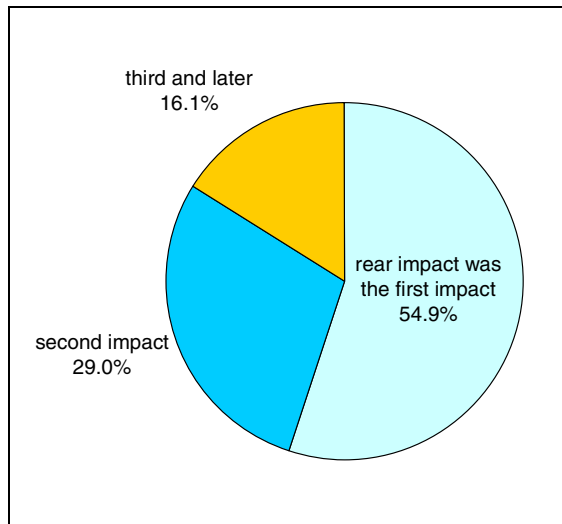


Figure 17. Sequence of the rear impact for cars with multiple impacts with at least one rear impact (n=1119).

The importance of the sequence is apparent in the delta v distributions for these impacts. When the rear impact is the first impact, the level of delta v is significantly higher than in single rear impacts. When the rear impact is not the first impact, the share of low speed impacts (up to 15 km/h) follows the curve for single impacts, but a higher proportion at the impacts occurred at higher delta v levels (Figure 18).

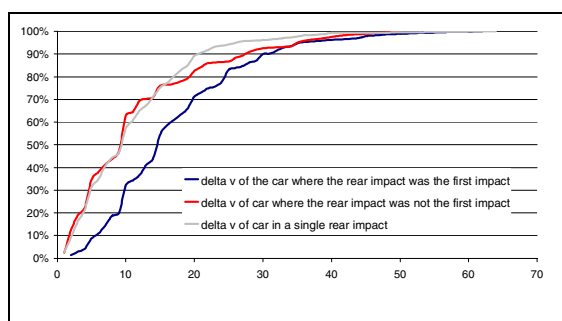


Figure 18. Delta v of the rear impact in multiple impacts with at least one rear impact

Considering only car-to-car rear impacts with multiple impacts where the rear impact occurred first, the cumulative delta v curves of the struck car and the cumulative impact speed of the striking car of cars are parallel to the cumulative values for single rear impacts, but on a much higher delta v

(Figure 19). Multiple impacts with rear impact first occur with a share (52 %) on rural roads.

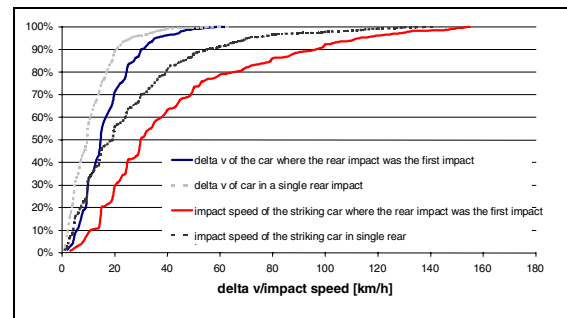


Figure 19. Delta v of the struck car and impact speed of the striking car in car-to-car rear impacts.

In terms of impact severity there is a significant difference between single rear impacts and rear impacts in multiple impacts with rear impact first. However there is only slight difference in the overlap distribution. More than the half of the cars, regardless if they are the struck car or striking car, had an overlap of more than 80 % (Figure 20).

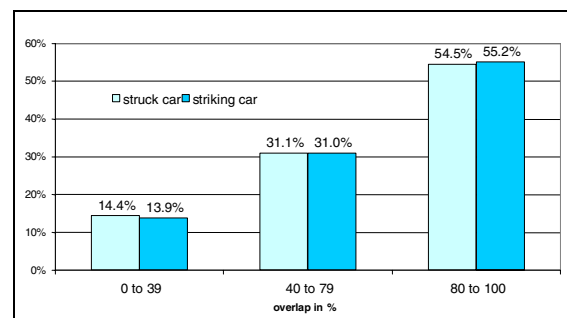


Figure 20. Overlap of the struck car and of the striking car in multiple impacts with at least one rear (rear was first impact).

Injury severity and injury description

The impact characteristics have also an effect on the injury severity. If the rear impact is the first impact, the injury severity of the front seat occupants is, on average, lower than for occupants in multiple impacts where the rear impact is the second or later impact (Figure 21).

Almost 42 % of the front seat occupants are uninjured if the rear is the first impact, but only 31.3 % are uninjured if the rear impact is not first. More significant is the difference in the share of occupants with MAIS2+ injury severity. Only 6 %/1.6 % of the occupants had MAIS2/MAIS3+ injuries if the rear impact is first, otherwise 11.4 %/7.2 % of the occupants have MAIS2/MAIS3+ injuries. The percentage of

occupants with MAIS2+ is more than doubled if the rear impact is not the first impact.

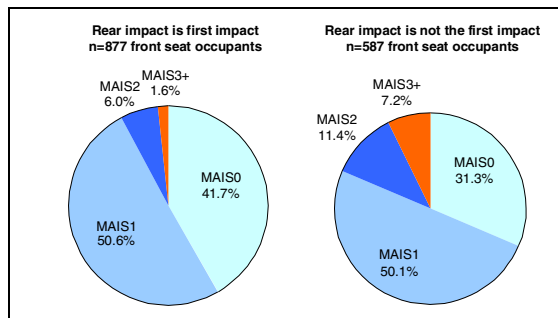


Figure 21. MAIS distribution of front seat occupants in multiple impacts with at least one rear.

Although there is no significant difference between the shares of occupants with MAIS1 in both groups, the shares of occupants with soft tissue neck injury are distributed differently.

When the rear impact is the first impact, two thirds of the injured front seat occupants received a soft tissue neck injury, 46.5 % as a unique injury. When the rear impact is not the first impact, only one third received this type of injury, 10.4 % as a unique injury. The other two thirds of the injured front seat occupants received no soft tissue neck injury but had other injuries (Figure 22).

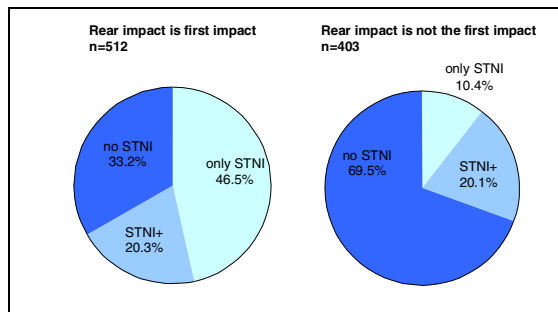


Figure 22. STNI distribution of injured front seat occupants in multiple impacts with at least one rear impact.

Effects of occupant parameters on STNI

Front seat occupants in cars with multiple impacts with at least one rear impact have only a slightly lower soft tissue neck injury risk (32 %) than occupants in cars with single rear impacts (34 %). As in the single rear impacts, the occupant parameters have a very similar influence on the STNI risk.

Seat belt use

The percentage of unbelted front seat occupants in multiple impacts with at least one rear impact is with 3 % higher than in single front impacts

(1.4 %). However for unbelted front seat occupants the risk of receiving a soft tissue neck injury is lower than for belted front seat occupants (Figure 23).

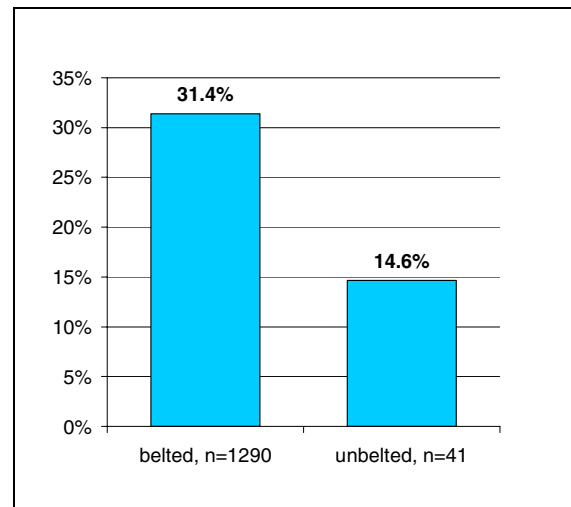


Figure 23. Belt use and STNI risk for front seat occupants in multiple impacts with at least one rear impact.

Age

The effect of age on STNI risk is not as significant as for occupants in single rear impacts. The STNI risk varies from 37 % to 21 % (Figure 24) compared with 38 % to 16 % in single rear impacts.

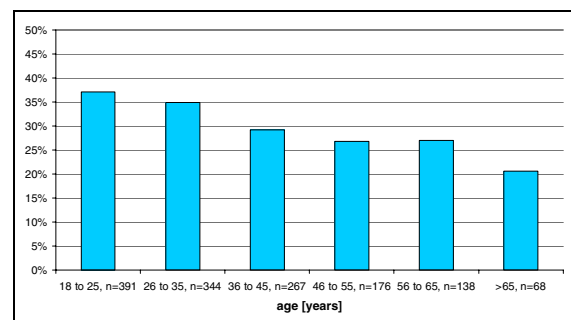


Figure 24. STNI risk of front seat occupants in multiple impacts with at least one rear impact by age.

Gender and seating position

In single rear impacts, the risk of receiving a soft tissue neck injury for female front seat occupants is significantly higher than for males. However there is no suggestion that front seat passengers seem to have a higher STNI risk than drivers in multiple impacts with at least one rear impact. The risk for female front seat occupants was significantly lower than for female drivers, but there is only a very slight difference for males (Figure 25).

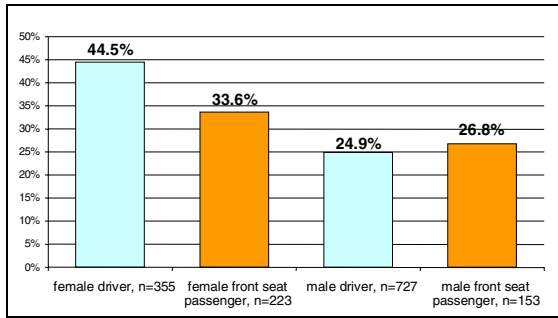


Figure 25. STNI risk of front seat occupants in multiple impacts with at least one rear impact by seating position and gender.

Body height

The results for multiple impacts with at least one rear impact show the same general trends for STNI risk by body height and gender as single rear impacts. The difference between male and female occupants is however not as high as for the occupants in single rear impacts (Figure 26).

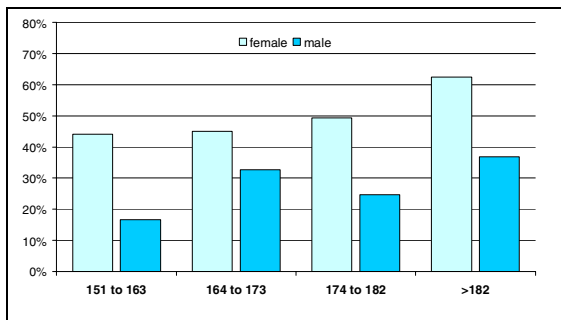


Figure 26. STNI risk of front seat occupants in multiple impacts with at least one rear impact by size and gender

Other injuries than STNI

In multiple impacts it is difficult to accurately determine which impact caused any individual injury. As the number of impacts increases, it becomes increasingly difficult. The final part of the analysis therefore looks only at which body regions are injured, without attempting to attribute the injuries to the rear impact itself.

Due to the higher impact severity of multiple impacts with at least one rear impact, compared to single rear impacts, the number of AIS2 and AIS3 injuries increases.

The most frequently affected body parts are the head, thorax and the extremities. Injuries to the face are more frequent than in single rear impacts and injuries to the abdomen are less frequent (Figure 27).

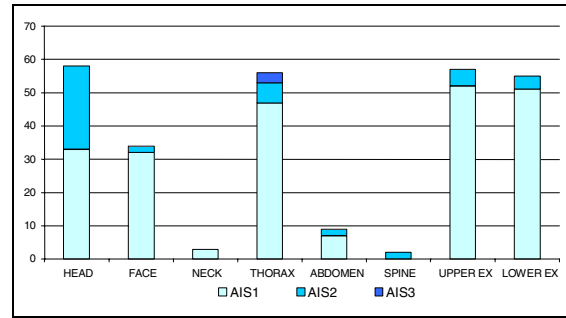


Figure 27. Injured body regions of front seat occupants with STNI and other injuries in multiple impacts with at least one rear.

For front seat occupants receiving no soft tissue neck injury, the most frequently affected body regions are the upper extremities, with a high share of fractures, and the head and thorax regions. In these body regions AIS4+ injuries also occur (Figure 28).

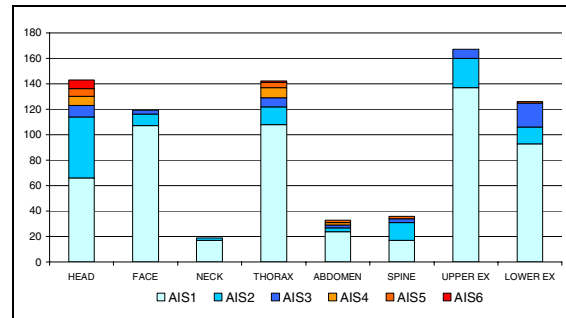


Figure 28. Injured body regions of front seat occupants with no STNI but other injuries in multiple impacts with at least one rear impact

CONCLUSIONS

This analysis included a wide range of information on the rear impacts of passenger cars in Europe.

Single rear impacts are the least frequent impact type for passenger cars and have the lowest impact and injury severity levels.

- Only 10 % of the passenger cars involved in accidents had a single rear impact
- 90 % of the passenger cars had a $\Delta v < 22$ km/h
- Only 0.2 % of the occupants received MAIS3+ injuries

Car-to-car impacts are the main group of single rear impacts (more than 70 % of total). Most of these impacts occur on urban roads, 90 % of the striking cars have an impact speed lower than 55 km/h. More than the half of the car-to-car impacts had an overlap level of more than 80 %.

Soft tissue neck injuries play an important role in single rear impacts.

- 78 % of the injured front seat occupants received a soft tissue neck injury, 65 % in absence of other injuries

With increasing age, especially from 65 years of age on, the risk of receiving a soft tissue neck injury decreases. Female front seat occupants are at significantly higher risk of receiving a whiplash than males, with an increasing risk as their height increases.

The most frequent AIS2 injury types in combination with whiplash are concussions. In the absence of soft tissue neck injuries the overall injury severity is higher, due to the relative higher delta v levels of the impacts. Concussions are the most frequent AIS2 injury type and the small number of AIS3+ injuries was found in the head and thorax.

With a quarter of all impact types of passenger cars multiple impacts are the second largest group. Multiple impacts have the highest injury severity level of all impact types. The present study focuses on multiple impacts with at least one rear impact, which are 9 % of all impact types, and therefore as big as the percentage of single rear impacts.

The injury severity of the front seat passengers in multiple impacts with at least one rear impact depends on the sequence of the rear impact. If the rear impact is the first impact, 55 % of the sample, the injury severity is significantly lower than in cars with multiple impacts where the rear was not the first impact.

The sequence of the rear impact also has an influence on the risk of receiving a soft tissue neck injury. Two thirds of the injured front seat occupants receive a soft tissue neck injury if the rear impact is the first impact, in contrast to only one third of the injured front seat occupants who had a rear impact as one of the following impacts.

The most injured body regions after soft tissue neck injury are head, thorax and the extremities. In the group of occupants without soft tissue neck injury the high percentage of injuries in the upper extremities is conspicuous. In head and thorax also MAIS4+ injuries occur.

REFERENCES

[1] Jacobsson, L.; Lundell, B.; Norin, H.; Isakksson-Hellmann, I.: WHIPS – Volvo's whiplash protection study. Accident Analysis and Prevention 32, 2000, pp 307-319

- [2] Morris, A.P., Thomas, P.A., 1996. Study of soft tissue neck injuries in the UK. Paper No. 96-S9-O-08. Proceedings of the 15th ESV Conference, Melbourne, Australia, May 1996, pp. 1412–1425.
- [3] Otte, D., Pohlemann, T., Blauth, M. 1997. Significance of soft tissue neck injuries at 1 in the accident scene and deformation characteristics of cars with delta-V up to 10 km/h. Proceedings of the IRCOBI Conference on Biomechanics of Impacts, Hannover, Germany, pp. 265–283.
- [4] Temming, J., Zobel, R., 1998. Frequency and risk of cervical spine distortion injuries in passenger car accidents: significance of human factors data. Proceedings of the IRCOBI Conference on Biomechanics of Impacts, Göteborg, Sweden, pp. 219–233.
- [5] Wissenschaftliche Informationen der Bundesanstalt für Straßenwesen: Gurte, Kindersitze, Helme und Schutzkleidung – 2002, Bundesanstalt für Straßenwesen Info 13/2003
- [6] Fay, PA; Sferco, R; Frampton, R. Multiple impact crashes — consequences for occupant protection measures. Proceedings of IRCOBI Conference, September 2001, Isle of Man.

DEVELOPMENT OF A RIDER SIZE AND POSITION MODEL TO DETERMINE MOTORCYCLE PROTECTIVE DEVICE TEST CONDITIONS

R. Michael Van Auken

Scott A. Kebschull

Peter C. Broen

John W. Zellner

Dynamic Research, Inc.

United States

Nicholas M. Rogers

International Motorcycle Manufacturers Association

Switzerland

Paper Number 05-0392

ABSTRACT

The benefits and risks of potential motorcycle protective devices (such as airbags) may depend on the pre-crash position of the rider on the motorcycle. Therefore an understanding of the range of riding positions is needed for research into the risks and benefits of these devices. A statistical model was developed that describes the range motorcycle riding positions, in terms of mean, variance, and correlation parameters; as a function of rider stature, motorcycle-rider interface geometry (seat, hand grips, footrest), and geographic region, based on data collected from Japan, Europe (the Netherlands), and the United States. The rider position and motorcycle-rider interface geometry data was digitized from images of 1390 riders as they were riding on public roadways. A graphical user interface was developed to enable a user to select from and view the range of riding positions described by the model.

INTRODUCTION

Background

The benefits and risks of potential motorcycle protective devices (such as airbags) may depend on the pre-crash position of the rider on the motorcycle (See Rogers and Zellner [1]). Therefore an understanding of the range of riding positions is needed for research into the risks and benefits of these devices.

In addition, motorcycle seating and control layout may affect other, various vehicle attributes, such as comfort, aerodynamics, visibility, stability and so on, and therefore the interaction with ride size and position are of general interest. For example, Reed et al. [2] have developed a similar model for automobile driving posture.

Objectives

The objectives of this study were to determine the range of motorcycle riding positions, as a function of rider stature, motorcycle-rider interface geometry (seat, hand grips, footrest), and possibly geographic region.

Approach

The distribution of motorcycle riding positions was quantified in terms of a mean and variation of the rider back angle and hip position in terms of the rider the hand grip location and seat height relative to the footrests, and rider stature. The mean location was determined by a regression analysis, assuming a constant (homogeneous) variation in riding position about the mean. The homogeneity of the variation were then assessed by subdividing the data into quartiles.

RIDER POSITION DATABASE

A rider position database was prepared comprising 1390 observations of riders operating motorcycles on public roads in Japan, the Netherlands, and the United States (Ohio) as indicated in Table 1. There were 56 variables for each observation, comprising coordinates of points on the rider and motorcycle that were digitized from video still images, and derived measures such as rider stature. Of the 1390 cases, 139 cases were not used in the analysis because they were outliers (> 5 standard deviations) or had missing data (e.g., a point was not visible on the still image and therefore could not be digitized).

Data Sources

The video and digitized data were provided by Honda, Kawasaki, Suzuki, and Yamaha of Japan, Harley-Davidson (USA), and Yamaha (Europe). The sources and regions are summarized in Table 1.

Table 1.
Rider Position Database Sources and Regions

Source	Region	Number of Observations
Harley-Davidson	US (Ohio)	218
Honda	Japan	150
Kawasaki	Japan	150
Suzuki	Japan	138
Yamaha (Japan)	Japan	144
Yamaha Motor Europe	Europe (Netherlands)	501
Total		1390

Rider Position Variables

The variables of interest for this analysis are as follows:

- Independent variables:
 - θ_{back} is the rider back angle in degrees relative to the vertical. A positive value indicates that the rider is leaning forward.
 - x_{hip} is the rider longitudinal hip position relative to the footrest.
- Dependent variables:
 - z_{seat} is the seat height (m),
 - x_{grip} is the rider longitudinal hand grip position (m),
 - z_{grip} is the rider vertical hand grip position (m),
 - S' is the estimated rider stature (m).

The X and Z coordinates are expressed in meters relative to the location of the motorcycle footrest. The Z-axis is perpendicular to the ground plane and the positive direction is pointed towards the ground. The X-axis is in the plane of symmetry of the motorcycle and perpendicular to the Z-axis; the positive direction is pointed towards the front of the motorcycle.

The rider stature was estimated from the distances between the head center, shoulder point, hip point, knee, and ankle, with corrections for the head height and ankle height.

Distribution of Rider Position Variables

The distributions of the position variables are illustrated in Figures 1 to 4. Figures 1 and 2 are histograms illustrating the univariate distributions for each of the dependent and independent variables. Figures 3 and 4 are scatter plots illustrating the distribution of the rider hip position and back angle vs the independent variables. These figures indicate a wide range of rider positions for which more detailed model is sought.

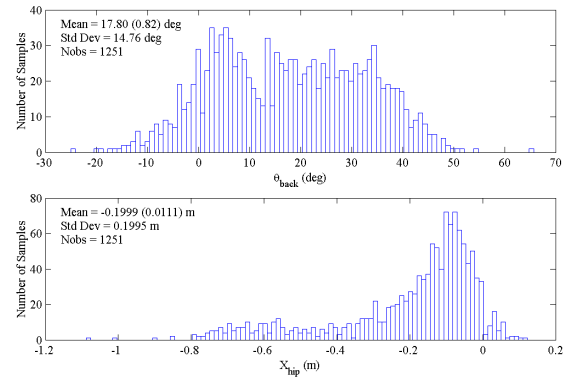


Figure 1. Distribution of rider longitudinal hip position and back angle.

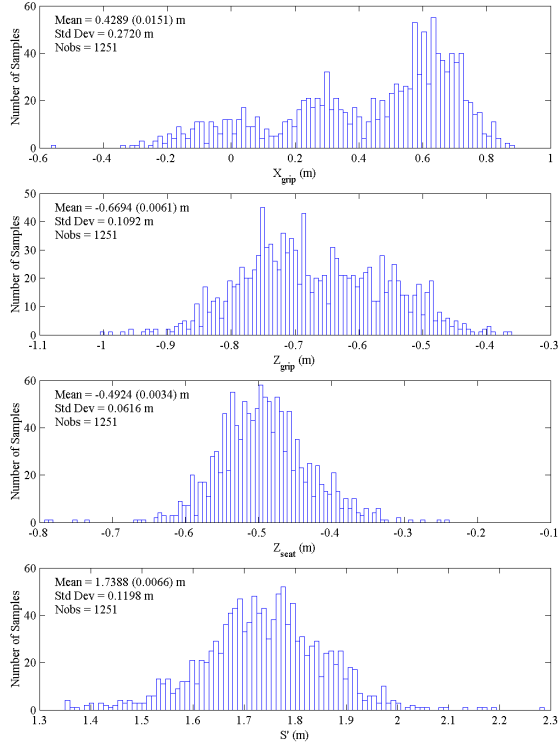


Figure 2. Distribution motorcycle seat height, hand grip location, and rider stature.

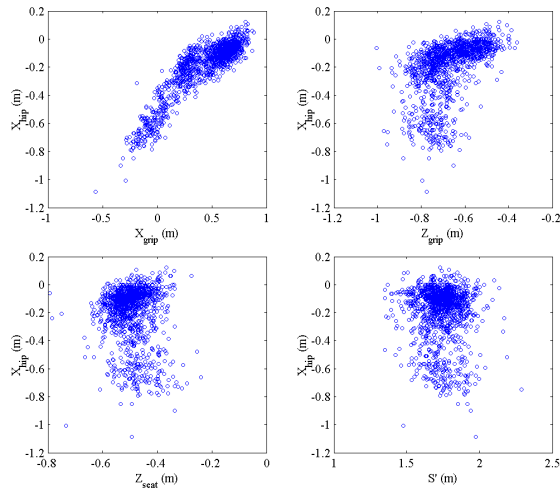


Figure 3. Distribution of rider hip position vs motorcycle seat height, hand grip location, and rider stature.

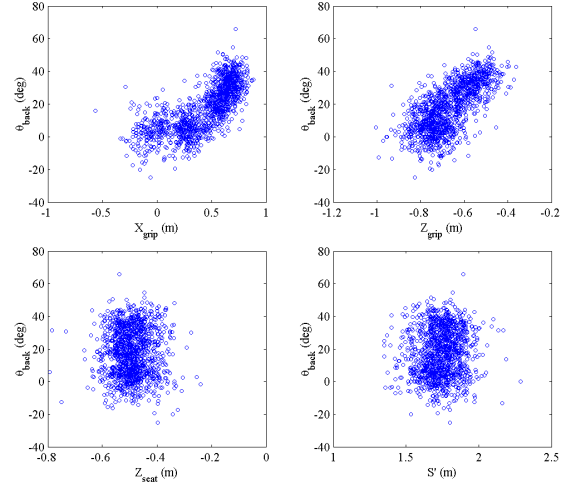


Figure 4. Distribution of rider back angle vs motorcycle seat height, hand grip location, and rider stature.

METHODOLOGY

Assumed Rider Position Distribution

It was assumed that the rider position can be characterized in terms of the longitudinal hip position (x_{hip}) and back angle (θ_{back}) that depend on the motorcycle seat height (z_{seat}) and hand grip position (x_{grip} , z_{grip}), rider stature (S'), region (R), plus some amount of random variation. More specifically, it is assumed that x_{hip} and θ_{back} are normally distributed with mean and variance as follows:

Mean:

$$\begin{aligned} E(x_{hip}) &= \mu_{x_{hip}} = F_x(x_{grip}, z_{grip}, z_{seat}, S', R) \\ E(\theta_{back}) &= \mu_{\theta_{back}} = F_{\theta}(x_{grip}, z_{grip}, z_{seat}, S', R) \end{aligned} \quad (1).$$

Variation:

$$\begin{aligned} E\left(\left(x_{hip} - \mu_{x_{hip}}\right)^2\right) &= \sigma_{x_{hip}}^2 \\ E\left(\left(\theta_{back} - \mu_{\theta_{back}}\right)^2\right) &= \sigma_{\theta_{back}}^2 \\ E\left(\left(x_{hip} - \mu_{x_{hip}}\right)\left(\theta_{back} - \mu_{\theta_{back}}\right)\right) &= \rho \sigma_{x_{hip}} \sigma_{\theta_{back}} \end{aligned} \quad (2).$$

where

$F(x)$ is a function of x ,

$E(x)$ is the expected value of x ,

and where $\sigma_{x_{hip}}$, $\sigma_{\theta_{back}}$, and ρ are constant values to be estimated.

It is furthermore assumed that $\mu_{x_{hip}}$ and $\mu_{\theta_{back}}$ in equation (1) are linear combinations of x_{grip}^p , z_{grip}^p , z_{seat}^p , and $(S')^p$, for p=1 and 2, for each region R separately and for all regions as a group. This can be expressed as follows:

$$\begin{aligned} \mu_{x_{hip}} &= \alpha_{0,R} + \alpha_{1,R}x_{grip} + \alpha_{2,R}x_{grip}^2 \\ &+ \alpha_{3,R}z_{grip} + \alpha_{4,R}z_{grip}^2 \\ &+ \alpha_{5,R}z_{seat} + \alpha_{6,R}z_{seat}^2 \\ &+ \alpha_{7,R}S' + \alpha_{8,R}(S')^2 \\ \mu_{\theta_{back}} &= \beta_{0,R} + \beta_{1,R}x_{grip} + \beta_{2,R}x_{grip}^2 \\ &+ \beta_{3,R}z_{grip} + \beta_{4,R}z_{grip}^2 \\ &+ \beta_{5,R}z_{seat} + \beta_{6,R}z_{seat}^2 \\ &+ \beta_{7,R}S' + \beta_{8,R}(S')^2 \end{aligned} \quad (3).$$

where the values for $\alpha_{k,R}$ and $\beta_{k,R}$ can be estimated by multivariable linear regression (Draper and Smith [1]).

Table 2.
Estimated rider distribution model coefficients

Distribution Model	Parameter	Japan	Europe	US	All Regions
Mean hip position $\bar{x}_{hip} = a_0 + a_1x_{grip} + a_2x_{grip}^2 + a_3z_{grip} + a_4z_{grip}^2 + a_5z_{seat} + a_6z_{seat}^2 + a_7S' + a_8(S')^2$	a_0	-0.42 (0.24)	-0.15 (0.15)	0.26 (0.32)	-0.089 (0.057)
	a_1	1.104 (0.053)	0.931 (0.056)	0.873 (0.071)	1.055 (0.038)
	a_2	-0.667 (0.097)	-0.279 (0.082)	-0.38 (0.13)	-0.599 (0.059)
	a_3	-0.62 (0.66)	0.60 (0.37)	1.08 (0.79)	0
	a_4	-0.41 (0.49)	0.41 (0.28)	0.73 (0.59)	-0.032 (0.041)
	a_5	0	0	0	0
	a_6	0	0	0	-0.103 (0.075)
	a_7	-0.161 (0.053)	-0.116 (0.049)	-0.22 (0.10)	-0.212 (0.037)
	a_8	0	0	0	0
<i>Regression model RPRED statistic</i>		<i>0.87</i>	<i>0.92</i>	<i>0.93</i>	<i>0.88</i>
Mean back angle $\bar{\theta}_{back} = b_0 + b_1x_{grip} + b_2x_{grip}^2 + b_3z_{grip} + b_4z_{grip}^2 + b_5z_{seat} + b_6z_{seat}^2 + b_7S' + b_8(S')^2$	b_0	105 (26)	13.4 (5.5)	27 (15)	51 (15)
	b_1	-10.2 (6.3)	15.2 (8.4)	17 (11)	6.9 (4.5)
	b_2	57 (11)	9 (11)	17 (18)	30.0 (6.7)
	b_3	282 (76)	0	64 (18)	117 (43)
	b_4	169 (56)	-48.5 (6.0)	0	47 (32)
	b_5	-31 (15)	-41 (12)	-34 (26)	-26.8 (8.7)
	b_6	0	0	0	0
	b_7	0	0	0	0
	b_8	0	0	0	0
<i>Regression model RPRED statistic</i>		<i>0.63</i>	<i>0.72</i>	<i>0.75</i>	<i>0.68</i>
Hip position standard deviation	$s_{x_{hip}}$	0.0686	0.0512	0.0585	0.0688
Back angle standard deviation	$s_{\theta_{back}}$	7.93	7.03	8.42	8.28
Correlation	r	-0.554	-0.434	-0.390	-0.432
<i>Number of observations</i>		<i>563</i>	<i>501</i>	<i>185</i>	<i>1251</i>

Note 95% confidence intervals are in parenthesis ().

Mean Rider Position Model

Given $a_{k,R}$ and $b_{k,R}$ are unbiased linear regression estimates of $\alpha_{k,R}$ and $\beta_{k,R}$, it follows that

$$\begin{aligned}\bar{x}_{hip} &= a_{0,R} + a_{1,R}x_{grip} + a_{2,R}x_{grip}^2 \\ &\quad + a_{3,R}z_{grip} + a_{4,R}z_{grip}^2 \\ &\quad + a_{5,R}z_{seat} + a_{6,R}z_{seat}^2 \\ &\quad + a_{7,R}S' + a_{8,R}(S')^2 \\ \bar{\theta}_{back} &= b_{0,R} + b_{1,R}x_{grip} + b_{2,R}x_{grip}^2 \\ &\quad + b_{3,R}z_{grip} + b_{4,R}z_{grip}^2 \\ &\quad + b_{5,R}z_{seat} + b_{6,R}z_{seat}^2 \\ &\quad + b_{7,R}S' + b_{8,R}(S')^2\end{aligned}\quad (4).$$

are unbiased estimates of $\mu_{x_{hip}}$ and $\mu_{\theta_{back}}$.

The form of equation (4), with linear and quadratic terms, was chosen in order to model possible nonlinear trends in the data. However, not all of these trends may be present in the data and therefore it is appropriate to remove terms that do not contribute to the “fit and predictive capability” of the model. This was accomplished by evaluating the RPRED statistic for all 255 possible models with different combinations of the input terms. The RPRED statistic is described in Appendix D. The model with the maximum RPRED was then chosen and the coefficients for the terms that were removed were set to 0.

Rider Position Variation Model

The difference between the observed and the mean rider position values can be expressed as

$$\begin{aligned}\Delta x_{hip_k} &= x_{hip_k} - \bar{x}_{hip} \\ \Delta \theta_{back_k} &= \theta_{back_k} - \bar{\theta}_{back}\end{aligned}\quad (5).$$

It then follows that

$$\begin{aligned}s_{x_{hip}}^2 &= \frac{1}{n-5} \sum_{k=1}^n \Delta x_{hip_k}^2 \\ s_{\theta_{back}}^2 &= \frac{1}{n-5} \sum_{k=1}^n \Delta \theta_{back_k}^2 \\ r &= \frac{1}{(n-5)s_{x_{hip}}s_{\theta_{back}}} \sum_{k=1}^n \Delta x_{hip_k} \Delta \theta_{back_k}\end{aligned}\quad (6).$$

are unbiased estimates of $\sigma_{x_{hip}}^2$, $\sigma_{\theta_{back}}^2$, and ρ respectively, where n is the number of observations that were used in the linear regression.

RESULTS FOR ALL GEOGRAPHIC REGIONS COMBINED

The distribution of rider position for all 1251 observations from Japan, Europe, and the US was assessed and the resulting distribution model coefficients are listed in the last column of Table 2. The actual distribution of the data was then compared to the distribution model to verify the assumptions.

Verification of the Assumed Equation for the Mean Rider Position

Scatter plots illustrating the distribution of rider longitudinal hip position (x_{hip}) and back angle (θ_{back}) vs the seat height, hand grip location, and stature, while controlling for the other independent variables, are illustrated in Figure 5 and Figure 6. These plots help to verify the assumed quadratic relationship between the dependent and independent variables that was assumed by equation (3). However, there are some small but statistically significant higher order mean deviations that are observable in Figures 7 and 8.

Verification of the Homogeneous Normal Distribution Assumption

The variations in the dependent rider position variables versus the mean values are illustrated in Figures 7 and 8. The colors of the points in the scatter plot at the bottom of each figure illustrate how the data were divided into four equally sized subsets or quartiles. Histograms of each quartile and the entire data set are illustrated at the top of each figure.

These results in Figure 7 suggest that there may be some lack of homogeneity in the Δx_{hip} variation, which is larger in the first quartile and smaller in the fourth quartile.

The back angle variation in Figure 8 appears to be consistent with the assumptions.

Verification of the Homogeneous Correlation Assumption

The correlation between Δx_{hip} and $\Delta \theta_{back}$ is illustrated in Figure 9. The size of the ellipse

represents the 95% confidence interval. The ellipsoid appears to be representative of the distribution.

Figure 10 illustrates the same correlation by quartile, in order to observe the homogeneity of the correlation. The quartiles were determined by \bar{x}_{hip} and $\bar{\theta}_{back}$ as illustrated by the scatter plot at the bottom of Figure 10. The correlation appears to be relatively homogeneous, except for the non-homogeneous variation in Δx_{hip} previously noted for Figure 7.

Comparison of the Modeled and Observed Rider Position Distributions

Figure 11 illustrates the agreement between the modeled and observed rider position distributions. The modeled distribution was calculated from

- the values for a , s , and r , listed in Table 2 that describe the mean, variance, and correlation of the dependent rider position variables as a function of the independent variables;
- the observed distribution of the independent variables (e.g., Figure 2); and
- the assumption that the distribution is normally distributed.

The results in Figure 11 indicate that the modeled distribution is in good agreement with the overall distribution. The results also indicate that there are some higher order variations in the distribution that are not modeled, and this may be attributed to the non-homogenous Δx_{hip} previously indicated, and differences due to geographic region (which are not included in this model).

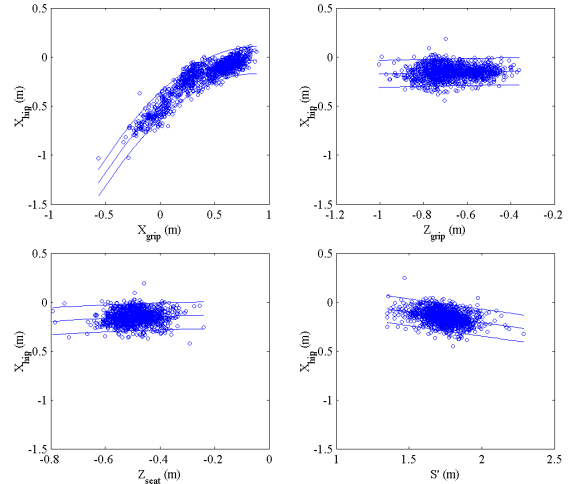


Figure 5. Rider longitudinal hip position vs motorcycle seat height, hand grip location, and rider stature, while controlling for the other independent variables.

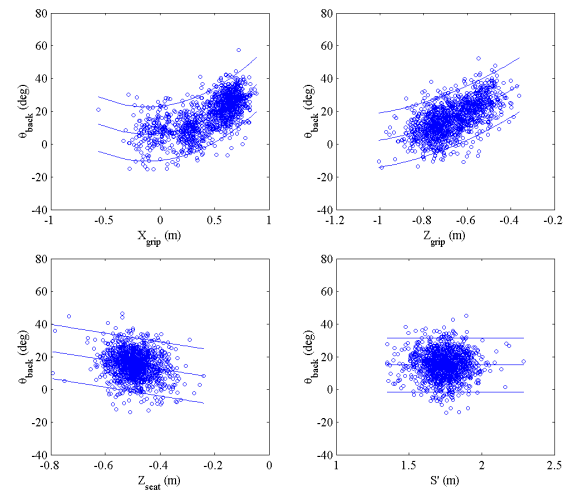


Figure 6. Rider back angle vs motorcycle seat height, hand grip location, and rider stature, while controlling for the other independent variables.

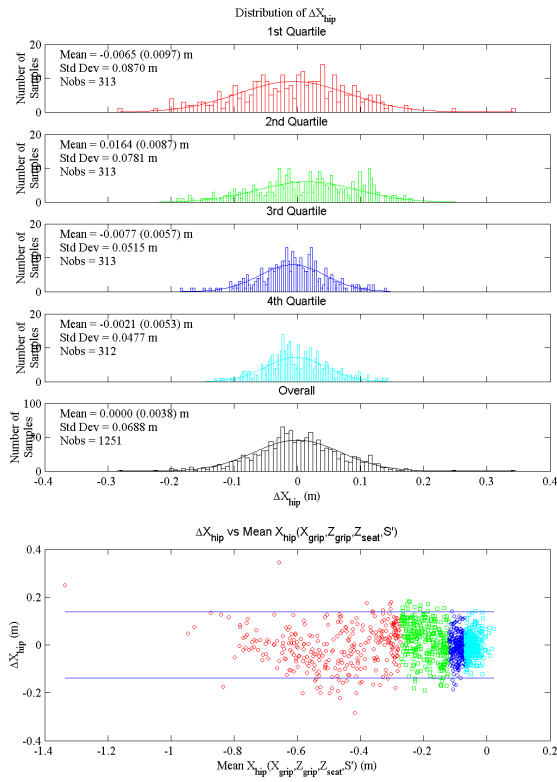


Figure 7. Distribution of the rider longitudinal hip position relative to the mean hip position.

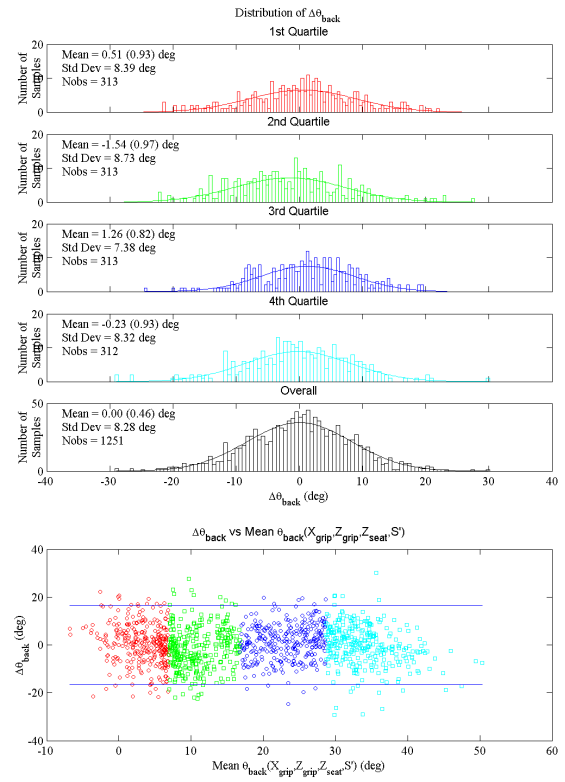


Figure 8. Distribution of the rider back angle relative to the mean back angle.

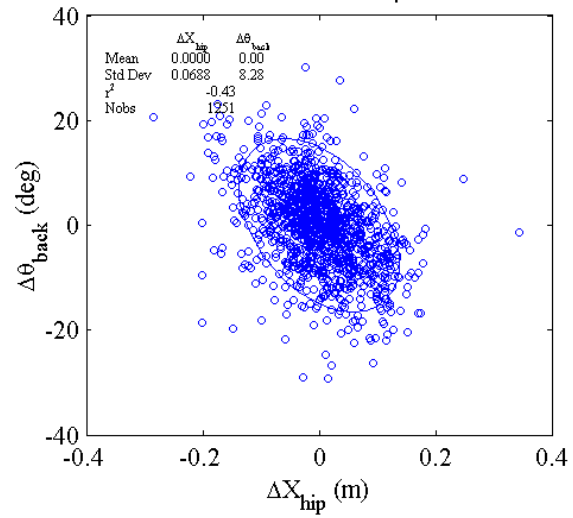


Figure 9. Variation in rider back angle vs longitudinal hip position.

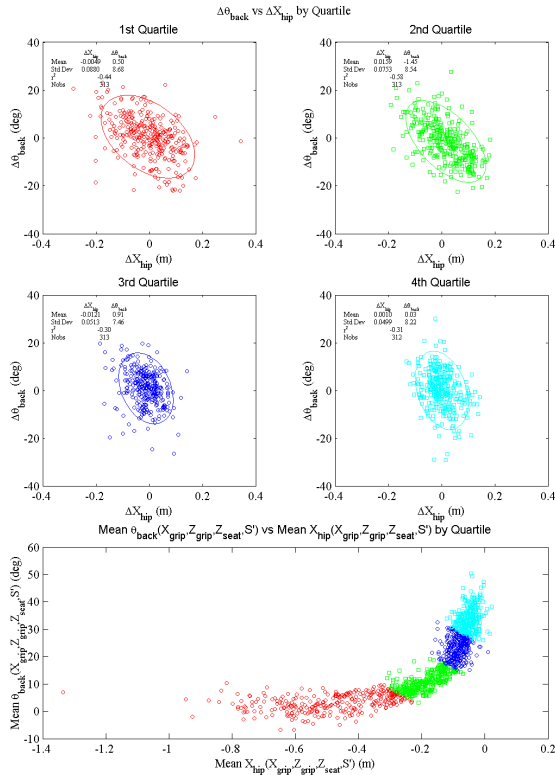


Figure 10. Variation in rider back angle vs longitudinal hip position by quartile.

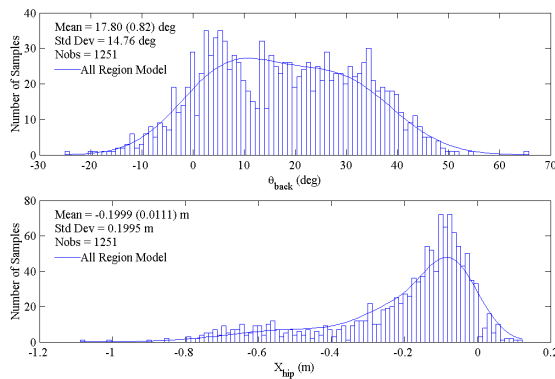


Figure 11. Modeled and observed distributions of rider longitudinal hip position and back angle.

RESULTS FOR EACH GEOGRAPHIC REGION SEPARATELY

The distribution of rider position for Japan, Europe, and the US were also assessed separately, and the resulting distribution model coefficients are also listed in Table 2. Plots illustrating the agreement

between the data and the distribution models are illustrated in Appendices A, B, and C.

SOFTWARE TOOL

The descriptive models for rider position (equations (7) and (3)) and Table 2) were incorporated into a user-friendly Microsoft Excel based computer program. As illustrated in Figure 12, the MS Excel program computes rider position based on the geographic region, motorcycle seat height and hand grip position, and rider stature, and displays the results.

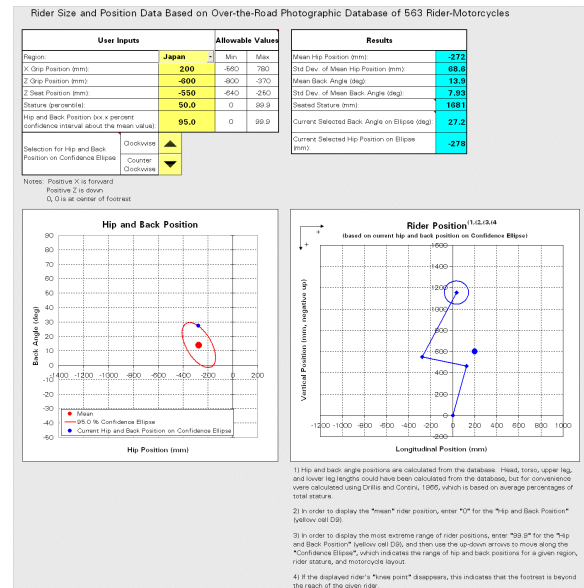


Figure 12. Rider position software tool.

CONCLUSIONS AND RECOMMENDATIONS

Descriptive statistical models for Europe, Japan, the US, and all regions were determined that describe the distribution of rider position as a function of the motorcycle-rider interface, rider stature, and geographic region. The dependent rider position variables are the longitudinal location of rider hip relative to the motorcycle footrest (x_{hip}) and rider back angle (θ_{back}). It was assumed that x_{hip} and θ_{back} are randomly distributed with normal distributions relative to mean values which are a function of the independent variables. The independent variables are the motorcycle seat height (z_{seat}) and hand grip position (x_{grip} , z_{grip}), relative to the motorcycle footrest, and the rider stature (S'). It was furthermore assumed that the standard

deviations and correlation of x_{hip} and θ_{back} , relative to the mean values, are constants. The coefficients that describe the mean, standard deviation, and correlation for each geographic region and for all geographic regions combined are listed in Table 2.

Given the motorcycle-rider interface geometry, rider stature, and geographic region, the distribution of motorcycle riding position can be estimated according to the model as follows:

1. Determine the appropriate set of coefficients listed in Table 2 to use based on the desired geographic region.
2. Calculate the mean rider position accord to the following equations:

$$\begin{aligned}\bar{x}_{hip} &= a_0 + a_1x_{grip} + a_2x_{grip}^2 + a_3z_{grip} + a_4z_{grip}^2 \\ &\quad + a_5z_{seat} + a_6z_{seat}^2 + a_7S' + a_8(S')^2 \\ \bar{\theta}_{back} &= b_0 + b_1x_{grip} + b_2x_{grip}^2 + b_3z_{grip} + b_4z_{grip}^2 \\ &\quad + b_5z_{seat} + b_6z_{seat}^2 + b_7S' + b_8(S')^2\end{aligned}\quad (7)$$

3. Calculate the approximate 95% confidence intervals for x_{hip} and θ_{back} according to the equations:

$$\begin{aligned}\bar{x}_{hip} - 1.96s_{x_{hip}} &\leq x_{hip} \leq \bar{x}_{hip} + 1.96s_{x_{hip}} \\ \bar{\theta}_{back} - 1.96s_{\theta_{back}} &\leq \theta_{back} \leq \bar{\theta}_{back} + 1.96s_{\theta_{back}}\end{aligned}\quad (8)$$

These calculations have been integrated into a Microsoft Excel computer program.

The overall agreements between the modeled and observed distributions of rider position are illustrated in Figures 11, A-11, B-11, and C-11.

It may be possible to further improve the agreement between the modeled and observed Δx_{hip}

distributions by scaling or weighting the longitudinal rider position in order to model the differences in the Δx_{hip} variation that were observed in Figure 7.

It is notable that, with regard to rider back angle, the Europe and Japan models are uni-modal (with means at 24 and 13 degrees of forward lean, respectively), whereas the US model is bi-modal with peaks at 1 and 28 degrees, reflecting the different seating preferences and layouts in the data from the regions.

ACKNOWLEDGEMENTS

This work was funded by the International Motorcycle Manufacturers Association. Honda, Suzuki, and Yamaha of Japan, Harley-Davidson

(US), and Yamaha (Europe) provided in-use rider position video and digitized data. DRI staff member Joe Kelly also assisted in digitizing the video data, and Brian Keschull prepared the MS Excel computer program

REFERENCES

- [1] Rogers, N.M., and Zellner, J.W., "Factors and Status of Motorcycle Airbag Feasibility Research", Paper No. 01-S9-O-207, Proceedings of the 17th International Technical Conference on the Enhanced Safety of Vehicles (ESV), Amsterdam, The Netherlands, June 4 - 7, 2001.
- [2] Reed, M.P., et al., "A Statistical Method for Predicting Automobile Driving Posture", Human Factors, Vol. 44, No. 4, Winter 2002, pp 557-568.
- [3] Draper, N.R., and Smith, H., Applied Regression Analysis, Second Edition, John Wiley & Sons, New York, 1981.

APPENDIX A – DISTRIBUTION OF RIDING POSITION IN JAPAN

The distribution of rider position in Japan, based on observations of 563 riders, is illustrated in Figures A-1 to A-5. Figure A-1 illustrates modeled and observed distribution of rider back angle and hip position. The modeled distributions of these dependent variables are based on the distribution of the four independent variables in Figure A.2. Figure A-3 illustrates the relationship between the rider hip position and back angle vs. the independent variables. Figure A-4 is similar to Figure A-3, but controlling for the variation in the other independent variables and illustrating the distribution model.

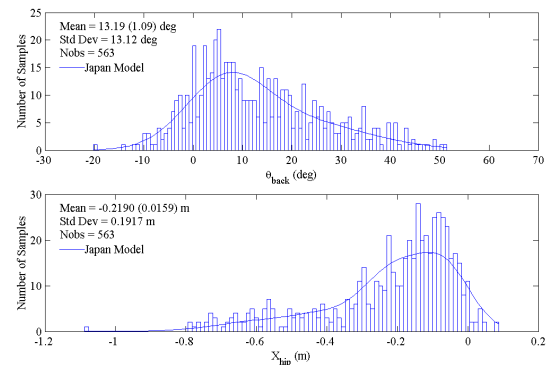


Figure A-1. Modeled and observed distribution of rider longitudinal hip position and back angle for 563 riders in Japan.

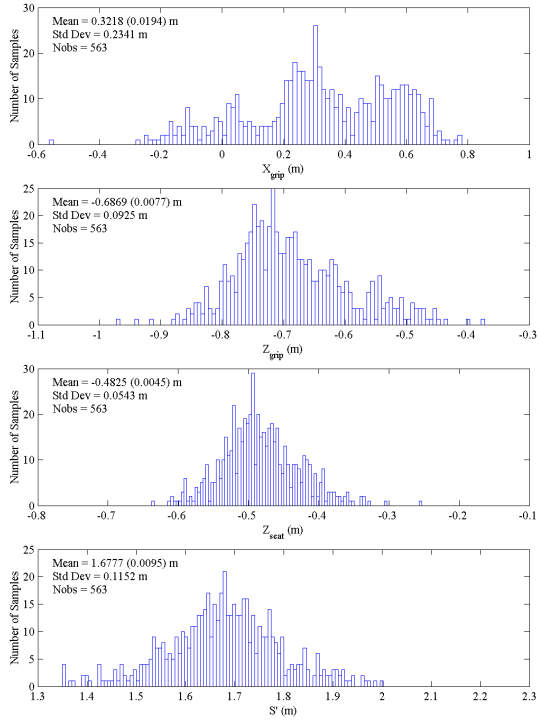


Figure A-2. Distribution of observed motorcycle seat height, hand grip location, and rider stature for 563 riders in Japan.

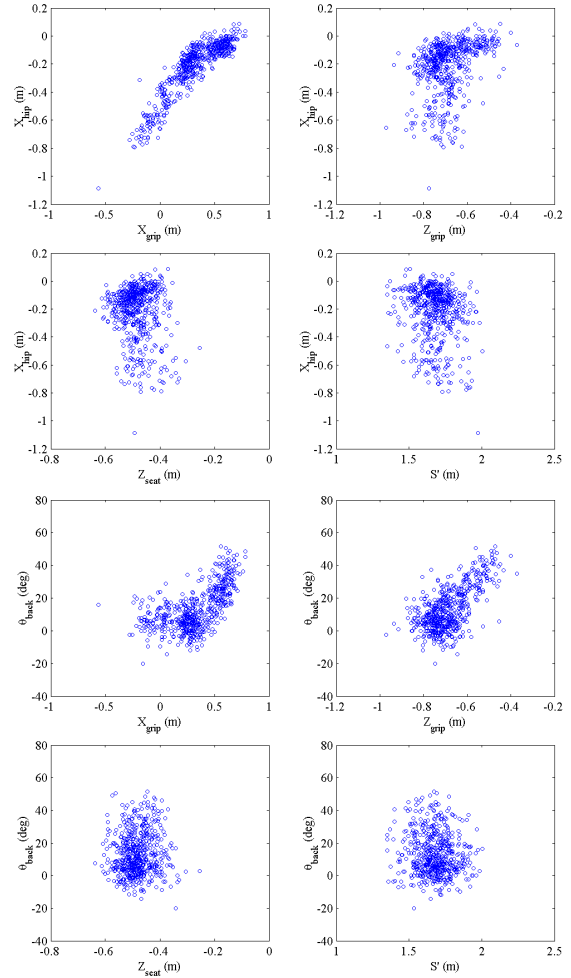


Figure A-3. Observed rider hip position and back angle vs motorcycle seat height, hand grip location, and rider stature for 563 riders in Japan.

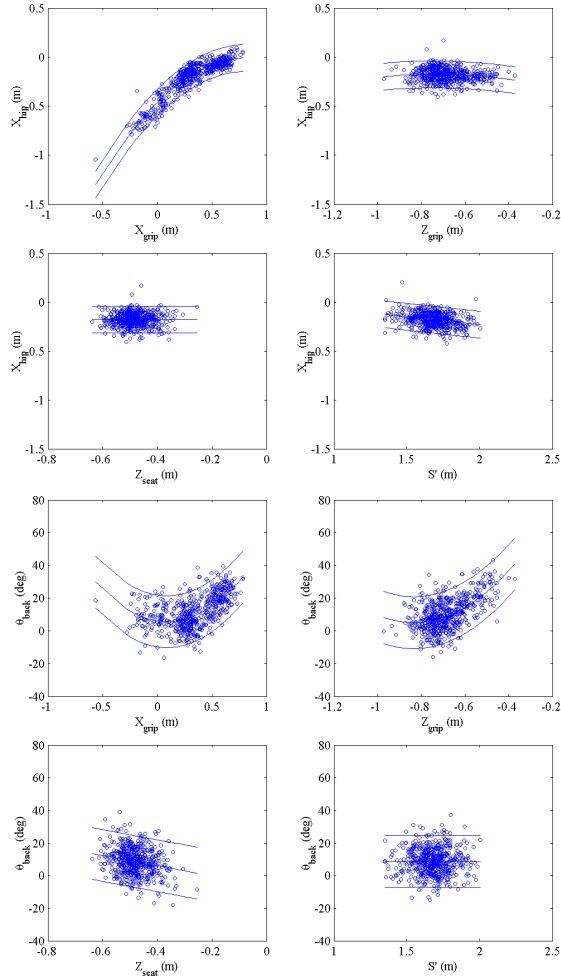


Figure A-4. Rider hip position and back angle vs. motorcycle seat height, hand grip location, and rider stature, for 563 riders in Japan, while controlling for the other independent variables.

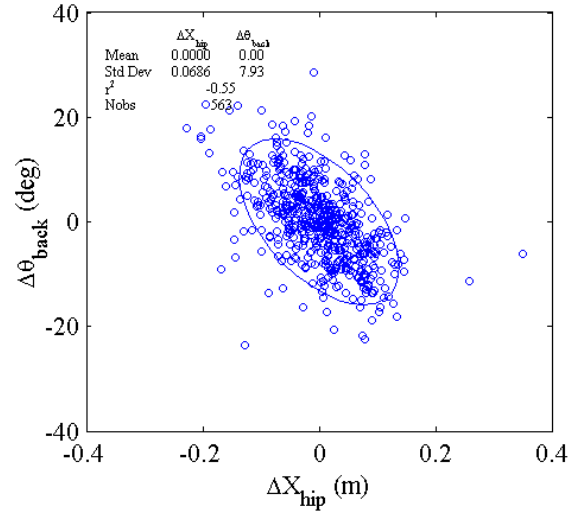


Figure A-5. Variation in rider back angle vs hip position for 563 riders in Japan.

APPENDIX B – DISTRIBUTION OF RIDING POSITION IN EUROPE

The distribution of rider position in Europe, based on observations of 501 riders in the Netherlands, is illustrated in Figures B-1 to B-5.

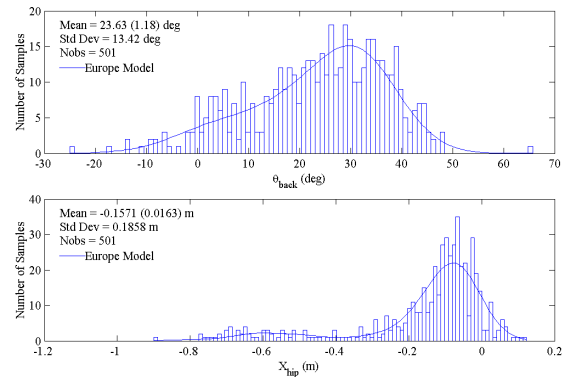


Figure B-1. Modeled and observed distribution of rider longitudinal hip position and back angle for 501 riders in Europe.

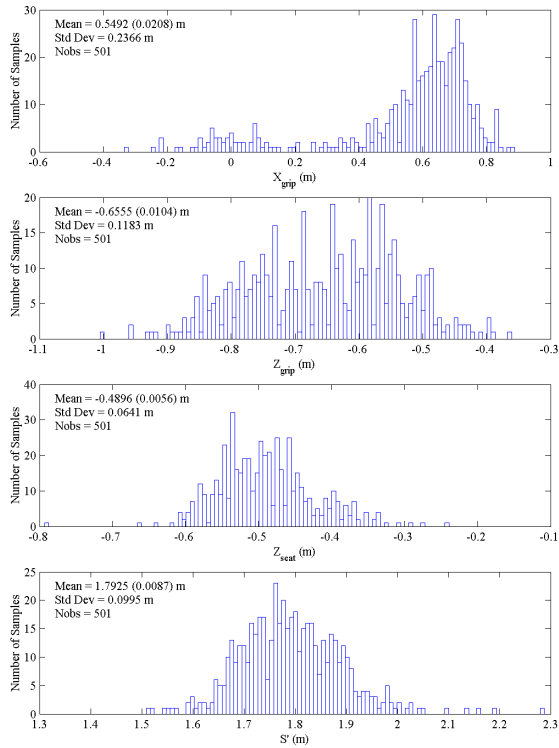


Figure B-2. Distribution of observed motorcycle seat height, hand grip location, and rider stature for 501 riders in Europe.

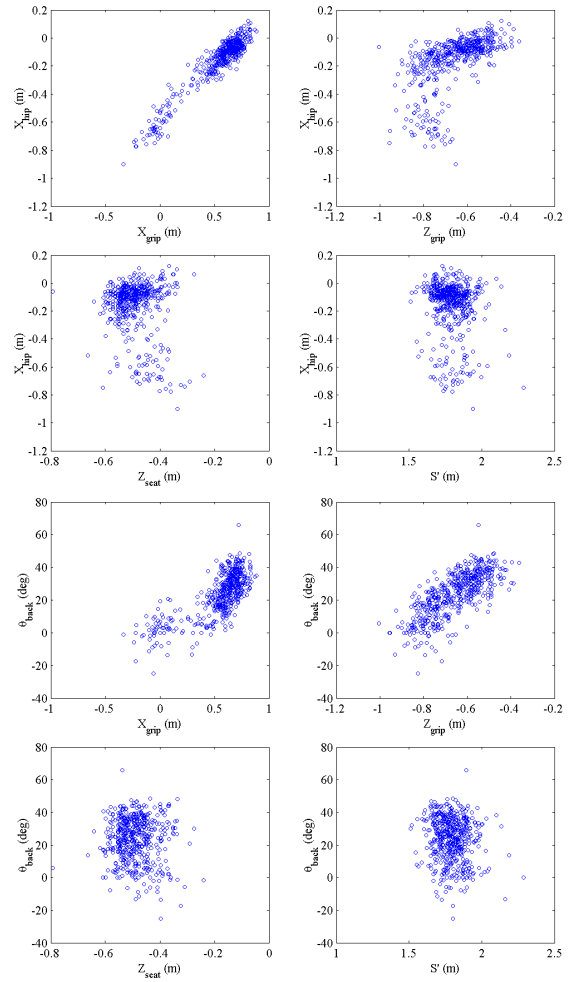


Figure B-3. Observed rider hip position and back angle vs motorcycle seat height, hand grip location, and rider stature for 501 riders in Europe.

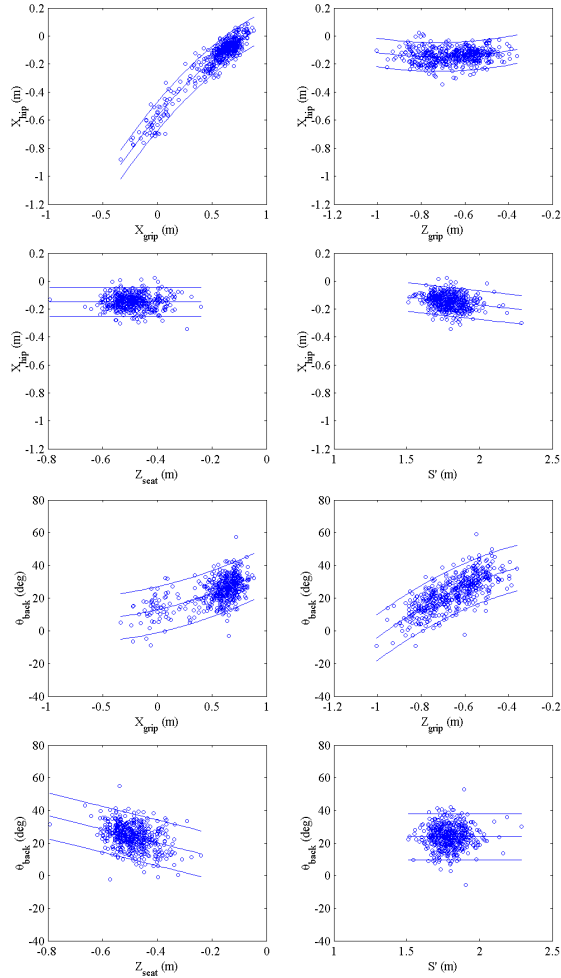


Figure B-4. Rider hip position and back angle vs. motorcycle seat height, hand grip location, and rider stature, for 501 riders in Europe, while controlling for the other independent variables.

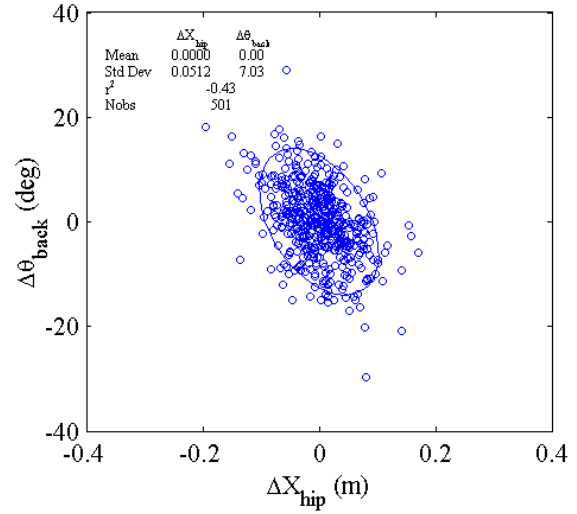


Figure B-5. Variation in rider back angle vs hip position for 501 riders in Europe.

APPENDIX C – DISTRIBUTION OF RIDING POSITION IN THE US

The distribution of rider position in the US, based on observations of 185 riders in the State of Ohio, is illustrated in Figures C-1 to C-5.

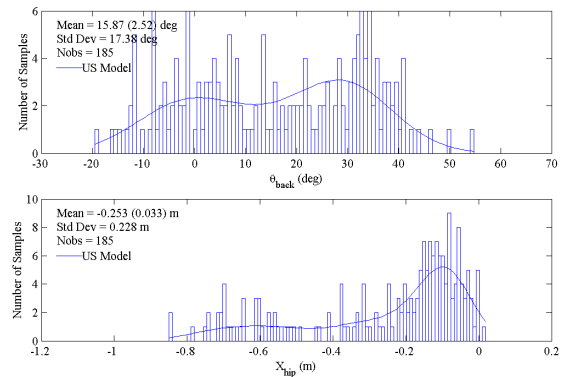


Figure C-1. Modeled and observed distribution of rider longitudinal hip position and back angle for 185 riders in the US.

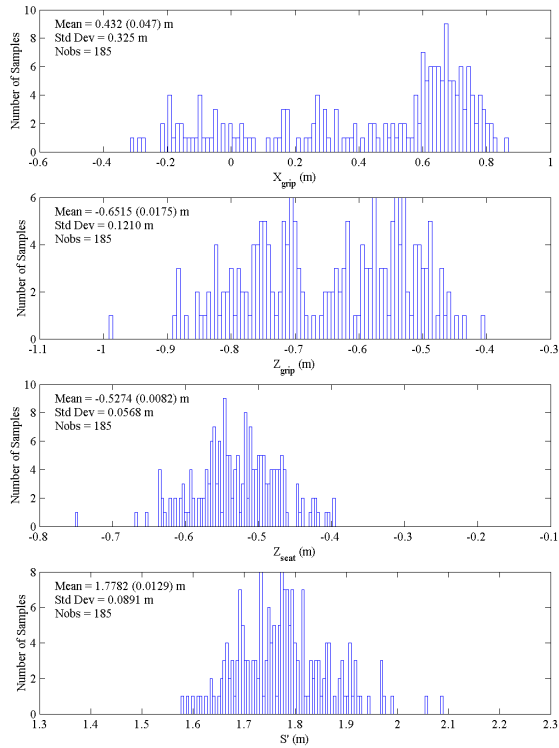


Figure C-2. Distribution of observed motorcycle seat height, hand grip location, and rider stature for 185 riders in the US.

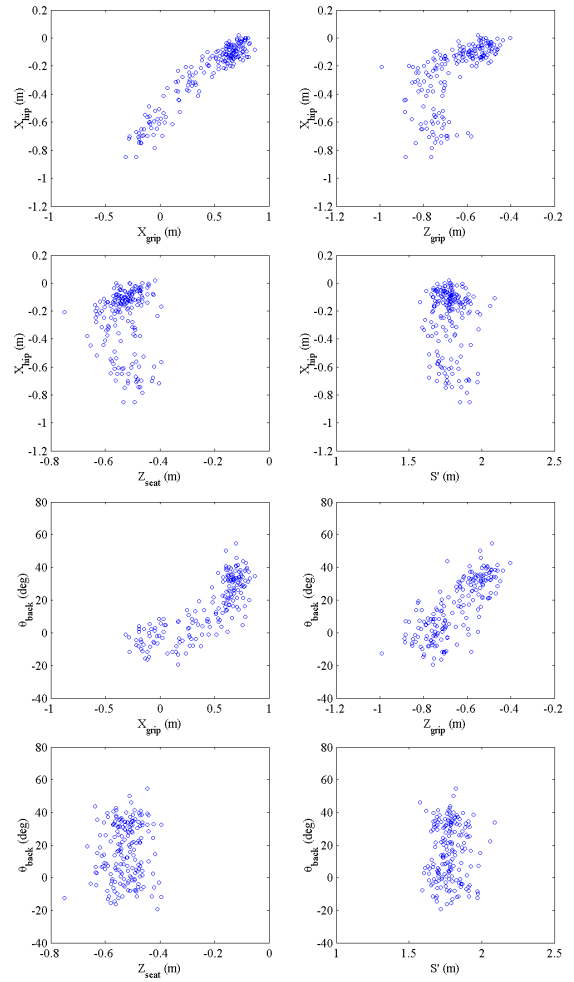


Figure C-3. Observed rider hip position and back angle vs motorcycle seat height, hand grip location, and rider stature for 185 riders in the US.

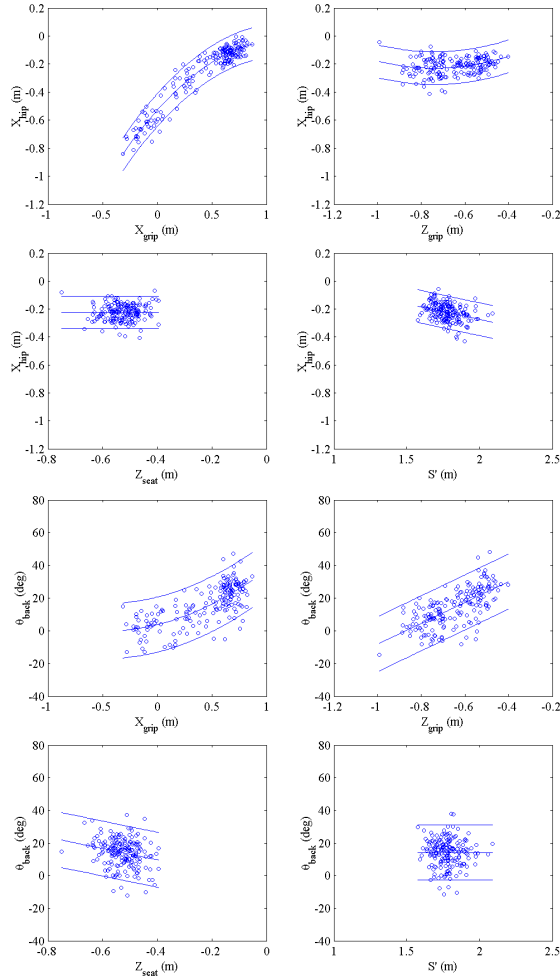


Figure C-4. Rider hip position and back angle vs. motorcycle seat height, hand grip location, and rider stature, for 185 riders in the US, while controlling for the other independent variables.

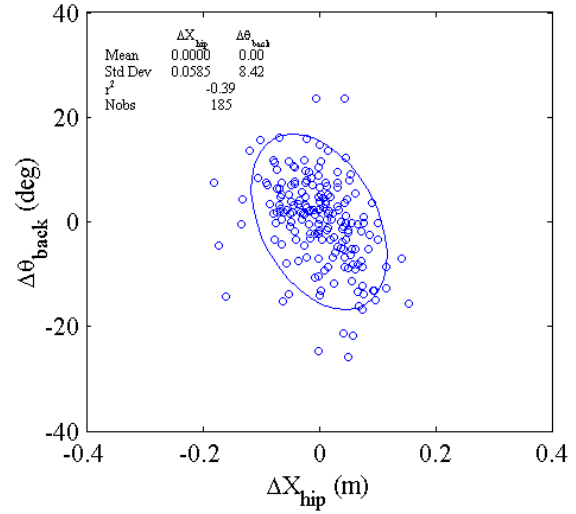


Figure C-5. Variation in rider back angle vs hip position for 185 riders in the US.

APPENDIX D

The RPRED statistic was the figure of merit used to select the regression models. It is based on the PRESS statistic described in Section 6.8 of Draper and Smith [3]. The RPRED statistic can be calculated according to the following equation:

$$RPRED = 1 - \frac{PRESS}{SS_{TOT}}$$

Where

$$PRESS = \sum_{k=1}^n (y_k - \hat{y}_{k,-k})^2$$

$$SS_{TOT} = \sum_{k=1}^n (y_k - \bar{y})^2$$

$$\bar{y} = \frac{1}{n} \sum_{k=1}^n y_k$$

The RPRED statistic is similar to the regression model R^2 statistic, except that PRESS residuals are used instead of ordinary residuals. Whereas ordinary residuals are the difference between the observed value for y and the estimated value \hat{y} , PRESS residuals are the difference between the observed y and \hat{y} predicted by a model in which one rating at a time had been set aside and not used to identify the model. Therefore RPRED is a measure of both the fit and the predictive capabilities, and RPRED values approaching 1 are desirable.

Experimental and numerical studies of muscular activations of bracing occupant

Hyung Yun Choi

Sung Jin Sah

Bumsoo Lee

Hongik University

Korea

Hyeon Seok Cho

Sung Jae Kang

Mu Seong Mun

Korea Orthopedics & Rehabilitation Engineering Center

Korea

Inhyeok Lee

Hankook ESI

Korea

Jinhee Lee

IPS International

Korea

Paper No. 05-0139

ABSTRACT

Occupants who recognize the approaching crash tend to brace themselves. This reflexive muscular activation can affect the kinematics and kinetics of occupant during the crash event but the mechanisms of potential muscle contraction in car crash event remains poorly understood. A quantitative investigation of muscular activation has been attempted by utilizing dynamometer, sled and EMG devices with human volunteers. The experimental findings have been incorporated into the numerical investigation by utilizing a finite element model of skeletal muscular structure of human body.

Eight male subjects were employed and the maximum amount of voluntary isometric muscular contraction for each limb joint at various joint angles was determined using a dynamometer and surface EMG. To mimic the approaching frontal crash and bracing, each volunteer was asked to brace himself when descending in inclined sled system began. During bracing, steering wheel and pedal forces were measured as well as the EMG signals at the volunteer's shoulder, elbow, wrist, knee and ankle joints. The pressure distributions between volunteer and seat back were also measured using a pressure mat.

Simulation of muscle activation for bracing occupant was performed using an optimization process for the joint muscle force calculations. The musculo-skeletal model with the optimized muscle parameters was utilized to validate its tensing behavior against the experimental results. The computed axial compressive loads on steering wheel were respectively 144N and

178N for two sled heights which correlates quite well with the average value of test measurements ($121.7 \pm 46.6\text{N}$ and $151.1 \pm 78.9\text{N}$). The computed reaction forces at pedal and seat back also exhibited quite good agreement with the test measurements.

INTRODUCTION

The bracing driver in pre-impact situation tends to extend elbow and knee joints, and consequently push the pelvis back into the seat and lean backward as shown in Fig. 1.



**Fig. 1 Postures of driver:
Before (left) and after (right) bracing**

The bracing induced by reflexive contractions of joint muscles change the kinematics and kinetics of occupant during the crash. Its effects on injury risk have been also investigated: Begeman et al [1] studied the response of the human musculo-skeletal system to impact acceleration. They employed volunteers and EMG technology to identify the muscular response before, during and after the impact acceleration. It was found that the tone of the lower extremity muscles changed the kinematics of occupant and force

distribution of restraints. However they only focused on the bracing of the lower extremity and also could not quantify the degree of the muscle activations. Klopp et al [2] also studied the effects of the reflexive bracing, a series of computer simulations, pendulum and sled tests with Hybrid III dummies and human cadavers. It was concluded that the effect of muscular preloading was to increase the efficiency of load transmission to the leg and the preloaded legs acted as additional restraints helping the occupant ride down the crash pulse. Gordon et al [3] performed static and dynamic characterizations of human hip, knee and ankle. They computed forces and torques acting on the joints by measuring seat and pedal loads.

In this study, the muscular activation of bracing occupants was quantified using a dynamometer, sled system and EMG devices with human volunteers. A deliberate process was taken in the selection of volunteers since the individual divergence in muscular structure between the volunteers might generate large deviations in the bracing test. Therefore, total 8 volunteers having similar body compositions as well as anthropometries were selected. Using the dynamometer, isometric voluntary maximal torques for 5 joints, shoulder, elbow, wrist, knee, and ankle of each volunteer were characterized. EMG signals at the pair of muscles, each representing an extensor and a flexor were also monitored for various joint angles. Assuming the maximal voluntary effort was made, the extension and flexion should have brought the maximum levels of EMG signals from the associated muscle group. The mean rectified EMG signals from the maximally contracted muscle were utilized as a reference value for computing the activation level of corresponding muscle in bracing test with a sled system. To mimic the approaching frontal crash, the inclined sled system driven by gravity was designed and built as shown in Fig. 2. Each volunteer was asked to brace himself when descending began on the slope until the sled stopped by striking an energy-absorbing barrier. During the bracing in the sled, steering wheel and pedal forces were measured from the installed load cells as well as the EMG signals from the volunteer's joint muscles. The pressure distributions between the back of volunteer and seat were also measured using a pressure mat

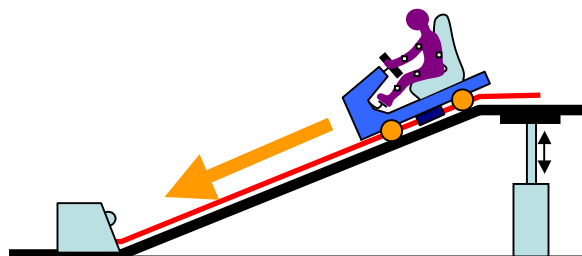


Fig. 2 Sled system for bracing test

Finite element modeling of skeletal muscular structure and numerical investigation of its activations were performed subsequently to the experimental study. An optimization scheme based on an ergonomic criterion [4] was adopted for the calculation of internal muscular force distributions around joints. The muscle tensing behavior of the model was validated against the test results.

EXPERIMENTAL STUDY

Selection procedure of volunteers

The lean balance, ratio of muscle mass to the body weight and isometric voluntary maximum torques at elbow and knee joints were extra indices in addition to the anthropometric data for selecting volunteers. During the first round of the two-stage selection process, 20 out of 128 volunteers were selected based on BMI (Body Mass Index, kg/m²). The selection criterion of the BMI was 22 ± 1 kg/m² (Height: 1.75 ± 0.01 m, Body mass: 67 ± 1 kg). Isometric voluntary maximal elbow and knee joint torques had been measured with those 20 volunteers in the second round and 8 volunteers with responses closest to mean values were then chosen for the final tests. As a consequence, the dispersion in the final group of volunteers, e.g., standard deviation of maximal joint torques had decreased from the first round selections by 41% and 26% for elbow and knee joints, respectively. The average and standard deviation of the final 8 volunteer's anthropometric data and body compositions are listed Table 1

Table 1 Volunteer data

	Age	Height (m)	Weight (kg)	BMI (kg/m ²)	RA lean balance (%)	RL lean balance (%) [*]
Mean	24.2	1.746	67.31	22.09	4.62	13.28
S.D	1.69	0.84	1.55	0.61	0.31	0.58

^{*}: Ratio of right arm muscle mass to total body mass (%)

^{**}: Ratio of right leg muscle mass to total body mass (%)

Measurement of isometric maximal joint torque and voluntary muscle contraction using dynamometer

In order to gauge the maximal voluntary contractions (MVC) of selected muscles, each volunteer was asked to produce the utmost isometric joint torques in a dynamometer (model: Biodex™ System 3 Pro). The EMG activities of a pair of muscles for extension and flexion were simultaneously measured using surface electrodes. The selected joint muscles for EMG measurement are listed in Table 2.

Table 2 Joint muscles for EMG activity monitoring in dynamometer test

Joint \ Muscl	Extensor	Flexor
Shoulder	Posterior deltoid	Anterior deltoid
Elbow	Medial triceps	Biceps brachii
Wrist	Extensor capri radialis	Flexor capri radialis
Knee	Rectus femoris	Biceps femoris
Ankle	Soleus*	Tibialis anterior**

*: plantaflexor, **: dorsiflexor

The dynamometer test setup with a volunteer is shown in Fig. 3. The measured maximal joint torques with various joint angles for five joints in upper and lower limbs (shoulder, elbow, wrist, knee, ankle) during isometric muscle contractions are shown in Fig. 4.



Fig. 3 Measurement of maximal voluntary joint torque in a dynamometer

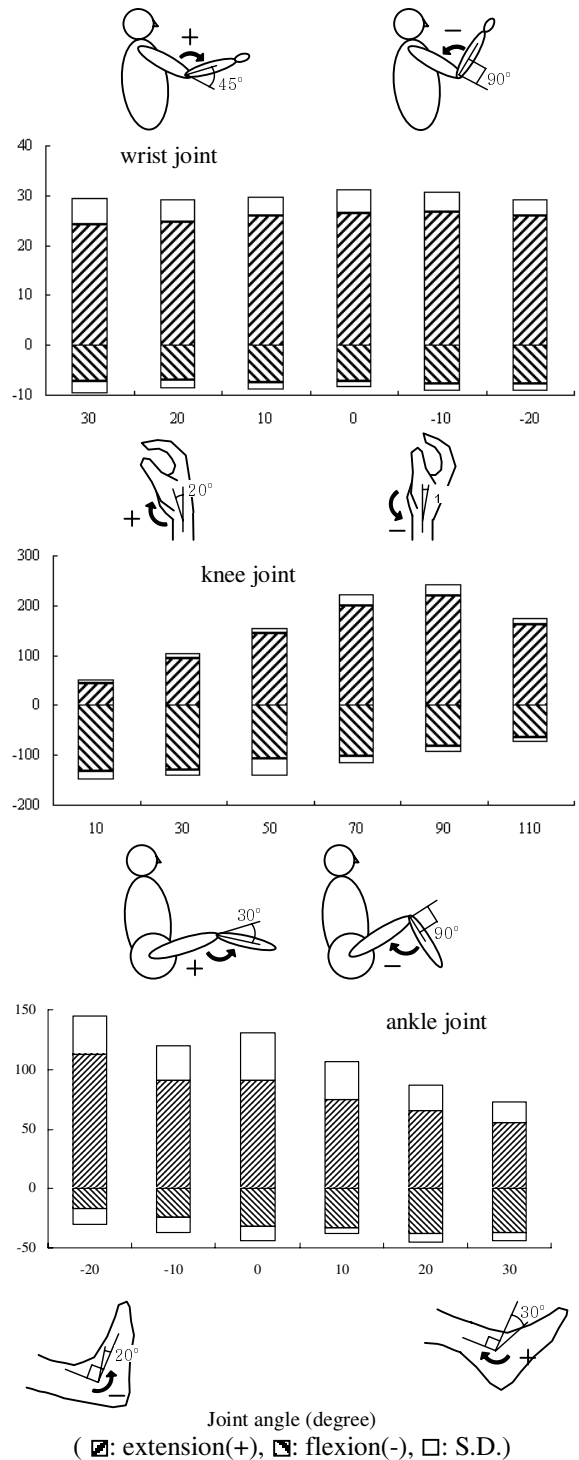
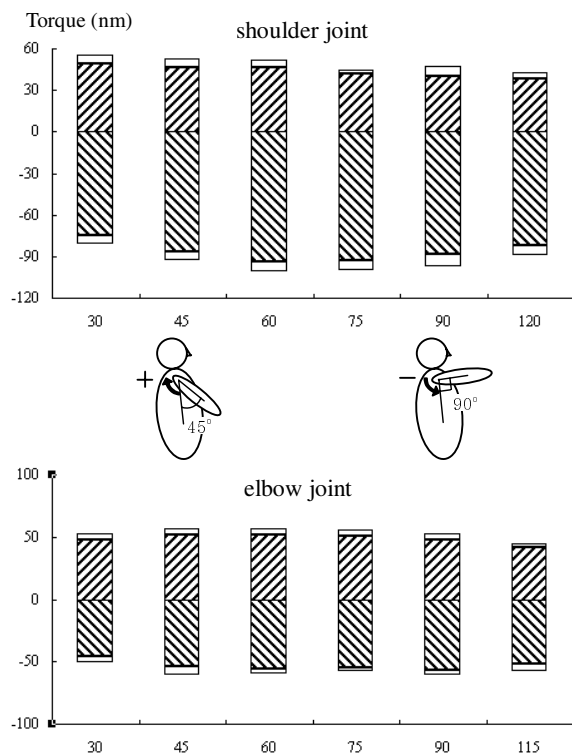


Fig. 4 Maximal isometric voluntary joint torques from dynamometer test

During the dynamometer test, EMG activities of representative pairs of joint muscles in Table 2 were monitored. Fig. 5 shows a typical raw data set of the elbow joint composed of torque and EMG signals

obtained from dynamometer and surface electrodes, respectively.

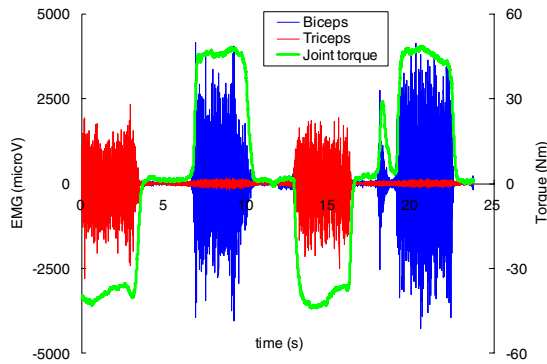
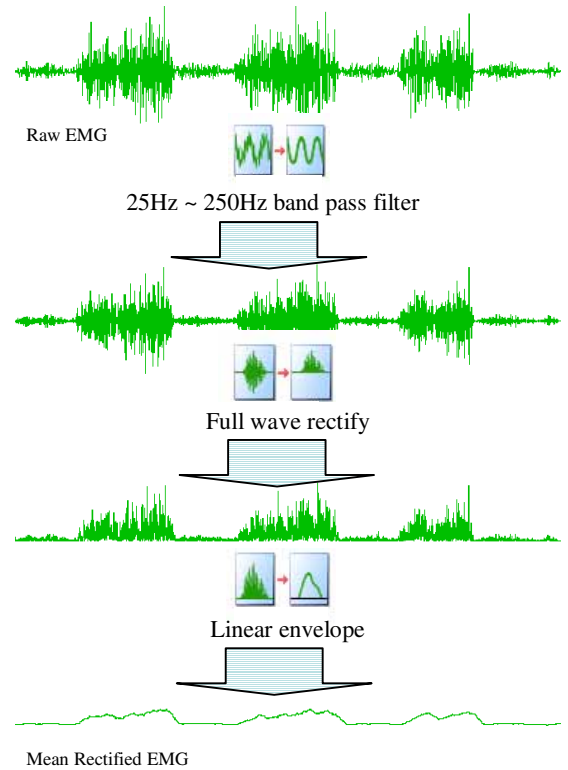


Fig. 5 Typical raw EMG signals and joint torque from dynamometer test (Elbow joint at 75° angle)

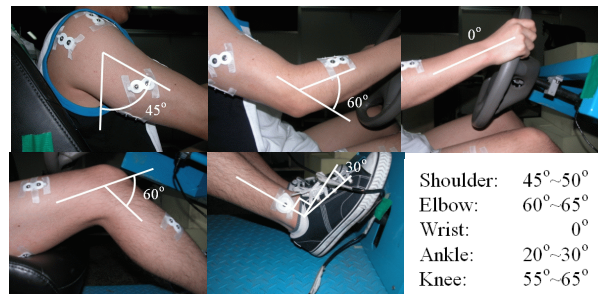
Processing the raw EMG signal, rectifying, filtering (low pass filter: 250 Hz, high pass filter: 25Hz), and smoothing (LP filtering), a MR EMG (Mean Rectified EMG) signal was obtained as shown in Fig. 6. A RMS (Root Mean Square) value was then computed from the MR EMG signal, which represents an intensity of the EMG signal and an index of muscle activation level at the maximal voluntary contraction (MVC). There were considerable divergences in RMS values between volunteers in spite of their similar lean balances. This might be due to the different amount of subcutaneous fat tissue between volunteers and variability in electrode positioning relative to active muscle fibers.



ig. 6 EMG signal processing

Measurement of activation level of bracing muscles in sled system

Fig. 7 shows a volunteer's configuration in sled test. Two different sled heights, 0.9m and 1.0m were tried twice each and the measurements were very repeatable.



(a) Initial joint angles in sled test



(b) Volunteer in descending slope (Left: before bracing, Right: after bracing)

Fig. 7 Configuration of volunteer in sled test

Typical profiles of reaction forces at steering wheel and pedal are presented in Fig. 8 with mean rectified EMG signals monitored at the muscles of the elbow and ankle joints. In general, the reaction force developed 0.3-0.5s after the onset of EMG activity, which is similar to the timing observed in an earlier volunteer test [1].

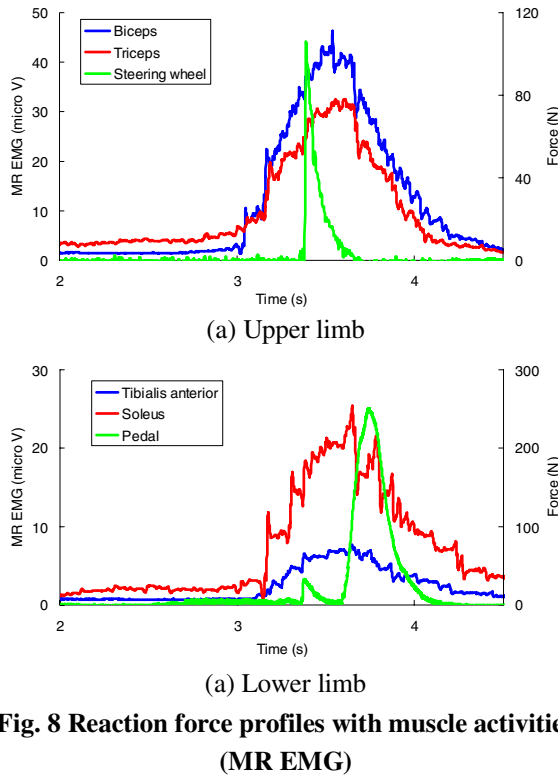


Fig. 8 Reaction force profiles with muscle activities (MR EMG)

The volunteer's pattern of bracing in sled test was quantified by computing his ratio of joint muscle activation levels to the maximal voluntary contractions from dynamometer test mentioned in previous section. Fig. 9 shows the %MVCs, the ratios of RMS of MR EMG signals between sled and dynamometer tests. The higher sled at 1.0m height tends to induce from 5% to 20% more muscle activations in both extensors and flexors than the lower sled at 0.9m height, -except the knee joint. But quite same ratios of activations between extensors and flexors were produced from both sled heights. The extensors were significantly more activated than flexors in elbow, wrist and ankle joints while the opposite tendency found in shoulder and knee joints. There were relatively large standard deviations in the sled test comparing to the dynamometer test since the styles of the bracing might have differed greatly between volunteers.

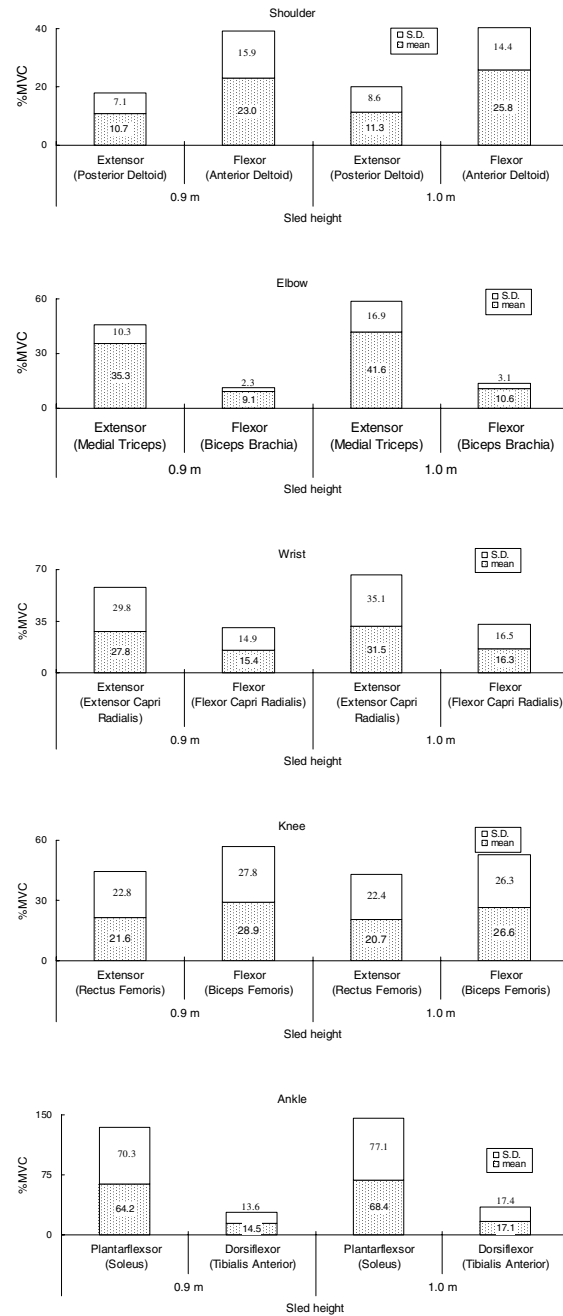


Fig. 9 %MVC of joint muscles from sled test

The average axial forces measured at steering wheel and pedal as shown in Fig. 10 also indicate that volunteers braced more at the higher sled drop resulting in larger reaction forces.

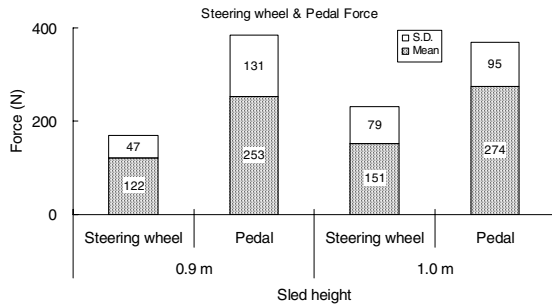


Fig. 10 Reaction forces at steering wheel and pedal

Elbow joint extension and subsequent rearward rotation of the upper body developed more contact pressure on seat back as displayed in Fig. 11. The average net normal reaction force at seat back, the area integration of increased pressure by bracing is shown in Fig. 12.

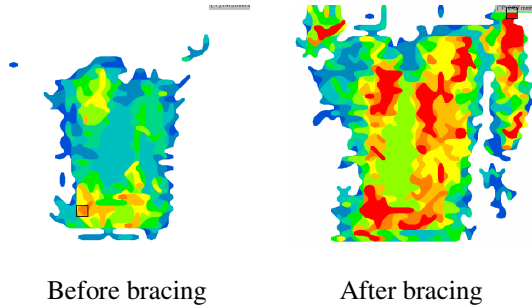


Fig. 11 Measured contact pressure distributions between volunteer and seat back

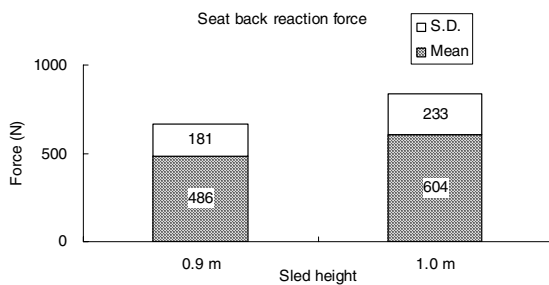


Fig. 12 Reaction force at seat back

NUMERICAL STUDY

Numerical investigation of muscular activation was performed subsequent to the experimental study presented in the first part of this paper.

Human body modeling

The H-model, shown in Fig. 13, is a finite element human body model representing the 50% male anthropometry. This model is widely used for

crashworthiness simulation [5]. Each body segment in the H-model, in a version aiming for muscle tensing simulation, was defined as a rigid body and was linked by the anatomical joints and with the relevant skeletal muscles represented by bar finite elements [5]. The incorporated sixteen major skeletal muscles modeled by Hill type one dimensional bar elements [6] are listed in Table 3. The articulated joints were modeled with kinematic joint elements whose characteristics were designed to have no resistance within the range of motion such that only muscle forces could be the source of joint torques. Seeking the average of active isometric muscle force-length relations of the model, the maximal forces (F_{max}) of each muscle at various lengths with different joint angles were computed based on the maximal isometric voluntary joint torques obtained from dynamometer test in Fig. 4. In the case when multiple muscles were involved for the same articulation DOF, e.g., biceps brachii, brachialis, and brachioradialis for elbow flexion, an optimization algorithm was adopted to determine the likely distribution of the muscle forces (design variable) by minimizing the active muscle energy (objective function) for static equilibrium (constraints). The sequential response surface method in HyperOpt [7] was selected for the optimization process. Fig. 14 shows the result of computed isometric maximum muscle forces for shoulder, elbow, knee, and ankle joints.

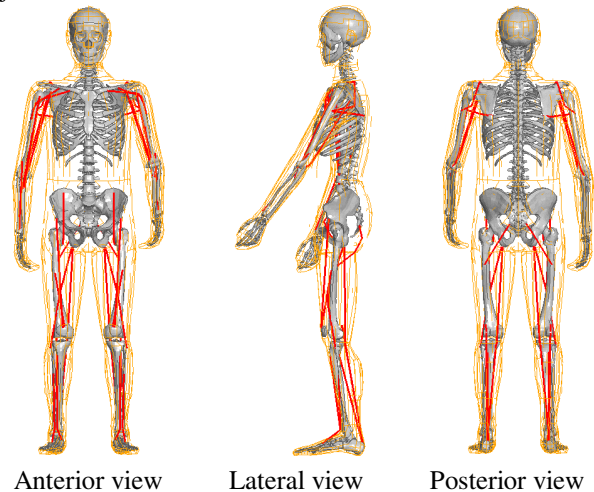
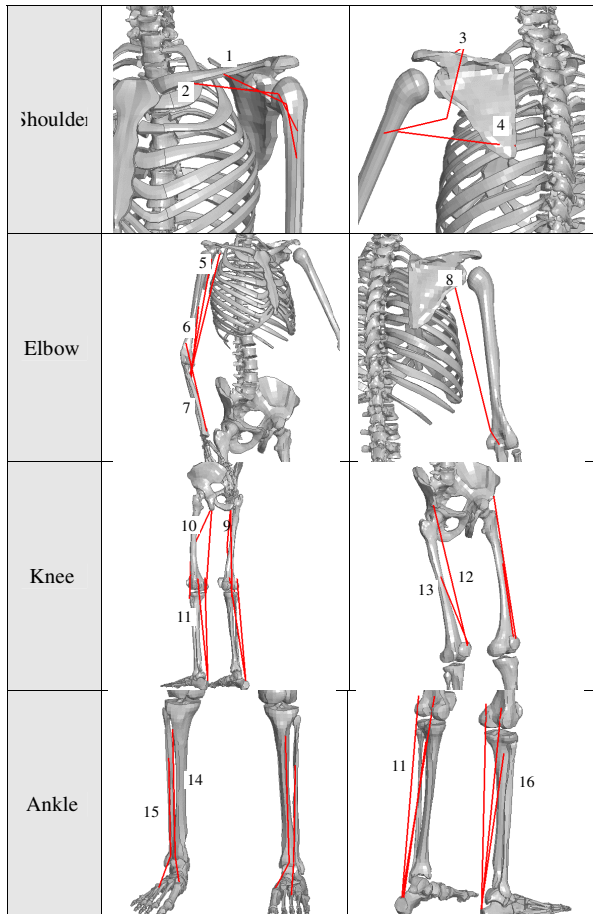


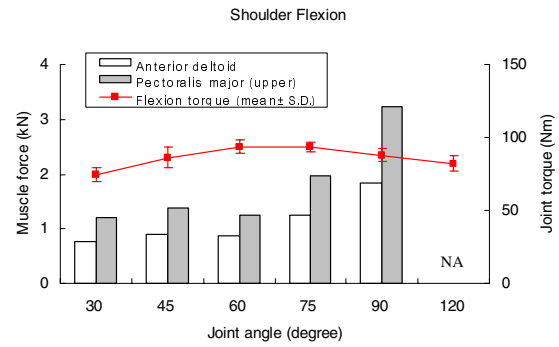
Fig. 13 H-model with skeleton and muscles

Table 3 Skeletal muscles in H-model for the simulation of bracing

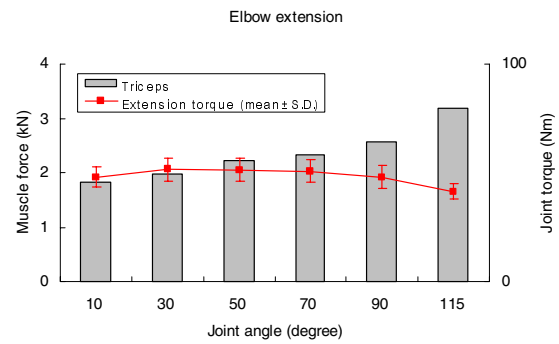
	Flexors	Extensors



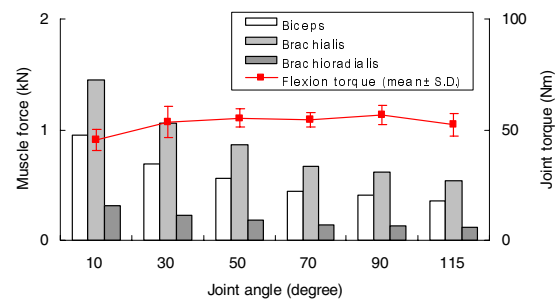
1. Anterior deltoid
2. Pectoralis major (upper part)
3. Posterior deltoid
4. Teres major
5. Biceps
6. Brachialis
7. Brachioradialis
8. Triceps
9. Biceps femoris
10. Semitendinosus
11. Gastrocnemius (lateral & medial)
12. Rectus femoris
13. Vastus intermedius
14. Tibialis anterior
15. Extensor digitorum
16. Soleus



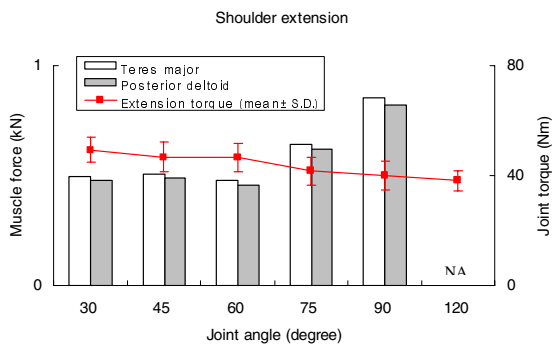
(a) Shoulder joint



Elbow Flexion



(b) Elbow joint



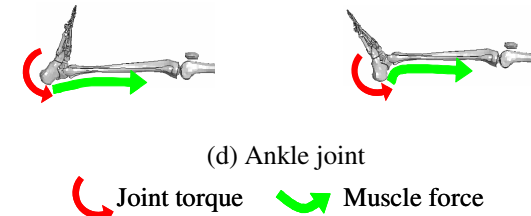
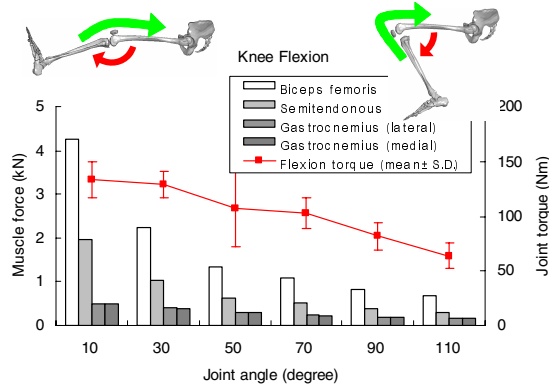
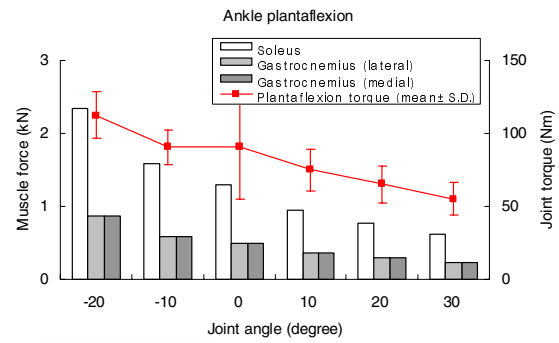
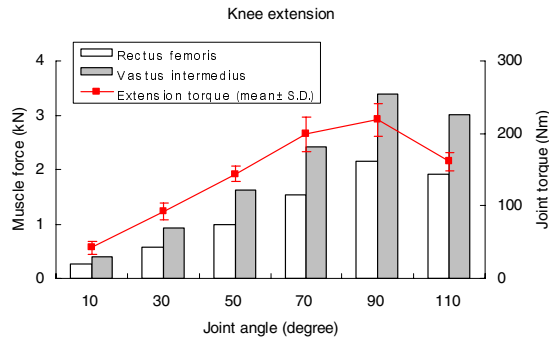


Fig. 14 Computed isometric maximum muscles forces (F_{max}) (wrist joint was not performed)

Simulation of bracing occupant

The seat, floor panel and steering wheel of the sled system were added to the H-model with driving posture as shown in Fig. 15. Sliding contact interfaces were defined between the seat and the skin part of the H-model. Translational motions of hands and feet were respectively tied to steering wheel and pedal such that the forces generated from the muscle bracing could be transmitted.

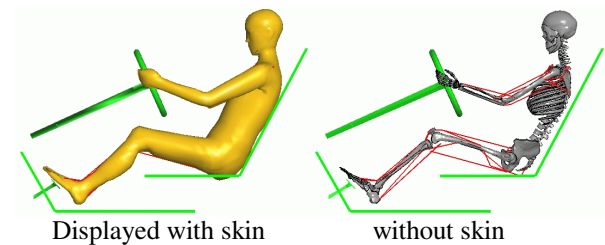
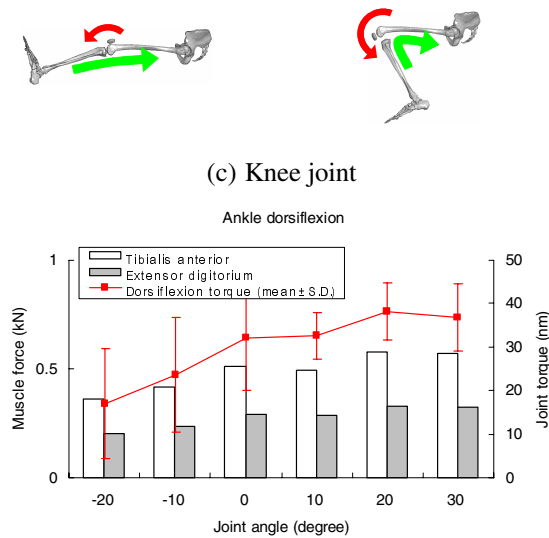


Fig. 15 Configuration of H-model for the simulation of bracing occupant

In the simulation, the average values of %MVC in joint muscles, the ratios of RMS of mean rectified EMG signals between sled and dynamometer tests which are listed in Table 4 were applied as activation levels of the bracing muscles. The reaction forces at the steering wheel, pedal, and seat back were then computed until they statically equilibrated with the imposed bracing muscle forces. The simulation results correlate quite well with the experimental measurements as shown in Fig. 16

Table 4 Average volunteer's muscle activation levels used for bracing simulation

Sled height	0.9 m			1.0 m		
Muscle joint	xtensc	Flexor	Ratio*	xtensc	Flexor	Ratio*
Shoulder	10.7	23.0	0.46	11.3	25.8	0.44
Elbow	35.3	9.1	3.88	41.6	10.6	3.93
Wrist**	15.4	27.8	0.55	16.3	31.5	0.52
Knee	21.6	28.9	0.75	20.7	26.6	0.78
Ankle	64.2	14.5	4.43	68.4	17.1	3.99

*: Ratio=Extensor/ Flexor, ** Wrist joint is not included in the model

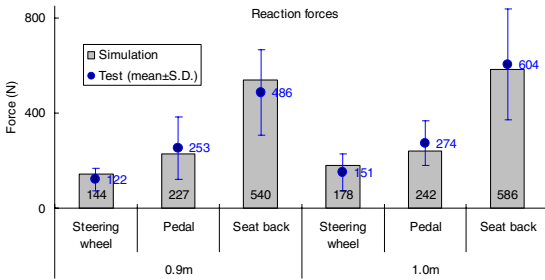


Fig. 16 Comparison of reaction forces between volunteer test and simulation

The simulated driving posture altered by muscle tensing is illustrated in Fig. 17. There is a noticeable straightening of arms and an elastic penetration into the seat surface in the bracing position.

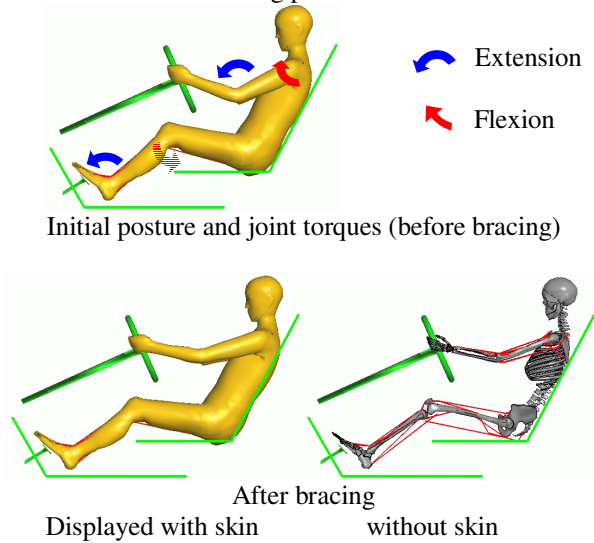


Fig. 17 Simulated bracing posture

The computed peak muscle forces during the bracing, which are proportional to the activation levels multiplied by the isometric maximum voluntary forces at corresponding joint angles, are shown in Fig. 18. The net joint torque generated by tensing of each muscle depends on the effective moment arm of the muscle with respect to the corresponding joint center.

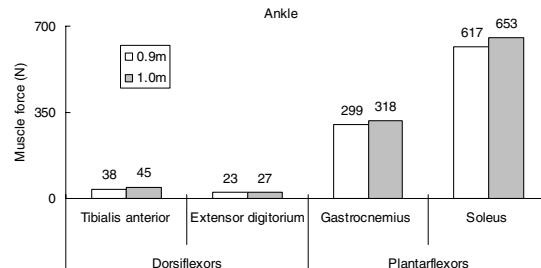
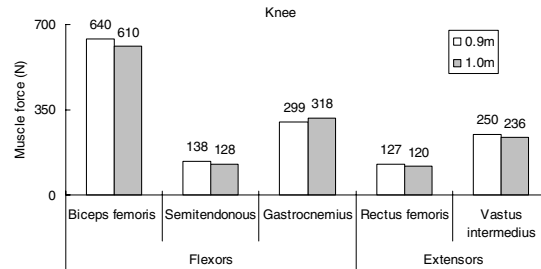
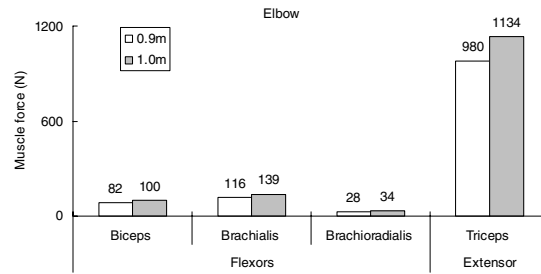
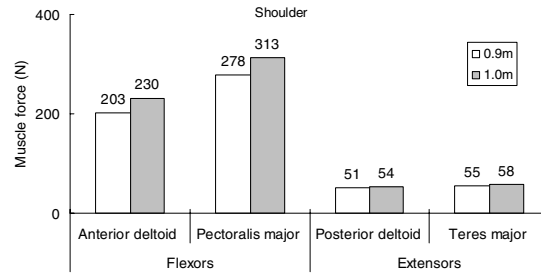


Fig. 18 Computed bracing muscle forces

CONCLUSIONS

Vehicle occupants tend to brace in anticipation of a crash and this pre-crash muscle tensing can change the kinematics and kinetics of the occupants. The pattern of extremity bracing, i.e., shoulder, elbow, wrist, knee and ankle joints was quantitatively analyzed by volunteers EMG test. For shoulder, elbow and ankle joints, activations of extensors were substantially higher than those of flexors. However, an opposite trend was found at wrist and knee joints. The reaction forces at steering wheel, pedal and seat back were also measured to identify the degree of muscle tensing.

Numerical simulation of muscle tensing was

performed to verify the finite element human body model. The simulated muscle tensing behavior of the model such as amounts of reaction forces at the steering wheel, pedal and seat back correlated quite well with the test results. It was the first step in the development of human body model to investigate the effect of muscle tensing on occupant kinematics and kinetics. A crash simulation with likely dynamic muscle activations taken into consideration would follow as a next step.

ACKNOWLEDGMENT

The authors would like to thank Prof. Richard Kent at Center for Applied Biomechanics of UVA for reviewing the manuscript and providing a constructive commentary. The authors also would like to thank Dr. Eberhard Haug for his advice on the simulation process.

This study was supported, in part, by Korean ministry of science and technology.
(Project No.: M10139080002-04L1008-00210)

REFERENCES

- [1] Begeman, P., A. King, R. Levine, and D.C. Viano. 1980. "Biodynamic response of the Musculoskeletal System to Impact Acceleration" Proc. 24th Stapp car crash Conf., SAE paper 801312
- [2] Klopp, G. S., J. R. Crandall, E. M. Sieveka, and W. D. Pilkey. 1995. "Simulation of Muscle Tension in Pre-impact Bracing", IRCOBI Conference on the Biomechanics of Impact
- [3] Gordon, S., P. Orticke, J. Prince, and R. Mcmeekin. 1977. "Dynamic Characteristics of Human Leg Joints" Proc. 21st Stapp car crash Conf., SAE paper 770924
- [4] Haug, E. Allain, J.C., and H. Choi. 2001. "Modeling of Ergonomics and Muscular Comfort" Journal of KSME, Vol. 15 No. 7, pp 982-994.
- [5] Handbook of Numerical Analysis, Volume XII: Computational Models for the Human Body – Human Models for Crash and Impact Simulation, pp 297-361, Elsevier, 2004
- [6] PAM-CRASH/SAFE USERS AND THEORY MANUAL, VERSION 2004, ESI GROUP, FRANCE
- [7] HYPER-OPT, ALTAIR ENGINEERING. INC, USA

DEVELOPMENT OF AN IMPROVED NECK INJURY ASSESSMENT CRITERIA FOR THE ISO 13232 MOTORCYCLIST ANTHROPOMETRIC TEST DUMMY

R. Michael Van Auken

John W. Zellner

Terry Smith

Dynamic Research, Inc.

United States

Nicholas M. Rogers

International Motorcycle Manufacturers Association

Switzerland

Paper No. 05-0227

ABSTRACT

The Motorcyclist Anthropometric Test Dummy (MATD) and injury risk/benefit analysis methods standardized under International Standard ISO 13232 allow the relative injury benefits and risks of rider protective devices fitted to motorcycles to be assessed, for a specific set of injury types. Research involving the feasibility of airbags fitted to motorcycles intensified the need to upgrade the crash test dummy neck injury assessment methods, and an improved dummy neck with multi-directional biofidelity and injury assessment capabilities and corresponding probabilistic four-axis neck injury criteria (upper neck axial compression and tension forces, lateral bending, extension and flexion, lateral bending, and torsion moments) were subsequently developed. The four-axis neck injury criteria originally proposed for ISO 13232 had a “trapezoidal egg” shaped injury index, based on mechanical stress ratio principles, which tended to under-predict injuries under tension-only loading conditions, compared to injurious tension force levels reported in the technical literature. A revised neck injury criteria was then developed having a “clipped trapezoidal egg shape” index that is similar in concept to the two-axis “clipped kite” shape criteria specified by the US Motor Vehicle Occupant Crash Protection Standard (FMVSS 208). The improved Neck injury criteria were developed by fitting the distributions of neck injury severities observed in on-scene in-depth investigations of 565 real-world motorcycle crashes, including the direction of neck motion indicated by special detailed neck dissections in 67 fatal cases, to the distributions of upper neck forces and moments measured in calibrated computer simulations of the MATD with the improved neck in the 565 crashes. The improved injury criteria can estimate the probability of neck injury, based on four-axis upper neck forces and moments measured with the new MATD neck with a higher level of overall agreement

with neck injury severity levels and directions observed in real world crashes, compared to the previous four-axis criteria.

INTRODUCTION

Background

INTERNATIONAL STANDARD 13232 specifying test and analysis procedures for the research and evaluation of rider crash protective devices fitted to motorcycles, first approved and published in 1996 [1], has undergone a comprehensive review as a result of experience with the Standard (e.g., Zellner, et al. [2]). Recommendations for changes and improvements were made in all aspects resulting in the draft first revision of ISO 13232 [3].

The recommendations included proposed changes to the motorcycle anthropometric test dummy (MATD) neck (in Part 3 of the revised Standard [3]), described in Withnall et al. [4]; and the neck injury probability analysis (in Part 5 of the revised Standard [3]), described in Van Auken et al. [5] and herein. These changes were considered necessary because the neck injury criteria in the original (1996) Standard:

- did not provide an indication of the AIS injury severity level;
- were “pass/fail” in nature, indicating either “likely [neck] fracture or dislocation [with] a fatal propensity” or non-injury [1], rather than probabilistic; and
- tended to over predict the number and likelihood of neck injuries ($\geq 30\%$) for a census sample, compared to actual injury data ($\leq 6\%$);

as explained in Annex J of Part 5 of the revised Standard [3]. Furthermore, the 1996 “pass/fail” neck injury criteria is fundamentally different than the probabilistic injury severity (AIS) and injury cost model for the head, chest, abdomen, and lower extremities, based on injury assessment variables

measured by the MATD, specified in Part 5 of the Standard. The initial basis for this injury model was reported in Newman et al. [6], with example application in Kebschull et al. [7]. These limitations in the 1996 neck injury criterion, due to the limited injury tolerance data that was available at the time, became especially important in airbag evaluations that involved severe neck loading. For example, Ramet et al. [8] reported severe upper neck lesions with cadavers positioned on prototype motorcycle airbags, suggesting that a better estimate of neck injury probability would be required.

A probabilistic four-axis neck injury criteria described by Van Auken et al. [5] was initially proposed for the revised Standard. This criteria was based on a “trapezoidal egg” shaped injury index which combined the effects of axial neck tension/compression force, flexion/extension moments, lateral bending moment, and torsion moment. This index was derived according to mechanical stress ratio principals. However, this “trapezoidal egg” based criteria tends to under-predict injuries under tension only loading conditions, compared to injurious force levels reported in the technical literature. For example, Wilber (AAMA) [9] reported that a neck tension limit of $F_T=4170$ N corresponds to a 3% probability of AIS 3+ neck injury, which is a much larger probability than would be predicted by the “trapezoidal egg” criteria in [5] at this force level. This paper describes the development of improved four-axis criteria that does not under-predict injuries in tension only loading conditions.

Objectives

The objectives of this study were to develop a new, improved, probabilistic neck injury criterion compatible with the criteria employed in other body regions of the MATD, and taking into consideration available information on the probability of neck injury due to neck tension. The criteria would be appropriate for assessing AIS 0 to 6 skeletal and ligamentous injuries to the upper neck defined by AO/C1/C2. The new neck design and injury criteria have been proposed in the draft first revision of the Standard for use in the risk/benefit analysis and injury severity and cost models.

In order to achieve these objectives the following refinements were accomplished:

- the computer simulations of the new neck were refined to better match existing and new test data,
- The LA/Hannover neck injury data were further screened to exclude non-relevant injuries such as

abrasions and lacerations,

- Three LA/Hannover cases were excluded from the analysis because they occurred at higher speeds than the corresponding USC fatal cases.
- The neck injury index was modified to include an additional term to account for increased injury potential due to axial tension/compression forces.

REQUIREMENTS FOR THE NECK INJURY CRITERIA DEVELOPMENT

The objective was to develop a probabilistic, objective injury criterion that would be:

- consistent with the form of the injury criteria for the other body regions in ISO 13232-5,
- consistent in general form with other neck injury criteria applicable to other mechanical necks (e.g., Eppinger et al., [10], [11])
- based on the force and moment time histories obtained from either computer simulations or full scale tests using the new MATD neck, according to the relevant parts of ISO 13232,
- suitable for predicting AIS 1 to 6 level injuries to the AO/C1/C2 region of the cervical spine,
- consistent with the frequency distributions of:
 - neck injury severities observed in the census of LA/Hannover non-fatal and fatal motorcycle-car accidents (ISO-13232-2) and USC fatal motorcycle-car accidents ([12], [13]);
 - AO/C1/C2 neck injury severities and directions observed in the USC fatal motorcycle-car accidents;
 - peak AO forces and moments observed in calibrated computer simulations of the LA/Hannover non-fatal and fatal motorcycle-car accidents and USC fatal motorcycle-car accidents, assuming the baseline helmet and opposing vehicle were present in all cases, and a GPZ 500 motorcycle was the subject motorcycle in all cases.

REFINED COMPUTER SIMULATION OF THE MATD NECK

A computer simulation of the new MATD neck was developed using the US Air Force Articulated Total Body (ATB) Program [7], [14] in order to estimate the neck forces and moments that would have been measured by the MATD in the LA/Hannover and USC accidents. The mathematical model of the new neck comprised 8 segments (lumped mass rigid bodies) connected in series between the lower neck pivot point and the head, with 26 motion degrees of freedom, as illustrated in Figure 1. The model was

originally validated by comparing the predicted results to those observed in component and full-scale tests as reported in [15]. This model was then further refined to improve the force-deflection characteristics of the “stops” in the neck slider, and to match the response to a vertical impact laboratory test (Figure 2). For example, Figure 1 illustrates a comparison of still images from high-speed video of a rearward neck extension sled test and the corresponding computer simulation. Figure 3 illustrates a similar comparison for a full-scale test. Time histories comparing the digitized motions and computer simulations for these and other laboratory tests are illustrated in Appendix A.

The distribution of the maximum neck forces and moments from computer simulations of 498 LA and Hannover cases and 67 USC fatal cases are illustrated in Appendix B.

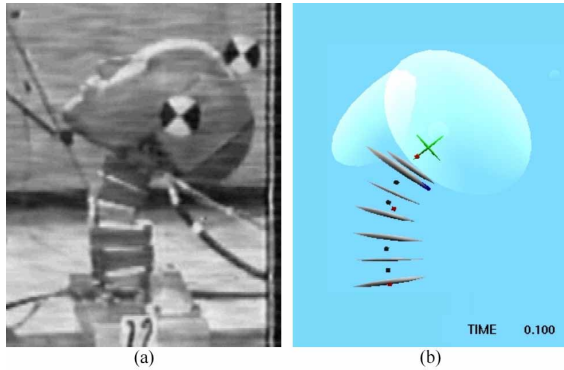


Figure 1. Rearward neck extension: a) dynamic laboratory sled test and b) computer simulation at 0.1 sec.

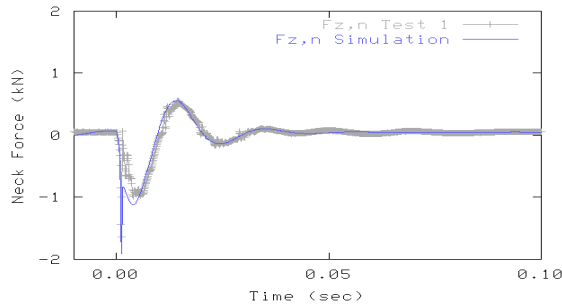


Figure 2. Axial neck force time responses measured in a laboratory head impact test and computer simulation.



(a)



(b)

Figure 3. Impact configuration 413-0/30: a) full scale test and b) computer simulation 0.1 sec after initial contact.

NECK INJURY PROBABILITY MODEL FORM

In order to maintain consistency of form with other injury functions in ISO 13232 and other scientific literature, it was assumed that the probability of a maximum $AIS_{AO/C1/C2} \geq k$ neck injury is related to an objective injury index NII_{max} as follows:

$$P(MAIS_{AO/C1/C2} \geq k | NII_{max} = x) = 1 - e^{-\left(\frac{x - \gamma_k}{\eta_k}\right)^{3.5}} \quad (1)$$

where γ_k and η_k are injury risk distribution coefficients to be determined. It was further assumed that this distribution approximates a normal distribution with mean μ_k , and standard deviation σ_k , according to the equations from SAE AE-9 [16] and Råde and Westergren [17]:

$$\mu_k = \gamma_k + 0.8997\eta_k \quad (2)$$

$$\sigma_k = 0.2847\eta_k \quad (3)$$

The objective injury index NII_{max} is defined as follows:

$$NII_{max} = \max_t NII(t) \quad (4)$$

$$NII(t) = \max \left\{ \underbrace{\left(\left(\frac{F_C(t)}{F_C^*} + \frac{F_T(t)}{F_T^*} + \left(\left(\frac{M_X(t)}{M_X^*} \right)^2 + \left(\frac{M_E(t)}{M_E^*} + \frac{M_F(t)}{M_F^*} \right)^2 \right)^{1/2} \right)^2}_{\text{Term 1}} + \left(\frac{M_Z(t)}{M_Z^*} \right)^2 \right)^{1/2}, \underbrace{\alpha \left| \frac{F_C(t)}{F_C^*} + \frac{F_T(t)}{F_T^*} \right|}_{\text{Term 2}} \right\} \quad (5).$$

where $NII(t)$ is defined by equation (5) and where

- F_C is the neck axial compression force,
 $F_C = -\min(F_Z, 0)$,
- F_T is the neck axial tension force,
 $F_T = \max(F_Z, 0)$,
- M_X is the neck lateral flexion moment,
- M_E is the neck extension moment,
 $M_E = -\min(M_Y, 0)$,
- M_F is the neck flexion moment, $M_F = \max(M_Y, 0)$,
- M_Z is the neck torsion moment,
- F_I^* and M_I^* are model coefficients corresponding to single axis failure criteria, to be determined for $I = \{C, T, X, E, F, Z\}$.

The first term in equation (5) corresponds to equation (5) in Van Auken et al. [5], which has a “trapezoidal egg” shape. It was adapted from the generalized stress ratio method for estimating the strength of materials under combined loading conditions described in many references (e.g., Shanley et al. [18], Bruhn [19], and US Department of Defense MIL-HDBK-5D [20]) and assuming that the generalized exponent has a value of either 1 or 2. For example Figure 1.5.2.5 of MIL-HDBK-5D ([20], pp 1-29) indicates that for various materials, the exponents in equation (5) in general can have real values in the range of $n=1$ to 3. The assumption is that biological material such as ligaments and vertebral facets exhibit material characteristics analogous to those for metallic materials. For strength of materials, in general, bending and axial stresses are considered to be linearly additive (i.e., $n=1$); moments about orthogonal axes are considered to be resultants (i.e., $n=2$); and combinations of shear (i.e., torsion) and axial stress are considered to be resultants. Equations C4.11, C4.16, and C4.16 in Bruhn [19] are examples of stress ratios for these types of interactions. Equation (5) allows for asymmetric strengths (e.g., extension-flexion), and strengths in each direction which are independent of the strengths in the other directions, which was considered to be appropriate for composite structures

such as the human neck.

The second term in equation (5) is only a function of axial neck force, and effectively “clips” the “trapezoidal egg” shape if the α “clipping” coefficient is greater than 1. This term is modeled after NHTSA’s neck injury criteria [21], which limit the allowable neck tension and compression forces to values less than those of allowed for a “Nij” limit based on a combination of axial tension/compression force and flexion/extension moment. This limit was incorporated into the criteria recommended by Eppinger et al. [11] and appears to be based on axial neck tension/compression limits recommended by Wilber (AAMA) [9].

Neck shear forces are not included in this model because shear motions were observed in 64 of the 67 cases in the USC fatal accident database with AO/C1/C2 neck injuries. As a result, it was considered that there was insufficient information in this database to identify injury criteria based on shear force. Possible explanations for this are that neck shear motion may be uniformly associated with motorcycle (and perhaps nearly all motor vehicle) neck injuries; or alternatively, that neck shear motion is a fully coupled variable, uniformly associated with the other motions that are present (e.g., bending, torsion, and compression-tension).

Equation (5) can be re-expressed in terms of normalized neck force and moment components according to equations (6) and (7) as follows:

$$NII_I(t) = \begin{cases} \left(\frac{F_I(t)}{F_I^*} \right) & \text{for } I = \{C, T\} \\ \left(\frac{M_I(t)}{M_I^*} \right) & \text{for } I = \{X, E, F, Z\} \end{cases} \quad (7).$$

It was then furthermore assumed that if an $MAIS_{AO/C1/C2} \geq k$ injury does occur, then the injuries

$$NII^2(t) = \max \left\{ \left(NII_C(t) + NII_T(t) + \left(NII_X^2(t) + (NII_E(t) + NII_F(t))^2 \right)^{1/2} \right)^2 + NII_Z^2(t), \alpha (NII_C(t) + NII_T(t))^2 \right\} \quad (6).$$

are associated with the neck force and/or moment directions, I , which satisfy the equation:

$$NII_I(t_{max}) \geq Q_k^* \mu_k \quad (8).$$

where t_{max} is defined such that

$$NII(t_{max}) = NII_{max} \quad (9).$$

The Q_k^* coefficients have positive values between 0 and 1 which are also to be determined.

MOTORCYCLE ACCIDENT DATABASES

The coefficients for the assumed neck injury probability model were estimated from data describing 498 Los Angeles and Hannover motorcycle-car accidents (ISO 13232-2) and 67 USC fatal motorcycle-car accidents [13]. Features of these databases are summarized in Table 1. Note that 3

LA/Hannover cases were excluded from the analysis because the relative normal closing velocity was greater than the range of speeds in the USC fatal accident data (i.e., less than 121 km/h).

METHODOLOGY FOR INJURY CRITERIA DEVELOPMENT

The neck injury criteria were estimated using methods based on the available motorcycle accident data and several assumptions.

Basic Assumptions

Basic assumptions for this analysis were that:

- The sought for neck injury criteria would be applicable to a majority of motorcycle-car crashes. However, the range of crash conditions in the available accident databases limit the domain

Table 1.
Summary of Accident Databases

Sample Criteria		Accident Database		
		LA	Hannover	USC
Accident	Reporting criteria	Police reported	Police reported	Police reported
	No. of vehicles	2	2	2
	Accident configurations	All, except untestable configurations	All, except untestable configurations	All, except runaway/snag
	Investigation method	On scene, in-depth	On scene, in-depth	On scene, in-depth, including in-depth medical autopsies, neck dissections
Subject vehicle		Motorcycle with seated, solo rider	Motorcycle with seated, solo rider	Motorcycle with solo rider
	Person	Rider	Rider	Rider
	Injury severity	Injured or killed	Injured or killed	Death within 10 days
Other vehicle		Passenger car	Passenger car	Passenger car
Region		Los Angeles	Hannover	Los Angeles County
Time period		1976-1977	1980-1985	Aug 1978-Mar 1981
Sample size		501		67
	Relative normal closing velocity ≤ 121 km/h	498		67
	Non fatal neck injuries	$\leq 2\%$		92.5%
	Fatal neck injuries	Unknown, but $\leq 3\%$		7.5%
	Fatal (all causes)	3%		100%
Comment		No neck dissections, neck injuries for fatal cases unknown		Detailed injury information
Reference		ISO-13232-2	ISO-13232-2	[12], [13]

Notes:

- Ruptures, dislocations, and fractures
- The fatal sample indicates that nearly all of these motorcycle accidents involved non-fatal neck injuries. This confirms the assumption that 3 percent of LA/Hannover accidents that were fatal all involved some (i.e., non fatal) levels of neck injury.

of validity of the injury criteria. The neck injury criteria are not applicable to high-speed crashes with relative normal closing velocity greater than 121 km/h.

- The assumed mathematical injury probability model described by equations (1) to (9) are valid within the sought for domain of validity.
- The neck rupture, dislocation, and fracture injuries reported in the LA/Hannover databases are AO/C1/C2 neck injuries.
- The distribution of neck AO/C1/C2 injury severities in the 67 USC fatal accidents are the same as the distribution of neck rupture, dislocation, and fracture injury severities in the 13 fatal LA/Hannover accidents.
- The distribution of neck forces and moments predicted by computer simulations (based on ISO 13232 computer simulations) of 67 USC fatal motorcycle accidents with a GPZ 500 motorcycle and a helmeted rider, are the same as those which occurred in the 67 USC fatal motorcycle accidents, and that these distributions are representative of all fatal motorcycle accidents.
- The distribution of forces and moments predicted by the 498 ISO 13232 calibrated computer simulations with a GPZ 500 motorcycle and a helmeted rider are the same as those which occurred in the 498 LA/Hannover injury accidents, and that these distributions are representative of all injurious motorcycle accidents.

These assumptions are also based on the underlying assumption that neck forces and moments and resulting injury severity are independent of helmet use. Orsay et al. [22] have found that there is no relationship between helmet use and the prevalence of neck injuries.

Additional Assumptions

It was further assumed that:

- The forces in the new MATD dummy upper neck are those that are relevant and correlated with human upper neck injuries. The new MATD neck dynamic response in three axes has been validated against volunteer human response corridors as described by Withnall et al. [4]. This general approach for developing neck injury criteria has been commonly used by others in the past;
- The simulated dynamic response of the new MATD neck correlates strongly with the dynamic response from full-scale tests, as described herein and in [15];
- The distributions of neck forces and moments from calibrated computer simulations of a GPZ 500 and a helmeted rider for the 67 USC fatal accident cases are assumed to correspond to the distributions of the observed injury severities and motions;
- The coefficients that describe the relative distribution of neck injuries by direction (F_C^* , F_T^* , M_X^* , M_E^* , M_F^* , M_Z^* , and Q^*) are assumed to be the same for both fatal and non-fatal motorcycle-car accidents, and for all neck injury severity levels;
- F_C^* , F_T^* , M_X^* , M_E^* , M_F^* , and M_Z^* have positive values, which are assumed to be less than the overall maximum values for F_C , F_T , M_X , M_E , M_F , and M_Z that occur in the computer simulations of the 67 USC fatal cases, because observed injuries were previously associated with motions in each of these axes;
- The α “clipping” coefficient that describes the injury potential for axial forces relative to the injury potential for combined forces and moments may be different in the LA/Hannover and fatal USC motorcycle accidents. It is furthermore assumed that there were no injuries in the fatal USC motorcycle accidents resulting from only axial forces and that $\alpha = 1$ for these cases.
- The overall probabilities of neck injury in fatal and non-fatal subsamples of motorcycle-car accidents may be different (i.e., the intercept value μ_k for riders in fatal accidents may be different from μ_k for injured riders);
- The standard deviation of the injury risk, σ_k , which is related to the slope of the probability of injury vs. injury index curve, is the same for all AIS injury severity levels (i.e., failure mechanism is similar at all AIS levels, e.g., as assumed with the ISO 13232-5 thoracic compression injury probability). This assumption eliminates the possibility of overlapping injury risk curves (e.g. the probability of an AIS 3+ injury being greater than the probability of an AIS 2+ injury for a given injury index value);
- The coefficient of variation (standard deviation divided by the mean) of the AIS ≥ 3 injury risk curve is 0.2 (i.e., $\sigma_3/\mu_3 = 0.2$). This assumption is based on results for neck extension moment and tension described by Mertz and Prasad [23];
- The probability of AIS>3 injury due to a 4.17 kN tension force is 0.03, based on AAMA [9].
- “Direction of force” corresponds to “direction of motion” for each neck injury observed in the USC fatal accidents. The later was based on detailed reconstructions of rider motions and in particular head and neck kinematics by a panel of experts.

Methods

The coefficients for the assumed mathematical injury probability model were identified in two steps. First, the injury direction coefficients were estimated from the neck injury severities and directions observed in the 67 USC fatal accident cases. Then, the injury risk probability coefficients were estimated from the neck injury severities observed in the 498 LA/Hannover cases. This process is further detailed in the informative annexes to the draft first revision of ISO 13232-5 [3].

Injury direction coefficients

The values for F_l^* , M_l^* , Q_k^* , and S_k were estimated by fitting the distribution of neck injury severities and direction components, which were predicted by the model from computer simulations of the 67 USC fatal accidents, to the observed distribution of injury severities and directions observed in the USC 67 fatal accident database. S_k was defined such that $NI_{max} \geq S_k$ corresponded to a $MAIS \geq k$ injury in the 67 USC fatal accidents.

The distribution of neck injuries in the USC fatal accident database can be described by the frequencies with which the contributing directions occur by injury severity level. Let $n_{k,c,t,x,e,f,z}$ be the number of riders in the USC fatal accident database according to the AO/C1/C2 neck injury severity and axis/direction, where the subscripts c, t, x, e, f, z are either 0 or 1 as follows:

$i=1$ if the rider had an $MAIS_{AO/C1/C2} \geq k$ injury, and the injury was associated with direction F_l or M_l .

$i=0$ otherwise.

Note that $n_{k,0,0,0,0,0,0}$ represents the number of riders with $MAIS_{AO/C1/C2} < k$ injuries. Values of $n_{k,0,0,0,0,0,0}$ for the USC fatal accident database are listed in Table 2. The total number of cases in the fatal accident database is

$$n_{total} = \sum_{c=0}^1 \sum_{t=0}^1 \sum_{x=0}^1 \sum_{e=0}^1 \sum_{f=0}^1 \sum_{z=0}^1 n_{k,c,t,x,e,f,z} \quad (10).$$

which is a constant ($n_{total}=67$) for all injury severity levels k .

In a similar manner, let $m_{k,c,t,x,e,f,z}$ be the number of computer simulations where AO/C1/C2 neck injury is indicated, where the subscripts c, t, x, e, f, z are either 0 or 1 as follows:

$i=1$ if $NI_{max} \geq S_k$ and $NI_1(t_{max}) \geq Q_k^* S_k$.

$i=0$ otherwise.

The total number of computer simulation cases is

$$m_{total} = \sum_{c=0}^1 \sum_{t=0}^1 \sum_{x=0}^1 \sum_{e=0}^1 \sum_{f=0}^1 \sum_{z=0}^1 m_{k,c,t,x,e,f,z} \quad (11).$$

which is also a constant ($m_{total}=67$) for all injury severity levels k .

Table 2.
Distribution of neck AO/C1/C2 injuries in the USC fatal motorcycle accident database

k	Number of Cases with $MAIS_{AO/C1/C2} = k$	Number of Cases with $MAIS_{AO/C1/C2} < k$ ($n_{k,0,0,0,0,0,0}$)
0	3	0
1	0	3
2	9	3
3	39	12
4	0	51
5	11	51
6	5	62

The injury criteria coefficients F_l^* , M_l^* , Q_k^* , and S_k were selected to minimize the difference between the distributions of predicted and observed injuries. Specifically, the coefficients $S_k F_l^*$, $S_k M_l^*$, and Q_k^* were determined by the numerical searches described in Annex M of ISO 13232-5 to minimize the difference function J ,

$$J = \sum_{k=1}^6 J_k \quad (12).$$

where

$$J_k = \sum_{c=0}^1 \sum_{t=0}^1 \sum_{x=0}^1 \sum_{e=0}^1 \sum_{f=0}^1 \sum_{z=0}^1 \left(\frac{n_{k,c,t,x,e,f,z}}{n_{total}} - \frac{m_{k,c,t,x,e,f,z}}{m_{total}} \right)^2 \quad (13).$$

and where

$$m_{k,0,0,0,0,0,0} = n_{k,0,0,0,0,0,0},$$

$$S_1 = 1, \text{ and}$$

Q_k^* is the largest value that satisfies

$$NI_1(t_{max}) \geq Q_k^* S_k \text{ for at least one direction, } l, \\ \text{for each of the cases that satisfy } NI_{max} \geq S_k.$$

The constraint that $m_{k,0,0,0,0,0,0} = n_{k,0,0,0,0,0,0}$ was imposed in order to facilitate the model coefficient identification process. With this constraint, S_k can be directly calculated from the F_l^* and M_l^* coefficients, thus eliminating one coefficient from the model coefficient search. The constraint that $S_1 = 1$ was

chosen in order to uniquely define the absolute magnitude of the F_I^* and M_I^* coefficients.

Injury risk probability coefficients

The values for μ_k were then estimated by fitting the distribution of neck injury indices predicted by the model from the computer simulations of the 498 generic LA/Hannover cases to the distribution of injury severities listed in Table 3. The injury severity distribution in Table 3 was estimated using the data and method described in Appendix C. The values for γ_k and η_k were then calculated from μ_k and σ_k assuming as noted previously that $\sigma_k = 0.2 \mu_k$.

Table 3.
Distribution of neck AO/C1/C2 injury severities in the LA/Hannover motorcycle accident database

k	Estimated Number of Cases with $MAIS_{AO/C1/C2} = k$ (from column 9 of Table C-1)	Estimated Number of Cases with $MAIS_{AO/C1/C2} < k$
0	479	0
1	4	479
2	3	483
3	9	486
4	0	495
5	2	495
6	1	497

For each injury severity level k , the numbers of LA/Hannover cases with $MAIS_{AO/C1/C2} \geq k$ injuries and computer simulation cases with $NII_{max} \geq \mu_k$ can be expressed according Table 4, where μ_k and m_k are to be determined. If the cases are sorted such that $NII_{max,i} \leq NII_{max,i+1}$, for $i = 1$ to 497, then μ_k and m_k satisfy the equation

$$NII_{max,m_k} < \mu_k \leq NII_{max,m_k+1} \quad (14).$$

The values for μ_k that satisfy equation (14) can be calculated from m_k according to the equation for the logarithmic mean,

$$\mu_k = \sqrt{NII_{max,m_k} NII_{max,m_k+1}} \quad (15).$$

The best estimate of μ_k , for $k=1$ to 6, satisfies equation (14) with $m_k=n_k$, the number of cases with $MAIS_{AO/C1/C2} < k$ listed in the 3rd column of Table 3. As a result, the distribution of $MAIS_{AO/C1/C2}$ injuries predicted by the 498 computer simulations will match the distribution of neck injuries observed in the LA/Hannover database as illustrated in Figure 4.

Table 4.
Number of cases with observed and predicted injuries

	Number of Cases	
	$MAIS_{AO/C1/C2} \geq k$ (LA/Hannover data)	$NII_{max} \geq \mu_k$ (computer simulations)
No	n_k	m_k
Yes	$498-n_k$	$498-m_k$
Total	498	498

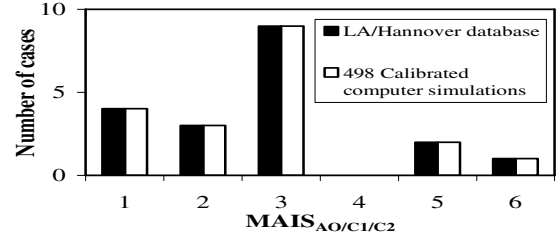


Figure 4. Distribution of observed and predicted neck injuries.

The 95% confidence intervals for μ_k can be considered to be the range of values for μ_k such that the portion of cases with $NII_{max} \geq \mu_k$ is not statistically significantly different than the portion of cases with $MAIS_{AO/C1/C2} \geq k$. This condition is satisfied for $m_k^- \leq m_k \leq m_k^+$ such that $\chi^2 \leq 3.84$, where χ^2 is calculated according to the following equation (based on equation 5.39 in Box, Hunter, and Hunter [24])

$$\chi^2 = \frac{(n_k(498 - m_k) - m_k(498 - n_k))^2 (2 \times 498)}{(n_k + m_k)(498 - n_k + 498 - m_k)(498)^2} \quad (16).$$

The range of values for m_k^- and m_k^+ that satisfy $\chi^2 \leq 3.84$ are listed in Table 5. These values are used in conjunction with equation (15) to estimate the 95% confidence limits for μ_k . The upper confidence limits for m_4 , m_5 , and m_6 (and thus μ_4 , μ_5 , and μ_6) are undefined because $\chi^2 \leq 3.84$ is satisfied for all $m_k^- \leq m_k \leq 498$.

Table 5.
95% Confidence limits for m_k

k	m_k^-	m_k^+
1	466	489
2	471	491
3	475	493
4	488	-
5	488	-
6	492	-

RESULTING MATD NECK INJURY CRITERIA

Injury Direction Coefficients

The injury direction coefficients listed in Tables 6 and 7 were identified according to the method described above. The resulting value for J was $462/67^2=0.103$. Table 8 lists the number of observed and predicted injuries by injury severity and direction, which summarizes the fit to the 64 individual bins. The correlation between the predicted and observed bin counts ($m_{k,c,t,x,e,f,z}$ and $n_{k,c,t,x,e,f,z}$), excluding the non-injury cases, was $r^2=0.56$.

Table 6.
Force and moment normalizing coefficients for the new MATD neck

Coefficient	Estimated Value
F_C^*	6.53 kN
F_T^*	3.34 kN
M_X^*	62.66 Nm
M_E^*	58.0 Nm
M_F^*	204.2 Nm
M_Z^*	47.1 Nm

Table 7.
Injury threshold coefficients for the 67 USC fatal cases with the new MATD neck

k	S_k	Q_k^*
1	1	0.619
2	1.00	0.619
3	1.50	0.650
4	3.74	0.594
5	3.74	0.594
6	5.20	0.564

Table 8.
Comparison of Number of Observed and Predicted Injuries by Injury Severity and Direction

Direction	Number of cases in the USC fatal motorcycle accident database with $MAIS_{AO/C1/C2} \geq k$ and indicated direction						I	Number of computer simulations of the USC fatal cases with $NII_{max} \geq S_k$ and $NII_f(t_{max}) \geq Q_k^* S_k$					
	k							k					
	1	2	3	4	5	6		1	2	3	4	5	6
Compression	5	5	4	0	0	0	C	8	8	1	0	0	0
Tension	18	18	16	4	4	0	T	12	12	11	1	1	0
Lat. Bending	42	42	35	11	11	2	X	42	42	30	7	7	1
Extension	33	33	29	8	8	4	E	28	28	23	6	6	2
Flexion	20	20	17	4	4	0	F	16	16	10	0	0	0
Torsion	20	20	17	7	7	2	Z	28	28	16	5	5	2
All	64	64	55	16	16	5	-	64	64	55	16	16	5

The shape and step-wise fit of the NII_{max} criteria to the USC data is illustrated in Figure 5. There are six scatter plots, one for each pair of F_z , M_x , M_y , and M_z axes. The numbers in each scatter plot are the maximum $AIS_{AO/C1/C2}=k$ predicted by $NII_{max} \geq S_k$ computed from the forces and/or moments at t_{max} , using the coefficients listed in Tables 6 and 7, for injuries associated with the forces and moments on the plot. For example, the graph in the upper left corner is a scatter plot of injuries that were only associated with tension ($NII_T(t_{max}) \geq Q_k^* S_k$), compression ($NII_C(t_{max}) \geq Q_k^* S_k$), and/or lateral bending ($NII_X(t_{max}) \geq Q_k^* S_k$) motion vs F_z and M_x . Envelopes of constant $NII_{max}=S_k$ are also shown on each plot, corresponding to the S_k values in Table 7. The envelopes tend to separate out the injuries by AIS level as intended.

Injury Risk (Probability) Coefficients

The injury severity coefficients listed in Table 9 were identified from the LA/Hannover data according to the methods as previously described and based on the clipping coefficient $\alpha = 3.1$. The value of 3.1 was selected for α in order that $F_T = 4.17$ kN would correspond to a 0.03 probability of a $MAIS \geq 3$ injury (AAMA [9]) as illustrated in Figure 6. The corresponding injury risk curves are illustrated in Figure 7. The distribution of neck injuries for the 498 computer simulations also matches the distribution of injuries in the LA/Hannover database, as previously illustrated in Figure 4.

A comparison of resulting injury criteria for the new ISO 13232 MATD neck to NHTSA's criteria for the Hybrid III 50th Percentile Adult Male [21] is located in Appendix D, bearing in mind that the two different dummy necks and injury criteria were developed entirely independently, and therefore would not be expected to be similar.

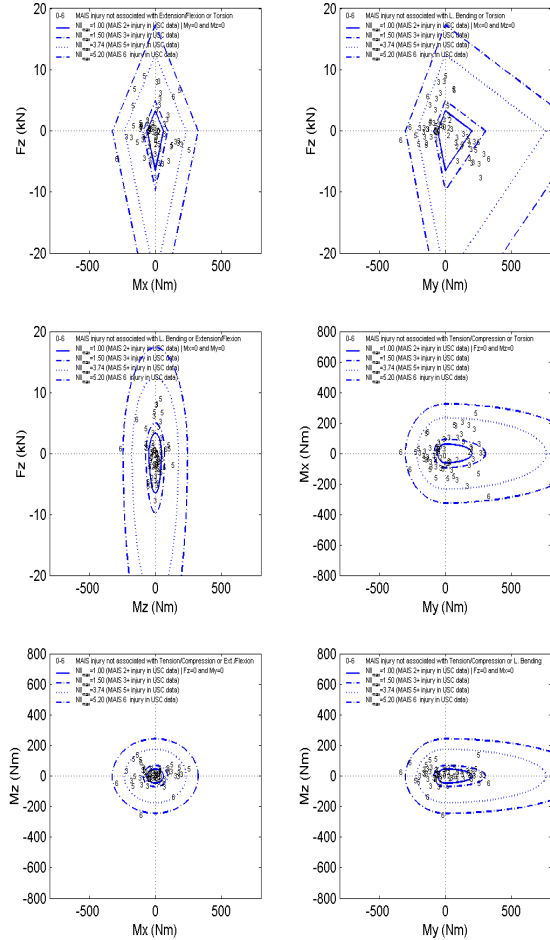


Figure 5. Forces and Moments at t_{max} from computer simulations of 67 fatal cases and the best step-wise fit envelopes of constant NI_{max} , providing the basis for the envelope shape (assuming $\alpha=0$).

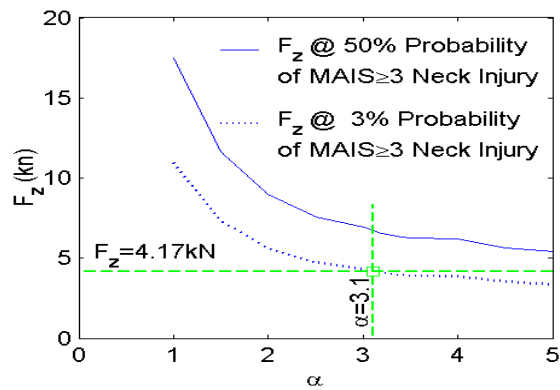
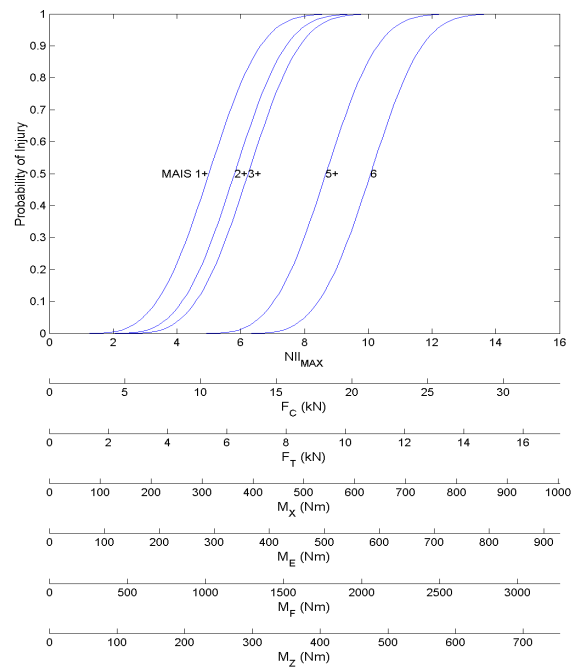


Figure 6. Critical neck tension force vs the “clipping” coefficient, providing the basis for selecting $\alpha = 3.1$.

Table 9. Injury severity risk coefficients for the new MATD neck

k	μ_k	σ_k ($=0.2\mu_3$)	γ_k	η_k
1	5.00 (4.33, 6.96)	1.247	1.06	4.38
2	5.80 (4.46, 7.42)	1.247	1.86	4.38
3	6.23 (4.70, 7.84)	1.247	2.29	4.38
4	8.67 (6.62, -)	1.247	4.73	4.38
5	8.67 (6.62, -)	1.247	4.73	4.38
6	10.07 (7.59, -)	1.247	6.13	4.38



Note: Each force and moment scale is only applicable if all of the other upper neck forces and moments are set equal to zero.

Figure 7. Neck AO/C1/C2 injury risk curves for the new MATD Neck.

CONCLUSIONS AND RECOMMENDATIONS

The need for a new multi-directional motorcycle test dummy neck and neck injury assessment method was identified during previous research studies with protective devices, in particular with prototype motorcycle airbags. A new neck and new improved neck injury criteria have been developed which satisfactorily meets these and other injury assessment needs of ISO 13232. The new neck and improved injury criteria are included in the draft first revision of the Standard [3].

The new improved probabilistic injury assessment criteria was developed to allow injury risk/benefit analysis of protective devices while incorporating the injury predictions for the neck at the AO/C1/C2 level for ligamentous and skeletal injuries at the AIS (1990) 1 to 6 level. The criteria employs the measured upper neck axial forces, and AP flexion-extension, lateral bending, and torsional moment responses from the new MATD neck to predict the injury outcome for use with injury risk/benefit analysis methods. The model currently predicts the same injury outcome for 565 reconstructions representative of field accident data based on the Los Angeles and Hannover studies. This is a substantial improvement from the previous criteria in ISO 13232 (1996) which resulted in the number of predicted injuries being 10 times larger than the number of observed injuries. The improved criteria are also in agreement with other published injury risk information for neck tension only forces.

The new neck injury criteria is based on several key assumptions which may be limiting: the equal injury-probability slopes at all injury severities, which might imply similar injury mechanisms for all severities; the accuracy of the $N=565$ computer simulations which have been only partially validated in component and full-scale tests; and the observed “associated neck motions” for the most severe upper neck injury in each accident being based on detailed case review and reconstructions by one group of experts. Although these assumptions could be subject to further refinement, the neck injury criteria are based on the best information available at this time, and produce predictions that are in closer agreement to real world accident data, using the specified methodology of ISO 13232. Additional in-depth motorcycle accident data would provide a larger validation sample.

ACKNOWLEDGEMENTS

This work was funded by the International Motorcycle Manufacturers Association. The full-scale test was funded by the Japan Automobile Manufacturers Association, and was conducted at the Japan Automobile Research Institute.

REFERENCES

[1] Anonymous, Motorcycles – Test and Analysis Procedures for Research Evaluation of Rider Crash Protective Devices Fitted to Motorcycles, ISO 13232, International Organization for Standardization, Geneva, 1996.

[2] Zellner, J.W., J.A. Newman, N.M. Rogers, “Preliminary Research into the Feasibility of Motorcycle Airbag Systems”, proceedings of the 14th International Technical Conference on the Enhanced Safety of Vehicles, Munich, Germany, National Highway Traffic Safety Administration, Washington DC, 1994, pp. 1198-1210.

[3] Anonymous, Motorcycles – Test and Analysis Procedures for Research Evaluation of Rider Crash Protective Devices Fitted to Motorcycles, ISO/DIS 13232, International Organization for Standardization, Geneva, 2004.

[4] Withnall, C., N. Shewchenko, K. Wiley, N. Rogers, “An Improved Dummy Neck for the ISO 13232 Motorcycle Anthropometric Test Dummy”, Paper No. 418, Proceedings of the 18th International Technical Conference on the Enhanced Safety of Vehicles, Nagoya, Japan, National Highway Traffic Safety Administration, Washington D.C., May 2003.

[5] Van Auken, R.M., et al., “Development of Neck Injury Assessment Criteria for the ISO 13232 Motorcyclist Anthropometric Test Dummy With The Revised Neck”, Paper No. 417, Proceedings of the 18th International Technical Conference on the Enhanced Safety of Vehicles, Nagoya, Japan, National Highway Traffic Safety Administration, Washington D.C., May 2003.

[6] Newman, J.A., S. Tylko, “Toward a Comprehensive Biomechanical Injury Cost Model”, proceedings of the 36th Annual Conference of the Association for the Advancement of Automotive Medicine, AAAM, Des Plaines, USA, 1992, pp. 271-287.

[7] Kebschull, S.A., et al., “Injury Risk/Benefit Analysis of Motorcycle Protective Devices Using Computer Simulation and ISO 13232”, proceedings of the 16th International Technical Conference on the Enhanced Safety of Vehicles, Windsor, Canada, National Highway Traffic Safety Administration, Washington D.C., 1998, pp. 2357-2374.

[8] Ramet, M., et al., “The Effect of Air Bag Inflation on the Cinematic and the Lesions of a Motorcyclist”, proceedings of the 14th International Technical Conference on the Enhanced Safety of Vehicles, Munich, Germany, National Highway Traffic Safety Administration, Washington D.C., 1994, pp. 1241-1246.

[9] Wilber, V.H., “American Automobile Manufacturers Association Comments to Docket No.

NHTSA Docket No. 98-4405; Notice 1 Advanced Technology Airbags: Attachment C”, American Automobile Manufacturers Association, December 17, 1998 (NHTSA Docket 98-4405-79).

[10]Eppinger, R., et al., Development of Improved Injury Criteria for the Assessment of Advanced Automotive Restraint Systems – II, National Highway Traffic Safety Administration, Washington D.C., November 1999.

[11]Eppinger, R., E. Sun, S. Kuppa, R. Saul, Supplement: Development of Improved Injury Criteria for the Assessment of Advanced Automotive Restraint Systems – II, National Highway Traffic Safety Administration, Washington D.C., March 2000.

[12]Thom, D.R., H.H., Jr., Hurt, T.A. Smith, and I. Rehman, "Atlas and axis injuries in fatal motorcycle collisions," Proceedings of the 39th Annual Conference of the Association for the Advancement of Automotive Medicine, 1995.

[13]Smith, Terry A., Summary report of the analysis of the USC fatal motorcycle accident data set, Head Protection Research Laboratory, July 2001.

[14]Fleck, J.T., and F. E. Buttler, Validation of the Crash Victim Simulator, Vol. 1: Engineering Manual – Part 1: Analytical Formulation, DOT HS-806-279, Washington, D.C., 1981.

[15]Van Auken, M., et al., Comparison of the new MATD neck computer simulation model to the full scale test and laboratory test responses, ISO/TC22/SC22/WG22 N305, 2001-05-22.

[16]Anonymous, Automotive Electronics Reliability Handbook, Publication No. AE-9, Society of Automotive Engineers, Warrendale, PA, February 1987, pp 32-33.

[17]Råde, L., and B. Westergren, Beta Mathematics Handbook, Second Edition, CRC Press, Boca Raton, FL, 1990, pp. 395.

[18]Shanley, F. R. and E. I. Ryder, "Stress Ratios; the answer to the combined loading problem", Aviation, June 1937, pp. 28-29:43:66:69-70.

[19]Bruhn, E. F., Analysis and Design of Flight Vehicle Structures, Jacobs Publishing, Inc., Indianapolis, 1973.

[20] Anonymous, Military Standardization Handbook Metallic Materials and Elements for Aerospace Vehicle Structures, MIL-HDBK-5D, US Department of Defense, Washington, D.C., June 1983.

[21] Anonymous, U.S. DOT/NHTSA - Final Rule: Interim Final Rule – Notice 1, Docket No. NHTSA 00-7013-1, RIN 217-AG70, National Highway Traffic Safety Administration, Washington, D.C., May 2001.

[22]Orsay, E.M., et al., “Motorcycle helmets and spinal injuries: Dispelling the myth”, Annals of Emergency Medicine 1994 April 23(4):802-6.

[23]Mertz, H.J., and P. Prasad, “Improved Neck Injury Risk Curves for Tension and Extension Moment Measurements of Crash Dummies”, Paper No. 2000-01-SC05, Society of Automotive Engineers, Proceedings of the 44th Stapp Car Crash Conference, November 2000.

[24]Box, G.E.P., W.G. Hunter, and J.S. Hunter, Statistics for Experimenters, John Wiley & Sons, New York, 1978.

APPENDIX A

The observed and simulated responses of the neck in component and full-scale tests are illustrated in Figures A-1 to A-5.

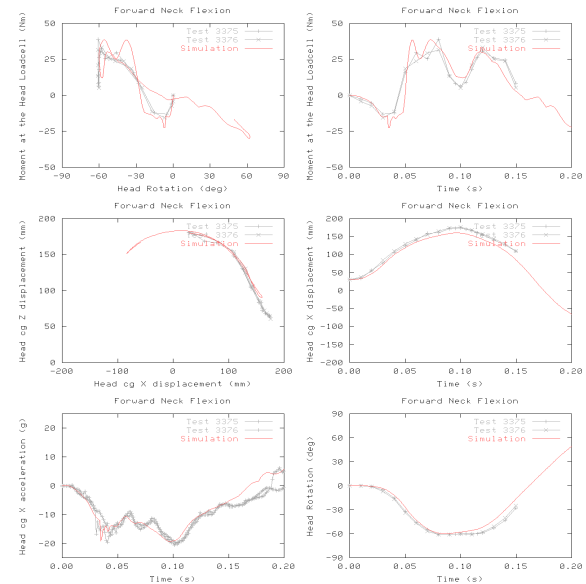


Figure A-1. Forward neck flexion sled test and computer simulation time responses.

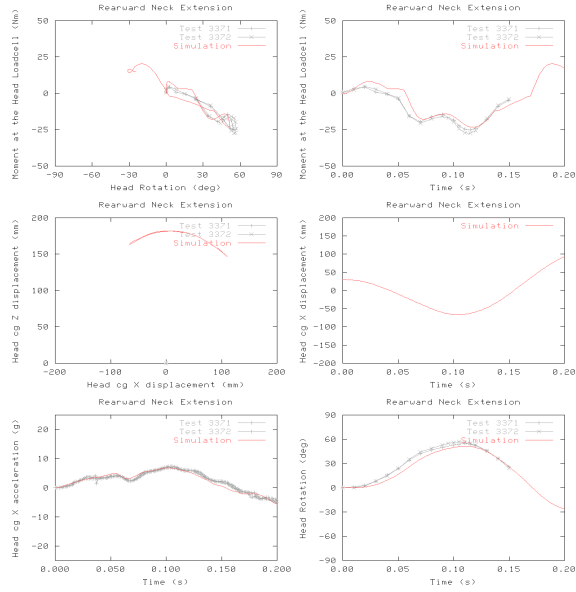


Figure A-2. Rearward neck extension sled test and computer simulation time responses.

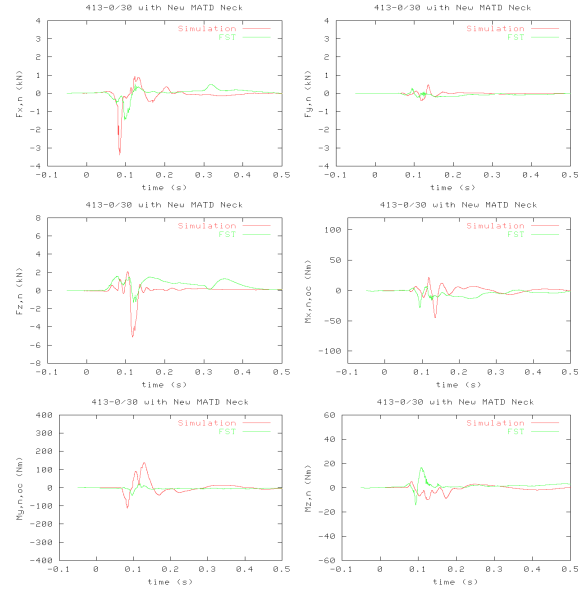


Figure A-5. Full scale test and computer simulation of impact configuration 413-0/30.

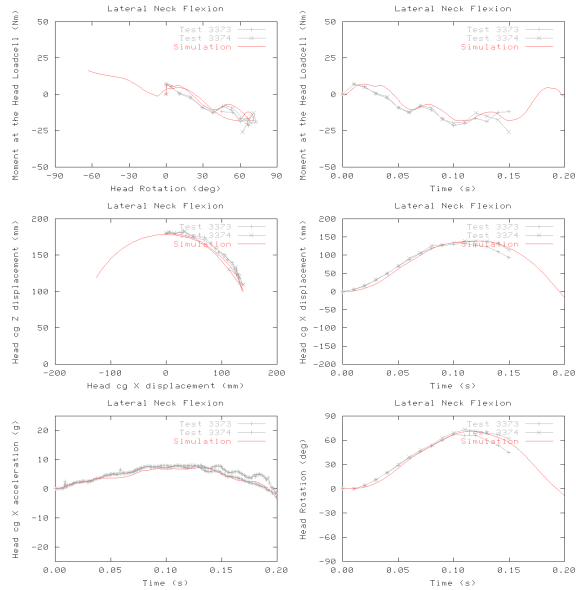


Figure A-3. Lateral neck flexion sled test and computer simulation time responses.

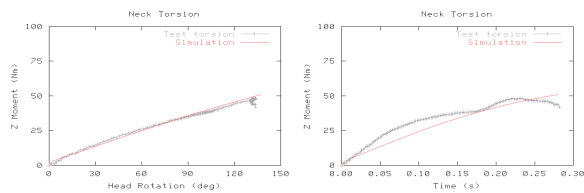


Figure A-4. Neck torsion test and computer simulation time responses.

APPENDIX B

Figure B-1 illustrates the distributions of maximum neck forces and moments for the 498 computer simulations used to identify the neck injury criteria for the new MATD neck. Note that these maximum forces and moments were the maximum values observed in the entire impact sequence, including ground contacts, up to 5 sec from the time of initial contact, for the purpose of correlating with injuries reported in the accident data. Furthermore, some of the collisions in this accident database represent high speed, severe impacts, with relative normal closing velocities up to 121 km/h. This could explain why some of the maximum forces and moments are of relatively large magnitude.

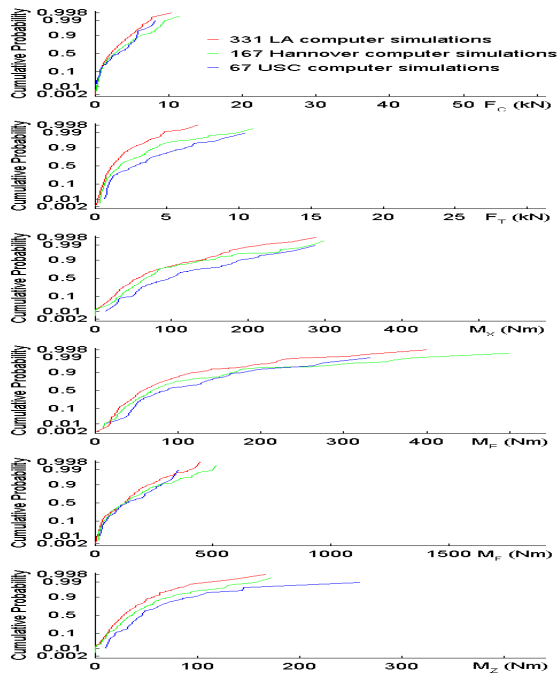


Figure B-1. Maximum neck force and moment distributions from computer simulations of 498 LA/Hannover cases and 67 USC fatal cases, including cases with high speed, severe impacts up to 121 km/h relative normal closing velocity.

APPENDIX C

The distribution of neck injuries in the 498 LA/Hannover accident database was estimated by

- imputing the distribution of neck injuries in the 13 fatal LA/Hannover cases according to the distribution observed in the 67 USC fatal cases; and
- redistributing the remaining 3 unknown injuries amongst the valid cases.

The data and results of this analysis are listed in Table C.1. The columns in Table C.1 are as follows:

- (1), (10) The maximum AO/C1/C2 AIS injury severity level ($MAIS_{AO/C1/C2}$).
- (2), (4) The numbers of non-fatal and fatal cases in the LA/Hannover database by neck rupture, dislocation, and/or fracture $MAIS_{AO/C1/C2}$. Note that 3 non-fatal cases and all 13 fatal cases have unknown neck injuries.
- (3), (5) The percentages of cases in the LA/Hannover database corresponding to columns 2 and 4. The percentages in these columns are equal to the number of cases/498 x 100%.
- (11) The numbers of cases in the USC fatal accident database by $MAIS_{AO/C1/C2}$.

Table C-1. Distribution of neck AO/C1/C2 injury severities in the LA/Hannover and USC fatal accident databases

$MAIS_{AO/C1/C2}$	(1)	(2)	(3)	(4)	(5)	(6)	(7)	(8)	(9)
	LA/Hannover Database								Estimated Number of Cases
	Non Fatal		Fatal		All				
	Observed Number of Cases ¹	Observed Percentage of all Cases	Observed Number of Cases	Observed Percentage of all Cases	Estimated Percentage of all Cases	Estimated Percentage of Cases	Estimated Valid Percentage of Cases	Estimated Number of Cases	
0	476	95.58%			0.12%	95.70%	96.28%	479	
1	4	0.80%			0.00%	0.80%	0.81%	4	
2	1	0.20%			0.35%	0.55%	0.55%	3	
3	1	0.20%			1.52%	1.72%	1.73%	9	
4	0	0.00%			0.00%	0.00%	0.00%	0	
5	0	0.00%			0.43%	0.43%	0.43%	2	
6	0	0.00%			0.19%	0.19%	0.20%	1	
unknown	3	0.60%	13	2.61%	0.00%	0.60%	-	0	
Total	485	97.39%	13	2.61%	2.61%	100.00%	100.00%	498	

Note:

¹Ruptures, dislocations, and/or fractures

$MAIS_{AO/C1/C2}$	(10)	(11)	(12)	(13)
	USC Database			Observed Percentage of USC Fatal Cases x 2.61%
	Fatal			
	Observed Number of Cases	Observed Percentage of Fatal Cases		
0	3	4.48%	0.12%	
1	0	0.00%	0.00%	
2	9	13.43%	0.35%	
3	39	58.21%	1.52%	
4	0	0.00%	0.00%	
5	11	16.42%	0.43%	
6	5	7.46%	0.19%	
Total	67	100.00%	2.61%	

- (12) The percentages of cases in the USC fatal accident database by $MAIS_{AO/C1/C2}$.
- (6), (13) The estimated percentage of LA/Hannover cases which were fatal by $MAIS_{AO/C1/C2}$. The percentages in this column are equal to the values in column 12 x 2.61%.
- (7) The estimated percentage of all LA/Hannover cases by $MAIS_{AO/C1/C2}$. The percentages in this column are equal to the values in column 3 plus the values in column 6.
- (8) The estimated valid percentage of LA/Hannover cases by $MAIS_{AO/C1/C2}$, which reapporitions the remaining 3 unknown cases amongst the valid cases. The percentages in this column are equal to the values in column 7 x 498 / (498-3).
- (9) The estimated number of LA/Hannover cases by $MAIS_{AO/C1/C2}$. The numbers in this column are equal to the values in column 8 x 498 / 100%. The estimated numbers of cases were rounded to the nearest integer values.

APPENDIX D

Figure D-1 illustrates the shapes of the new injury criteria for the MATD neck and NHTSA's criteria for the Hybrid III 50th percentile adult male neck [21]. Keeping in mind that the respective dummy necks are mechanically quite different, and the two dummy necks and criteria are not interchangeable, this figure indicates that the shapes of the two criteria are very similar in the F_z vs M_y plane. This figure also illustrates the differences between the two criteria in lateral flexion and torsion.

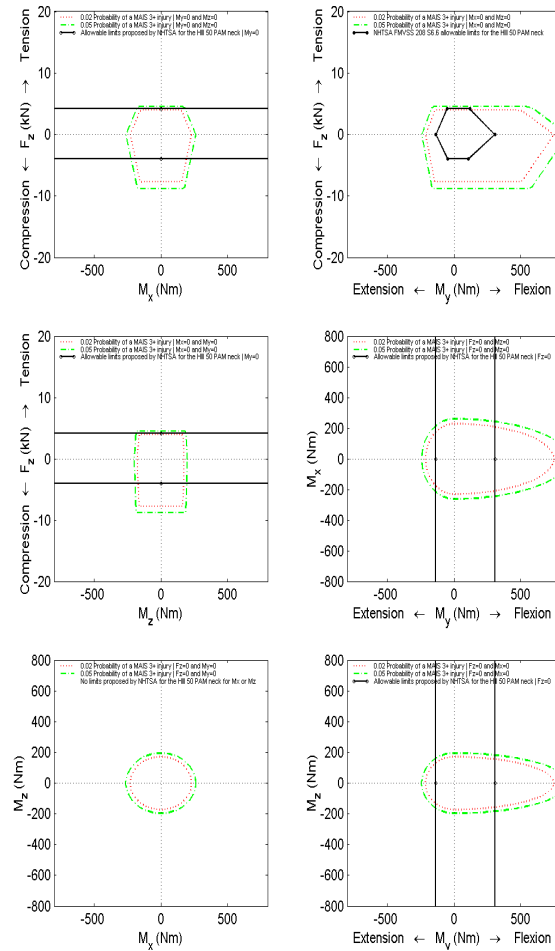


Figure D-1. Comparison of the general shape and axes of the improved neck injury criteria for the new ISO 13232 MATD neck to the allowable limits proposed by NHTSA for the HIII 50 PAM neck (recognizing that the necks have very different stiffness)

EVALUATING PEDIATRIC ABDOMINAL INJURIES

Kristy B. Arbogast, D. Andrew Mong, Shresta Marigowda

The Children's Hospital of Philadelphia
The University of Pennsylvania

Richard W. Kent, Stephen Stacey, Jason Mattice

University of Virginia

Hiromasa Tanji, Kazuo Higuchi

Takata Corporation

Stephen W. Rouhana

Ford Motor Company

United States

Paper Number 05-0046

ABSTRACT

Abdominal injuries, along with lumbar spine fractures, are part of a constellation of injuries referred to as "seat belt syndrome". Geometrical characteristics of the pelvis and abdomen of younger children place them at higher risk for these injuries. Efforts to design restraints that mitigate these injuries are limited as no current pediatric anthropomorphic dummy (ATD) can accurately quantify the abdominal response to belt loading. This paper describes progress on a four-phase project to address this gap involving pediatric anthropometrics, real-world abdominal injury risk, abdominal biomechanical structural response and injury tolerance from a porcine model, and development of an abdominal insert for the 6-year-old ATD based on these data.

Internal anthropometric measures consisted of radiological assessment of abdominal depth, height, and circumference at multiple horizontal planes. External measures consisted of distances, determined by digital photography, taken between skeletal markers while the child was seated on a vehicle seating apparatus with and without a booster seat.

Field investigation identified three unique kinematic patterns resulting in abdominal injury: pre-submarining where the belt is initially out of position, classic submarining where the belt starts in position and the pelvis moves under the belt with the torso reclined, and submarining/jackknifing where the pelvis slides under the belt, and the torso flexes forward.

The biomechanical studies developed age- and size-based correlations between pediatric swine and humans. Biomechanical tests performed using the most appropriately sized porcine model will be used to define the structural and injury response of the pediatric abdomen to realistic loading conditions.

INTRODUCTION

The abdomen is the second most commonly injured body region after the head/face in young children using vehicle seat belts and can be associated with significant health care costs and extended hospitalization (Durbin et al. 2001; Bergqvist et al. 1985; Tso et al. 1993; Trosseille et al, 1997). Injuries to this region, along with fractures of the lumbar spine, are part of a constellation of injuries known as seat belt syndrome (Kulowski and Rost 1956; Garrett and Braunstein 1962; Hoy and Cole 1993; Lane 1994).

Children of all ages are at risk of sustaining seat belt syndrome, but the poor fit of the belt in younger children likely places them at higher risk than older children. In a case series of 98 children with seat belt syndrome, the mean age was 7.3 ± 2.5 years and 72% were between 5 and 9 years of age. (Gotschall et al, 1998) The exposure of children to adult seat belts is large: data from the Partners for Child Passenger Safety study, an on-going, child-focused crash surveillance system, identify the adult seatbelt as the most common form of restraint for passengers age 5 years and older. (Winston et al. 2004)

Our previous work, based on an analysis of over 200,000 children in crashes, identified key predictors of elevated abdominal injury risk in seat belt-restrained child occupants: child age, vehicle type, and seat row (Arbogast et al, 2004). Children 4-8 years of age were at the highest risk of abdominal injury: they were 24.5 times and 2.6 times more likely to sustain an AIS2+ abdominal injury than those 0-3 years and those 9-15 years, respectively. The injury risk for children 4-8 years of age was 6 and 10 times higher in passenger cars and SUVs, respectively, compared to minivans. No reduction in abdominal injury risk was seen with rear seating as compared to front row seating. The role of direction of impact on injury risk varied by child age,

indicating diverse injury sources influenced by developmental differences and changes in restraint practices among the age groups. These findings provide a baseline understanding of abdominal injury patterns and suggest mechanistic hypotheses to be tested with additional in-depth data.

According to the American Academy of Pediatrics and the National Highway Traffic Safety Administration, the proper restraint for many of the children sustaining abdominal organ injuries associated with seat belt syndrome (those less than 9 years old) is a booster seat. There have been tremendous legislative, regulatory, and educational efforts to increase booster seat use in the recent past. Discussion has emphasized the need to ensure outstanding impact performance of booster seats while at the same time considering how vehicle belt systems can evolve to provide protection for this age group. In order to evaluate the safety performance of these new and emerging restraint technologies, a mechanical child surrogate that accurately assesses the risk of abdominal injuries in the motor vehicle environment is needed. Current pediatric anthropomorphic test devices (ATD) are limited in this ability.

None of the child frontal crash test dummies specified in the Code of Federal Regulations Part 572 have the ability to make any abdominal injury measurements. While several adult frontal impact dummies at the research stage have abdominal injury assessment capability (Hybrid III with Frangible Abdomen and THOR, both in mid-sized male and small female dummies), none of the child dummies have any instrumentation in the abdominal area. The Q series of dummies has taken abdominal biofidelity into account by scaling the force-deflection properties of the adult abdomen. It is not known how well this compares to the properties of real children. In addition, the dummies do not have abdominal instrumentation.

Rouhana (2002) reviewed abdominal injury criteria for various impact modes. Miller et al. (1989) and Rouhana et al. (1989) showed that given the low velocity nature of the belt to abdomen interaction, abdominal compression was well correlated to abdominal organ injury. For this reason, both the THOR dummies and the Hybrid III Frangible Abdomen dummies measure abdominal compression as the injury assessment metric.

This paper describes progress on a four-phase project to address this gap involving pediatric anthropometrics, real-world abdominal injury risk,

abdominal biomechanical tolerance from a porcine model, and development of an abdominal insert for the 6-year-old ATD based on these data. The long-term objective of this 3-year research effort is to develop a modification to the current 6-year-old Hybrid III anthropometric dummy so that the risk of abdominal injury can be accurately assessed in the motor vehicle crash environment. In order to achieve this objective, the biomechanical response of the pediatric abdomen must be understood. Traditional methods used to measure the impact response of adults such as cadaver or volunteer tests are unable to be used for children. As a result, we are utilizing a multidisciplinary approach that combines 1) an assessment of the anthropometry of the pediatric abdomen, 2) analysis of an extensive database of real-world crashes involving children who sustained abdominal injury, and 3) definition of the biomechanical response of the abdomen using a well-controlled animal model.

METHODS

Anthropometry

Two methods for obtaining geometry and anthropometry were implemented: retrospective review of abdominal radiological films and prospective measure of anthropometrics and seat belt fit parameters on healthy pediatric human volunteers.

Retrospective radiology – With this component, we determined abdominal compartment and intra-abdominal organ measures on a representative sample of children who closely approximate the size of the 6-year-old ATD. The current 6-year-old ATD measures 48 inches in height and 52 pounds. According to the current US pediatric growth charts produced by the Centers for Disease Control and Prevention (CDC, 2000), these measures approximate a 50th percentile, 7-year-old child. Intra-abdominal geometry of children was determined by examining abdominal computed tomography (CT) scans of a representative sample of children in the target age and weight range.

Subjects were identified via a retrospective review of abdominal/pelvic CT scans performed at The Children's Hospital of Philadelphia. An initial review of the Department of Radiology database at CHOP identified all children from 6-8 years of age who underwent abdominal CT scans. The most common indications for abdominal CT scanning in children include the evaluation of blunt abdominal trauma and the evaluation of abdominal pain suggesting appendicitis. In order to select a sample of CT scans that best approximates the intra-abdominal anatomy

of otherwise healthy children, only CT scans performed for suspected acute appendicitis or trauma evaluation which demonstrate no significant intra-abdominal injury were selected. Children with intra-abdominal free fluid, or solid organ injuries or pathology were excluded. Scans from 35 children were included in the study.

Specific inclusion criteria were children age 6-8 years of age who weigh between 20.4-27.3 Kg (+10% of the Hybrid III 6 year old ATD's weight). All CT scans included were reviewed by a single radiologist, board certified in pediatric radiology and experienced in the interpretation of pediatric abdominal CT scans.

All radiographs were taken with the children in a supine position (on their backs). Using scout views, axial and sagittal reconstructions, the following measures were obtained on all scans:

1. Abdominal depth and circumference at level of umbilicus and at level of last appearance of the anterior ribs.
2. Transverse width of the abdomen at the level of the iliac crests and at the level of the largest anterior-posterior diameter of the pelvis.
3. Vertical distance between the end of the 11th false rib and the top of the iliac crests.
4. Abdominal height from diaphragm insertion to pubic symphysis, both anteriorly and posteriorly.
5. Vertical dimension of the pelvis as measured from the top of the iliac crests to the most inferior point on the ischial tuberosity.
6. Pelvic inlet – distance from the sacral promontory at S1 to the superior aspect of the pubic symphysis in the midline sagittal plane

Examples of these dimensions are contained in the appendix. Means and standard deviations were calculated.

Prospective anthropometrics - The specific aim of this component of the research study was to describe a variety of external anthropometric measures on a representative sample of target age children taken on a stylized vehicle seat with and without a booster seat.

Children eligible for the study were those from 5-9 years of age presenting to the Primary Care Clinic of The Children's Hospital of Philadelphia. Effort was made to enroll subjects between 43-47 inches in height, and weighing 16-27 kg so that the findings were most applicable to the 6-year-old ATD. Any child with an existing neurologic, orthopedic, genetic, or neuromuscular condition was excluded. 60 children were enrolled in the study.

On each child, several skeletal landmarks were palpated by a research nurse and marked with a small bright sticker. The child wore bike shorts and a tight fitting T-shirt to facilitate the identification of anatomic landmarks and optimize the accuracy of the measurements. The skeletal landmarks included:

1. ASIS (anterior superior iliac spines) - the anterior most portion of the iliac crest of the pelvis
2. AIIS (anterior inferior iliac spine) - AIIS is found immediately below the ASIS and is a bony prominence on the lower part of the anterior margin of the iliac bone of the pelvis between the ASIS and the acetabulum.
3. Greater trochanter - the lateral most protrusion of the proximal femur bone
4. PSIS (posterior superior iliac spine) - PSIS is the upper protrusion on the posterior border of the ileum; a readily apparent dimple occurs in the skin overlying the PSIS
5. End of 11th false rib - the end of the bottom most rib (11th) on the lateral aspect.
6. Shoulder joint - right lateral greater tubercle of the proximal end of humerus at the center of the tuberosity
7. Knee joint - right lateral epicondyle of the distal end of femur at the center of the tuberosity
8. Ankle joint - right lateral malleolus of the distal end of fibula at the center of the tuberosity
9. Xiphoid (center point of the bottom tip of sternum)
10. Manubrium (center point of the top edge of sternum)

The child was then positioned on the stylized vehicle seat in a standardized symmetrical position with their head forward and hands at their sides. (Figure 1) The research nurse re-palpated the skeletal landmarks to assure proper placement of the markers. Photographs were taken with a high-resolution digital SLR camera mounted in a standardized location for all study subjects and remotely operated from a laptop computer. Photos were taken from the front as well as the side.

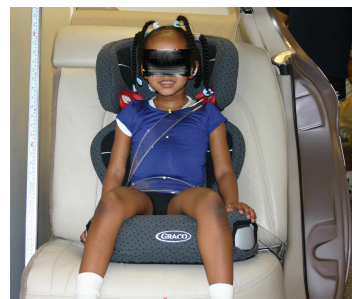


Figure 1: Subject for the prospective anthropometric study in the standard position with her head forward and hands at her side seated on the full back booster.

The stylized vehicle seat was fitted with a transparent seat belt representing the geometry of an actual rear seat 3-point seat belt. Front photographs were taken with and without the belt. The belt was applied by the research nurse and fitted snugly to the study subject. Once the belt was applied, three additional markers were placed on the subject:

1. Shoulder belt outer (lateral edge of the shoulder belt where it crosses the clavicle)
2. Shoulder belt center (bottom edge of the shoulder belt where it crosses the midline)
3. Superior edge of lap belt (top edge of the lap belt where it crosses the midline)

The entire study protocol was repeated for the vehicle seat alone and seated on two different belt-positioning booster seats: a backless booster and a fullback booster. Digital measurements from the photos were calculated using SigmaScan Pro image analysis software. Specific measures obtained were as follows (specific locations described above):

From front view photo:

- Vertical distance between the xiphoid and a horizontal line drawn between the right and left ASIS
- Distance between right and left ASIS bilaterally
- Vertical distance between a horizontal line drawn through manubrium where it intersects with the sternum to the bottom edge of shoulder belt along the midline of the body.
- Horizontal distance between a vertical line drawn through manubrium where it intersects with the sternum and the outer edge of shoulder belt at the level of the clavicle
- Vertical distance between horizontal line drawn between the right and left ASIS and superior edge of lap belt along the midline of the body
- Difference in the vertical heights of right and left ASIS relative to the seat base

From side view photo:

- Pelvic tilt (angle formed by the intersection of a vertical line and the line connecting the ASIS and PSIS)
- Pelvic angle (angle formed by the intersection of a vertical line and the line connecting the ASIS and AIIS)
- Hip angle (angle formed by the intersection of a line joining the shoulder joint and greater trochanter with a line joining the greater trochanter and the knee joint)
- Vertical distance between the ASIS and the greater trochanter.

- Knee angle (angle formed by the intersection of a line joining the greater trochanter and the knee joint with a line joining the knee and ankle joint).
- Tibia/Fibula angle (angle formed by the intersection of a vertical line and the line connecting the knee and ankle joint)

All measurements were compared across the different restraint systems and by size of child (standing height, seated height, weight and/or body mass index (BMI)). All data obtained in this study were continuous in nature. Analyses consisted of the calculation of mean, standard deviation, range, and interquartile range for each measure obtained.

Crash Investigation review

Cases of seat belt restrained children in motor vehicle crashes who sustained abdominal organ injury were analyzed from the Partners for Child Passenger Safety (PCPS) Study. Detailed descriptions of the study population and methods involved in data collection and analysis have been previously published (Durbin et al. 2001). PCPS consists of a large scale, child-specific crash surveillance system: insurance claims from State Farm Insurance Co. (Bloomington, IL) function as the source of subjects, with telephone survey and on-site crash investigations serving as the primary sources of data. The telephone interviews provide data for a surveillance system used to describe characteristics of the population including risk factors for injury while the crash investigations provide detailed mechanisms and sources of injury.

Crashes qualifying for inclusion in the surveillance system were those involving at least one child occupant ≤ 15 years of age riding in a model year 1990 or newer State Farm-insured vehicle. Qualifying crashes were limited to those that occurred in fifteen states and the District of Columbia, representing three large regions of the United States (East: NY, NJ, PA, DE, MD, VA, WV, NC, DC; Midwest: OH, MI, IN, IL; West: CA, NV, AZ). On a daily basis, data from qualifying and consenting claims were transferred electronically from all involved State Farm field offices to researchers at The Children's Hospital of Philadelphia and University of Pennsylvania (CHOP/Penn). Data in this initial transfer included contact information for the insured, the ages and genders of all child occupants, and a coded variable describing the medical treatment received by all child occupants.

In order to gain more detailed information about the kinematics of the child and the mechanisms and

sources of the injury, a subset of these cases was chosen for in-depth crash investigation. Cases were screened via telephone with the policyholder to confirm the medical details of the case. Contact information from selected cases was then forwarded to a crash investigation firm and a full-scale on-site crash investigation was conducted using custom child-specific data collection forms.

Crash investigation teams were dispatched to the crash scenes within 24 hours of notification to measure and document the crash environment, damage to the vehicles involved, and occupant contact points according to a standardized protocol. The on-scene investigations were supplemented by information from witnesses, crash victims, physicians, hospital medical records, police reports, and emergency medical service personnel. From this information, reports were generated that included estimates of the vehicle dynamics and occupant kinematics during the crash and detailed descriptions of the injuries sustained in the crash by body region, type of injury, and severity of injury. Delta v (the instantaneous change in velocity) was calculated using WinSmash and crush measurements of the vehicles involved.

Medical, crash, and child characteristics of 26 cases of pediatric abdominal injuries in restrained child occupants in frontal crashes were analyzed. The mechanism of each abdominal injury was determined by an assessment of the specific location of impact and the resultant kinematics.

Development of the Porcine Model

In order to design an abdominal element for use in a dummy, it is necessary to define the structural and injury characteristics of the 6-year-old human's abdomen. The field investigations described above allow the study of meaningful clinical outcomes on real children in real crashes; however, data obtained from these analyses are limited in that the engineering input is derived rather than measured directly. An experimental model, in contrast, allows the application of an exact loading condition and documentation of specific injuries but is limited by the knowledge of the exact transfer function between the experimental model and the human.

For adults, abdominal characteristics are typically determined using human cadavers (Hardy et al. 2001). For the child, however, such data are not available. Scaling techniques may be used to estimate pediatric force-deflection characteristics based on those measured for adults, but these techniques require assumptions about age-related

changes in geometry and material properties that remain largely unproven, particularly for the complex and inhomogeneous abdomen. Additionally, injury threshold values and the correlations between injury criteria and injury outcome cannot be reliably scaled from adults to children. It is necessary, therefore, to identify a surrogate that mimics to an acceptable degree the child's anatomy, size, organ development, and other characteristics and to quantify this surrogate's abdominal characteristics. The porcine model is reasonably well established for studying thoracoabdominal impact and injury response of both adults (Stalnaker et al. 1973, Trollope et al. 1973, Gogler et al. 1977, Miller 1989, Miller 1991a, Miller 1991b) and children (Aldman et al. 1980, Mertz et al. 1982, Prasad and Daniel 1984). The studies by Miller et al. focused specifically on belt loading to the abdomen, but used an adult pig. The other studies listed above focused on loading mechanisms other than abdominal belt loading (e.g., hub loading or air bag loading on an out-of-position occupant). Recent research has utilized a pediatric porcine model to evaluate the influence of active muscle tensing on the structural response of the thorax (Kent et al. 2003, 2004) and to study resuscitation of a choking child (Woods et al. 2002). This history provides the basis for selecting the pig as a reasonable representation of the human abdomen, but the porcine model has not been sufficiently developed to apply directly to the study of abdominal loading to a 6-year-old human. This study will, therefore, identify the porcine age that best correlates with the size and development of a human six year old and will characterize the abdominal structure and injury tolerance of these swine as a reasonable approximation of the human child.

This identification was accomplished via an imaging and necropsy study, which correlated the geometric and mass properties of the pig and the 6-year-old. Twenty-five pigs, age 14 days to 429 days, were included in the study. Whole-body mass ranged from 4 kg to 101 kg. Females were chosen preferentially, and only one male was included in the study. Over 30 geometric and inertial characteristics of each subject were measured and compared with similar characteristics of humans. Human data were taken from four primary sources. External body dimensions were obtained from the GEBOD database (Grunhofer 1975, McConville et al. 1980, Clauser et al. 1972, Young et al. 1983, and Snyder et al. 1977), the University of Michigan data compiled under the name "Anthrokids" (Owings et al. 1975, Snyder et al. 1977, see <http://ovrt.nist.gov/projects/anthrokids/>), and the data from Children's Hospital of Philadelphia collected as part of this project. In cases of

apparently contradictory values, the GEBOD data were used preferentially (note that the GEBOD database and the Anthrokids database draw from overlapping sources, but are not identical). The organ masses for the pigs were compared with data compiled by Stocker and Dehner (2002), who list average organ weights for children for each year from birth through age 19 years.

Since the goal of the necropsy study was to identify the best overall representation of the 6-year-old human, two functions defining a series of characteristics were used instead of a single target to identify the most appropriate pig model. These functions included $i = 1..5$ external measures (f^1_i) and $j = 1..4$ internal organ masses (f^2_j). The external parameters considered in f^1 were :

- a. Abdominal depth (at umbilicus) (target = 15.1 cm),
- b. Abdominal breadth (at umbilicus) (target = 18.5 cm),
- c. Sitting height (defined for the pig as the distance from the proximal end of the tail to the cranial surface of the head, with the neck in a neutral position) (target = 64.5 cm),
- d. Distance in the midsagittal plane from the cranial end of the sternum to the umbilicus along the ventral surface of the trunk (target = 25.4 cm), and
- e. Trunk weight (target = 11.8 kg).

The organs used for mass comparison in f^2 were the liver, kidneys, and lungs. The targets were 660 g (liver), 66 g (right kidney), 67 g (left kidney), and 328 g (both lungs).

The value of each of these parameters for each pig was defined as a percentage of the human target. The average percentage of the 5 external parameters was then defined as f^1_{avg} , and the average percentage of the organ parameters was f^2_{avg} . Regression equations were used to relate f^1_{avg} and f^2_{avg} to the pig's age, a , and mass, m :

$$f^1_{avg} = g(a, m) \quad [1]$$

$$f^2_{avg} = h(a, m) \quad [2].$$

A second-order polynomial regression was then developed defining the relationship between pig age and whole-body mass:

$$m = A + Ba + Ca^2 \quad [3].$$

The pig age and mass that best represent the 6-year-old human were then determined by setting

$$f^1_{avg} = f^2_{avg} = 1 \quad [4]$$

and minimizing the error in equations [1] and [2] simultaneously subject to the constraint imposed by equation [3].

Development of Test Matrix

There are several factors that could influence abdominal force-penetration and injury response to belt loading. The goal with the experimental test matrix and fixture was to evaluate as many of these factors as practical while limiting the number of test subjects required. The six factors identified for study were:

1. The degree of belt "wrap-around" (i.e., the degree of belt-abdomen contact). The testing will involve two conditions: 105° and 160°.
2. The loading location (upper and lower abdomen). Previous research has shown that the upper abdomen (primarily solid organs) and the lower (primarily hollow organs) exhibit markedly different responses to loading (Rouhana 2002). The field data component of this project showed that most young belted children who sustain abdominal injury have those injuries in the lower abdomen, but that injuries can occur in either location.
3. The shape of the displacement wave. A ramp-hold wave will be used to define the viscous force relaxation (Kent et al. 2003), while a ramp-release wave will be used to define injury tolerance.
4. The presence of active muscle tensing (Kent et al. 2004).
5. The magnitude of abdominal compression. Tests will be performed to 25%, 50%, and 65% of the unloaded abdominal depth.
6. The peak deflection rate (3 m/s and 6 m/s). While most of the injuries identified in the field component of this study were thought to be mechanistically related to deflection magnitude, there is evidence in the literature that organs can be injured via a viscous mechanism if the rate of deformation is sufficiently great.

The conditions chosen for the testing in this project are intended to maximize the information gleaned while minimizing the number of subjects to be sacrificed. This project is designed as a multi-level parametric study with 6 parameters and multiple levels of each: belt wrap-around (2 levels), loading location (2 levels), waveform (2 levels), muscle tensing (2 levels), compression depth (3 levels), deflection rate (2 levels). Inter-specimen variability is assessed by repeated tests of all test combinations. If all possible combinations of these levels were tested, including repeated tests of each combination, a total of $2 \times 2 \times 2 \times 2 \times 3 \times 2 \times 2 = 192$ subjects would be required. The number of required subjects

can be decreased substantially if certain assumptions are made about the influence of interactions between parameters. In the proposed test plan, the following rationale is used to reduce the number of required tests.

1. The influence of muscle tensing will be assumed to be most pronounced in the maximal wrap-around condition. Since muscle activation will be either none or full tetanus, information about intermediate muscle effects is not needed.

2. The effect of muscle tensing in the upper and lower abdomen will be assumed to be similar. Muscle tensing will therefore not be stimulated in tests loading the upper abdomen.

The levels of abdominal compression chosen should generate an acceptable distribution of injury and non-injury outcomes. Multiple levels of abdominal compression are tested since many tests (both with and without injury) are required in order to develop an injury risk function using censored data. The influence of loading rate will be evaluated to a limited extent by performing the 50% compression tests with the ramp-release wave at two loading rates. Repeated tests on the same subject shall not be used, even in the case of the 25% compression tests, since some injuries may result from these tests and because the initial condition will probably be changed after even a non-injurious test. In previous UVA tests of porcine thoracic response, a long-time viscous effect and superficial soft tissue damage have made repeated tests inappropriate, even when the first test did not generate hard tissue injury (Kent et al. 2003). There is also the potential to weaken the statistical modeling if repeated tests are performed on the same subject, since clustering will have to be considered.

Test Methods

Live anesthetized porcine subjects will be intubated, ventilated, instrumented, and positioned for testing on a pneumatically driven test table similar in concept to that described by Kent et al. (2003, 2004) (Figure 2). Immediately prior to loading, the subject will be euthanized, the lungs will be inflated to maximal physiological inhalation, and the tracheal tube will be occluded. The tube will remain occluded throughout the displacement wave. The pulmonary system will therefore be assumed to be closed during the loading and the effects of airflow from the lungs will be ignored.

Pressure transducers will be inserted via catheters into the abdominal aorta, the thoracic aorta, the trachea, and at other locations. For tests involving simulated muscle tension, pairs of external electrodes

will be positioned bilaterally over the abdomen anterolaterally and posterolaterally. A load transducer will be positioned between the subject and the table. Load transducers will also be used to measure the applied force on the anterior abdomen. Potentiometers will measure anterior-posterior displacement of the anterior abdominal wall. Digital video of the tests will be taken and digital still images will be used to document test conditions and the necropsy findings.

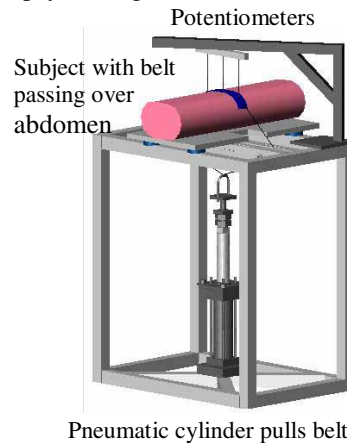


Figure 2. Schematic depiction of loading frame.

Following positioning of the subject on the table, the belt will be positioned on the abdomen. Immediately prior to the application of loading, the subject will be euthanized using a solution of pentobarbital, a barbiturate that affects the central nervous system and can therefore be assumed to have no effect on the muscles' response to an external stimulus. Immediately after death, the muscles will be stimulated when applicable and the displacement wave will be applied. In all ramp-hold tests, the displacement will be held until a nominal steady-state condition is achieved (i.e., until force relaxation is complete). Viscoelastic structural models will be developed for each ramp-hold test (Kent et al. 2003). The validity of these models will be assessed by using them to predict the measured response in all ramp-release tests. At the completion of the test, a detailed necropsy will be performed to document all macroscopic thoracoabdominal injuries.

The Institutional Review Boards and Institutional Animal Care and Use Committees of The Children's Hospital of Philadelphia, The University of Pennsylvania School of Medicine, and The University of Virginia approved the conduct of relevant components of this project. All testing will be overseen by personnel from the UVa Center of Comparative Medicine and Department of Emergency Medicine. All procedures comply with the guidelines of the Animal Welfare Act and Public

Health Policy on the Humane Care and Use of Laboratory Animals. All subjects will be euthanized prior to any biomechanical testing.

RESULTS

Anthropometrics

Retrospective radiology – Radiology films from 35 study subjects, 18 females and 17 males, were analyzed to determine the geometrical measures. The average age and weight were 6.9 ± 0.8 years and 24.4 ± 1.7 kg, respectively. ¹

Table 1: Results from the retrospective radiology study of 35 subjects. Figures showing these dimensions are contained in the Appendix.

Measure	Average (cm)	Std. Dev.
Abdominal depth at umbilicus	13.6	1.3
Circumference at umbilicus	51.6	4.0
Abdominal depth at lower ribs	15.0	1.2
Circumference at lower ribs	54.8	3.5
Inner distance between iliac crests at first appearance	9.0	1.9
Outer distance between iliac crests at first appearance	16.0	1.2
Transverse dimension of abd. at iliac crest first appearance	20.2	1.4
Inner distance between iliac crests at largest AP diameter	7.2	1.1
Transverse dimension of abdomen at largest AP diameter	21.4	1.6
Right lowest rib to iliac crest	6.5	0.9
Left lowest rib to iliac crest	6.8	1.0
Right iliac crest to ischial tuberosity	13.9	0.7
Left iliac crest to ischial tuberosity	13.8	0.8
Lower border of the lung to the pubis - anteriorly	24.7	1.6
Lower border of the lung to the pubis - posteriorly	23.1	1.8
Pelvic inlet	9.0	0.8

Prospective anthropometrics – Anthropometric measures from 60 study subjects, 29 females and 31 males, were obtained. The average age and weight were 6.2 ± 1.3 years and 23.7 ± 5.2 kg, respectively. Preliminary analysis is complete on 30 subjects and several representative measures are shown below.

¹ This data was presented at the May 2005 Annual Meeting of the Society of Pediatric Radiology.

Figure 3 shows the angle made by the right fibula/tibia relative to a vertical line in space. In general, this angle is largest for those children seated directly on the vehicle seat followed by those on a back less booster, then those on a full back booster. A smaller value corresponds to a more comfortable position.

The distance between the lateral edge of the neck to the lateral edge of the shoulder belt along the line of the clavicle is shown in Figure 4. Again the role of the restraint is evident with the backless booster providing a vertical “boost” to the child and making his stature more adult like. The shoulder belt guide on the full back booster moves the belt even farther off the neck.

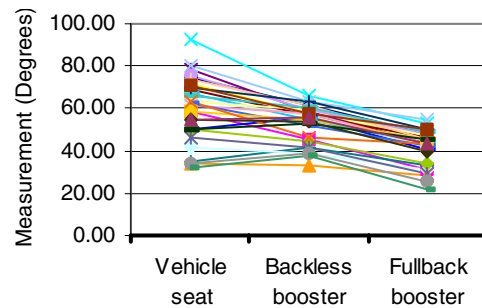


Figure 3: Right tibia/fibula angle (relative to vertical)

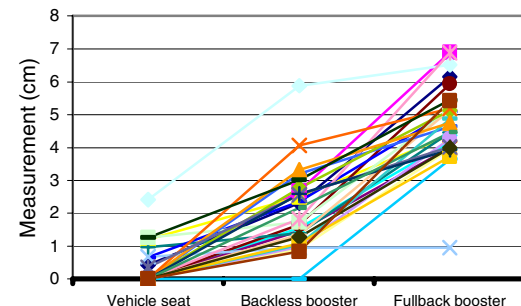


Figure 4: Distance from lateral edge of the neck to lateral edge of shoulder belt at the level of the clavicle.

Crash Investigation

Twenty-six cases meeting the following selection criteria were reviewed and analyzed: seat belt restrained child occupant age 4-11 who sustained an AIS 2+ abdominal injury in a frontal crash. Specific observations from the cases were as follows:

- Hollow organ injuries (stomach/intestine) were associated with higher delta v (47 kph) than those injuries to the solid organs (spleen/liver/pancreas/kidney) (26 kph)
- Belt compression was the primary mechanism of injury however the compression derived from both the lap and the shoulder belt.

- Belt misuse or older designs were predominant in those with injury; for example, children with the shoulder belt behind the back, automatic shoulder belts, and single manual lap belts.

The case review identified three unique kinematic patterns that resulted in abdominal injury: pre-submarining where the belt is initially out of position, classic submarining where the belt starts in position and the pelvis moves under the belt with the torso reclined, and submarining/jackknifing where the pelvis slides under the belt, and the torso flexes forward. Three cases are described here for illustration.

Case 1 - The case vehicle (1995 Honda Civic) was traveling north, vehicle 2 (1996 Mazda MPV) directly ahead of the case vehicle. Vehicle 3 (1996 Mercury Villager) was also traveling north in the lane to the right of the case vehicle and vehicle 2. Vehicle 3 lost control on the wet pavement and entered the path of vehicle 2. Vehicle 2 hit Vehicle 3 on the left side. Vehicle 2 was rear ended by the case vehicle. The PDOF was 0° and the delta v was calculated to be 20 kph. A 7-year-old male was seated in the left rear seat restrained by the lap and shoulder belt with the shoulder portion of the belt behind his back.

AIS 2+ injuries:

- Hematoma of the small bowl mesentery (AIS2)

AIS 1 injuries:

- Horizontal abrasion to the lower abdomen
- 2 cm forehead laceration

Proposed injury source:

- Submarining with jackknifing - lap belt loading

MAIS other occupants:

- Adult restrained driver (AIS 1)
- Adult restrained right front passenger (AIS 1)
- 3 year old - booster seat in right rear (none)



Figure 5: Photo of case vehicle damage from Case 1.

Case 2 - Vehicle 2 (1993 Pontiac Sunbird) was traveling north on inside lane and rear-ended vehicle 3 (1997 Honda Accord), traveled over the yellow line into oncoming traffic and struck the front of the case vehicle (1994 Mercury Grand Marquis). Vehicle 4

(1992 Jeep Wrangler) was traveling behind the case vehicle and struck it in the rear. The case vehicle struck a roadside sign with its rear plane before coming to a rest. The PDOF was 330° for the frontal impact and the delta v was calculated to be 37 kph. A 4-year-old male was seated in the center rear seat restrained by the lap belt.

AIS 2+ injuries:

- Proximal ileal serosa tear of the distal jejunum
- Several mesenteric hematomas
- Grade 1 liver laceration.

AIS 1 injuries:

- Contusion/ abrasion to forehead
- Contusion to lower abdominal area
- Laceration over the right eye.

Proposed injury source:

- Pre submarining with lap belt loading

MAIS other occupants:

- Adult restrained driver (AIS 2)
- 2 year old in child restraint in left rear (AIS 1)



Figure 6: Photo of case vehicle damage from Case 2.

Case 3 - The case vehicle (1994 Nissan Sentra) was traveling eastbound behind a non-contact vehicle. Vehicle 2 (1997 Honda Accord) was traveling westbound at about 65mph, when vehicle 2 lost control due to hydroplaning after hitting a water spot on the road. Vehicle 2 skid sideways into the traveling path of eastbound traffic. The non-contact vehicle in front of the case vehicle steered to the right. The front of the case vehicle was struck by the right side of vehicle 2. The PDOF was 330° and the delta v was calculated to be 43 kph. A 7-year-old female was seated in the right front seat restrained by the automatic shoulder belt and manual lap belt.

AIS 2+ injuries:

- Lacerated spleen
- Small liver laceration
- Epidural bleeding along the skull base
- Fractured left ribs #9 and #10.
- Contused right lung

AIS 1 injuries:

- Contused right abdominal area

- Abdominal abrasion, left side
- Proposed injury source:*
- Classic submarining - lap/shoulder belt loading
- MAIS other occupants:*
- Adult restrained driver (AIS 1)



Figure 7: Photo of case vehicle damage from Case 3.

Necropsy Study

The multiple linear regressions described in Equations [1] and [2] were both significant, though the age term was not significant in Equation [1]. This term was therefore dropped and the forms of Equation [1] and [2] used for the subject identification were

$$f_{avg}^1 = 1 = 0.217 + 0.0327m \quad [5]$$

and

$$f_{avg}^2 = 1 = 0.536 + 0.00266a + 0.0179m \quad [6]$$

where

$$m = -2.5239 + 0.1812a + 0.0017a^2 \quad [7].$$

Minimizing the error in [5] and [6] subject to the constraint imposed by Equation [7] results in a pig age and mass of 76.7 days and 21.4 kg as the best representation of a 6-year-old human based on the external dimensions and masses, and organ masses, described earlier. As shown in Figure B.1 in the Appendix, the constraint imposed by Equation [7] makes it impossible for the pig to match all characteristics of the 6-year-old human. The age and mass chosen, however, do result in a very good representation of the set of characteristics chosen for comparison (see large dot in Figure B.1). A visual comparison of a to-scale adult human skeleton, a 73.4 kg pig, and a 21.2 kg pig (i.e., the best representation of a 6-year-old) is shown in Figure 8.

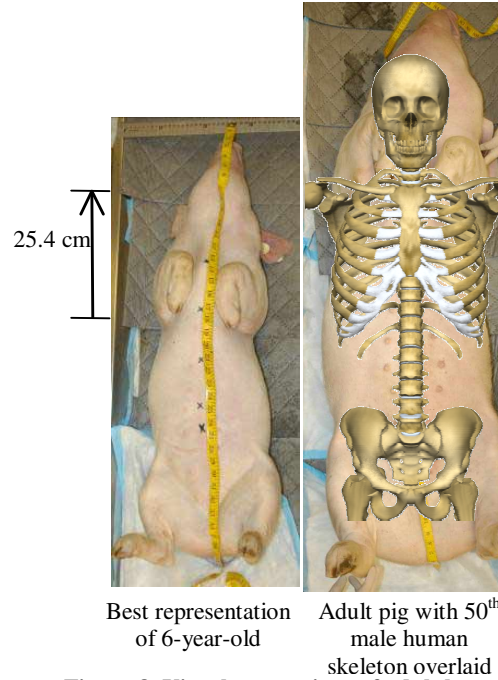


Figure 8. Visual comparison of adult human, adult pig, and chosen pig model (77 days old).

DISCUSSION AND CONCLUSIONS

Abdominal injuries, along with lumbar spine fractures, are part of a constellation of injuries referred to in the medical literature as "seat belt syndrome". Geometrical characteristics of the pelvis and abdomen of young children place them at higher risk for these injuries. Efforts to design restraints that mitigate these injuries are limited as no current pediatric anthropometric dummy (ATD) can accurately quantify the abdominal response to belt loading. This manuscript describes progress on a four-phase project to address this gap involving pediatric anthropometrics, real-world abdominal injury risk, abdominal biomechanical tolerance from a porcine model, and development of an abdominal insert for the 6-year-old ATD based on these data.

The two sources of anthropometric and geometrical data serve several purposes in the overall research project. First they facilitate the identification of the relevant porcine model and second they provide geometrical guidelines for the development of the ATD insert. Use of the measures to guide the choice of the appropriate age animal is discussed below. Although the ATD does not have many of the skeletal landmarks used in either the retrospective radiology or prospective anthropometric studies, some measures can be compared to the current ATD dimensions. All ATD measures were taken from the

current Hybrid III 6 year old ATD drawing package (US DOT, 2002).

Table 2: Comparison of human measures with current Hybrid III 6 year old ATD measures taken from the ATD drawing package

Measure	ATD (cm)	Human (cm)+	Diff. (%)	ATD source*
Abdominal depth	15.7	13.6	-15%	p.70
Hip width	21.6	20.2	-7%	p.7, U
Waist circ.	57.2	51.6	-11%	p.7, Z
Sitting height	63.5	61.5	-3%	p.7, A
Stature	114.0	119.5	5%	p.7, Q
Height of pelvis	14.3	13.85	-3%	p.70, 71
Dist. between iliac crests	15.3	12.5	-23%	p.71

+From either the retrospective radiology measurements shown in Table 1 or the prospective anthropometrics study
*Page number and measurement symbol, if noted, from Hybrid III 6-year-old ATD drawing package

In addition to the project specific relevance of these measures, these data provide critical information regarding belt fit and how that improves with age and booster seat use and will be summarized in a future publication.

Review of the field data provides an understanding of the conditions in which abdominal injury occurs in seat belt restrained children. An important finding is that abdominal injuries can occur in low severity crashes with little injury to the other restrained occupants as illustrated by Case #1. The delta v in this case was 20 kph and all other restrained occupants (driver, right front passenger, booster seat restrained rear seated child) sustained either no injuries or only bruising and contusions.

In almost all of the cases reviewed, the abdominal injury was due to compression by the belt. It varied whether that compression was due to the lap belt or the shoulder belt depending on the likelihood for submarining. This is illustrated in case #3 where the child was restrained by an automatic shoulder belt and manual lap belt. The position of the shoulder belt and the lap belt anchors was more aft than in a traditional manual lap and shoulder belt. Substantial submarining occurred in this case and both belts played a role in loading the upper abdomen and thorax as evidenced by the spectrum of injuries: liver and spleen lacerations, rib fractures, and a lung contusion. The role of belt compression as the mechanism of injury confirms the hypothesis highlighted in the introduction that the injury

measure needed to accurately reflect abdominal injury risk for children should be deflection based, as has been suggested for adults.

Review of the possible kinematics in these cases suggested three distinct patterns of movement in the crash. Not all children sustained their abdominal injury through the jackknifing over the seat belt, the traditional view of how these injuries occur in children (Weber 2002). Although this was the suggested kinematics for some as evidenced by associated head or facial injury (Case #1), some children were injured due to poor initial belt placement (Case#2) and some were injured due to classic submarining, where the belt starts in position and the pelvis moves under the belt with the torso reclined (Case #3). In those cases with poor initial belt placement, these children were often restrained by a manual lap belt and were scooted forward on the seat causing the belt to ride high on their abdomen pre-crash. Several of these cases are being modeled using MADYMO in order to more clearly study the kinematics and relate it to the velocity and direction of belt loading, the amount of head excursion and head acceleration. The extreme stiffness of the Hybrid III 6-year-old ATD's abdomen prevents meaningful values of abdominal compression from being extracted from the models.

The necropsy component of this project identified the pig having an age of 77 days and a whole-body mass of 21 kg as the best representation of a 6-year-old human. The finding that both age and mass contributed information to a statistical model of external body dimensions indicates that pediatric pigs, like human children, are not simply scaled-down versions of adults. This supports the necessity of this type of study since scaling adult data to represent pediatric response requires the assumption of geometric similitude.

Since one of the end goals of this project is the development of an abdominal insert having the appropriate structural response, we decided that the geometry and inertial properties of the human were the most important characteristics to match. It should be noted, however, that other markers of development, such as sexual maturity or bone ossification, may not show the same age correlation between humans and pigs.

It is also important to acknowledge that, while the pig is a commonly used and reasonable model of the human for many applications, there are some important limitations for the study of abdominal response to belt loading. The most obvious are the

marked differences in pelvic structure. These differences make the pig a poor model with which to study, for example, the kinematics of submarining. This study has therefore focused only on those situations where the belt is initially mis-positioned over the abdomen. There are also some abdominal anatomy differences that are significant. Some of these are discussed in detail by Huelke et al. (1986). In the case of abdominal loading using a pig model, one important factor to consider is the tethering of the abdominal contents. The quadrepedal nature of the pig results in organ tethering that reacts against gravitational forces in the dorsoventral direction, as opposed to the superior-inferior direction in a standing human. Furthermore, the subjects used in these experiments will be tested in a supine position, so the organ geometry will not be an exact match of the seated human's. Another important anatomical consideration is the spleen. In a human, the spleen is shaped somewhat like a fist, while the pig's spleen, which is long and thin, has been described as "tongue-like". The liver is also different in the pig, having many "leaf-like" lobes. Finally, the intestinal structure of the pig is different from the human, primarily in the arrangement of the ascending colon. In the pig, this structure is coiled to form a cone-shaped mass with its axis oriented dorsoventrally. The cecum is at the base of the cone.

The abdominal insert development will follow using the information provided by the aforementioned parts of the study. Specifically, a reusable, rate-sensitive abdominal insert will be developed for the Hybrid III 6-year old child dummy following the development reported by Rouhana et al. (2001). Initial prototypes will utilize equal stress equal velocity scaling for the response. The response data from the porcine tests will be used for the final design.

Based on the field data analyzed to date, the authors anticipate the measurement of abdominal deflection and/or functions of deflection will be important for the injury assessment part of the project. Therefore, initial instrumentation efforts will concentrate on deflection measurements. Data from the porcine study will also be analyzed to confirm that hypothesis and thereby, drive the injury assessment instrumentation included with the new abdomen. If the field accident data or biomechanical data indicate otherwise, the efforts will be refocused.

ACKNOWLEDGEMENTS

Funding for the anthropometric, field data and injury tolerance research activities contained in this manuscript is from the Takata Corporation. Funding

for the abdominal insert research and development activities contained in this manuscript is from Ford Motor Company. The authors would also like to acknowledge the commitment and financial support of State Farm Mutual Automobile Insurance Company for the creation and ongoing maintenance of the Partners for Child Passenger Safety (PCPS) program, the source of crash investigation data for this study. The authors also thank the many State Farm policyholders who consented to participate in PCPS. The results presented in this report are the interpretation solely of the author(s) and are not necessarily the views of State Farm or Takata.

REFERENCES

- Aldman, B, A Anderson, O Saxmark. (1980) Possible effects of air bag inflation on a standing child. Proceedings of IRCOBI.
- Arbogast, K.B, I Chen, ML Nance, D Durbin and FK Winston (2004). "Predictors of pediatric abdominal injury risk." *Stapp Car Crash Journal* 48: 479-494.
- Bergqvist, D, H Hedelin, B Lindblad and T Matzsch (1985) "Abdominal injuries in children: an analysis of 348 cases." *Br J Accident Surgery* 16: 217-220.
- Centers for Disease Control (2000) <http://www.cdc.gov/growthcharts/>
- Clauser, C, P Tucker, J McConville, E Churchill, L Laubach, J Reardon. (1972) Anthropometry of Air Force women (Report No. AMRL-TR-70-5). Wright-Patterson Air Force Base, Ohio. (DTIC No. AD 743 113).
- Durbin, DR, E Bhatia, JH Holmes, KN Shaw, JV Werner, W Sorenson and FK Winston (2001). "Partners for child passenger safety: a unique child-specific crash surveillance system." *Accid Anal Prev* 33(3): 407-12.
- Durbin, DR, KB Arbogast and EK Moll (2001). "Seat belt syndrome in children: a case report and review of the literature." *Pediatr Emerg Care* 17(6): 474-7.
- Garrett, J and P Braunstein (1962). "The seat belt syndrome." *J Trauma* 2: 220-238.
- Gogler, E, A Best, H Braess, H Burst, G Laschet. (1977) Biomechanical experiments with animals on abdominal tolerance levels. Paper 770931, SAE, Warrendale, PA
- Gotschall, C., A. Better, D. Bulas, M. Eichelberger, F. Bents and M. Warner (1998). *Injuries to children restrained in 2- and 3-point belts. 42nd Annual Meeting of the AAAM, Charlottesville, VA.*
- Grunhofer, H (1975) A review of anthropometric data of German Air Force and United States Air Force personnel (Report No. AGARD-AG-205). (DTIC No. AD-A010 674).
- Hardy, W, L Schneider, S Rouhana. Abdominal impact response to rigid-bar, seatbelt, and airbag loading. (2001) *Stapp Car Crash Journal* 45:1-32.

- Hoy, G and W Cole (1993). "The paediatric cervical seat belt syndrome." *Injury* 24: 297-299.
- Huelke, D, G Nusholtz, P Kaiker. (1986) Use of quadruped models in thoraco-abdominal biomechanics research. *J. Biomech.* 19(12):969-77.
- Kent, R, C Bass, W Woods, C Sherwood, N Madeley, R Salzar, Y Kitagawa. (2003) Muscle tetanus and loading condition effects on the elastic and viscous characteristics of the thorax. *Traffic Injury Prevention*; 4(4):297-314.
- Kent, R, C Bass, W Woods, R Salzar, J Melvin. (2004) The Role of Muscle Tensing on the Force-Deflection Response of the Thorax and a Reassessment of Frontal Impact Thoracic Biofidelity Corridors. Proc. 2004 IRCOBI, Graz, Austria.
- Kulowski, K and W Rost (1956). "Intra-abdominal injury from safety belts in auto accidents." *Arch Surg* 73: 970-971.
- Lane, J (1994). "The seat belt syndrome in children." *Accid Anal & Prev* 26: 813-820.
- McConville, J, C Clauser, T Churchill, J Cuzzi, I Kaleps. (1980) Anthropometric relationships of body and body segment moments of inertia. (AFAMRL-TR-80-119), Air Force Aerospace Medical Research Laboratory, Wright-Patterson Air Force Base, Ohio.
- Mertz, H, G Driscoll, J Lenox, G Nyquist, D Weber. (1982) Responses of various animals exposed to deployment of various passenger inflatable restraint system concepts for a variety of collision severities and animal positions. 9th ESV.
- Miller, M (1991a) The biomechanics of lower abdominal steering-wheel loading. *J Trauma* 31:1301-1309.
- Miller, M (1991b) Tolerance to steering wheel-induced lower abdominal injury. *J Trauma* 31:1332-1339.
- Miller, MA (1989) "The biomechanical response of the abdomen to belt restraint loading." *J Trauma*, 29(11) 1571-1584.
- Owings, C, D Chattin, R Snyder, R Norcutt. (1975) Strength characteristics of U.S. children for product safety design. University of Michigan Final Report, #FDA-73-32, Prepared for CPSC, Bethesda, MD.
- Prasad, P and R Daniel (1984) A biomechanical analysis of head, neck, and torso injuries to child surrogates due to sudden torso acceleration. Paper 841656, SAE, Warrendale, PA.
- Rouhana, SW (2002) "Biomechanics of Abdominal Trauma", in *Accidental Injury: Biomechanics & Prevention*, Nahum and Melvin, eds., Springer-Verlag, NY.
- Rouhana, SW, AM Elhagediab, A Walbridge, WN Hardy, LW Schneider. (2001) "Development of a Reusable, Rate-Sensitive Abdomen for the Hybrid III Family of Dummies" *Stapp Car Crash Journal*, 45: 1-10.
- Rouhana, SW, DC Viano, EA Jedrzejczak, JD McCleary (1989) "Assessing Submarining and Abdominal Injury Risk in the Hybrid III Family of Dummies", 33rd Stapp Car Crash Conference, SAE Paper No. 892440.
- Snyder, R, L Schneider, C Owings, H Reynolds, D Golomb, M Sckork. (1977) Anthropometry of infants, children, and youths to age 18 for product safety design. UM-HSRI-77-17, CPSC, Bethesda, MD.
- Stalnaker, R, J McElhaney, V Roberts (1973) Human torso response to blunt trauma. in *Human Impact Response Measurement and Simulation*, pp. 181-199. Plenum Press, New York.
- Stocker, J and L Dehner. (2002) *Pediatric Pathology*. Lippincott Williams & Wilkins, Philadelphia, PA..
- Troiseille, X, F Cassan and M Schrooten (2001). Child restraint system for children in cars - CREST results. 17th ESV, Amsterdam, the Netherlands
- Trollope, M, R Stalnaker, J McElhaney, C. (1973) The mechanism of injury in blunt abdominal trauma. *J Trauma* 13(11):962-970.
- Tso, E, B Beaver and JA Halter (1993). "Abdominal injuries in restraint pediatric passengers." *J Pediatric Surgery* 28(7): 915-919.
- United States Department of Transportation. (2002) "Hybrid III 6-year-old Anthropomorphic Test Device Drawing Package." http://dmses.dot.gov/docimages/pdf1a/181357_web.pdf
- Weber, K (2002) Child Passenger Protection. in *Accidental Injury: Biomechanics & Prevention*, Nahum and Melvin, eds., Springer-Verlag, NY.
- Woods, W, Kent, R, Ullman, E, Bass, C. (2002) Effect of multiple exhalation ports in a simulation of transtracheal ventilation with a porcine model of an obstructed airway. AAP 2002 National Conference and Exhibition, Boston, Massachusetts
- Winston, FK, IG Chen, MR Elliott, KB Arbogast and DR Durbin (2004) "Recent trends in child restraint practices in the United States" *Pediatrics* 113(5): e458-64.
- Young, J, R Chandler, C Snow, K Roginette, G Zehner, M Lofberg. (1983) Anthropometric and mass distribution characteristics of adult females. FAA-AM-83-16, Office of Aviation Medicine, Federal Aviation Administration, Oklahoma City, OK

APPENDIX

Dimensions used for the retrospective radiology anthropometric study

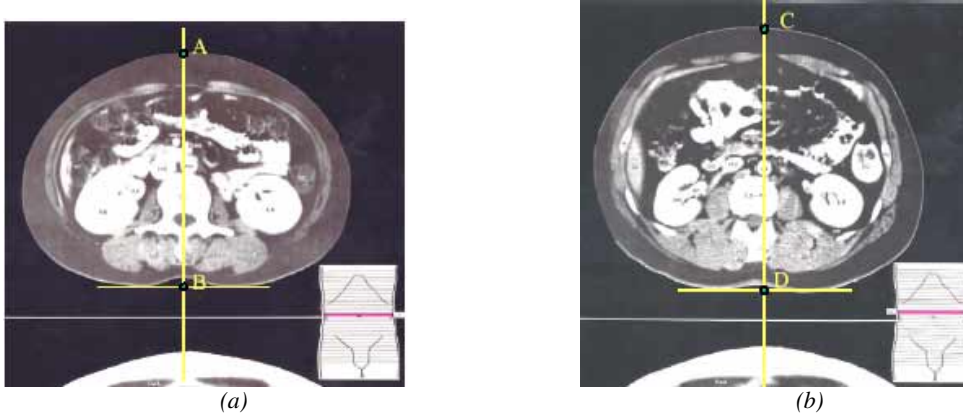


Figure A.1 (a) Depth (AB) and circumference at the level of the umbilicus. For the circumference, continuation across the umbilicus was assumed. (b) Depth (CD) and circumference at the level where the anterior ribs last appear.

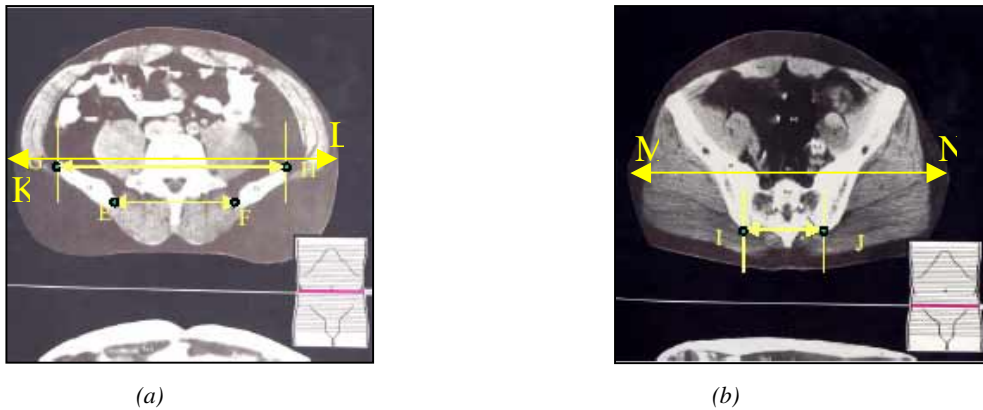


Figure A.2 (a) At the level of the first appearance of the iliac crests, the widest transverse dimension of the abdomen (K-L), the inner dimension of the iliac crests (EF), and the outer dimension of the iliac crests (GH). (b) At the level of the largest AP diameter of pelvis, the widest transverse dimension of the abdomen (MN) and the inner dimension of the iliac crests (IJ).

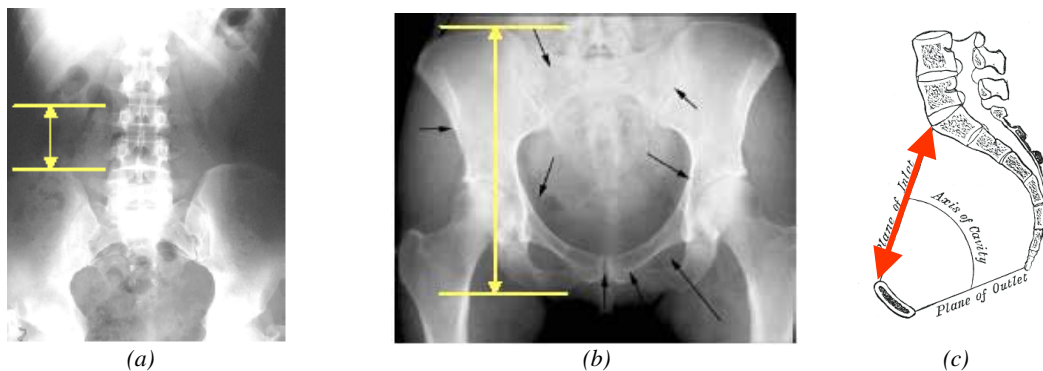


Figure A.3 (a) From the abdominal AP film, the vertical distance from the most superior points of the iliac crest to lowest inflection point of 12th rib anteriorly measured on both the right and left side. (b) the vertical distance from the most superior point of the iliac crest to most inferior point of the ischial tuberosity measured on both the right and left side. (c) Distance from the sacral promontory at S1 to the superior aspect of the pubic symphysis in the midline sagittal plane (defined as plane of inlet in figure). Figure from *Anatomy of the Human Body*, H. Gray, 20th Edition, 2000.

Results of necropsy study

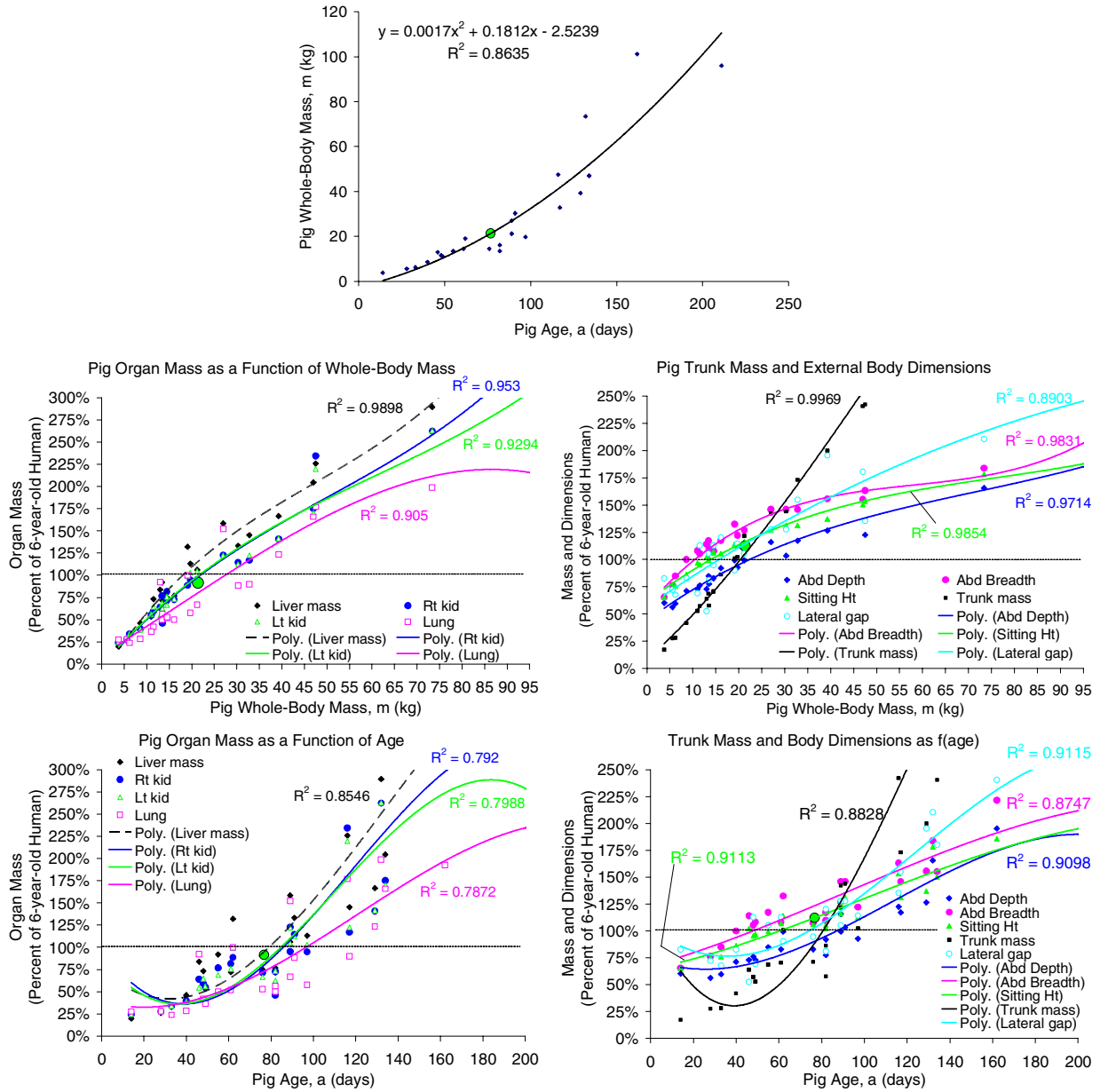


Figure B.1. Results of human-to-pig correlation. Large dot is the subject age and mass identified as the best representation of the 6-year-old human.

THE REPEATABILITY AND REPRODUCIBILITY OF PROPOSED TEST PROCEDURES AND INJURY CRITERIA FOR ASSESSING NECK INJURIES IN REAR IMPACT

Céline Adalian

PSA Peugeot Citroën,
France

Raimondo Sferco,

Paul Fay

Ford of Europe,
Germany and UK

(on behalf of the ACEA Whiplash Sub-Group)

Paper number 05-0340

ABSTRACT

The European Automobile Manufacturers Association (ACEA) has carried out a study looking at the repeatability and reproducibility of the proposed test procedures and injury criteria. For repeatability, 3 repeat tests were carried out on 3 different seats using a 16 km/h delta-V test pulse. To evaluate reproducibility, the same 3 seats were tested to a common protocol at 5 different test labs using two different test pulses (16 and 25 km/h delta-V). The sleds used included both acceleration and deceleration types. A wide range of acceleration, simple force/moment and combined force and moment injury criteria were evaluated. In general, repeatability of the sled pulses was reasonable but significant variations in pulses and test set up were found between laboratories. As a result, more precise procedures, test pulse corridors and an agreed definition of T_{zero} (beginning of impact) are needed. Repeatability of most of the injury criteria at 16 km/h was acceptable but reproducibility was poor, with variations of up to 40% for some of the criteria. The situation was even worse at 25 km/h, with some criteria showing variations of over 100%. Great care therefore needs to be exercised in selecting appropriate injury criteria, in selecting the stringency of assessment limits and in comparing results from different laboratories. The variation in results also questions the use of high severity pulses for neck injury assessment.

INTRODUCTION

A number of organisations are carrying out or planning sled tests on car seats to assess the risk of soft tissue neck injuries and to make comparisons between vehicles. Most of these tests will use a recently developed dummy (BioRID) but a number of different test pulses and injury criteria have been proposed. There is little experience available in the

use of these test procedures and limited knowledge of their repeatability and reproducibility. Nevertheless, data are widely exchanged for comparisons, without checking if the test protocols followed exactly the same data processing definitions.

The European Automobile Manufacturers Association (ACEA) has carried out a study looking at the repeatability and reproducibility of the proposed test procedures and injury criteria. This study helped in identifying the different problems which may be encountered if a test protocol is not sufficiently detailed enough. It aimed at highlighting the possible improvements to reduce dispersion and the test configurations or criteria that should not be used to assess whiplash because of non reproducibility.

PRESENTATION OF THE STUDY

In order to determine reliability of current whiplash assessment, a whiplash testing programme has been defined. The purpose is :

- to assess the feasibility and reproducibility of the contemplated test procedure and test tools
- to find the key test parameters/ conditions which would ensure that the test are reproducible/repeatable
- to prepare recommendations for the exploitation of test measurements/ results and for the ways and means to obtain them
- to record unexpected problems/risks of problems with the contemplated test procedure and tools

Description of the test matrix

The defined test matrix is made of 36 tests :

- two different pulses that are thought to be used to assess whiplash and seat stability by EuroNCAP

- three different seat models with different levels of performance in published ratings

- the same model will be tested three times in one laboratory to assess repeatability

- five different laboratories with different tests set-ups and tools to carry out the tests to assess reproducibility

The tests have been carried out according to the test procedure which is currently studied within Euro-NCAP whiplash working group (whiplash test procedures such as Thatcham and IIWPG [1], ADAC [2], SNRA [3]). Therefore, the key test conditions which should be monitored by test laboratories (the dummy and dummy installation, the pulses, the seat adjustments) are described in the following paragraphs.

Seat adjustment

Seats were rigidly mounted on sled with actual rail angle and standard heel point values. Care was taken to reproduce similar configuration in all the labs for each seat model.

Seats were set in mid position and mid height as usually required in whiplash test procedures. Head Restraints (HR) were set according to the RCAR procedure [4] : mid locking position when Z-lock available or else fully down.

Dummy adjustment

The Head Restraint Measuring Device (HRMD) defined by RCAR together with an SAE J826 H-point machine was used to define H-point and backset (horizontal distance between head and HR). Backset used to control the BioRID head position was measured with HR in its fully up position in order to have easy and reproducible data to record in all the labs in whiplash test procedures. The BioRID dummy was installed in the seat by controlling the parameters presented in table 1.

Table 1.

Control parameters to install BioRID dummy in the seat.

Location	Target Measurements	Tolerance
X Dummy H-Point	Seat H point + 20mm (Forward)	± 10mm
Z Dummy H-Point	Seat H point + 6mm (Lower)	± 10mm
Pelvis angle	26,5°	± 2,5°
Head plane	0° (Level)	± 1°
Dummy backset	HRMD backset + 15mm (Forward)	± 5mm

In order to prevent the dummy from jumping out of the seat during rebound, a 2 point seat belt was used to restrain the dummy during rebound phase. It was loose with same amount of slack for all the seats and in all the labs, so that the lap belt could

not interfere on the behaviour of the dummy during the rear impact.

Test pulses and type of sled

The IIWPG pulses have been used : deltaV = 16 km/h and 25 km/h. They are presented in chapter “sled pulses”, later in this paper.

Different sled facilities have been used :

- TNO and Fiat used an hydraulic acceleration sled,

- Thatcham used a pneumatic acceleration sled

- ADAC used a deceleration sled with hydraulic brake as stopping device

- Faurecia used a pendulum device for the 16 km/h tests and a deceleration sled with hydraulic brake as stopping device for the 25 km/h tests

Parameters analysed and definition

The first definition needed to analyse the data is the definition of T_{zero} (beginning of impact). T_{zero} is defined as the first point above 0.5 g on the sled X-accel channel filtered at CFC 60. Change of velocity (or “deltaV”) is calculated from the sled X-channel filtered at CFC 180.

All the criteria that could be measured or calculated for whiplash studies have been used :

- accelerations of BioRID head, spine and pelvis

- force and moment on BioRID upper and lower neck

- combined criteria such as NIC, Nkm and LNL

- contact between BioRID head and HR

- ...

An example of the method of assessment for repeatability and reproducibility is presented below. For a given parameter, X, measured during the 16 km/h tests for all the same seat model, seven values will have to be compared (one for each test). They are presented in Equation 1.

$$\left\{ \begin{array}{l} \text{Thatcham} = X_{Ta}, X_{Tb} \text{ and } X_{Tc} \\ \text{ADAC} = X_A \\ \text{Faurecia} = X_F \\ \text{TNO} = X_{T1} \\ \text{Fiat} = X_{F1} \end{array} \right. \quad (1).$$

The following definitions are used to assess repeatability (see Equations 2 to 6).

$$X_{Tmean} = \frac{(X_{Ta} + X_{Tb} + X_{Tc})}{3} \quad (2).$$

$$\text{Max}_3 = \text{MAX}(X_{Ta}; X_{Tb}; X_{Tc}) \quad (3).$$

$$\text{Min}_3 = \text{MIN}(X_{Ta}; X_{Tb}; X_{Tc}) \quad (4).$$

$$\text{Dispersion} = \Delta_3 = \text{Max}_3 - \text{Min}_3 \quad (5).$$

$$\text{Scattering} = \frac{\text{Max}_3 - \text{Min}_3}{X_{\text{Tmean}}} \times 100 \% \quad (6).$$

The following definitions are used to assess reproducibility (see Equations 7 to 11).

$$X_{\text{mean}} = \frac{(X_{\text{Tmean}} + X_A + X_F + X_{T1} + X_{F1})}{5} \quad (7).$$

$$\text{Max}_5 = \text{MAX}(X_{\text{Tmean}}; X_A; X_F; X_{T1}; X_{F1}) \quad (8).$$

$$\text{Min}_5 = \text{MIN}(X_{\text{Tmean}}; X_A; X_F; X_{T1}; X_{F1}) \quad (9).$$

$$\text{Dispersion} = \Delta_5 = \text{Max}_5 - \text{Min}_5 \quad (10).$$

$$\text{Scattering} = \frac{\text{Max}_5 - \text{Min}_5}{X_{\text{mean}}} \times 100 \% \quad (11).$$

ANALYSIS OF RESULTS

Initial set-up

The assessment of the initial position for the seat and for the dummy is made using the HRMD + SAE J826 H-point machine (also called Oscar + HRMD). Measurements recorded were :

- stem angle of HR with respect to vertical
- torso angle
- H-point
- backset and height (measured with different position of HR)

BioRID data are also used :

- H-point
- backset and height (measured with HR in its fully up position and with HR in its tested position)
- pelvis angle

The following paragraphs present the analysis of some of these parameters linked to the initial set-up.

Torso angle

The set-up procedure requires a torso angle of 25 +/- 1°. This requirement was fulfilled, but the whole band of tolerance, as proposed in the protocol, was needed to achieve it. None of the lab shows any particularity with respect to the others, such as seat set-up always in the extreme part of the band of tolerance for all the seats and seat models. Figure 1 shows that the set up of the seat can lead to torso angle variations of up to 1.6° depending on where the test was carried out. This is due to the fact that seat back recliner could be a step adjustment, not a continuous one. Even on a seat with continuous adjustment, it could take a long time to set-up the seat at exactly 25°.

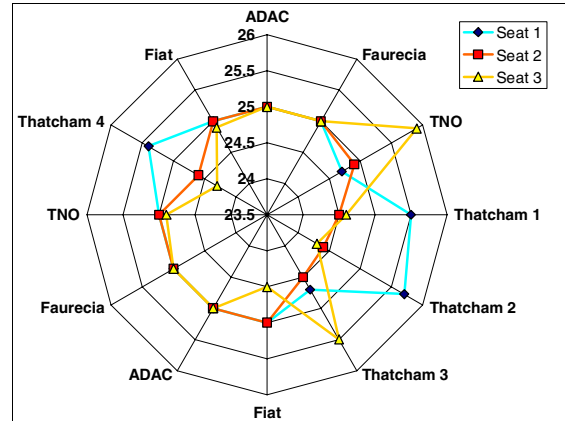


Figure 1. Torso angle dispersion.

Oscar + HRMD H-point

For H-point coordinates, the reference point is the seat back articulation. In the following graphs (figure 2 to 5), white crosses represent repeatability results. Maximum dispersion is represented by a coloured dotted rectangle for each seat model. Mean value is also given thanks to a different coloured symbol.

The combination of X and Z H-point measured on Oscar + HRMD and their dispersion is shown in figure 2 with an extensive analysis of the results. We can notice that none of the lab shows any particularity with respect to the others. Dispersion appears in the H-point X and Z coordinates for all the seat models (up to almost 20 mm in X and up to 22 mm in Z).

We can also notice that repeatability (white crosses) is better than reproducibility for X and Z H-point except for Seat 1 in Z. Up to twenty millimetres of dispersion occurred in X and Z for H point location. This dispersion is present for the 3 seat models for X H-point location.

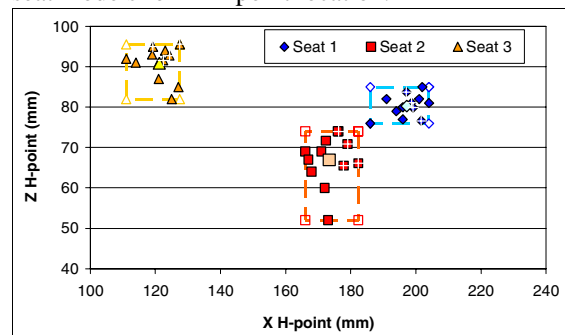


Figure 2. H-point distance measured on Oscar+HRMD.

Head to HR distance measured with HRMD

Backset and height are combined in figure 3. The commonly used HRMD rating zones are also presented: The green line is the border between “good” and “acceptable” rating zones, the yellow line is the border between “acceptable” and “marginal” rating zones and the orange line is the border between “marginal” and “poor” rating zones according to RCAR geometrical rating procedure [4].

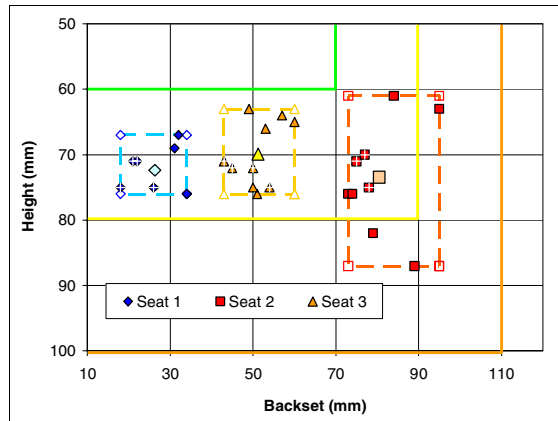


Figure 3. Head to HR distance measured on HRMD

We can see that each seat model has a different backset average (from 26 mm for Seat 1 to 80 mm for Seat 2) and a height average (from 69.9 mm for Seat 3 to 73.4 mm for Seat 2). This is due to the fact that each seat has its own structure design and its own HR volume. We can also add that none of the lab presents a specific trend, such as smaller backset than the ones measured in the other labs. Maximum dispersion for backset is 22 mm and maximum dispersion for height is 26 mm.

Since dispersion can be above 20 mm for each direction, this means that theoretically, the geometrical rating for the same seat can go from "Good" (green) to "Marginal" (orange).

If we suppose training to install HRMD can be improved, we can focus on Thatcham points (repeatability). In this case, dispersion is lowered since backset gets maximum dispersion of 11 mm and height gets maximum dispersion of 5 mm).

BioRID H-point

The combination of X and Z H-point measured on BioRID and their dispersion is shown in figure 4. Dispersion appears in the H-point X and Z coordinates for all the seat models but not to the same amount (up to 28 mm in X and up to 33 mm in Z). None of the lab can be distinguished from the others with respect to the use of the band of tolerance.

We can notice that repeatability (white crosses) is better than reproducibility for X and Z H-point.

Maximum dispersion in reproducibility assessment is about 30 mm in X and Z for BioRID H-point location.

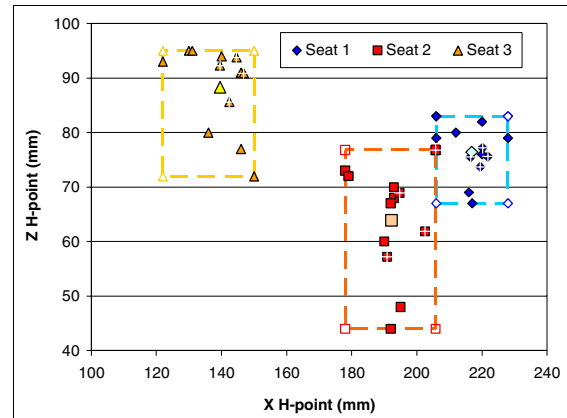


Figure 4. H-point distance measured on BioRID.

Head to HR distance measured with BioRID

Backset and height are combined in figure 5.

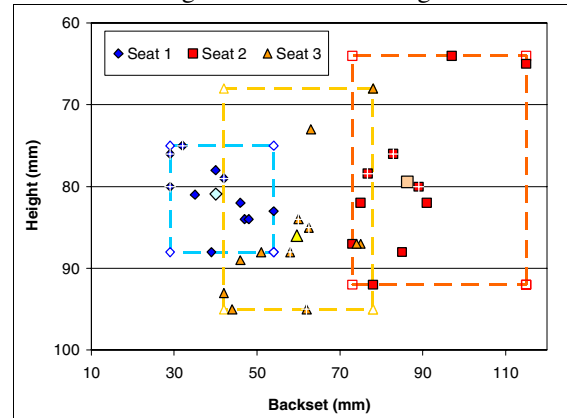


Figure 5. Head to HR distance measured on BioRID.

Each seat model has more dispersion for BioRID than for HRMD backset. Backset average ranges from 40 mm for Seat 1 to 86 mm for Seat 2. We can see that there is not so much difference for height since height average ranges from 79 mm for Seat 2 to 86 mm for Seat 3.

Moreover, maximum dispersion for BioRID backset is 42 mm and maximum dispersion for height is 28 mm.

It is also important to notice that in the current test procedures, there are different ways to measure backset for BioRID. In our opinion, it is important to distinguish the purpose of the measurement. One measure is used to ensure the head to be placed 15 mm forward from the HRMD head. This measure can be done with any reference point (seat, sled or even north pole thanks to GPS) and has no need to be linked to the actual HR position. But this measure is not useful for engineers. What is interesting for engineering purposes is the actual distance between BioRID's head and HR. For this, a specific method of measurement has to be defined. This should be discussed within BioRID Users Meeting.

Dummy final set-up : H-point

In order to check whether BioRID has been correctly installed with respect to HRMD, we can analyse the difference in H-point coordinates between the two machines. For reminder, BioRID X H-point should be 20 mm forward of HRMD one, and Z H-point should be 6 mm downward as already specified in table 1.

Figure 6 shows X delta H-point for all the tests carried out (16 and 25 km/h). X H-point shift seems to be easy to achieve. The average shift ranges from 18.3 mm for seat 3 to 19.69 mm for seat 1. But the large band of tolerance proposed in the test protocol is used by the different labs since maximum dispersion goes up to 15 mm.

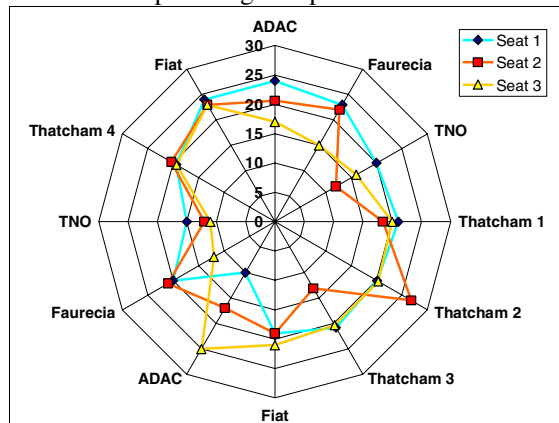


Figure 6. Difference of H-point in X between BioRID and Oscar + HRMD.

Figure 7 shows Z delta H-point for all the tests carried out. For this parameter, all the seat models can be compared since they should all reach the same target.

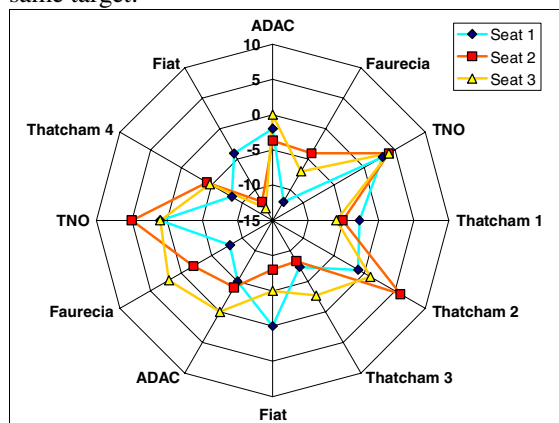


Figure 7. Difference of H-point in Z between BioRID and Oscar + HRMD.

Z H-point shift seems to be less easy to achieve than X one. The theoretical shift should be -6 mm but average shift between -2.53 mm for seat 3 and -3.87 mm for seat 1. Here again the large band of tolerance proposed in the test protocol is used by the different labs since maximum dispersion is 18 mm.

Figure 8 presents the same results in a 2-D format. White crosses represent repeatability results. Maximum dispersion is represented by a coloured dotted rectangle for each seat model. Mean value is also given thanks to a different coloured symbol. A fourth set of information has been added to this graph (green dotted rectangle + green circle point). It represents the official target for BioRID H-point with respect to HRMD.

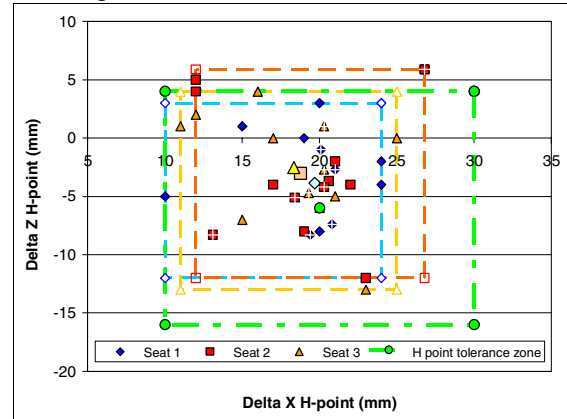


Figure 8. Difference of H-point in X and Z between BioRID and Oscar + HRMD – comparison with BioRID official H-point tolerance.

For the three seat models, average points are really close together. White crosses highlight the repeatability points, and we can notice they are closer together than reproducibility points. Training would help improving BioRID installation. But even with repeatability points, it can be noticed that Z H-point target should be modified, since the majority of points are above the theoretical target. Therefore, it should be recommended to modify Z H-point target for BioRID. Our proposal would be to require BioRID H-point to be at the same height than Oscar + HRMD one.

Dummy final set-up : distance between head and HR

Figure 9 shows difference in backset and height between BioRID and HRMD for all the tests carried out.

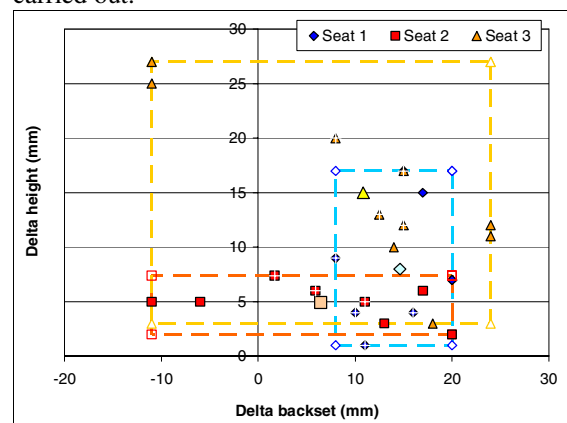


Figure 9. Difference of head to HR distance in X and Z between BioRID and Oscar + HRMD.

Backset shift seems not to be so easy to achieve. Theoretical shift is 15 mm (with HR in its fully up position), and BioRID positioning fulfilled this requirement. But when backset was measured with HR in its tested position, the average shift ranges from 6.45 mm for seat 2 to 14.63 mm for seat 1. The large band of tolerance is, here again, fully used since maximum dispersion is 35 mm between the two extreme positions.

Height shift between Oscar + HRMD and BioRID seems to be dispersive and linked to the seat model. The average shift ranges from 4.93 mm for seat 2 to 15 mm for seat 3. This means that HRMD is always lower than BioRID. Here again the large band of tolerance is fully used since maximum dispersion is 24 mm. Measurement method for backset and height between BioRID and HRMD has to be improved if we want to get good reproducibility.

A clear method for measuring backset has to be defined. It should take into account the possible different geometries a HR could have.

Sled pulse

The comparison of the pulses carried out in the different test lab is made in the following sections. They are compared with the target pulse (defined by IIWPG) for both 16 and 25 km/h severity, and with the corridor already defined by IIWPG for 16 km/h.

All the pulses are analysed thanks to the T_{zero} definition which was described in chapter "Parameters analysed and definition".

DeltaV = 16 km/h

Seven pulses can be compared for the 16 km/h test severity, for each seat model. Figure 10 presents this comparison for seat 2.

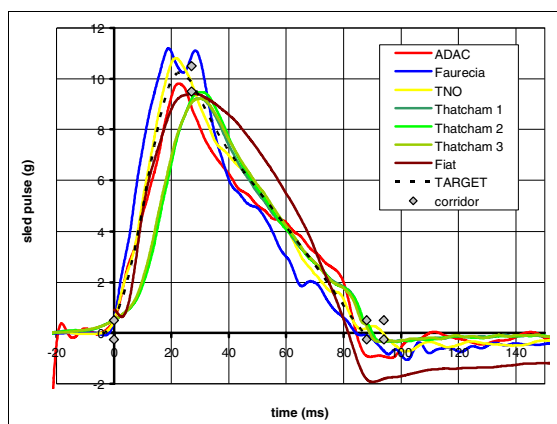


Figure 10. Comparison of sled pulses for the different 16 km/h tests carried out on seat 2.

Results were similar for seat 1 and seat 3. We can notice that the peak is between 9.2 g and 11.2 g. None of the sleds fulfils the corridor requirements. The shift in time can be explained because of the T_{zero} definition used here which is different from the one currently used by IIWPG (*IIWPG T_{zero} is such that peak pulse occurs at 27 ms*), but there is not such an explanation for the magnitude of the sled pulse.

Moreover, it is difficult to distinguish between the curves whether the sled is a deceleration one or an acceleration one. The only comment we can make is that T_{zero} definition as proposed by IIWPG would be difficult to apply to the Faurecia pulse (double peak pulse).

The resultant change of velocity for seat 2 is presented in figure 11. The change of velocity is calculated from T_{zero} up to the time when sled acceleration goes below 0.5 g.

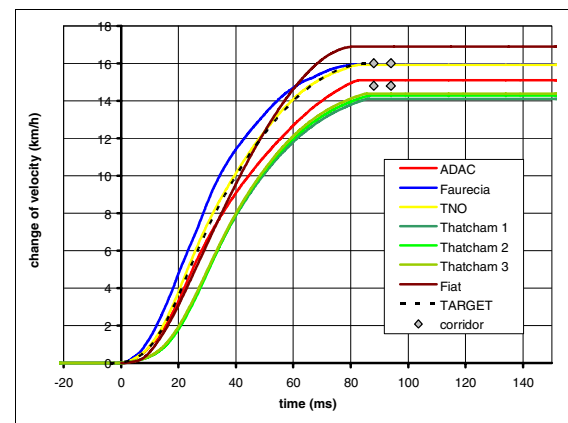


Figure 11. Comparison of sled pulses for the different 16 km/h tests carried out on seat 2.

Results were similar for seat 1 and seat 3. We can notice that this change of velocity is between 14 and 17 km/h.

It is acknowledged that there is a need to better define the pulse characteristics. The data presented here is being used by groups such as Euro NCAP to define the pulse more precisely, probably using a combination of requirements for acceleration levels and deltaV.

Moreover, after the ACEA tests had been performed, Thatcham subsequently improved their pulse performance and meet now the corridor.

DeltaV = 25 km/h

Five pulses can be compared for the 25 km/h test severity, for each seat model. Figure 12 presents this comparison for seat 3.

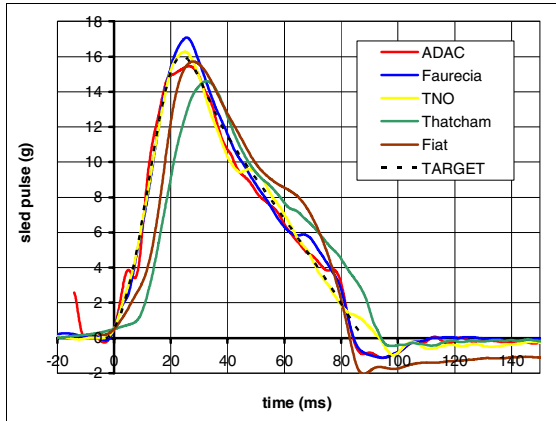


Figure 12. Comparison of sled pulses for the different 25 km/h tests carried out on seat 3. Results were similar for seat 1 and seat 2. We can notice that for this severity, the peak is between 14.7 g and 17 g.

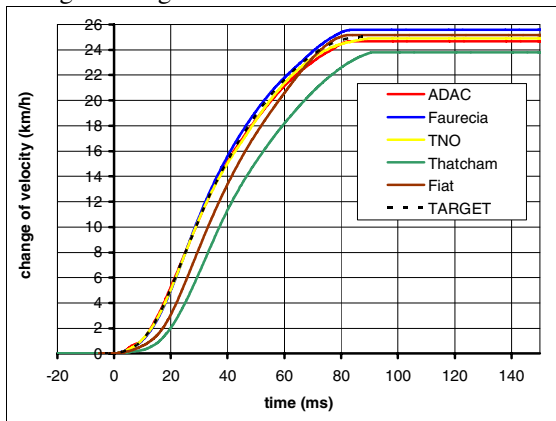


Figure 13. Comparison of sled pulses for the different 25 km/h tests carried out on seat 3. The change of velocity up to the time when sled acceleration goes below 0.5 g is between 23.8 and 25.6 km/h.

Conclusion on sled pulse

We can conclude that significant variation in pulse and set up have been documented. But repeatability of sled pulses is acceptable. Future work should be devoted to define more accurate requirements on sled pulse and change of velocity. The first action would be to define a corridor for the 25 km/h (impact severity dedicated to seat stability only). Moreover, general accepted definition of T_{zero} is needed since 3 different definitions are currently proposed.

Finally, there is no clear influence of sled type on pulse characteristics and on initial position.

Influence of the different set-ups and sled pulses on dummy readings

Dummy readings have been compared for repeatability and reproducibility tests in order to assess the dispersion that could be due to difference in dummy set-up, sled pulse and type of sled. For this purpose, minimum, maximum and average

values are presented for the main criteria studied in the different current ratings (see figure 14 to 25). In order to assess the consequences of dispersion with respect to a final rating, it has been decided to use thresholds (upper and lower thresholds) for each criterion.

In the following figures, the thresholds are represented as follows:

- upper level of rating - - - - -
- lower level of rating - - - - -

It is important to note that the thresholds used in this study are **NOT** proposed by ACEA but are mainly the ones currently used or proposed in published whiplash ratings (Thatcham and IIWPG, SRA, ADAC). They are presented in table 2.

Table 2.

High and low performance level for assessing influence of rating on dispersion at different impact severities.

	High performance	Low performance
HRMD data		
Backset (mm)	70	90
Height (mm)	60	80
BioRID data		
Fx+ upper (N)	130	400
Fz+ upper (N)	700	1400
NIC	10	20
Nkm max	0.3	0.5
LNL	1.5	3.0
T1 (g)	9	15
THRC	70	120
TreIHRC	43	93

In this chapter, the type of graph used is as follow : 3 x 3 bars representing the 3 seat models in the 3 type of tests (repeatability at 16 km/h, reproducibility at 16km/h and reproducibility at 25 km/h). For each bar, the dark blue part shows the minimum value recorded for the criteria under study (Min_3 for repeatability and Min_5 for reproducibility), the light blue shows the maximum one (Max_3 for repeatability and Max_5 for reproducibility) and the yellow symbol shows the mean value (X_{Tmean} for repeatability and X_{mean} for reproducibility).

T1 acceleration

Maximum value of T1 acceleration in X CFC 180 up to the end of contact between head and HR as defined in [6] is studied in this section.

Figure 14 presents the results for T1 acceleration.

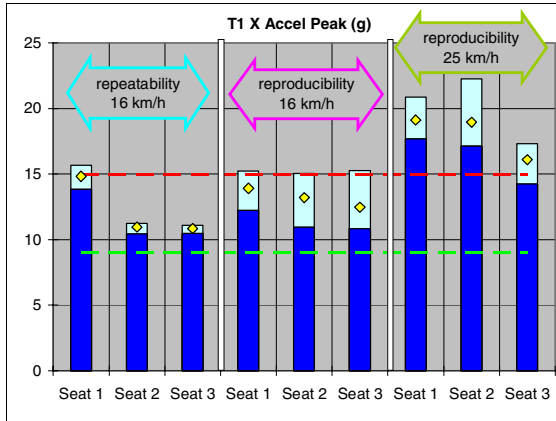


Figure 14. Comparison of dispersion analysed on T1 acceleration.

Repeatability is far much better than reproducibility for this parameter. Dispersion at 16 km/h is almost as large as the band of tolerance. This means that a seat could be rated green in one test and red in the other.

In order to decrease dispersion, a different CFC filter can be used, or 3ms duration values. The three seats show approximately the same trend in reproducibility tests. Whereas seat 1 shows a different trend in repeatability tests than the two other ones.

NIC

Figure 15 presents the results for NIC. NIC is calculated from Head accel and T1 accel in X filtered at CFC 180. Maximum value is taken up to the end of contact between head and HR as defined in [6].

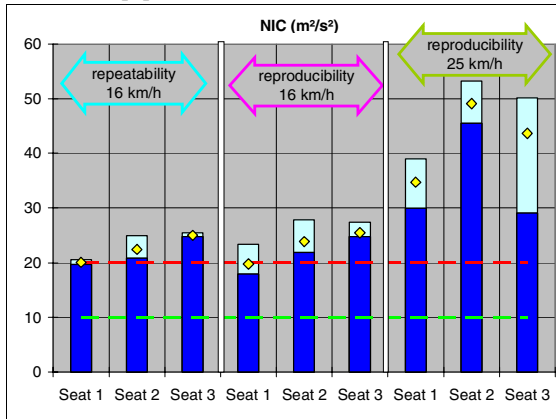


Figure 15. Comparison of dispersion analysed on NIC.

Here again, dispersion is less important in repeatability than in reproducibility tests. But it is large enough to be above or below the red line. Data at 25 km/h shows the very large dispersion of this parameter for all the seat models.

THRC : 1st time of contact between head and HR

Figure 16 presents the results for THRC (absolute values).

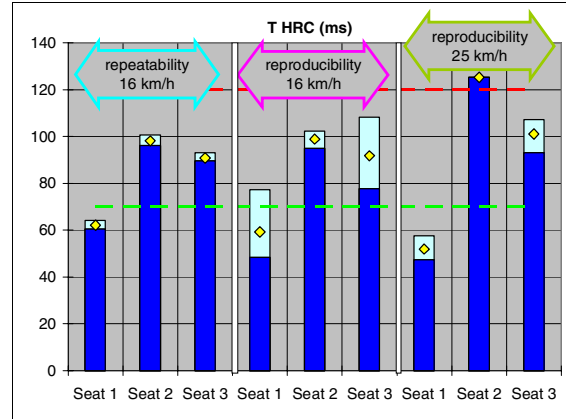


Figure 16. Comparison of dispersion analysed on THRC.

This figure shows the raw data which could be seen as strongly dependent on T_{zero} definition. Here again, repeatability is good, but reproducibility is not.

It should be noted that only 1 result was reliable for seat 2 at 25 km/h.

In order to remove the influence of T_{zero} definition and of the first ms of the sled acceleration, it has been proposed to determine a relative time of HR contact. In theory, if this time is taken with respect to peak sled pulse, T_{zero} definition will have no more influence. This is why we have computed a 2nd THRC, a relative one, TrelHRC. The thresholds have been computed by subtracting 27 ms from the threshold proposed for THRC. Therefore we have an assessment of dispersion for head to HR contact time with no influence of T_{zero} definition.

Figure 17 presents the results for TrelHRC (relative values).

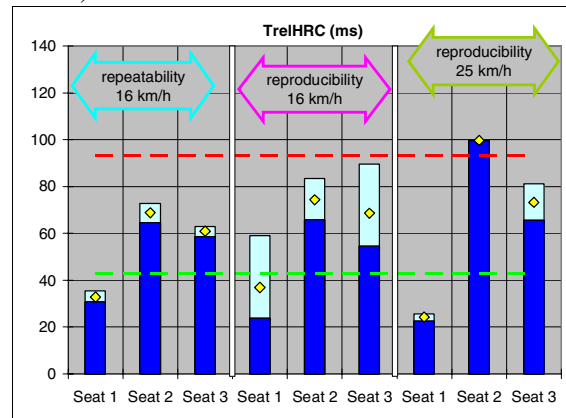


Figure 17. Comparison of dispersion analysed on TrelHRC.

Unfortunately dispersion has not been improved thanks to this solution. Therefore, it is not possible to say that difference in THRC is only due to difference in T_{zero} definition. This is an intrinsic dispersion, because of difference in seat set-up that

may generate a difference in backset between the different seats from the same model and because of measurement dispersion.

Fx : Shear force – upper neck

Figure 18 presents the results for Fx, upper neck shear (positive value only).

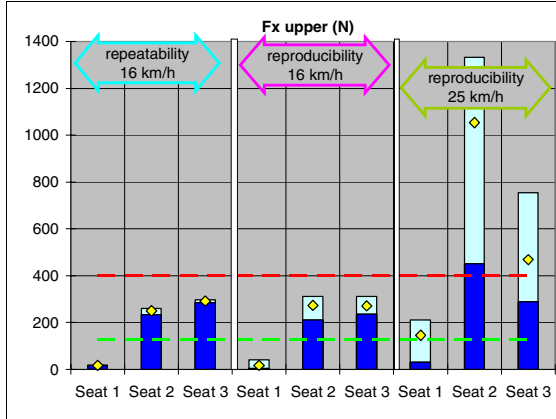


Figure 18. Comparison of dispersion analysed on Fx upper neck.

Positive shear force measured on the upper neck shows very good repeatability results, and slightly worse reproducibility results at 16 km/h but reproducibility at 25 km/h is not acceptable at all.

Fz : Tension force – upper neck

Figure 19 presents the results for Fz, upper neck tension.

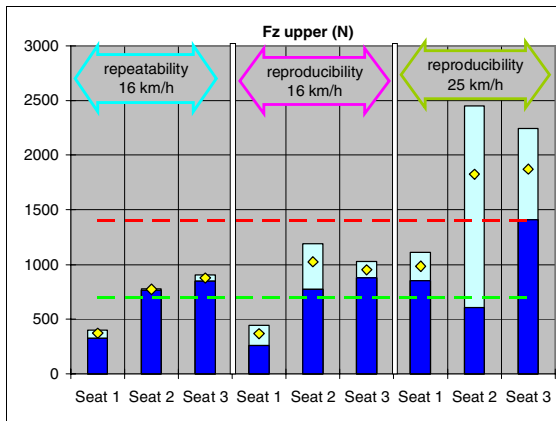


Figure 19. Comparison of dispersion analysed on Fz upper neck.

Tension force measured on the upper neck also shows very good repeatability results, moderate reproducibility results at 16 km/h. But reproducibility at 25 km/h is not acceptable at all.

Nkm and its 4 components

Figure 20 to 24 present the results for Nkm and its 4 different components.

If we first analyse the 2 components made with flexion ($M_y > 0$), i.e Nfa and Nfp (figures 20 and 21), we can see repeatability is very good and reproducibility at 16 km/h is acceptable. But reproducibility at 25 km/h is unacceptable.

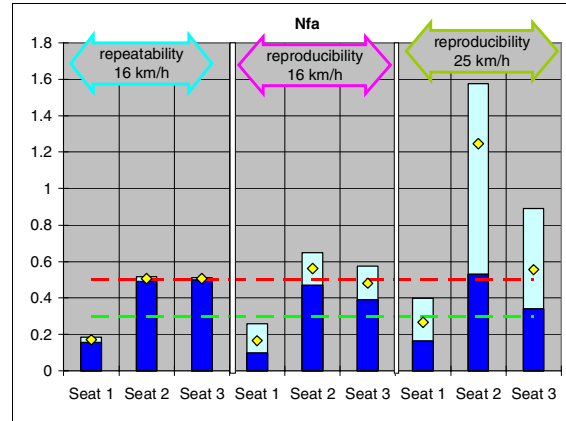


Figure 20. Comparison of dispersion analysed on Nfa.

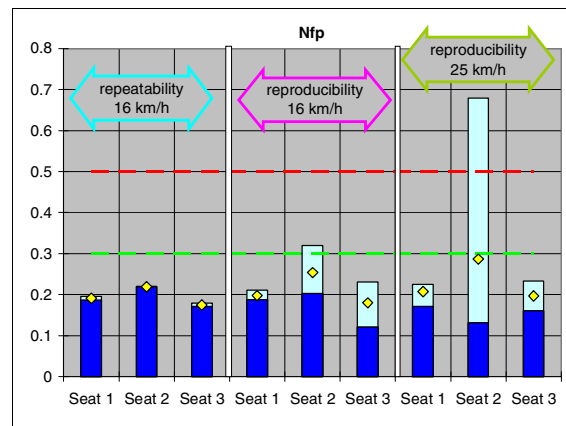


Figure 21. Comparison of dispersion analysed on Nfp.

We can also notice that Nfa is higher than Nfp for all impact severities. Nfa is generally close to the red limit whereas Nfp is close to the green one.

Then, if we analyse the 2 components made with extension ($M_y < 0$), i.e Nea and Nep (figures 22 and 23), we can see repeatability is very good and reproducibility at 16 km/h is acceptable. But reproducibility at 25 km/h is unacceptable.

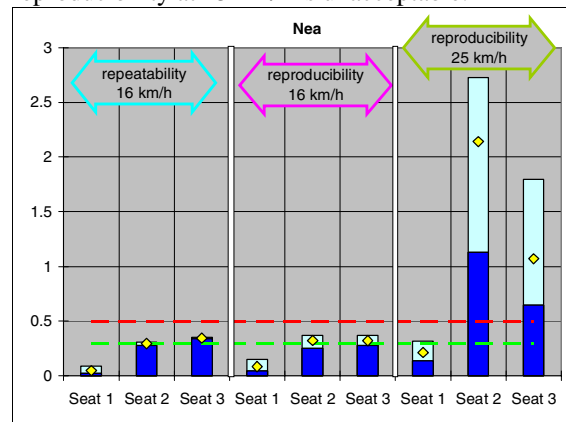


Figure 22. Comparison of dispersion analysed on Nea.

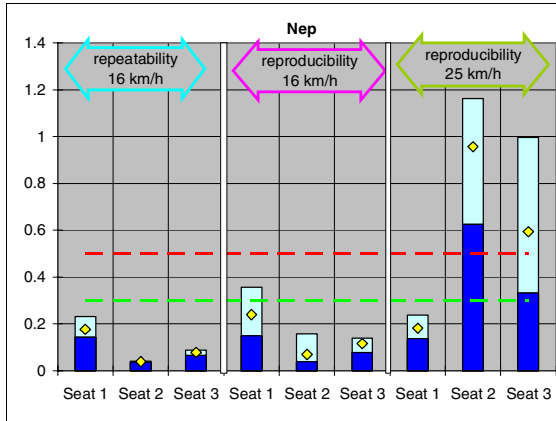


Figure 23. Comparison of dispersion analysed on Nep.

We can also notice that Nea is higher than Nep for all impact severity. For 16 km/h tests, Nea is generally above the green limit whereas Nep is below.

By taking into account all the 4 components of Nkm, we can create a graph with Nkm max values (see figure 24).

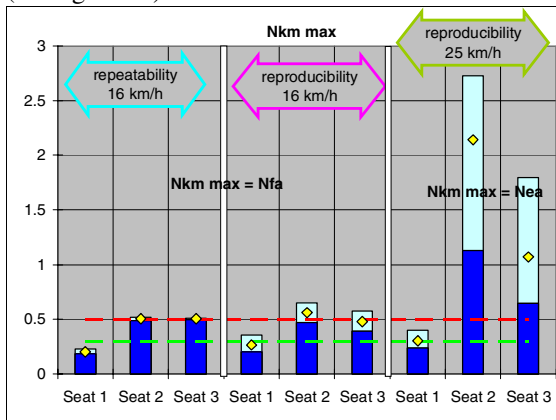


Figure 24. Comparison of dispersion analysed on Nkm max.

For the 16 km/h tests, maximum values are made by Nfa. But it is the Nea component that gives the maximum magnitude for 25 km/h tests. This is the reason why it is not recommended to compare Nkm results without separating the components.

LNL : lower neck load index

Figure 25 presents the results for LNL index (a combination of shear, tension and extension lower neck loads as defined in [6]).

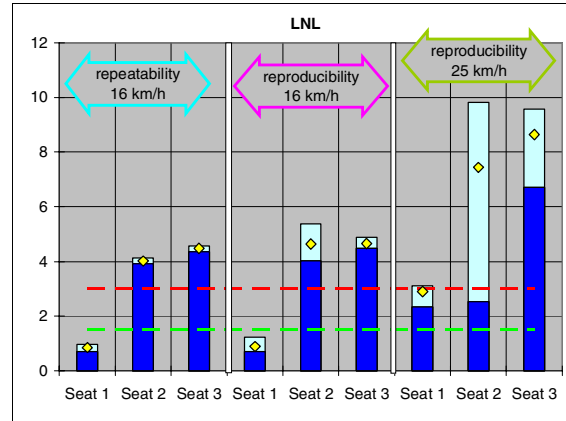


Figure 25. Comparison of dispersion analysed on LNL.

Here again, we can see repeatability is very good and reproducibility at 16 km/h is acceptable. But reproducibility at 25 km/h is unacceptable for two of the seat models.

DISCUSSION

Maximum scattering with respect to test severity

In order to quantify dispersion, the 3 following figures present the scattering, as defined in equations (6) and (11) of several parameters analysed in this study (backset, height, and biomechanical parameters) and for each seat model. There is one graph per type of analysis (repeatability, reproducibility 16 km/h and reproducibility 25 km/h).

Maximum scattering for repeatability assessment at 16 km/h

Repeatability at 16 km/h (see figure 26) shows that scattering is acceptable (around 20%) for all the parameters except for Nkm (mainly Nea and Nep which reached more than 50% of dispersion).

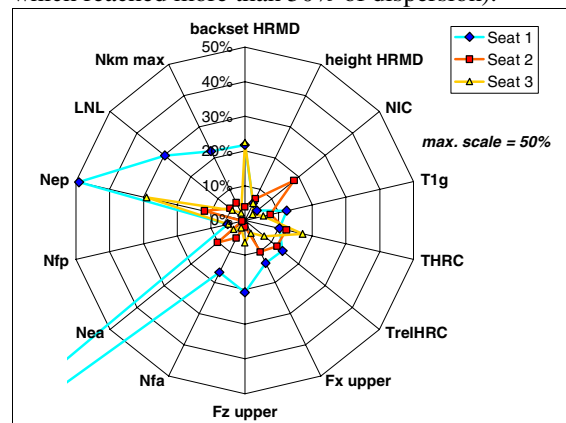


Figure 26. Maximum scattering for repeatability assessment at 16 km/h.

Maximum scattering for reproducibility assessment at 16 km/h

Reproducibility at 16 km/h (see figure 27) shows that scattering is higher than for repeatability but still acceptable (generally between 10 and 40%) for all the parameters except for THRC and Nkm (mainly Nea and Nep which reached more than 50% of dispersion). Fx, Fz and LNL show high scattering for seat 1 only because the values are really low.

Improving training for seat and dummy set-up and defining sled pulse corridor will help to decrease scattering to the level of repeatability.

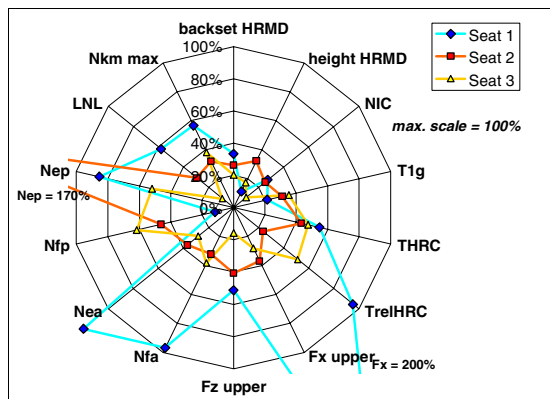


Figure 27. Maximum scattering for reproducibility assessment at 16 km/h.

Maximum scattering for reproducibility assessment at 25 km/h

If we want to do the same comparison for reproducibility at 25 km/h it is needed to enlarge scattering scale. With a maximum scale of 100% we can notice that all the parameters show unacceptable dispersion (generally between 30 and more than 100%) for all the parameters except for backset and height that have no link with impact severity (see figure 28).

It definitively proves that biomechanical criteria cannot be used at this impact severity.

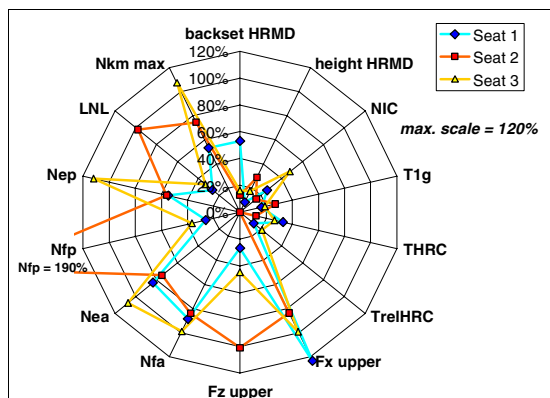


Figure 28. Maximum scattering for reproducibility assessment at 25 km/h.

In conclusion, repeatability (16 km/h) is acceptable, with the exemption of the Nep value (no influence on Nkm max for these tests).

For the delta v 16 km/h tests Nkm (all) and THRC show variations of more than 50%. Forces (Fx/Fz), LNL and T1 are between 20 to 40% variation. NIC showed the lowest variation with values below 30%.

Reproducibility is significantly degraded when delta v 25 km/h pulse is used compared to delta v 16 km/h. In particular the forces and force based criteria show extreme variations (> 100%) with delta v 25 km/h pulse. Result variations clearly question the suitability using these measures at the high severity pulse (delta v 25 km/h).

Combined criteria (« ratings »)

Presentation

When these results were first presented to EuroNCAP, a question was raised : whether the fact to use a combination of several criteria would decrease or not dispersion (like a balance between several criteria dispersion). For this purpose, this paragraph presents dispersion assessed for several ratings inspired by current whiplash rating already published for several years or under construction [1], [2], [3].

As already mentioned earlier in this paper (see Table 2), these ratings are **NOT** proposed by ACEA, they are only based on ratings currently published or under construction.

The philosophy taken to create the ratings is based on the same philosophy as EuroNCAP adult frontal or side score. When a parameter is below the green limit, the maximum score is given. When it is above the red limit, the minimum score is given. When it is between the two limits, a sliding scale is applied.

In order to have a correct scale to compare the results, the sliding scale proposed is between 10 and 0 points. ACEA is not suggesting whiplash score to be 10 points. The reason of choosing 10 points is to get sufficient scale to compare the results.

The method of calculation of the rating is described below:

- each parameter gives a score between 0 and 10 points thanks to the sliding scale.
- the rating is made of 2 to 6 criteria.
- the rating score is the average of 2 to 6 criteria scores.

Therefore:

- a rating score of 10 points means a seat with all the criteria below the green limit
- a rating score of 0 point means a seat with all the criteria above the red limit

We have taken into account three different ratings, named “A”, “B” and “C”. The criteria used for each rating are:

- rating A : NIC, LNL, Nkm
- rating B : NIC, Nkm
- rating C : Fx, Fz, T1g, TrelHRC

A fourth rating has also been used, it combines all the criteria foreseen in the EuroNCAP whiplash WG :

- rating W : NIC, Nkm, Fx, Fz, T1g, TrelHRC

Results

In order to assess consequences on dispersion, the rating has been calculated for all the 16 km/h tests, but also with the average value of each criteria (X_{Tmean} and X_{mean}) and with the extreme values too : maximum value for all the criteria (Max_3 and Max_5), and minimum values for all the criteria (Min_3 and Min_5). This is called respectively “rating with average scores”, “rating with maximum scores”, “rating with minimum scores”.

The three different ratings and the whole one would give homogeneous scores for seat 1 (see figure 29) and different ones for seat 2 (see figure 30) and seat 3 (see figure 31).

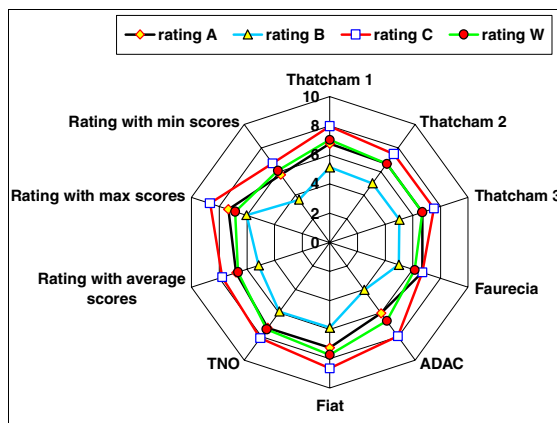


Figure 29. Seat 1 - influence of rating combination on dispersion for 16 km/h whiplash test.

Figure 29 shows that dispersion can lead to 20 % of difference in the rating score for seat 1. Generally extreme scores are close to lab scores. This means all the minimum (or maximum) values appear in the same test.

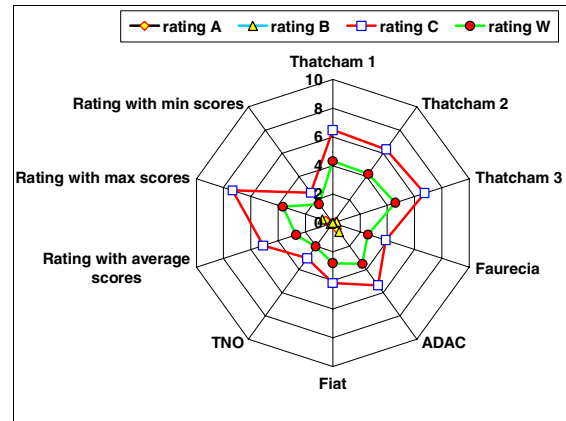


Figure 30. Seat 2 - influence of rating combination on dispersion for 16 km/h whiplash test.

For seat 2, dispersion is important and can bring up to 40 % of difference in the rating score.

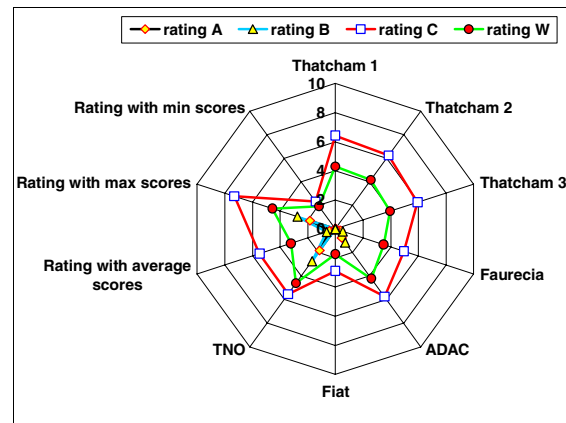


Figure 31. Seat 3 - influence of rating combination on dispersion for 16 km/h whiplash test.

For seat 3, dispersion is important and can bring up to 40 % of difference in the rating score.

Conclusion of rating combinations

In conclusion, no improvement in dispersion occurs when a combination of criteria is used. Therefore, the need is clearly to decrease dispersion by improving reliability of seat and dummy set-up and of pulse reproductibility.

T_{zero} definition

T_{zero} is defined as the first point above 0.5 g measured on the sled accelerometer filtered at CFC 60. The reason why 0.5 g was chosen is because the current definition (1 g) can be in conflict with mechanical systems that are triggered when the acceleration goes above 1g. Moreover 1 g represents 10 % of the maximum value of a 16 km/h test. It was thought to be too high to use as T_{zero} definition.

Whatever the level of T_{zero} (1 g or 0.5 g), it is interesting to notice that defining T_{zero} for an accelerated sled is not so easy because before the beginning of the impact the sled is not at rest (see figure 32) before impact (setting the sled acceleration to 0 before impact could be difficult with such a sled device.

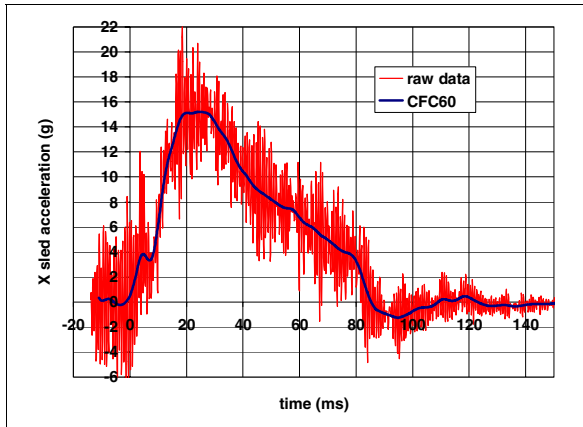


Figure 32. Illustration of possible difficulties to define T_{zero} or accel peak max for a deceleration sled.

What could be added is that it would also be difficult to define any peak in this example (figure 32) where the maximum value is not unique but represented by a plateau.

One of the solutions to improve T_{zero} definition could be to use a specific sensor with a low amplitude range (20 g) in order to define more accurately the 1st point above 0.5g.

CONCLUSION

Initial position

We can sum up the trends by saying that :

- Oscar+HRMD H-point dispersion was within 20 mm for x and 22 mm for z
- BioRID H-point dispersion was within 28 mm for x and 32 mm for z
- BioRID X H-point target with respect to Oscar+HRMD is easily respected but the large band of tolerance is needed since maximum dispersion for X delta H-point was 15 mm
- BioRID Z H-point target with respect to Oscar+HRMD is very difficult to achieve and should be modified (ACEA proposal : same height as for the Oscar + HRMD). Maximum dispersion for Z delta H-point was 18 mm
- HRMD backset dispersion was up to 22 mm
- HRMD height dispersion was up to 26 mm

- BioRID is taller than HRMD (up to 15 mm in the tests performed)

- there is a need to define a BioRID backset for which confidence is enough to help in predicting biomechanical results since current dispersion is 42mm (and 28 mm in height)

Biomechanical criteria

Repeatability tests showed good results of scattering, and reproducibility was acceptable at 16 km/h. Training in seat and dummy set-up will help to improve the results. But the scattering at 25 km/h showed that biomechanical results cannot be used at this impact severity. Indeed, dispersion at 25 km/h was generally between 30 % and more than 100% on biomechanical criteria.

It definitively proves that biomechanical criteria cannot be used at this impact severity.

The three different ratings and the whole one do not show any improvement in dispersion which can lead to 40 % of difference in the rating score. Therefore, in order to improve dispersion one has to put an effort on initial position.

ACEA whiplash subgroup recommendations

Following this extensive analysis, ACEA recommend :

- a clear T_{zero} definition
- a more accurate pulse corridor
- training for seat, HRMD and BioRID set-up
- an update test procedure with pictures to clearly understand the requirements
- an update of Z H-point target for BioRID
- a clearer definition for backset measurement for BioRID to ensure a repeatable position of the BioRID head but also to get a useful parameter for engineers
- clear definition of biomechanical criteria (computer procedure to calculate each criteria)
- no biomechanical criteria at 25 km/h.

ACKNOWLEDGMENTS

ACEA wishes to thank all the labs and all the car manufacturers and seat manufacturers that were involved in this study.

REFERENCES

- [1] IIWPG Ratings of seats and head restraints for neck injury prevention - International Insurance Whiplash Prevention Group - V 1.3 - January 12, 2004
- [2] Dynamic testing and assessment procedure of vehicle seats to examine the risk of injury for the neck in rear impacts - ADAC - January 2004 (Draft 30/01 prepared by Ralf Ambos)
- [3] Folksam/SNRA standard test method for rear end impact crash tests - March 16, 2004
- [4] Research Council for Automobile Repairs (RCAR) – 2001 - A procedure for evaluating motor vehicle head restraints - Issue 2 - February 2001.
- [5] ACEA whiplash test set-up – V2 – January 2004
- [6] ACEA - Data processing for Whiplash- – September 2004

DEVELOPMENT AND VALIDATION OF A NEW FINITE ELEMENT MODEL OF HUMAN HEAD

Giovanni Belingardi
Giorgio Chiandussi
Ivan Gaviglio

Politecnico di Torino, Dipartimento di Meccanica
Italy
Paper Number 05-0441

ABSTRACT

Head injuries are one of the main causes of death or permanent invalidity in everyday life.

The main purpose of the present work is to build and validate a numerical model of human head in order to evaluate pressure and stress distributions in bones and brain tissues due to impact.

Geometrical characteristics for the finite element model have been extracted from CT and MRI scanner images, while material mechanical characteristics have been taken from literature. The model is validated by comparing the numerical results and the experimental results obtained by Nahum in 1977.

The proposed numerical model is promising even if some quantitative differences with the experimental results can be found due to the fact that all the inner organs are considered as a continuum (without sliding interfaces or fluid elements) and due to the geometrical difference between the head used in the experimental test and the head used as reference to build the numerical model.

The protecting action of the ventricles and of several membranes (dura mater, tentorium and falx) has been evaluated taking into account known injury mechanisms.

INTRODUCTION

Head injuries are one of the main causes of death or permanent invalidity in everyday life, especially among young people. Head injuries do not occur only on road accidents, but also during sport or work activities. During many years scientists have been trying to explain pathologies due to cerebral trauma searching for injury mechanisms, psychophysic consequences and possible treatments. In the last fifty years the consequences of head trauma have been studied also from a biomechanical point of view through the use of mathematical models.

Currently the parameter used in order to quantify the severity of a head damage as a consequence of a collision is the Head Injury Criterion (HIC). This parameter has been widely criticized. Its main limits are related to the fact that only linear accelerations are taken into account and that it

should be used only when impacts against rigid surfaces are analyzed. Instead, several studies [1,2,3] concerning cerebral lesions demonstrates the influence and the importance of many other mechanical aspects as, for example, the angular accelerations and contacts responsible of stress and pressure distributions inside the cranium.

An effective way to predict several different head injuries (skull fracture, contusions, hemorrhage, diffuse axonal injury...) is the implementation and application of a finite element human head models validated by means of results obtained in experimental tests. Head models can be used to study the possibility of injury due to an external load (See figure 1).

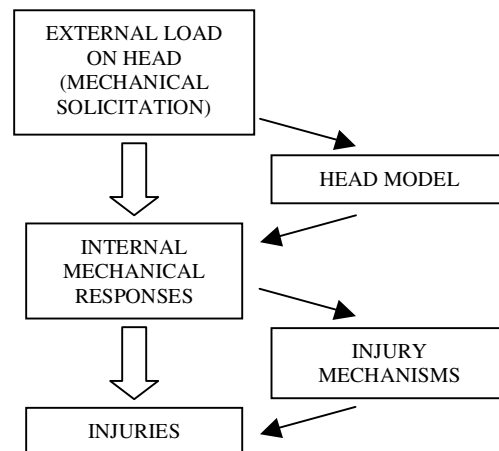


Figure 1. Block diagram representing injury sequence model.

Accelerations and forces are applied to the head model that tries to reproduce the behavior of a real human head in terms of internal mechanical responses. Injury mechanisms found by scientists (especially medicine doctors) for different biological tissues allow to estimate the possibility and severity of injuries due to the evaluated internal responses.

Different authors have proposed FEM models of human head during last years.

One of the first three dimensional model has been developed by Nahum, Smith and Ward in 1977 [4] in order to reproduce the experimental tests carried out on corpse heads. In this model the brain has

been modeled by means of 189 eight node brick elements while dura mater, falx and tentorium membranes have been modeled by means of 80 four node shell elements. A linear-elastic behavior has been adopted to model tissue mechanical properties.

A few FEM models of the human head have been proposed starting from this, each one characterized by several improvements:

- more realistic geometrical data due to the use of diagnostic medical instruments as Computer Tomography (CT) scans or Magnetic Resonance Images (MRI) ,
- introduction of different tissues and anatomical parts previously not present,
- more complex material models,
- higher number of elements due to the increased computational capabilities.

In 1993 Ruan, Khalil and King [5] developed a model of human head with 6080 nodes and 7351 elements where the scalp, the cranium, the cerebrospinal fluid (CSF), the dura mater and the brain were represented. In this model a visco-elastic behavior was introduced for the brain tissue. This model is known as the first version of the WSUBIM (Wayne State University Brain Injury Model) and has been continuously improved. In 1995 Zhou, Khalil and King [6] built a model with 17656 nodes and 22995 elements representing: the scalp, the cranium, the grey matter, the white matter, the brainstem, the CSF, the ventricles, venous sinuses, the dura mater, the falx, the tentorium, the parasagittal bridging veins and the facial bones. In one of the last versions (WSUBIM 2001) proposed by Zhang, Hardy, Omori, Yang and King [7] the number of elements grew up until 245000.

In 1996 Willinger et al. [8] proposed a head model focusing his attention on CSF and made some in vivo experimental tests to find its mechanical properties. The same author in 1997 developed a

model with Kang and Diaw [9,10] where a elastic-brittle constitutive law has been introduced to describe the mechanical behavior of the bone and to simulate fractures.

In 1997 Claessens et al. [11] developed a model of human head where the elements of the skull and the brain tissues have been separated by introducing a sliding interface.

In 2001 Kleivin and von Holst [12] proposed a parametric model to evaluate the influences of geometrical dimensions on impact response. They introduced particular formulations to model the brain tissue and to simulate the sliding interface between brain and skull.

Papers found in literature have been analyzed in collaboration with several doctors leading to the conclusion that the presence of some inner elements as the ventricles and the veins and of the differentiation between grey and white matter should be investigated with more attention in order to improve the knowledge of injury mechanisms. The objective of the present work is the development and the validation of a finite element model of human head to be used to evaluate the intracranial pressure and stress distribution due to a frontal impact, with particular attention toward the protective effects of some inner organs as membranes and ventricles.

MODEL DESCRIPTION

The geometrical model of the head has been build by taking advantage of CT scan and MRI images. More than 160 CT scan images corresponding to sections at a 1.25mm distances of a 31 year old patient with a cranium trauma without serious cerebral consequences have been used to build the internal and external surfaces of the cranium and the facial bones. Surfaces describing the inner soft tissues, as the ventricles, have been taken from MRI images of another patient scaled and adapted

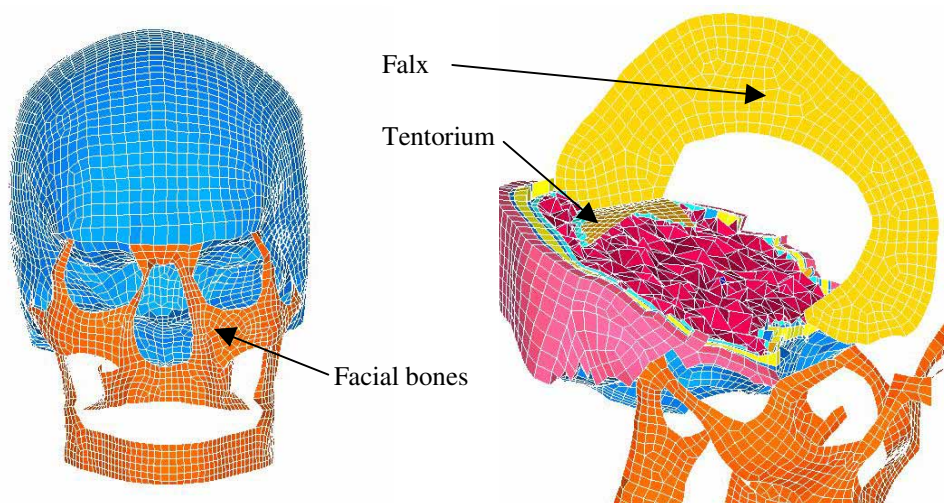


Figure 2,3. Frontal and perspective view of the head model.

to the surfaces obtained by the CT scan images. CT scan images in the DYCOM format have been manipulated by using the software AMIRA. Triangulated surfaces in the STL format have been imported in PARASOLID and transformed in analytical surfaces for a better manipulation with the meshing code.

Finite Element Model

The finite element model (fig. 2-5) has been obtained by using Hypermesh 5.1. A continuous model has been adopted and contact elements between organs have not been defined. The proposed numerical model is characterized by the following components:

- an external layer of brick elements with a 6mm thickness to represent the scalp,
- three layers of eight node brick element (two external layers of compact bone and one internal layer of cancellous bone) to represent the cranial bones,
- shell elements with only inertial contribution to describe the facial bones,
- four nodes shell elements to describe the dura mater, the falx and the tentorium membranes,
- eight node brick elements to describe the CSF,
- tetrahedral elements to model the brain tissues,
- tetrahedral elements to model the ventricles.

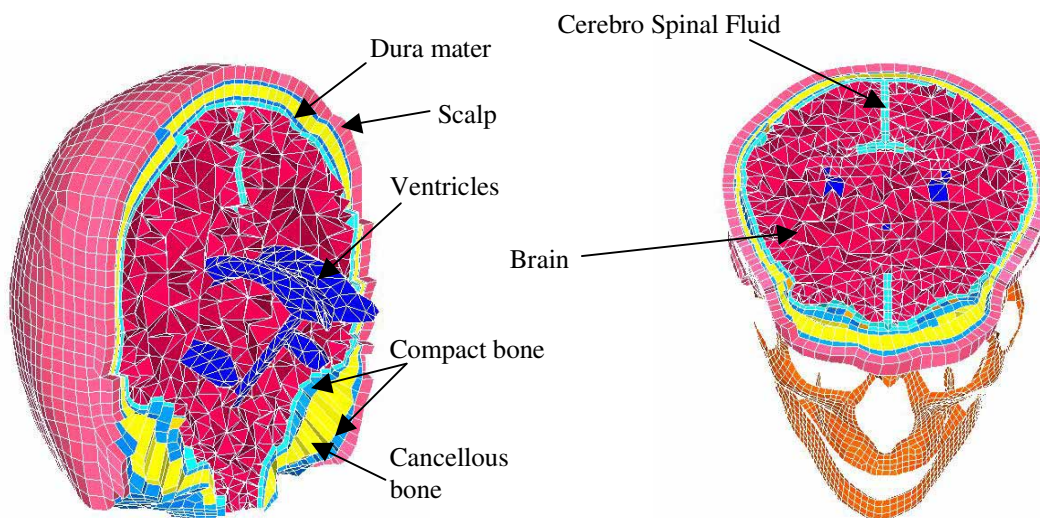


Figure 4.5. Coronal and axial section of the head model.

Dura mater has been obtained from the internal surface of the skull, while falx and tentorium have been built manually based on anatomical images. Cerebro spinal fluid has been obtained with a 2 mm offset from membrane surfaces. A layer of CSF surrounds all membranes and the brain. Internal surfaces of the CSF have been used as external surfaces for the brain volume. The overall model is composed of 55264 elements and about 26000 nodes.

Tissues' Mechanical Property

It is very difficult to estimate the mechanical properties of the different tissues used in the model. They are very variable, depending on the experimental tests used to evaluate them. In this work literature data have been considered. For some parameters an average value of different literature values has been used, while other parameters have been adapted to the model. All the tissues, except the brain, have been modeled with a linear-elastic behavior. The mechanical properties of the different components of the FEM model are summarized in table 1. Mechanical properties used to model the scalp are $\rho=1200 \text{ Kg/m}^3$, $E=16.7 \text{ MPa}$ and $\nu=0.42$. This values have been used in WSUBIM [5], in the model by Zhou et al. [6] and in the model proposed by Willinger-Kang-Diaw [9,10]. A lot of experimental tests have been done by different authors in order to evaluate the bone mechanical properties. It has been chosen to adopt the same values used in Willinger et al. [9,10] to model the cranium bones. For the compact bone it has been used a Young modulus $E=15000 \text{ MPa}$, a Poisson ratio $\nu=0.21$ and a material density $\rho=1800 \text{ Kg/m}^3$.

For the cancellous bone it has been chosen a Young modulus $E=4500 \text{ MPa}$, a Poisson ratio $\nu=0.01$ and a material density $\rho=1500 \text{ Kg/m}^3$. Mechanical stiffness properties of the facial bones are not relevant for the proposed model and only inertial properties have been considered. The material density of the facial bones has been evaluated in order to keep a realistic mass. For membranes, it as been found a general agreement in using the values ($E=31.5 \text{ MPa}$,

$\nu=0.21$, $\rho=1133\text{kg/m}^3$) obtained by Nahum et al. and used in their FEM model [4].

CSF surrounding the membranes and filling the lateral ventricles has been modeled using a linear-elastic material with a 'fluid' option. In this case the element loses its ability to support shear stress and only compressive hydrostatic stress states are possible. For the fluid option the bulk modulus (K) has to be defined as the Young modulus and the Poisson ratio are ignored by the computational code. With the fluid option fluid-like behavior is obtained where the bulk modulus K is given by:

$$K = \frac{E}{3(1 - 2\nu)} \quad (1).$$

and the shear modulus is set to zero. The mechanical properties introduced in (1) are not well defined. The bulk modulus K varies in literature from 4.76MPa in Zhou et al. [6] to 2125 MPa in Willinger et al. [9,10]. Considering a value of the Young modulus $E=0.012\text{MPa}$ and of the Poissons ratio $\nu=0.49$ (nearly incompressible material) a bulk modulus K equal to 0.2MPa has been obtained [8]. The CSF material density has been set to $\rho=1040\text{kg/m}^3$.

The brain tissue has been modeled by using a visco-elastic material model with shear relaxation behavior described by:

$$G(t) = G_{\infty} + (G_0 - G_{\infty}) \cdot e^{-\beta t} \quad (2).$$

where:

G_{∞} = long-time (infinite) shear modulus,

G_0 = short-time shear modulus,

β = decay coefficient,

t = time.

Considering the first [8] and the second [9,10] model proposed by Willinger the decay coefficient β varies from $\beta=0.035\text{ms}^{-1}$ to $\beta=0.145\text{ms}^{-1}$, the short-time shear modulus G_0 from $G_0=528\text{KPa}$ to $G_0=49\text{KPa}$ and the long-time (infinite) shear modulus G_{∞} from $G_{\infty}=168\text{KPa}$ to $G_{\infty}=16.7\text{KPa}$.

According to a previous model developed in our department [13] it has been chosen to set up the bulk modulus equal to 5.625MPa, the decay coefficient β equal to 0.145ms^{-1} , the short-time shear modulus G_0 equal to 490KPa and the long-time (infinite) shear modulus G_{∞} equal to 167KPa. A material density value of $\rho=1140\text{Kg/m}^3$ has been used for brain tissues. A total mass value of about 1.4Kg has been obtained: it is acceptable considering the cerebrum weight (1.2÷1.5Kg), the pons and medulla oblongata weight (50÷75g) and the cerebellum weight (about 150g).

Table 1.
Material characteristics.

Tissue	Material model	ρ (kg/m ³)	E (MPa)	ν
Compact bone	Linear elastic	1800	15000	0.21
Cancellous bone	Linear elastic	1500	4500	0.01
Facial bone	Linear elastic	4500	10000	0.3
Brain	Visco-elastic	1140		
CSF	Linear elastic	1040	0.012	0.49
Ventricles	Linear elastic	1040	0.012	0.49
Scalp	Linear elastic	1200	16.7	0.42
Dura mater	Linear elastic	1133	31.5	0.45
Tentorium	Linear elastic	1133	31.5	0.45
Faulx	Linear elastic	1133	31.5	0.45

Simulations have been solved using dynamic finite element code LS-DYNA.

Boundary Conditions

The model has been considered as free in correspondence of the neck because the impact phenomenon is too fast to be influenced by neck constraints.

Experimental tests carried out by Nahum in 1977 [4] have been taken into consideration in order to set up the loading condition and to validate the numerical model. In these tests pressurized corpse heads have been frontally hit by means of a metal impactor. In particular, test number 37 has been considered as reference due to the geometrical similarities between the impacted head used in the test and the proposed FEM model.

The impact force and the pressure distribution in correspondence of the frontal area of the skull and of the posterior-fossa subarachnoid space have been considered as reference parameters for the validation.

Experimental tests also consider the pressure distribution on the frontal, occipital and parietal lobes. These data have not been considered because of the difficulty to find the exact corresponding area on the FEM model, whose position depends on the unknown layout of the cranial sutures.

The impactor has been modeled by the finite element method. It is characterized by the same mass (5.6kg) as in the experiment 37 and has been covered with a layer of elements with an elasto-plastic behavior. Contact between impactor and scalp has been defined as surface/surface contact in LS-DYNA code by using a static and dynamic friction coefficient equal to $f=0.2$.

Several mechanical parameters have been maintained constant in all simulations while others have been changed, in a significative range, to find a better correlation with experimental tests.

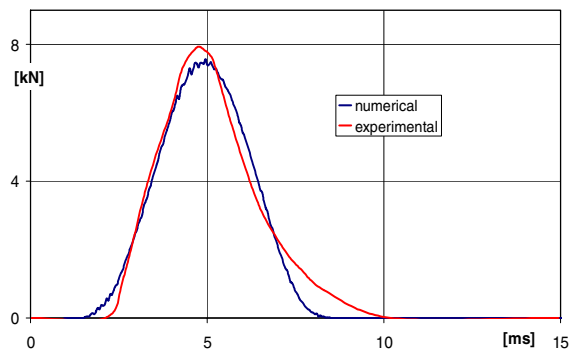


Figure 6. Impact force behavior.

The impact force behavior obtained by Nahum, related to the impact energy that has to be absorbed by head tissues, has been used as the first reference response to be reproduced with the numerical model.

Impactor mechanical properties influence the behavior of the impact force: the impactor speed influences mainly the peak value while the mechanical properties of the covering layer of the impactor control the time length and the shape of the force impulse.

In order to obtain the same peak of impact force, the impactor speed has been decreased from the real value of 9.6 m/s to a value of 7.0 m/s. This value is quite different from the experimental one used by Nahum in the analyzed experimental test (-27.5%) and it is probably due to differences in geometry, mass and stiffness distribution and to energy absorption mechanisms that are present in human tissues and have not been considered in the proposed numerical model. This difference became more relevant if kinetic energy of impactor is considered (-47%).

By setting up the impactor speed at $V=7.0\text{m/s}$, the best correspondence between numerical and experimental impact force behavior (see figure 6) has been obtained by using the mechanical properties of the impactor and of the covering layer shown on table 2.

Table 2.
Mechanical characteristics of impactor.

Tissue	Material model	ρ (kg/m ³)	E (MPa)	ν
Impactor	Rigid	5304	210000	0.3
Covering layer	Elasto-plastic	1050	1500	0.3

RESULT ANALYSES

Impact force has a peak value of $F=7.56\text{kN}$, nearly the same obtained by Nahum (7.9kN), and also the general behavior is quite similar (see figure 6). Once the correct impact force has been obtained, the mechanical responses of the proposed numerical model have been evaluated and compared to those obtained by Nahum in the experimental tests. In particular the influence of the value of some mechanical properties used to model the brain tissues and the CSF has been studied.

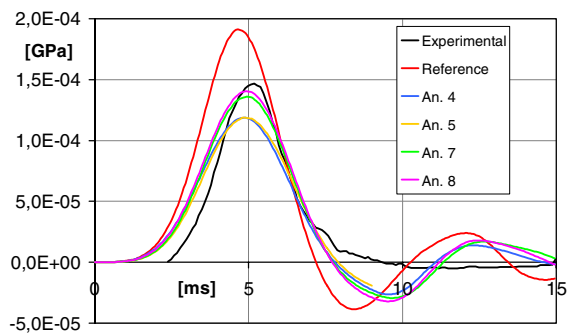


Figure 7. Frontal pressure behavior.

Different analyses have been carried out with different values of the bulk modulus for the CSF material and of the bulk modulus and of G_0 for brain material. The initial values chosen have been taken as reference and multiplied for a range of values varying between 0,1 and 10.

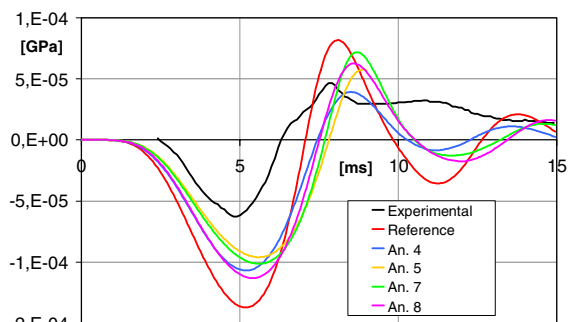


Figure 8. Posterior fossa pressure behavior.

Figure 7 and 8 show the numerical and the experimental pressure value evaluated in the frontal area of the cranium and in the posterior fossa for different values of the multiplying factors

(summarized in Table 3). The pressure has been evaluated as an average value on four elements.

Table 3.
Multiplying factor for material characteristics in different analyses.

	CSF bulk	Enc. bulk	Enc. G_0
Reference	1	1	1
An. 4	1	0.2	2
An. 5	0.5	0.2	2
An. 7	0.5	0.3	2
An. 8	0.75	0.3	1.5

The general behavior is similar in both cases but there are differences concerning the peak values, especially for the posterior fossa pressure. Even with different values of the mechanical characteristics it has not been possible to obtain a significative improvement. This does not seems to be due to a wrong value in these mechanical parameters but to a lack of the model that seems to need the introduction of elements with a damping and/or retaining action for the brain tissues. One of the main problems could be the modelization of the CSF. A structural analysis without fluid elements cannot correctly simulate the fluid damping and the fluid-dynamic migration

of the CSF in different areas during impact although the very short duration of the phenomenon .

The activation of the fluid option for elastic elements improves the results by introducing a damping factor that reduces pressure oscillations but it is not sufficient to obtain accurate quantitative results.

Even if on the basis of some experimental tests [14] the bulk modulus has been evaluated equal to 2125MPa (nearly incompressible) we have obtained better results (fig. 7,8) considering the brain compressible (bulk modulus less than 5.625Mpa). This is probably due to the fact that the compressibility assigned to the brain allows to take into account the mechanisms of movement of the CSF through the occipital foramen and of the blood flow of the inner vascular system that influence the history of the intracranial pressure during impacts. Figures 9-17 shows the pressure distribution on a median sagittal section. A gradual transition from compression in the frontal zone to tension in the occipital zone can be observed. This is due to inertia forces that push the brain against the frontal portion of the skull and pull it from the occipital portion leading to large stresses in the connecting tissues between brain and bone. After the first

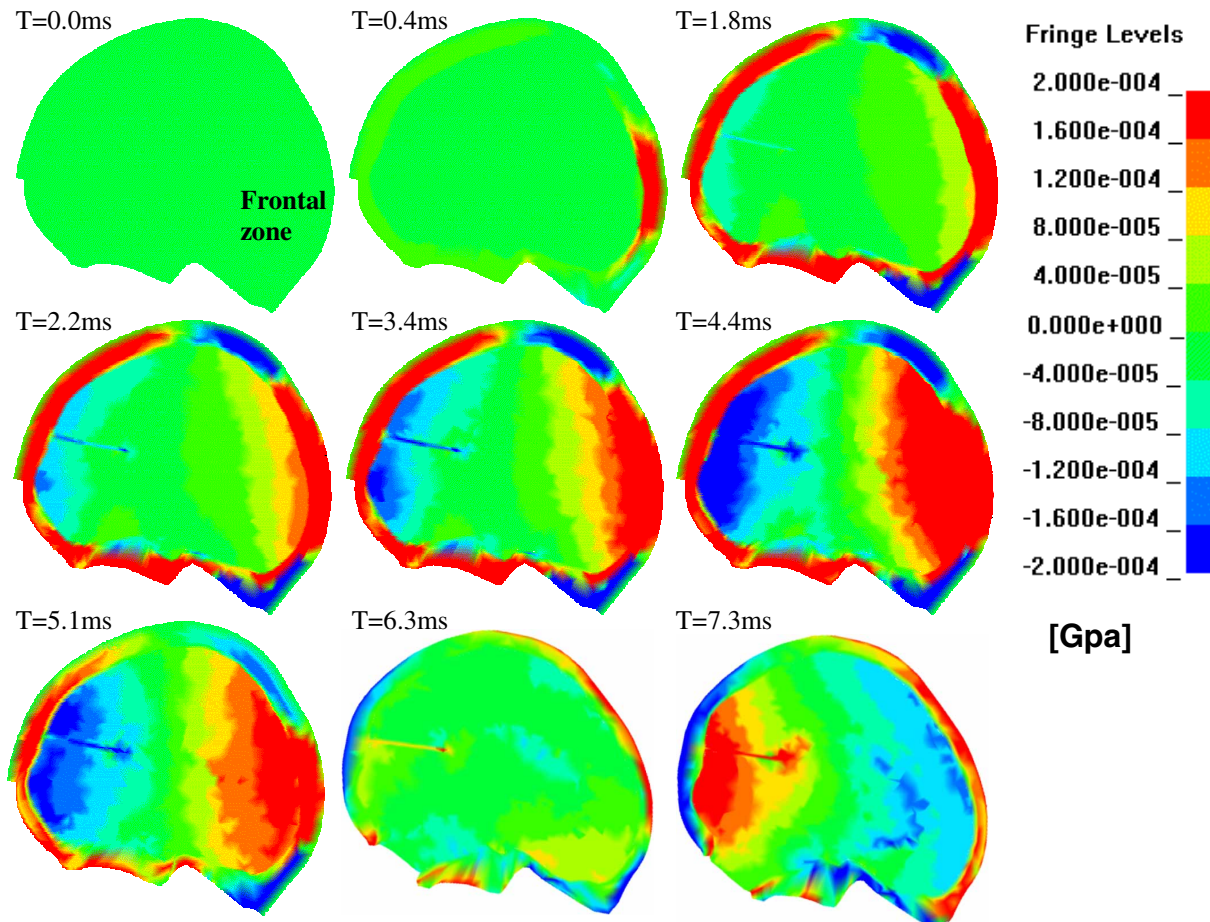


Figure 9-17. Pressure distribution on a sagittal section during impact.

bounce the brain return in the equilibrium position (about $T=6.3\text{ms}$) and the pressure distribution comes back to normality but the relative velocity between brain and skull, due to different inertial properties, creates the countercoupling effect when the brain is compressed towards the occipital zone (about $T=7.3\text{ms}$).

The analysis of the pressure distribution in different moments allows also to study the load transfer mechanism from the impacted area of the skull to the brain. In particular it is worth to notice the time delay of the mechanical responses in bone tissues and in the brain: high pressure values are reached in the bone about 1.8ms after impact while brain is still floating in the CSF and maximum values of pressure are reached after about 4.4ms in brain (figure 9-17.).

Influence of Ventricles and Membranes

Several medical studies have demonstrated the protecting effect of the ventricles and the membranes inside the cerebral mass. Some simulations have been done to investigate this behavior with the proposed model.

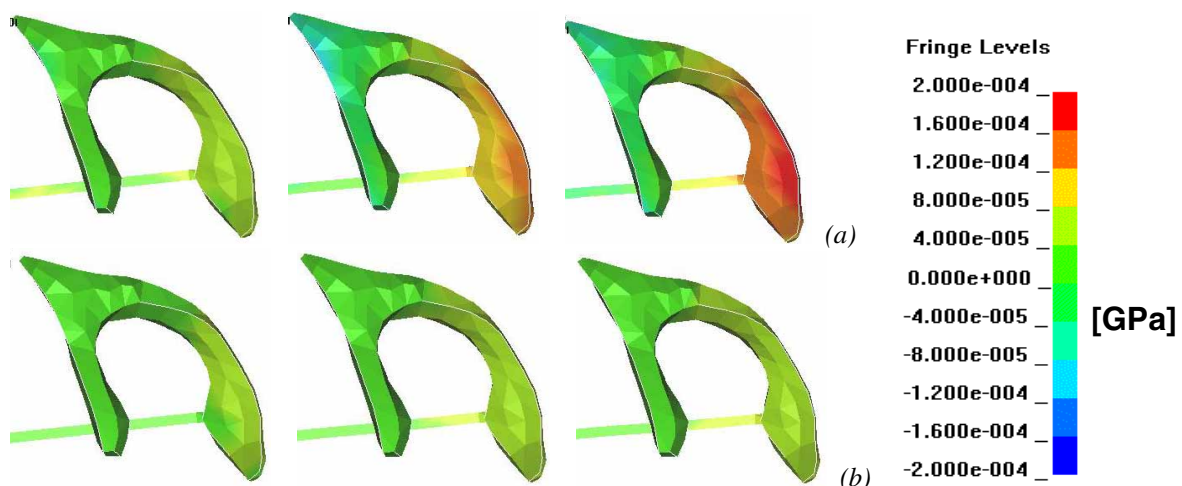


Figure 18. Pressure distribution in correspondence of ventricles after 3, 5 e 7ms (a) if they are modeled with brain material and (b) if they modeled with CSF material.

At first, attention has been focused on ventricles. The intracranial pressure distribution obtained by using the proposed model has been compared with that obtained by eliminating the ventricles. Ventricles elimination has been obtained by assigning to the corresponding elements the same mechanical properties of the surrounding brain tissues.

Pressure distribution in the frontal area of the skull and in the posterior fossa is not significantly different from that obtained by using the complete model. Otherwise relevant differences can be found in areas corresponding to ventricles surfaces (fig. 18) where peak pressure are strongly increased

(about +300%) showing their protective effect in brain's central area.

Attention has then been focused on membranes. In this case elements corresponding to dura mater, falx and tentorium have been deleted. The absence of membranes leads to higher pressure peaks (+17% in the frontal zone and +18% in the posterior fossa, fig. 19) confirming also for these tissues an important protective effect.

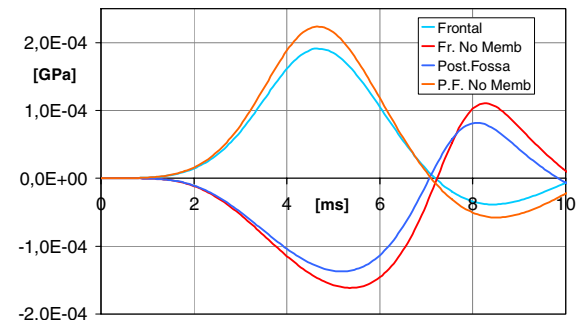


Figure 19. Pressure behavior with and without membranes.

The mechanical effect of membranes has been taken into consideration also by Claessens [11]. Also in his paper an increasing value for pressure distribution can be found eliminating membrane tissues.

Brain Injuries

Shear stress distribution has been analyzed on a median sagittal section and on a coronal section of the brain. Injuries concerning the brainstem and diffuse axonal injury (DAI) are usually related to the presence of large shear stresses.

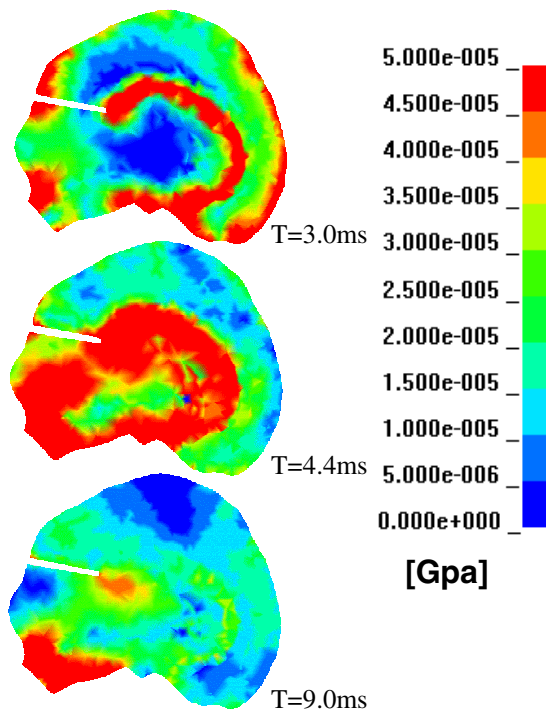


Figure 20-22. Shear stress distribution on sagittal section.

On the sagittal section maximum values of shear stress can be found at first in correspondence of corpus callosum, while later in correspondence of brainstem (fig. 20-22). Medical studies indicate this two tissues as the most affected by DAI. Some shear stress concentration can also be found in

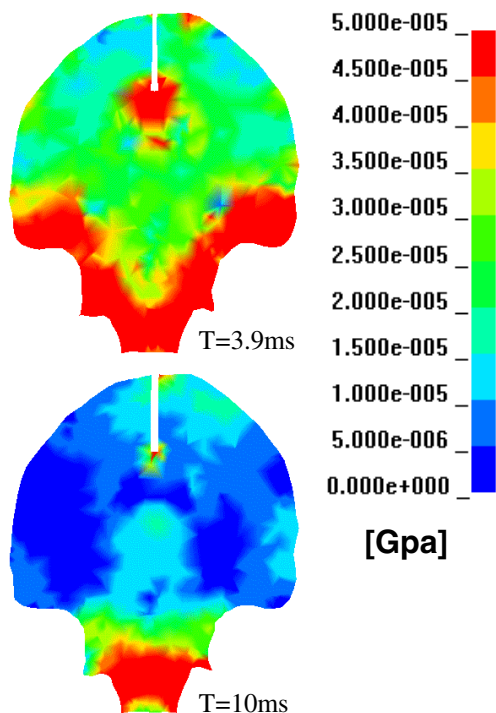


Figure 23-24. Shear stress distribution on coronal section.

correspondence of the falx border, but this could be due mainly to the numerical model that does not allow sliding between tissues.

A high value of shear stress can also be seen in the coronal section in correspondence of the brainstem. This area keeps being stressed for the greatest part of the impact phenomenon, also when all other tissues are almost relaxed (fig. 23-24). This behavior confirms the hypothesis that the brainstem is like a pivot for brain movements and may be seriously damaged by shear stresses.

CONCLUSIONS

A FEM model of human head has been built to study injury mechanism due to impacts. The use of images obtained by TC or MRI scanners revealed fundamental to obtain a realistic geometry to be used as a starting point for the numerical model. Unfortunately it is not always possible to obtain the necessary TC or MRI images of the same head to build all the surfaces needed for the numerical model. In fact, in most cases, these medical analyses are focused on a particular pathology and there are some tissues that are put in evidence and other that are not visible.

The mechanical properties of several tissues to be used are not well known. In this work literature data have been considered to define the mechanical properties. For some parameters an average of different literature values has been used, while other parameters have been modified during the validation phase.

Some mechanical parameters have been kept constant in different simulations while others have been changed, in a significative range, to find a better correlation with experimental tests. Impact force intensity obtained by Nahum has been used as reference value to be obtained with the numerical model. Impactor speed has however been varied from the real value of 9.6 m/s to a value of 7.0 m/s to obtain the same peak of impact force. This difference is probably due to differences in geometry and in mass and stiffness distribution between head used in Nahum experiments and our model.

Good results have been obtained for the impact force and the pressure distribution behavior while there have been difficulties in simulating pressure behavior in posterior fossa. The same problem has been encountered also by others authors and is probably due to the material model adopted to simulate the cerebrospinal liquid. Using a continuous mesh and an elastic material with a low stiffness value (with fluid option), it is possible to simulate the “floating” effect of brain inside the cranium but not the motion of fluid in the subarachnoid space and the ventricles. The solutions, as already proposed by Claessens [11], could be a coupled analysis with fluid-solid

interaction or a contact interface between brain and dura mater to allow tissue sliding, as proposed by Kleiven and Von Holst [12].

Importance of some tissues introduced in this model for injury prevention has been investigated. In particular tentorium and falx structural stiffening function with respect to soft tissues has been pointed out. An important pressure absorbing capability of the ventricles has also been put in evidence.

The highest values of shear stress have been found in area where DAI lesions are usually found. They seem to be also responsible for injuries to brainstem and corpus callosum.

The model could be improved from an anatomical point of view, for example by introducing the bridge veins or the brain tissue differentiation between white matter, grey matter, cerebellum and brainstem behavior. Improvements could be reached by introducing more complex material models like, as an example, the real fluid behavior of the CSF or the fracture criterion for skull bones. These considerations agree with some medical studies and more qualitative conclusions could be drawn with more experimental or clinical data. A close collaboration with doctors is considered as fundamental to obtain clinical data and information necessary to build more accurate models, to validate them and for a better comprehension of injury mechanisms.

ACKNOWLEDGEMENT

The contributions of the unit of intensive care of the Molinette hospital of Torino (Prof. L. Mascia) and of the neuroradiology unit of the CTO hospital of Torino (Prof. C. Valentini) are kindly acknowledged.

REFERENCES

- [1] David C. Viano. 1988. "Biomechanics of head injury: Toward a theory linking head dynamic motion, brain tissue deformation and neural trauma". SAE n° 881708.
- [2] Jesse S. Ruan, Priya Prasad. 1994. "Head injury potential assessment in frontal impacts by mathematical modeling". SAE n°942212.
- [3] Frank P. Di Masi. 1995. "Computational analysis of head impact response under car crash loadings". SAE n°952718.
- [4] Nahum, R. Smith, C. C. Ward. 1977. "Intracranial pressure dynamics during head impact", Proc. 21st Stapp Car Crash Conference SAE n° 770922.
- [5] Jesse S. Ruan, Tawfik B. Khatil, Albert I. King. 1993. "Finite element modeling of direct head impact", SAE 933114.
- [6] C. Zhou, T. B. Khalil, A. I. King. 1995. "A new model comparing impact responses of the homogeneous and inhomogeneous human brain". SAE n°952714.
- [7] Zhang, L., Hardy, W., Omori, K., Yang, K.H., King, A.I. 2001. "Recent advances in brain injury research: a new model and new experimental data", Bioengineering Center, Wayne State University.
- [8] Willinger, R., Trosseille, X., Lavaste, F., Tarriere, C., Domont, A., Kang, H.S. 1996. "Validation study of a 3D finite element head model against experimental data". SAE 962431.
- [9] Willinger, R., Kang, H.S., Diaw, B.M. 1997. "Développement et validation d'un modèle mécanique de la tête humaine".
- [10] Willinger, R., Kang, H.S., Diaw, B.M., Chinn, B. 1997. "Validation of a 3D human head model and replication of head impact in motorcycle accident by finite element modelling". SAE 973339.
- [11] Claessens, M., Sauren, F., Wismans, J. 1997. "Modeling of the human head under impact conditions: a parametric study". SAE 973338.
- [12] Kleiven, S., Von Holst, H. 2001. "Consequences of head size following trauma to the human head".
- [13] Luera, A., 2001. "Simulazione agli elementi finiti del fenomeno di impatto in una testa umana". Politecnico di Torino.
- [14] Shuck L. Z., Advani S. H. 1972. "Rheological response of human brain tissue in shearing", JBE.